Neuronal networks in absence epilepsy : dynamics of seizure transitions

Patrick Pierre O'Brien
ORCID : 0000 0003 0956 2184

Doctor of Philosophy

March 2021

Faculty of Engineering and Information Technology
Department of Biomedical Engineering
The University of Melbourne

Submitted in total fulfilment of the requirements of the degree of Doctor of Philosophy

Abstract

Epilepsy is the most common recurrent neurological condition, affecting a little over 1% of the world's population. It is often debilitating because of significant psychological, social and cognitive burdens apart from the seizures themselves. Advancing treatment options for generalised epilepsy syndromes has proven a challenging problem, since they are often refractory to treatment with anti-epileptic medication, and are currently not amenable to surgical treatment, so that it is rarely ethical to conduct invasive intracranial EEG studies in human patients with these conditions in order to study them further.

Although there has been controversy over the origin and networks involved in absence seizures, previous work by our group has shown that alternative areas of somatosensory cortex are important parts of the thalamocortical circuit in the generation of seizures. The work of this thesis aims to extend those studies by showing that the coupling between cortex and thalamus is altered during seizures. It is established that there is a process of resonance ocurring prior to and during seizures in relevant deep layers of cortex, and the mechanisms behind this are studied.

Novel aspects of the work presented in this thesis include the examination of the EEG in the GAERS rat, a whole animal model of absence epilepsy, at the scales of both individual cortical microcircuits and whole cortical areas using simultaneous depth electrodes, and also at both very fine and long time scales.

The studies described in this thesis show that the somatosensory cortex leads the thalamus in the first second of seizure onset, in agreement with the results of previous work. To account for the mechanisms behind this increased coupling at seizure onset, an analysis of the properties of resonance in different parts of cortex is presented. This indicates altered phase coupling prior to seizures, in the form of increased phase entrainment, phase coherence, and cross-frequency coupling. These changes are most marked in the junction between primary and secondary somatosensory cortex, with earlier, larger increases prior to seizures, and earlier decoupling at seizure termination.

Dynamical analysis points to a number of processes underlying such increases in cortical resonance. Alterations in scaling behaviour are observed in different cortical regions, and also prior to seizures. Analysis of the Lyapunov spectrum of cortical depth and tetrode EEG data shows evidence for a separation in timescales of dynamics at seizure onset, and changes consistent with critical slowing. Further, gradual changes in the statistics of the largest exponents are seen with approaching seizures, suggesting an alteration in dynamical properties giving rise to critical slowing.

The results of this thesis support the recently proposed cortical focus theory of ab-

sence seizure generation in GAERS rats, and provide new insight into cortical network changes relevant to seizures. This work provides a basis to explore the mode of action of antiepileptic drugs, and more targeted therapy for generalised absence seizures.

Declaration

This is to certify that

1. the thesis comprises only my original work towards the PhD,
2. due acknowledgement has been made in the text to all other material used,
3. the thesis is less than 100,000 words in length, exclusive of tables, maps, bibliographies and appendices.

Patrick Pierre O'Brien, March 2021

Preface

All of the analysis and results in this thesis is unpublished material not yet submitted for publication. The tetrode experiments described in Chapter 2 were carried out jointly by Dr Thomas Zheng and myself. The depth electrode experiments described in Chapter 2 were carried out by Dr Thomas Zheng.

The work described in this thesis was supported by NHMRC postgraduate scholarship 1040028.

Acknowledgements

Thanks to my supervisors, Professors Tony Burkitt, Terrence O'Brien, and Jamie Evans for their time and patience - my path through the PhD has been longer and more meandering than most! Dr Thomas Zheng is a wonderful teacher, colleague, and friend, as are Drs Andre Peterson and Alan Lai. Thanks also to my friend Dr David Hoxley, for his honest encouragement, I have learnt a lot about life in general from him too.

Practising clinical medicine always seems to me to be a great privilege, especially to learn life experience from patients, but I also value the opportunity to combinine the 'pragmatic' aspects of patient care with a deeper perspective rooted in neuroscience. In my day job, I run the neuropsychiatry service at St Vincent's Hospital in Melbourne. I have loved getting the chance to learn a rigorous approach to clinical neurology from Prof Mal Horne, a great doctor and teacher. Sorry to Kate for all the late nights after outpatient clinics meandering through the interesting byways of neuroscience. Looking back now, my first attempts to write an outline of some projects that would eventually comprise this thesis were truly woeful, and I'm glad to have the opportunity to learn how to approach scientific thinking in a more organised way from Tony. I've particularly loved the chance to observe Tony's rigorous scientific thinking, because although I'm not a professional physicist this was my first field of study with medicine. I've also loved spending time with Terry and learning electrophysiology from him, because I hope to continue combining these fields and move into some clinical research into the future.

I had always hoped that my wife Kate would acclimatise to physics and learn to like it - but perhaps this thesis is the nail in the coffin for her! Don't worry Kate, I'll keep trying :-). Looking at the bright side, at least now you'll not have to fear further requests to read it! Seriously though, thanks to the beautiful Kate for being such an honest friend, a resplendently gutsy person who is true to herself in every way I can think of.

I used the John Papandriopoulos Latex template for this thesis. Code written in this thesis is mine - except : thanks to Prof Adriano Tort, who provided the cross frequency coupling routine that I used as a core for further code used in chapter 5; Dr Alan Lai, who wrote the piecewise linear interpolation routine that I used to calculate nonlinear association measures used in Chapter 4; I used the FieldTrip routine for the phase slope index calculations; and I used Phillip Rinn's R package, Langevin, to help learn how to code the Fokker-Planck analysis, and which I used for the two-dimensional analysis. Lastly, to import the intan data files into Matlab their proprietary code was used. It can be provided on request.

Contents

List of Figures

List of Symbols

Acronym	What (it) Stands For
GAERS	Genetic Absence Epilepsy Rats from Strasbourg
AED	Antiepileptic Drug
SWD	Spike and Wave Discharge
EEG	Electroencephalogram
ECoG	Electro Corticogram
MEG	Magnetoencephalogram
IGE	Idiopathic Generalised Epilepsy
CAE	Childhood Absence Epilepsy
BOLD	Blood Oxygen Level Dependent
MRI	Magnetic Resonance Imaging
VB	Ventrobasilar thalamus
TRN	Thalamic Reticular Nucleus
EPSP	Excitatory post synaptic potential
IPSP	Inhibitory post synaptic potential
TLE	Temporal Lobe Epilepsy
EEP	Event evoked potential
AP	Antero-posterior
ML	Medial - lateral
S1	Primary somatosensory cortex
S1Fl	S1 - forelimb area
S1Ul	S1 - Upper lip (i.e. vibrissae)
S2	Secondary somatosensory cortex
IC	Insular cortex
MC	Motor cortex
KM	Kramers-Moyal expansion
FP	Fokker-Planck Equation
MPC	Mean phase coherence
PSI	Phase slope index

Chapter 1

Literature review

1.1 Introduction

Ours is a rapidly evolving age, dubbed by some the Fourth industrial revolution, where large data sets and complex systems abound. Numerous technological advances have resulted from our ability to deduce hidden relations amongst a forest of data. To paraphrase Arthur C. Clarke's Third Law[1], the results of a sufficiently advanced algorithm is 'indistinguishable' from magic : Netflix *knows* what movie you'd like to see next[2]. Weather predictions or large scale integrated circuit designs are modelled with greater accuracy than ever before. Alongside all of this, natural challenges have been explaining the complex system dynamics found in such self-organising systems as social media, cosmology, or in the case of this thesis, aspects of brain dynamics.

Many authors have nominated equilibrium statistical mechanics as the triumph of nineteenth century science. Apart from advancing our understanding of the behaviour of gasses and fluids known at the time, it enabled scientists to define temperature and ushered in the formalism for analysing the large-scale behaviour of microscopic constituents in a systematic way. Into the 20th Century, it paved the way for our understanding of the atom and electromagnetic radiation amongst many other developments.

More recently, there has been deeper insight into many classes of complex systems displaying sensitive dependence on initial conditions. Despite a long-held view that deterministic equations completely describe a system's internal dynamics, methods from the

[1] Arthur C. Clarke, *Profiles of the Future*, 1962
[2] This quote is from *Choice* Magazine, October 2015

analysis of chaotic and multifractal processes have advanced a more nuanced understanding of dynamics over the last 30 years or so. Since the 1980s, advances in computer simulations have accelerated progress with applications to such problems as the analysis of protein folding, or space flight.

Stochastic and nonlinear deterministic analysis methods have offered valuable insights. But methods from dynamical systems, in which it is attempted to find low dimensional descriptions of complex behaviour, are only valid or possible if higher dimensional degrees of freedom are not important in the dynamics of the system. It has also been realised that the study of chronotaxic systems[44][3] - with their innate time varying behaviour characteristic of living systems such as heart rate variability - need new approaches, and a corresponding new mathematics to accommodate these new approaches.

Consider for instance the example of turbulence where complex patterns emerge with many degrees of freedom under different conditions. Two such examples could be Bénard instabilities [86](Fig 1.1) or Taylor-Couette flow[44]. In the latter, laser light has been used to find oscillatory modes in fluid and uncover changes in dynamics with time. This is one striking example of how complex dynamics can be rendered understandable by a lower order time series.

Many complex real world biological systems are nonlinear, such as cellular processes (with their building blocks of nonlinear signalling pathways, protein or energy synthesis), from which much more complex behaviour (such as circadian rhythms, mitochondrial oscillations, or other time varying effects) emerge. This increasing complexity is accompanied by a dizzying increase in the number of degrees of freedom. In the face of such "'unpredictable' dynamics", our incomplete knowledge of the system and multiplicity of states which cannot be measured at all times, one might resort to statistical methods. However, the techniques of equilibrium statistical physics are not built for non-autonomous out of equilibrium systems[44] - precisely because of their complexity in spatial and temporal scales.

This thesis is concerned with one attempt to analyse brain electroencephalgram (EEG)

[3]this term was coined by [44],[211] to distinguish the dynamical properties of living systems, far from thermodynamic equilibrium, often having their own internal driving dynamics as well as responses to environmental interactions

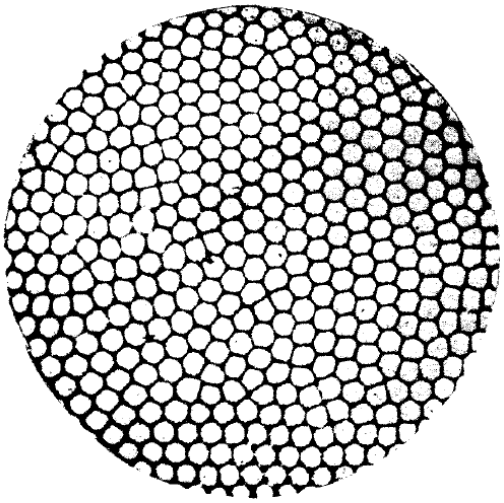

Figure 1.1: Example of self organisation in complex systems from fluid dynamics - the Bénard instability. As fluid is heated gently from below and kept at a constant temperature from above, convection currents form. The resulting fluid motion can be surprisingly well regulated forming rolls, or hexagons, and is stable i.e. after perturbation, resuming its stable homeostatic state. From [86]

signals to understand the changes associated either with disease or transitions in brain states - in this case, absence seizures. Here, the added difficulty is that the system under study cannot be simply controlled or perturbed from its natural state. In the awake, whole, living brain this is not possible without resort to invasive techniques such as microstimulation, which in many circumstances may be either ill advised or ethically not possible.

Since the development of technology enabling recording of the brain's electrical activity, or electroencephalogram (EEG) signals by Berger in 1929 [20], neural oscillations have been recognised as a prominent feature. Central questions in neuroscience are those of how brain activity is self-organised, how it relates to behaviour or consciousness, how information flow occurs, and the mechanisms by which its function is altered in disease states such as epilepsy.

A variety of cognitive processes have been shown to require the integration of brain activity across distinct spatiotemporal timescales ([216, 233, 144]) with a high degree of temporal precision (for example, in the case of neural avalanches, to within milliseconds over the course of tens of hours [18]). Singer and Gray proposed the role of synchrony

in interconnecting networks of cell assemblies in a flexible way, either binding together or segregating different features and anatomical regions[205], as an efficient method of communication between networks [199, 76].

Alterations of brain oscillation dynamics have been demonstrated in a variety of neurolgical disorders [76], psychiatric disorders [212] and disorders of cognitive function [157]; epilepsy may result in manifestations of all of these. Various and different types of synchronous oscillation between both remote and distant brain regions have been described by different authors, for example :

- synchronous variability in amplitude within and between frequency bands, coinciding with activation and deactivation of various sensory and cognitive modalities [138];
- synchronisation of phase, independent of amplitude, alongside coincident neuronal firing patterns in different regions
- synchronisation across different frequency bands [66], altered in different brain states

In 2001, Steriade and colleagues demonstrated the role of groupings between several lower and higher frequency bands in modulating the interactions between neural assemblies. While the cortex generated slower frequency oscillations, other brain rhythms were efficiently grouped together through cortico-cortical connections and the corticothalamic oscillating circuit [214]. The corticothalamic system is important in synchronising both cortical and thalamic areas[60], and in the modulation of this synchrony[150].

Sherman and Guillery have also detailed the role of thalamus in the processing of visual and other cortical sensory information [191]. In their reasoning, the lateral geniculate nucleus (LGN) is seen as a relay for subcortical sensory information from the retina whose response is modulated by descending input, from visual cortex layer 6 cells, and ascending input, from brainstem structures. The “response mode” of LGN neurons related to the attentional demands at that time, and depended on the neurons’ membrane potential, in turn carefully controlled by ascending and descending input (Section 1.2.1).

Alteration in synchronisation patterns have been linked to a number of neurological diseases, for example Alzheimer’s disease [209],[96], ADHD [108], or schizophrenia [143].

A striking example of altered synchronisation patterns is in epilepsy ([164],[166]), the most common recurrent neurological disorder affecting more than 1% of the worlds' population.

On one level this thesis will outline a description of network changes occurring in a rat models of absence epilepsy, the Genetic Absence Epilepsy Rat from Strasbourg (GAERS). On another level the theme underlying this work is a heirachical application of analysis methods which are appropriate to understanding the different factors in the dynamics associated with these seizures. It presents a mix of analysis techniques from applied physics and nonlinear dynamics to shed light on mechanisms behind synchrony, and aberrations of this, associated with seizures.

1.2 Absence epilepsy

Absence epilepsy is characterised by recurring generalised non convulsive seizures. These manifest in brief recurrent episodes of altered consciousness, often occurring in quiet, resting wakefulness with or without accompanying automatisms. In contrast with other types of focal onset seizures (such as complex partial seizures) normal consciousness returns, rather than post ictal confusion [165]. They are often treatment resistant in that anti epileptic drugs (AEDs) will fail to attain seizure freedom in up to 50% of patients either because of intolerable side effects or inadequate seizure control.

Gibbs[80] recognised the hallmark of absence epilepsy, of bilaterally synchronous high amplitude spike and wave discharges (SWD) on electroencephalogram (EEG), very shortly after the first reported studies of the human EEG. Similarly Lennox[109] described a disorder with onset in childhood or adolescence characterised by SWDs and absence events. No clear pathology was seen on examination of brain tissue, leading to the belief that this condition arose from a normally functioning brain and the classification of Idiopathic Generalised Epilpesy (IGE) [151]. This term has now been revised to Genetic Generalised Epilepsy (GGE) because of mounting evidence of genetic abnormalities giving rise to a propensity to seizures and also evidence of subtle functional abnormalities to be described below.

Generalised spike-wave discharges can also be seen in symptomatic or secondary

epilepsies such as the epileptic encephalopathy associated with Lennox-Gastaut syndrome, occurring at a lower primary frequency of 1.5 to 2 Hz, or the severe myoclonic epilepsy associated with Dravet's syndrome, or absence status epilepticus [24]. SWDs can also be associated with focal epilepsy and a diverse number of focal lesions including infarcts, neoplasms, cortical dysplasia, infections (e.g. HSV, CJD, SSPE), trauma, or hypoxic or metabolic encephalopathic disorders (e.g. hepatic or dialysis encephaopathy).

Clearly the generation of these diverse epileptic disorders above will be associated with very different pathophysiological processes even though they share the rhythmic oscillations manifesting as SWDs[24]. The most well known generalised spike-wave discharge is that seen in childhood absence epilepsy (CAE) as a 3-4 Hz rhythm consisting of large amplitude slow waves alternating with either single or double spikes [24] (Fig 1.2). These are seen to arise seemingly spontaneously and bilaterally from a normal desynchronised EEG, with an abrupt onset.

In 1950 William Lennox described two twins aged 6 with almost coincident onset of absences[109]. It is now known that monozygotic twins have a high concordance of seizures, of 80%[4], as compared with a concordance of 28% for dizygotic twins[22]. Patients will often have a combination of different seizure types, including absences, myoclonic and tonic-clonic seizures.

This led to the description of an overlap of paediatric epilepsy syndromes based on the clinical emergence and progression of syndromes with overlapping features, but different patterns of progression. Childhood Absence Epilepsy often arises in the first decade of life, whereas Juvenile Absence Epilepsy, often commences in the second decade. These are clinically separate conditions from Juvenile Myoclonic Epilepsy, characterised by early morning myoclonic jerks as was first described by Janz in the 1950s[181].

Genetics of absence epilepsy

Over the last 20 years evidence has accumulated that many absence epilepsy syndromes have a genetic basis, both from twin studies [21], more rarely from studies of families with inherited rare GABA subunit anomalies [165], and from genome wide association studies,

[4] in that if one twin has generalised epilepsy the other has an approximately 80% chance of developing the condition

which have revealed several loci[50]. However, it seems that for most patients with absence epilepsy the genetic basis is more complex, and most probably polygenetic in nature [21], [140].

Absence seizures are often controlled by sodium valproate or ethosuxamide, but it is well known that some medications such as carbamazepine and drugs with GABA activity can exacerbate absence seizures. However there is individual variability in which these drugs can actually improve seizure control in some patients[165]. Clinically, asymmetric EEG changes before generalised seizures are occasionally observed, for example during video EEG monitoring. Whilst the majority of JME patients will be free of seizures with sodium valproate[181], approximately 15% will experience treatment-resistent seizures, and other patients will experience side effects from their medication. Unfortunately current treatments are either not effective in controlling seizures or not tolerated by the patient in around 50% of cases[165], making the search for a greater understanding of this disease and new treatments a priority.

It has been known that aberrant function at a number of points in the thalamocortical system can generate SWDs for a long time, and also that an intact thalamocortical system is required for seizures to occur. There is clear evidence that absence seizures arise from the thalamocortical system, and require intact connections within this system for generalised bilateral seizures to occur [237]. Vergnes [237] studied SWD generation in what would become known as the Genetic Absence Epilepsy Rats from Strasbourg (GEARS) model, finding that SWDs arose both from cortex and the dorsal thalamus, particularly nuclei related to somatosensory areas. Vergnes and Marescaux showed that ablation of either deep layers of cortex or posterior thalamus will abolish seizures in GAERS rats [236],[165].

However there has been wide debate around what relative contributions of these regions generate these seizures, and how interactions between them lead up to SWDs. Specifically, until recently it has not been clear whether an abnormality in the cortex or the thalamus is responsible.

In the 1950s, Penfield and Jasper conducted electrophysiological studies suggesting that absence seizures originated in the thalamus [153] - the ‘centrencephalic hypothesis’. They hypothesised the existence of a subcortical rhythm generator in intralaminar thala-

mic neurons, in analogy with the reticular activating system [130] which sets its rhythm on thalamocortical relay cells. Buszaki instead proposed the 'clock' hypothesis [33], with the thalamus as the rhythm generator. Gloor [81] introduced the 'cortico-reticular theory', suggesting that the thalamus acted as a rhythm generator, and that an excitable cortex transformed sleep spindles generated from the thalamic reticular nucleus and thalamocortical relay cells into SWDs. Meeren [131] found from deep electrophysiogy recordings that seizures started locally, mainly from perioral somatosensory cortex in WAG/Rij rats.

A number of authors ([172], [207]) have found that deactivation of S1 suppressed SWDs. Polack [171] recorded from layers V and VI in the S1 region in GAERS rats, finding that pharmacological deactivation of neurons in deep layers of this region suppressed SWDs, suggesting that this may be a focus of absence seizures.

Studies of the causes of generalised epilepsy and the chain of events in its emergence (i.e., epileptogenesis) are important for a clear understanding of this disease, emergence of new treatment pathways, in addition to providing the opportunity to understand how the normal brain functions in more detail.

Functional MRI findings in absence epilepsy

Functional MRI experiments from a number of groups also support findings that thalamus and cortex show altered functional activity prior to and after seizures. Carney and Jackson [38] studied functional MRI changes in blood oxygen level dependent (BOLD) signal changes in human patients with absence seizures during SWD activity. The results of their analyses showed increased thalamic activity, whereas analysis of the time course of activity showed that the earliest detectible signs of altered activity prior to SWDs occurred in areas associated with the default mode network such as parietal and posterior cingulate cortex [38].

Voxel-based morphometry (VBM) analysis of grey matter show a relative decrease in thalamic grey matter and increase in mesial frontal cortex. In line with this result, studies utilising fibre density tractography have shown a decrease in the fibre density of tracts linking cingulate gyrus to thalamus.

Alongside these imaging studies and electrophysiology studies, there is increasing evi-

dence of subtle abnormalities in the cognitive functioning of patients with absence epilepsy from neuropsychology studies. Cohort studies have found evidence of decreased educational attainment, subtle frontal dysfunction. Findings from Camfield's study[35] of the Novia Scotia cohort, comprising of patients with JME or IGE with generalised tonic-clonic seizures, suggest that even if the epilepsy remits, these patients do not do as well educationally or vocationally. Studies of the psychosocial functioning of adults from this cohort suggest higher rates of social isolation, unemployment and psychiatric disorders [35]. These observations would seem to provide sound evidence in support of Janz's clinical observations in the 1960s.

1.2.1 The thalamocortical system

The thalamus is intimately connected with neocortex, the limbic system and deep subcortical structures, and it is involved with cortical rhythms subserving many high order brain functions including perception, wakefulness, attention / other cognitive functions such as attention and sensorimotor processing, as well as sleep [98].

The cortex is comprised of different cytoarchitectural areas found to serve different roles, and divided into layers I to VI on the basis of distinct neuronal types and connections. The thalamus is the major source of input to the cortex, and is composed of many distinct, separate nuclei. Dorsal thalamic neurons were thought to take input from subcortical neurons, and project to cortex. For example, studies of human visual pathways reveal classical somatotopic organisation from sensory relay nuclei, most notably the lateral geniculate nucleus, to layer IV of the visual cortex, and with modulating descending input from layer VI cells. It seems ([61],[98]) that other cortical areas are more pleiomorphic.

Thalamocortical cells have common membrane properties and synaptic circuitry. Afferents to each nucleus tend to be from one major functional source in the cortex, and efferents from each to one major cortical area in turn. The architecture of thalamocortical system is shown in Fig 1.3, showing a loop between pyramidal cells in cortex synapsing with thalamic nuclei cells, and TRN inhibitory connections. The thalamic reticular nu-

cleus (TRN) is on the pathway between thalamus and cortex, and receives afferents from both [202]. Efferent neurons back to the thalamus are inhibitory.

The major neurotransmitters of corticothalamic neurons in the thalamocortical network are excitatory (i.e. glutamatergic) in cortex, and inhibitory (i.e. GABAergic) in thalamus. Most notably, the TRN is populated with $GABA_A$ and thalamocortical relay neurons have longer acting $GABA_B$ synapses. Thalamocortical neurons terminate mostly in layers IV and II of cortex, synapsing with cortico-cortical neurons [98]. Corticothalamic neurons arise as pyramidal neurons in layers V and VI of the cortex and project back to the TRN and the thalamus. The TRN receives excitatory input from both thalamocortical and corticothalamic neurons, whereas all thalamic relay neurons receive inhibitory GABAergic projections from TRN. In this way, the TRN strongly regulates both thalamocortical and corticothalamic relay neurons via GABAergic connections as an "attentional gate"[48],[84], [162].

The primary and secondary somatosensory cortex are reciprocally connected with each other and also with the ventral posteromedial (VPM) and Ventral posterolateral (VPL) thalamic nuclei. The main role of the thalamus appears to be in the relay of sensory information. The VPM thalamic nuclei are the primary relay pathway for incoming sensory stimuli [40, 39], whereas dorsal ventral and lateral thalamic nuclei correspond to sensorimotor outputs[237]; posterior thalamic and VPM nuclei [51].

In rats, VPM nuclei receive sensory information from whiskers via the leminiscal tract [40] in addition to other inputs from the thalamocortical circuit (i.e. corticothalamic synapses arising from cortex as well as post synaptic inhibitory input from TRN).

The somatosensory cortex has been classified as primary (S1), consisting of the barrel cortex and peri-oral and forelimb areas more ventrally, and secondary somatosensory cortex (S2). Studies of the architecture and connections of the S2 cortex suggest that its neurons are responsive to multiple sensory stimuli and play a role in integrating somatosensory input with information from other sensory modalities to parallel the functions of association cortex in humans[30].

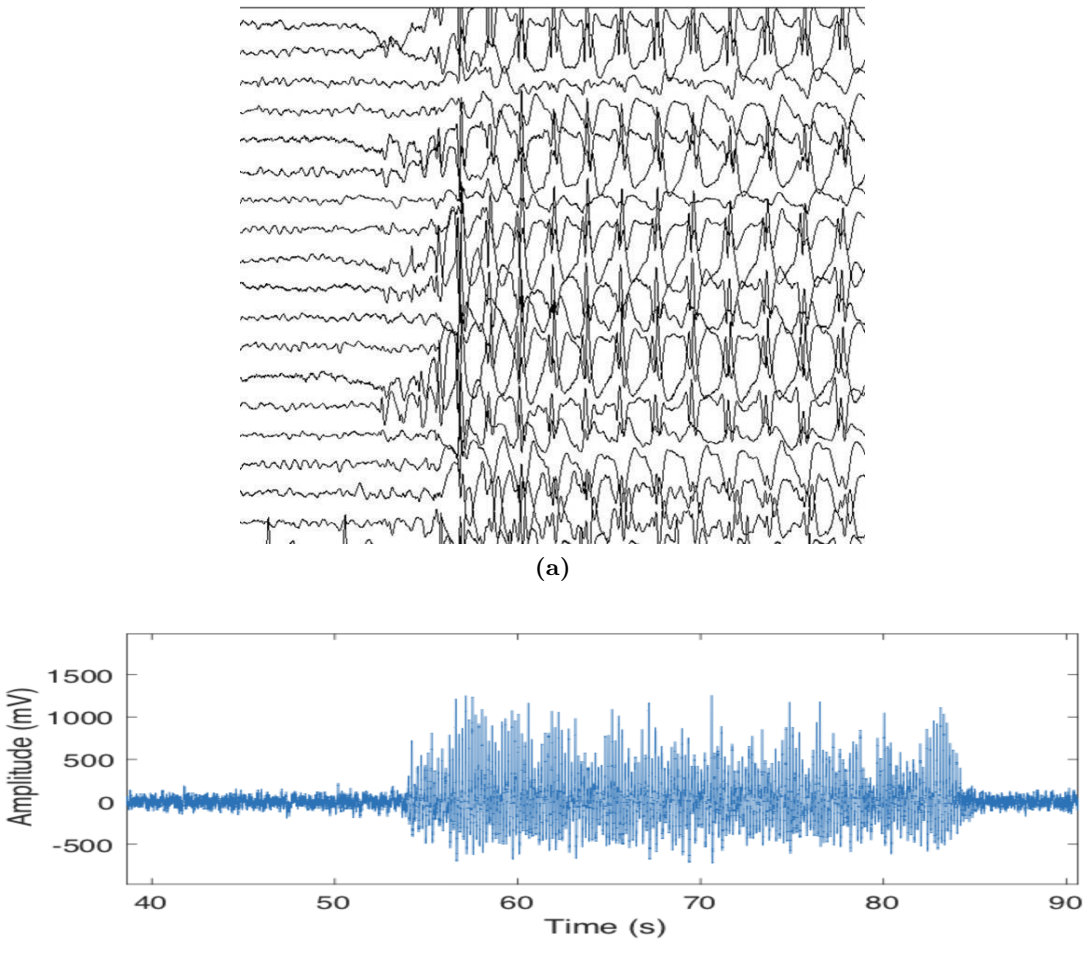

(a)

(b)

Figure 1.2: (a) Appearance of spike-wave discharges in a human EEG. (b) Appearance of SWDs in the GAERS rat

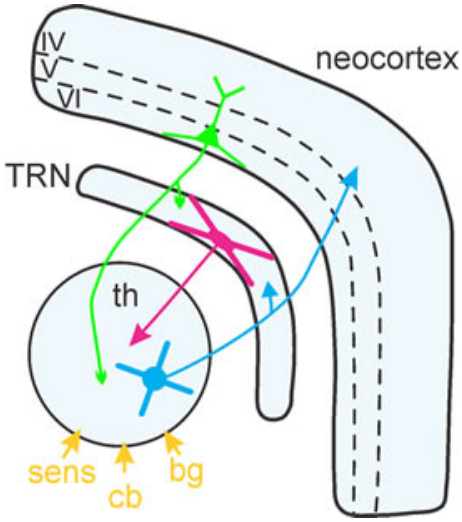

Figure 1.3: Structure of thalamocortical loop, showing efferent connections from thalamus to cortex and reciprocal corticothalamic neurons emerging from deep layers of cortex, and incoming sensory connections from other subcortical structures and periphery. From [162].

The thalamus as pacemaker

Initially thought of in simpler terms as a relay station for gating sensory information, the thalamus is now seen as having intrinsic dynamics of its own as a consequence of its neurons' electrical characteristics[98]. Physiological thalamic oscillations form part of regulating functions across sensory, motor, and limbic cortex. Alterations in thalamic cell behaviour to different inputs result in marked changes in EEG morphology such as spindles, delta, and slow (0.5 to 1Hz) waves seen during slow wave sleep, to beta and gamma activity in waking and active states including REM[5] sleep.

Faster beta and gamma activity arise from relatively depolarised membrane potentials [114], [214], generated and synchronised by corticothalamic neurons in cortical layers II to VI. These have been linked to other cortical and thalamic generators of similar oscillations [215, 214].

As modulated by corticothalamic input, thalamic neurons appear to have two different modes of oscillations [126],[98]. These are either voltage dependent tonic firing, which acts to synchronise high frequency components, or burst firing, which has an indirectly inhibitory effect via the TRN and which has the function of synchronising low frequency

[5]rapid eye movement

oscillations in the thalamocortical network.

The first of these modes occur during wakefulness or arousal and is characterised by fast, Na^+/K^+ mediated action potentials. In this state, thalamic neurons are more depolarised to -55mV, allowing the relay of sensory information to pass on to cortex where perception or information processing occurs [179]. The second mode occurs during drowsiness or sleep. Intrathalamic dopaminergic and cholinergic systems in thalamocortical neurons are capable of modulating neuronal membrane properties. When hyperpolarisation occurs to $<$ -60 mV, this results in a de-inactivation of Ca^{2+} conductance.

This hyperpolarisation is mediated through GABAergic TRN inhibitory neurons providing rhythmic, synchronous inhibitory postsynaptic action potentials to thalamic neurons. The TRN is GABAergic, with collateral input from thalamocortical and corticothalamic relay neurons as these pass bidirectionally through. Most sensory cortical areas are connected with dorsal thalamic nuclei. Contreras and Steriade showed this is reinforced by cortical glutaminergic projections resulting in oscillatory bursts occurring as sleep spindles as slow-wave sleep, in which relay thalamic and TRN neurons are hyperpolarised, and which rarely occur during consciousness [215]. In this state, sensory information arriving at the thalamus is not relayed to the cortex, so is not perceived. This produces a state of reduced responsiveness during sleep which can be overridden by strong stimuli causing a change to the tonic firing patterns described above.

During the wake-related medium voltage synchronised oscillations TRN cells have an observed firing pattern of packets of bursts with a frequency of 5-9Hz, arising due to synchronisation with cortical pyramidal cells and inhibitory interneurons. During sleep or drowsiness related spindle oscillations, TRN cells fire in a short 'rounds' of action potentials in a 11 - 16 Hz pattern. These different rhythms arise from distinct cellular mechanisms which are clearly distinguishable [166].

Von Stein[239] studied thalamocortical oscillations, finding that information is transferred through multiple pathways : higher frequencies (beta and gamma) allow synchronisation across local networks, whilst theta and alpha frequencies facilitate synchronisation over longer distances such as thalamus and cortex, and are linked to perception or tracking changes in evironmental stimuli.

Sarnthein and colleagues[195] studied the coherence between microelectrode recordings from thalamus and cortical scalp EEG in patients with chronic pain, epilepsy or treatment refractory movement disorders. They found increased theta thalamocortical coherence and also phase coupling between theta and beta frequency bands, a pattern found in thalamocortical dysrhythmia [180]. Buszaki [76] studied how cross frequency modulation may be linked to cognitive control. He found that cognitive control may be regulated through modulation of oscillations at specific frequencies, and coupling through different frequency bands.

Thalamic oscillation modes are relevant to the pathology of absence-related seizures [167],[161] in providing reinforcement to the somatosensory rhythms generated from somatosensory cortex. The next question is that of the relationship between cortical and thalamic networks at the time of seizures, and which cortical structures are involved.

Evidence of cortical excitability from electrophysiology changes in Absence Epilepsy

Evidence of cortical excitability

Seizures clearly have to start "*somewhere*". The question of whether an excitable cortex is involved in this process has been studied in a range of animal models. In the feline generalised penicillin model Avoli[11] found rhythmic firing in cortex before thalamus, which occurred 2 - 3 cycles later. In the so-called stargazing mice model (Table 1.1), layer V pyramidal neurons in cortex were found to have increased excitability [56]. This was subsequently linked to increased levels of expression of a transmembrane AMPA receptor regulating protein, now called stargazin. Interestingly this protein is also found in the somatosensory cortex of GAERS rats [173].

GAERS rats have been found to have a higher firing rate of layer V and VI neurons in somatosensory cortex both before and during seizures, and also increased bursting activity when compared to non epileptic control rats of the same strain [171]. This may possibly be augmented by increased NMDA receptor function, which has been reported in both GAERS and WAG/Rij rats [1], in that AMPA and NMDA receptor activity changes may

increase the probability of transition from non rhythmic to rhythmic generation of action potentials.

Pinault [161] investigated the changes in behaviour of thalamocortical cells, finding that the corticothalamic layer VI neurons phase lead functionally connected TRN and thalamocortical cells by an average of 7 msec. During SWDs, TRN and thalamocortical neurons tended to fire in synchronous, phase-locked manner, milliseconds after associated cortical action potentials in his study. From these results he hypothesised that the mechanism for this is that the corticothalamic cells trigger simultaneous excitatory post synaptic potentials (EPSP's) to both relay and TRN cells, both of which would combine to trigger low-threshold Ca^{2+} potentials, causing high frequency bursts of action potentials.

This leads to the possibility that layer VI cortical neurons lead the generalised synchronous spread to other cortical areas, via cortico-cortical projections, and thalamus during SWDs.

Additionally, a number of intracellular mechanisms might also explain why an excitable cortex may predispose to SWDs involving the intact thalamocortical circuit[1], [24].

Significant amongst these are changes to the hyperpolarisation-activated cation current, I_h. This current has multiple functions in different brain regions[219], including regulation of the firing behaviour and pacemaker function of thalamic neurons (as described in Section 1.2.1). For example, in entorhinal cortex, this current is important in stabilising the sub-threshold activity of neurons, acting as a 'buffer'. Because channel density on pyramidal cell dendrites is not uniform it can serve to attenuate summed dendritic synaptic events[219]. A reduction in this current was associated with slower kinetics for both activation and inactivation of one of the four proteins, the HCN1 protein, known to be associated with the 'fast gating' subunit of the channels controlling this current, and was associated with seizures.

An upregulation of Na channels as well as reduced expression of HCN1 channels have been found in genetic rat models of epilepsy, and associated with an increase in cortical excitability [24, 25]. Blumenfeld showed that treatment with ethosuxamide altered

the expression of these ion channels in rats with absence seizures, and also reduced the imbalance in ion channel expression [25].

There is also evidence of ecreased GABAergic inhibition of thalamocortical neurons by TRN, and reduced efficiency of GABAergic inhibition in cortex [**?**], [24], [165].

It has been observed that abnormalities in the expression of low-threshold calcium channels are associated with higher rates of absence epilepsy. For example, mutations in the low threshold calcium channel $CaV_{3.2}$ were found in 14 of 118 Han Chinese patients with absence epilepsy, but no controls, in one study[165]. O'Brien[165] and others have also established that abnormalities in T-type calcium channels are implicated in changes in reciprocal thalamocortical interactions and increased burst firing found to underlie absence seizures.

Changes in thalamic and TRN neurons during seizures

Thalamic relay neurons have a background 5 - 9 Hz oscillation as described in Section 1.2.1. This, with their background hyperpolarisation during wakefulness underlies a propensity for waves of rhythmic depolarisation when volleys of excitatory post synaptic potentials arrive, leading to low threshold Ca^{2+} spikes, which in turn causes bursts of APs to occur. This hyperpolarisation is augmented by increased chloride conductance, which occurs because of TRN GABAergic induced IPSPs[164, 163, 161].

Tsakiridou has shown that during each SWD cycle, TRN cells experience a prolonged hyperpolarisation, likely potentiating a de-inactivation of T-type calcium channels, which result in the generation of a new SWD cycle. Both TRN and thalamic relay neurons undergo a recurrent depolarising wave triggering low threhold Ca^{2+} potentials and a new cycle results as the summation of depolarising potentials.

Pinault showed that layer VI corticothalamic neurons phase lead these changes in TRN and thalamic relay cells[161]. He also reported that both TRN and thalamic relay neurons were observed to discharge synchronously 12 msec before the spike of the SWD complex, suggesting the likelihood of a common cortical input in to the thalamocortical loop [164].

Taken together, the results of these cellular physiology and EEG studies suggest that

SWDs are the result of rhythmic oscillations, indicating a process of resonance between cortex and thalamus [161]. He suggested that the cellular activity above, coupled with some cortical neurons generating a somatosensory rhythm possibly trigger these normal oscillations to become pathological SWDs.

The observations quoted above, from both human MRI imaging studies and animal model data lead to the conclusion that changes are not generalised across the brain prior to SWDs, and specific neural networks involving both cortical and subcortical structures are involved which centre around the thalamocortical network and related cortical structures.

1.2.2 The GAERS model

The results from electrophysiology studies above are almost exclusively involve experiments in animal models of epilepsy. Invasive electrophysiological studies of the origins and dynamics behind these seizures in humans are not usually possible in humans for ethical reasons, since most idiopathic generalised epilepsies are not usually amenable to surgical treatment. For this reason we must turn to appropriate animal models instead.

Similarities between the GAERS model and human absence epilepsy

As pointed out by O'Brien and Pinault [165], one can divide animal models of absence epilepsy into models of seizures and models of epilepsy. In the first, animals with an otherwise non-epileptic brain have seizures induced by either chemotoxic or electrical stimulation. In true models of epilepsy animals have recurrent seizures and depending on the cause of their epilepsy, the process of epileptogenesis can also be studied.

There have been a number of models put forward for the study of absence epilepsy (Table 1.1). These could be classed as arising from either genetic mutations or through exposure to neurotoxic agents during development[165]. Other models, which have a monogenetic basis, such as the stargazer, tottering, and lethargic mice models are less relevant because the other neurological deficits producing their phenotype, such as ataxia, are less applicable to human absence epilepsy. Apart from this, in clinical practice monogenetic

modes of inheritance are rarer (Section 1.2).

Amongst the whole animal models of absence epilepsy, two main models appear in the literature, both of which originated from Wistar rat colonies, the GAERS and WAG/Rij models[54].

In contrast with many models of 'seizures' such as in vitro slice preparations or induced seizure models (e.g. tetanus toxin, penicillin induced post status epilepticus models)[165], the Genetic Absence Epilepsy Rats from Strasbourg (GAERS) model has many advantages. Chiefly among these, this model resembles human absence epilepsy from the behavioural, pharmacological and electrophysiological perspectives, and can also be studied in the whole, awake, behaving animal.

Seizures in GAERS resemble that of human absence epilepsy behaviourally, pharmacologically and physiologically. Seizures occur around once a minute in fully developed rats. These episodes are not accompanied by any behavioural manifestation. Physiologically, these seizures involve enhanced synchrony between the cortex and thalamus, and appear on the EEG as large amplitude spike-and-wave discharges (SWDs). They usually last for less than 15 seconds.

The GAERS rat model also shows many similarities with human absence epilepsy. Most importantly, in the GAERs rat bilaterally synchronous spike and wave discharges - the hallmarks of absence epilepsy - seem to arise from a normal, desynchronised, background EEG, and also cease abruptly, without postictal slowing or depression (compared with other partial or generalised epilepsies involving convulsive seizures). As in humans seizures are most common in quiet resting wakefulness, often following or preceding slow wave sleep, and are less common in states of high arousal or other stages of sleep. Drugs that can be effective in suppressing human absence seizures such as ethosuxamide or sodium valproate are also effective in suppressing SWDs in GAERS rats, and medications known to aggravate absence seizures in humans such as carbamazepine or oxcarbazepine also have this effect on the SWDs in this rat model. Drugs that are known to aggravate seizures (eg. carbamazepine and oxcabazepine) increase the time rats spent in seizures by more than 200%. Blumenfeld[25] showed that early treatment with AEDs can impede later SWD development, and also treat the analogues of common neuropsychiatric syndromes

Table 1.1: Models of Absence Epilepsy, with a comparison of seizure characteristics to those seen in children with absence seizures. From [240, 169]

Model	Species	Seizure characteristics	SWD frequency (Hz)
Chemically induced epilepsy models			
Penicillin	cat	seizures last 6 - 8 hr	3
PTZ	rat	bilat, synchronous, from 3 weeks of age	7 - 9
THIP	rat	bilateral, synchronous SWD lasting 1 - 7 s	4 - 6
Genetic mouse models - single gene mutations			
Model	Chromosome (gene)	phenotype	SWD frequency
Lethargic	Chr 2 (CC, β_4 subunit)	Lethargy, ataxia, focal motor sz's	5 - 7
Stargazer	Chr 15 (CC, γ_2 subunit)	ataxia, neck dystonia	5 - 7
Tottering	Chr 8 (CC, α_{1A} subunit)	ataxia, motor seizures	5 - 7
Polygenetic rat models			
Model	Seizure onset	remission	SWD frequency
GAERS	30 - 40 days. All animals by 13 weeks	no	7 - 12
WAG/Rij	all animals by 4 months	no	7 - 11

seen in patients with focal epilepsies such as TLE such as anxiety and depression.

Earlier findings that SWDs arise from sleep spindles mainly arose from the studies which used the feline penicillin model of generalised epilepsy, which is less relevant to the human situation. Absence related SWDs are documented to be more common in wakefulness than sleep. Niedermeyer [139] found that almost 80% of patients only had absences recorded during wakefulness in his series of 50 patients, and also found that smaller 'sub ictal' bursts of synchronous generalised SWDs can also occur during light sleep as well as quiet wakefullness or drowsiness. Sleep spindles are a feature of deeper sleep (i.e. stage II or III)[214] which is a time when absence events rarely occur[165].

Pinault found that SWDs can arise from a natural, medium voltage (< 0.4 mV) sensorimotor rhythm either in quiet wakefulness or during neuroleptanalgesia. This rhythm is found in a desynchronised EEG in non epileptic rats and so in itself is not sufficient for SWDs. Its function is believed to be a normal, wake related sensorimotor rhythm and was found in frontal and parietal cortices and also related thalamic nuclei[166].

Intracellular correlates of absence seizures are less suggestive of associations with sleep spindles when looking at data from GAERS rats. For example, thalamic relay and reticular neuronal sensorimotor oscillations are associated with a more depolarised membrane potential (more than -65 mV) and a lower membrane input resistance [167, 161]. SM oscillations can also coexist with delta oscillations, a condition in which spindles are rare. Pinault [166] found higher beta and gamma power from a Fourier analysis prior to sensorimotor oscillations as compared with sleep spindles. Pinault found a condition of more tonic irregular firing in layer VI corticthalamic neurons as precursor to both occurrence of SM oscillations and also SWDs. This observation fits with data from experiments suggesting that irregular tonic firing from deeper layer corticothalamic neurons is important in the development of SWDs (Section 1.2.1), whereas spindles are much briefer, not lasting > 2 seconds, and most usually arise from a synchronised EEG.

While the GAERS model may share a common phenotype with the WAG/Rij model it is also interesting that there might also be subtle differences between these very close 'cousin' models too[54]. For example there are subtle differences in the EEG of WAG/Rij rats compared with GAERS, such as higher 8 - 14 Hz EEG power before seizures. The

frequency of their SWDs (5 Hz) differs from that seen in human absence seizures (3 Hz). Differences in these and other animal models are summarised in Table 1.1.

1.3 EEG studies of Absence Epilepsy

As part of the long debate as to whether there is a focal origin of 'generalised' seizures, the concept of a 'focus' suggests that there is an identifiable area capable of generating seizure activity, and that this usually 'drives' other areas of the brain to participate in seizure activity. Lutjohann and van Luitjelaar[116] describe three characteristics of an epileptic focus : (1) that it drives other participating structures; (2) that it has local rhythm generating properties; and (3) it shows features of "locally enhanced excitability", i.e., resonance.

1.3.1 Cortical or Thalamic Focus, or Both?

Meeren [131] used nonlinear association (regression) analysis (Sec 1.3.2) to assess driver-response relationships between intra- and inter-hemispheric cortex and VB /VPM thalamus during the progression to SWDs. He found that during the first 500 msec of seizures the cortex was leading thalamus, with a 'focus' region leading other areas of cortex at the most lateral sites recorded, located between 6 and 8 mm laterally from bregma, and from +2 to -3 mm anteroposterior to bregma. Synchronous activity quickly spread to other areas of cortex. Interestingly, they found that when an electrode was mistakenly placed in the perirhinal cortex, just ventral to the rhinal sulcus (coordinates : anteroposterior (AP) -2 mm, mediolateral (ML) 4.8 mm) this lagged behind somatosensory cortex.

They concluded from their results that the focus of absence seizures is in ventrolateral regions of S1 cortex, in the perioral or S1Ul region. The homunculus of this region most clearly corresponded to peripheral stimulation of the nose; the vibrissae in 5 of 8 rats studied, and contralateral upper lip (Ul) in 7 of 8 rats.

Sitnikova and van Luitjelaar studied changes in coherence the last second prior to, and the first second after, the first SWD[59]. The largest increase in coherence was

found between S1 forelimb (S1Fl) and other areas in the low-gamma range of 40 - 60 Hz, whereas low-frequency coherence increases were found in the sub 6 Hz range in S1Fl and S1(vibrissae) somatosensory cortex. Coherence increases between hemispheres did not follow any specific pattern, and bilateral ipsilateral hemispheric coherence changes did not tend to decrease with distance. Coherence increases appeared symmetrical and to arise from functionally similar networks in this study. Network synchronisation was mainly seen in the vicinity of the 8 - 11 Hz frequency band and its first harmonic.

The presence of the somatosensory rhythmic oscillations first described by Pinault and seen prior to seizures may either represent precursor activity to a seizure [249], or may be an epiphenomenon reflecting an underlying shift in system dynamics as part of the transition into a seizure state (as discussed, for example, in [94],[52],[89]). To investigate this possibility, Wagner and colleagues [241] used optogenetic stimulation to stimulate neocortical neurons and further investigate seizure initiation. They found that rhythmic activation of excitatory cortical neurons could trigger after discharges, and seizures, in GAERS rats. They also found that the probability of inducing a seizure was influenced by brain state, which correlated with the level of neuronal excitation (as measured by LFP power, and response amplitudes to optogenetic stimulation). Very interestingly, the dynamics of seizure onset were the same whether these seizures were optogenetically induced or spontaneous, suggesting that the same seizure neronal networks were involved.

The resonant frequency of optical stimulation in this study was 10 Hz [241]. Historically, this is in agreement with findings by Steriade [119] that single or repeated 10 Hz electrical stimulation of thalamic neurons in awake monkeys, or either cortical or thalamic stimulation in cats under light barbituate anaesthesia [120] would result in seizures.

In both GAERS and WAG/Rij rats, this seems to arise from developmental changes in excitability. For example, Mares and Tolmacheva found that cortical stimulation of immature WAG/Rij rats induced after discharges, but without any specific differences between that genetic absence epilepsy model and other rats without a predisposition to absence seizures.

Neckelmann established that spread of synchrony to the rest of cortex was most likely along corticocortical, rather than corticothalamic, connections because this could be in-

terrupted by transection of deep layers of cortex in cats.

The question of whether there is indeed evidence of increased cortical excitability has been considered by Sitnikova and van Luitjelaar [206]. They analysed the power spectrum 1 second before the first cortical thalamic spike, finding increased delta (1 - 4 Hz) and theta (defined, in this study, as 4.5 - 8 Hz) power in somatosensory cortex before seizures. In their analysis, the theta component was not composed of a single rhythm, as might be supposed if this corresponded to the 5 - 9 Hz physiological rhythm found by Pinault and colleagues in single cell and network recordings summarised above[161, 167, 166]. Sitnikova and colleagues also found an increase in thalamocortical coherence, between VPM or TRN thalamus and intracortical coherence betweeen frontal and occipital cortices, in the 9.5 - 14 Hz band, but they concluded that no features of EEG coherence could be considered unique for a pre-seziure state.

Luttjohann [1] performed cortical stimulation experiments to either S1 or MC to directly assess cortical excitability using a double pulse of 0.4 msec width, 0.4 seconds apart in wAG/Rij rats. They measured evoked potentials (EEPs) in three vigilance states i.e. alert wakefulness, drowsiness and non REM sleep with five pulse intensities (20,40, 60, 80, 100 μA) in each of three states of vigilance (), leading to 15 different stimulus 'conditions' . Responses to approximately 30 stimulations per stimulus condition were averaged to form each EEP, for an average of 15 EEPs per rat.

Given the higher frequency of seizures in the drowsy transitions to or from sleep they expected a higher EEP early (N1) amplitude in this vigilance condition, which they found. They found this was higher for S1 than MC and that the more delayed N3 component, perhaps a consequence of 'subcortical' spread from other neighbouring regions by this time, independent of the animal's vigilance state. In their study after discharges had the same EEP morphology as SWDs and occurred three times more in the drowsy state at a frequency of 8 Hz and its lower harmonics. These did not differ by stimulation site, so the authors suggested these could be the result of sub cortical interactions.

In potential agreement with this observation, other authors have noted increased coherence between MC and S1 during SWDs[59].

1.3.2 EEG network analysis

Luttjohann and colleagues have published a number of papers analysing the thalamocortical system in the WAG/Rij rat model of absence epilepsy.

van Luitjelaar et al [3] used pairwise phase consistency (PPC) analysis to explore the changes between PO, VPM thalamus, the TRN, and layers IV, V, and VI of cortex (the latter with histological confirmation of the site of recording). They found a reduction in PPC values up to 1.2sec prior to seizures, rostral TRN and PO and VPM thalamus, and also layer V or cortex. They interpreted this as evidence of decoupling between RTN and cortex before seizures, suggesting that a decrease in inhibitory TRN control on an excitable cortex was likely to increase the likelihood of seizures. Given that PO has strong connections with layer V of cortex, they suggested that a decoupling of caudal TRN with cortex would be a significant step towards preparing the cortex for a pro-epileptic state.

To follow this study of cortical network changes in more detail, Luttjohann and colleagues used frequency resolved Granger Causality to investigate network activity changes in areas of cortex and thalamus in 16 WAG/Rij rats[4]. They implanted electrodes into layers 4 to 6 of cortex, rostral and caudal thalamic reticular nucleus, and three thalamic nuclei (VPM, anterior, and posterior thalamic nuclei). They found that most thalamic nuclei showed increases in their Granger Causality measure during seizures, but of the cortical areas, most corticothalamic showed increased drive from cortex to thalamus, in the first 500msec of a seizure. Higher coupling was seen between cortex and PO thalamus, lasting up to 1.5sec after seizure termination, and higher directional coupling was seen between caudal and rostral TRN areas in the second prior to seizure termination.

On the basis of these findings they hypothesised that the rostral TRN may be a resonator for relevant deep layers of cortex, and that caudal TRN inhibition of this maybe relevant in seizure termination. Their findings add further weight to the hypothesis that cortex leads thalamus during seizure onset, and also that seizure termination is a gradual process involving changes in inhibition in thalamus and the TRN.

In summary, the majority of evidence for increased cortical excitability has come from either :

1. examining driver-response relationships across cortex, as in Meeren's study [131];
2. experiments of electrical stimulation[1]; or
3. examination of the intracellular correlates of increased excitability in deep layers of cortex, as in the works of Pinault [167, 161, 166].

On the other hand, to our knowledge, only one other study has examined the question of excitability in alternative areas of cortex [249]. Despite a number of previous studies of network EEG behaviour in relation to absence seizures, studies of the network mechanisms of increased resonance apart from altered functional connectivity have, in the words of Luttjohan and colleagues[115], been surprisingly rare.

Studies of synchrony in epilepsy

The study of synchrony has enjoyed prominent attention in many areas of neuroscience and physics in recent years, reflecting an increasing awareness of the implications of a rich variety of neural oscillations (Section 1.1) in cognitive and sensory processing, and potential complexity of their interactions [97].

The literature abounds with examples of the challenges of disentangling the complexity of interactions between brain regions, leading Jiruska [97] to observe that from a rigorous statistical perspective, it can be hard to conclude that regions are *not* synchronised.

To illustrate this point consider for example the system discussed by Sugihara [78] and described by the equations

$$\begin{aligned} x(t+1) &= x(t)[\alpha - \alpha x(t) - 0.02y(t)] \\ y(t+1) &= y(t)[\beta - \beta y(t) - 0.1x(t)]. \end{aligned} \tag{1.1}$$

These are plotted in Fig. 1.4 for the example of $\alpha = 3.8$ and $\beta = 3.5$. The equations indicate that each variable depends on the last values of the other, and Figure 1.4 shows that the correlation between the two constantly changes between positive and negative correlations, even though there is clearly a relationship between these variables. In establishing the causative relation that exists between these variables, general statistical

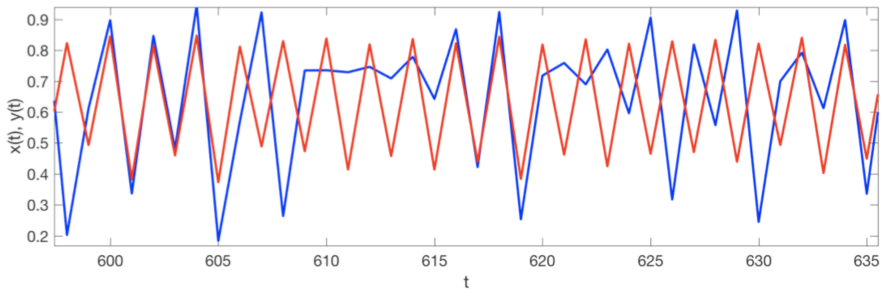

Figure 1.4: Example of complex correlation between two systems $x(t)$ and $y(t)$, given by Eq. 1.1. 2000 time points of this system were generated for $\alpha = 3.8$ and $\beta = 3.5$. Contemporaneous behaviour between the time series can be seen to move between positive and negative, and zero amplitude correlation, even though there is clearly some relation between them. Pearson's correlation is $\rho = 0.0054$, at a significance level of $p = 0.864$. From [78]

approaches such as the Pearson's correlation coefficient fail, because the two variables are not separable.

Fig 1.5 shows three types of coherence. In (a), both top and bottom signals align in peaks or troughs, producing phase coherence. In (b), the envelopes of both top and bottom signals align in their peaks and troughs producing a pattern of signals which are correlated in amplitude. In (c), cross-frequency coherence is shown, where the constituent higher-frequency signal envelopes are modulated by the lower frequency signal. In the many studies of synchrony in neuroscience the main ways of measuring synchrony are techniques based on linear cross correlation, coherence (either using wavelets or the Hilbert transform), techniques demonstrating phase locking such as that discussed in section 5.2.4, or mutual information, which are summarised in [154]. Given the variety of more than 42 methods described to date[14], care is needed in interpreting different studies using different techniques, or across different types of epilepsy.

The many studies of the direction and strength of coupling between brain regions prompt reflection on how best to measure correlated brain activity across time, and the statistical question of inferring both the existence of synchrony and then directed influence. This has been considered extensively in studies of the physical properties of the EEG in epilepsy, and also in the literature studying the predictability of epileptic seizures.

Breakspear [29] investigated the phenomenon of desynchronisation in human EEG

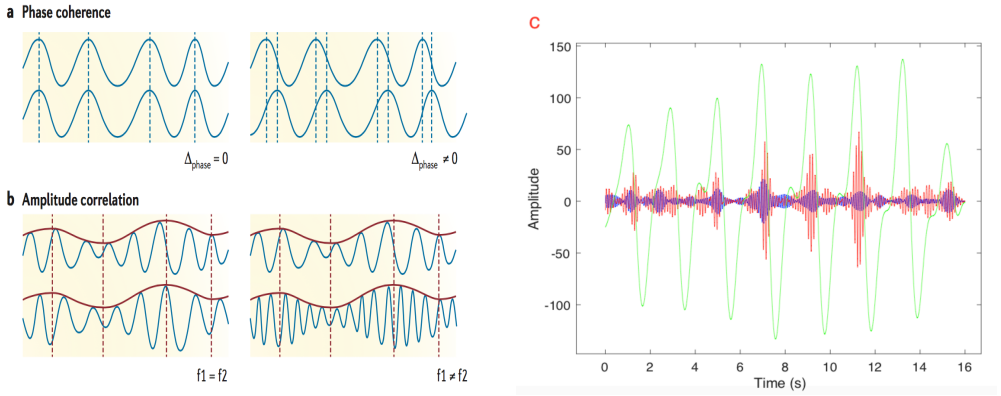

Figure 1.5: Illustration of (a) phase and (b) amplitude coherence. From ref. [203]. (c): cross frequency coupling. In this example the waveform in red oscillates at 80 Hz. It is modulated by a base waveform of $\sim$ 2 Hz (in green), and the 80 Hz waveform in turn modulates the blue 120 Hz signal.

recordings from the viewpoint of coupled networks of local nonlinear systems. He studied the EEG in 40 people without symptoms of psychiatric or neurological illness using a measure of bivariate phase entropy to investigate the balance between episodes of chaotic phase synchrony and bursts of desynchronisation. He observed that setting local dynamics into a chaotic regime permitted a greater variety of signal behaviour.

He suggested that if present, this phenomenon may provide a means of tuning to either local (nonlinear) parameters or global, modulatory, parameters such as the brain would require when flexibly binding to environmental stimuli. He suggested that this allowed the flexible binding of relevant networks and allowing brain networks to minimise entropy and maximise information transfer. He further noted that the seemingly idiosyncratic periodic attractors in the normal EEG could be dynamically similar to absence episodes in the EEG. By analogy with the modulation of cortico-cortical connections by subcortical circuits (such as thalamus), this may explain how the interruption of this process may result in disruption to core brain processes such as producing meaningful behaviour and processing information.

He used surrogate data to test a null hypothesis that dynamic variation in EEG alpha activity could be the result of random fluctuations in linearly correlated noise. (He noted that the assumption of linearly correlated noise could be confounded by the presence of

nonstationarity as well as nonlinearity, and the co-mingled effects of this could be hard to distinguish.) He found that this null hypothesis could be rejected in between 2 to 5 % of EEG epochs studied. The coherence between channels was different for these epochs of nonlinear interdependence when compared with those of other EEG epochs studied.

Studies of nonlinear systems have revealed that these can synchronise in complex ways. As one example, Rosenblum[187] showed the existence of phase coupling between chaotic oscillators, and that analysis of phase synchronisation was a better determinant of coupling than amplitude coupling in this instance. However the theoretical system studied had a strongly defined dominant frequency and phase [137] and so care will be needed in neural systems in determining the frequency range of interest, and whether broadband or more narrow band frequency ranges are used when assessing phase synchronisation.

Phase coherence

Correlations in brain activity can be studied in a number of ways. Given the oscillating quality of EEG it is not surprising that frequency based measures of correlation such as amplitude and phase coherence are very popular. Visual inspection of the EEG at the time of seizure onset may tempt us to infer the presence of widespread synchrony, as found by Penfield and Jackson in 1954.

The results of studies of synchrony at seizure onset are mixed. Many studies have actually found a decrease in synchronisation leading up to seizures, though others report increases at this time [231]. Many studies involve a difference in the type of epilepsy and frequencies of interest, or technique used to study this phenomenon.

Studies of neural synchronisation have traditionally made use of time-based measures of correlation, or frequency-based measures such as coherence. Chavez and colleagues studied synchrony during neocortical seizures using either phase coherence (as a measure of phase synchrony) or measures of amplitude correlation such as the nonlinear association index (Sections 1.3.2 and 4.1.3) and found concordant results [42]. They found decreases in phase synchrony in the focal area in the minutes prior to seizures. On the other hand, one would suspect that each measure will reflect different phenomena. Tass[224] found

that amplitude coherence is not necessarily equivalent to phase coherence.

Methods of calculating the degree of phase coherence between two time-varying signals are first based on extracting phase information from them. There are three ways to extract this phase information : the Fourier transform, a wavelet transform, or the Hilbert transform. Empirical Mode Decomposition is another method of breaking down a nonstationary signal into successsive oscillating components which are not from uniform basis functions [42].

The Fourier transform allows for fine frequency resolution, but being based on a superposition of periodic sinusoidal signals as basis functions, it requires relative long windows of data in time, and any time-varying properties of the signal within those windows of time are lost. On the other hand, wavelet based methods offer better temporal resolution by convolution of the signal with a wavelet of finite width at different scales. This results in a 'tessellation' of the time-frequency domain inhabited by the data with either finer resolution in time at the expense of frequency information, or vice versa.

The Hilbert transform takes a time varying signal and decomposes it into amplitude and phase components without the need for breaking the data into windows. It then allows the concept of 'instantaneous phase'. Breakspear and Terry observe that it allows the characterisation of instantaneous phase of broadband nonlinear oscillations because, in their words, "the highly structured ordering of the phases of the signal across different frequencies imparts an unambiguous emergent phase" to the signal. Breakspear and Terry also point out that for noisy signals the noise will impart a random phase structure across different frequencies, and will require band-pass filtering. In this sense the concept of instantaneous phase will have more meaning within the context of a narrow band set of frequencies. A number of questions arise regarding the interpretation of instantaneous phase as a concept and are handled differently by a number of authors. Chavez [42] points out that the physical meaning of wide band instantaneous phase is less clear than that of a narrow band signal. This issue is further explored by Boashash[27].

A common technique is to start by calculating the instantaneous phase difference between two time series F_i and F_j using Hilbert transform wavelet coefficients. In the notation of Kitzbichler et al[101], the Hilbert wavelet transform in the frequency band

defined by the kth wavelet scale is $\mathcal{W}_k(F)$, and the instantaneous phase difference $C_{ij}(t)$ over that frequency interval is

$$C_{ij}^k(t) = \frac{\langle \mathcal{W}_k(F_i)^\dagger \mathcal{W}_k(F_j)\rangle}{|\mathcal{W}_k(F_i)^\dagger||\mathcal{W}_k(F_j)|}. \tag{1.2}$$

This is based on the "analytic signal approach" of Gabor (1946), also summarised in Hurtado [88] and Mormann [136]. The starting point of this method is to use a Hilbert transform to extract the instantaneous phase $x(t)$ from the time series F_i. The expression

$$H(x) = \frac{1}{\pi}\text{p.v.}\int_{-\infty}^{\infty}\frac{x(\tau)}{t-\tau}d\tau, \tag{1.3}$$

where p.v. is the Cauchy principal value of the integral, returns the instantaneous phase $H(x)$ of the time series, with the same power spectrum of the original data, phase shifted by $-\frac{\pi}{2}$. Following Hurtado [88] and Mormann [136] the Hilbert transform is taken in practice by taking the discrete Fourier transform of the signal, setting negative frequencies to zero, then taking the inverse Fourier transform of the result.

One then obtains a 'phase series' by taking the argument of complex analytic signal $s(t)$ projected onto the unit circle: If $s(t) = x(t) + i\vec{x}(t)$ where x(t) is the real part of the filtered signal and $\vec{x}(t)$ is the imaginary (Hilbert transformed) component, then

$$\phi(t) = \arg(s(t)) = \arctan\frac{\vec{s}(t)}{s(t)}. \tag{1.4}$$

Mormann [136] makes the point that for noisy data like ECoG signals or chaotic time series, where phase discontinuities occur, an instantaneous "relative frequency" $\omega_{m,n} \equiv n\langle\omega_n\rangle - m\langle\omega_m\rangle$ is inadequate because it is strongly affected by noise. In this thesis, his definition of "phase entrainment" is used, as in $|\varphi_{n,m}| = |n\phi_n(t) - m\phi_m(t)| <$ constant. This can be found through the trigonometric addition theorem, for example, for n = m = 1,

$$\varphi_{1,1}(t) = \phi_i(t) - \phi_j(t) = \arctan[\frac{\vec{s}_i(t)s_j(t) - s_i(t)\vec{s}_j(t)}{s_i(t)s_j(t) + \vec{s}_i(t)\vec{s}_j(t)}]. \tag{1.5}$$

In this thesis, unless otherwise specified, it is supposed that n = m = 1 as what ratios of synchronisation may be present in the data are not known *a priori*. This renders the

relative phase to be naturally bounded to [0,2π].

In applying these concepts to EEG analysis, Mormann and colleagues [135],[67] used a moving-window technique combining measures of cross correlation and mean phase coherence to detect a decrease in synchronisation between EEG recording sites prior to seizures. Using intracranial EEG data spanning 117 hours of recording from 18 patients with medically refractory focal epilepsy being considered for epilepsy surgery, they found this measure predicted changes leading to 26 out of a total 32 seizures recorded. Of these seizures, three synchrony changes were not seen in the 'physiological' or normal, inter ictal EEG [135].

Many authors have concluded that mean phase coherence is well suited to EEG analysis, but studies of MPC in epilepsy have yielded conflicting results regarding what changes precede seizures. Perhaps this is partly explained by the many different types of epilepsy studied.

Dominguez and his co-workers [58] studied the characteristics of local versus distant synchrony present in the MEG studies of four patients with a number of different types of epilepsy, and seizures, compared with six healthy control subjects. They used phase coherence analysis between 3 - 55 Hz with narrow bands($\pm$2 Hz) of interest at a time, and the Hilbert transform, in sliding windows of 2.5 seconds. They did not find a consistent pattern of synchrony dynamics prior to seizures, but did find a broad pattern of increased local synchrony.

Netoff and Schiff [137] studied the comparative sensitivity of 'traditional' cross correlation, mutual infromation, or mean phase coherence to detect weak synchronisation in hippocampal CA1 cortical slices. By increasing the potassium concentration from a physiologically realistic 3.5 mmol to 5.5 mmol they could increase the synchrony observed between CA1 pyramidal cells from a baseline of 1 in 18 cell pairs to 6 in18 pairs. While cross correlation was reasonably sensitive to increases in synchrony, mutual information was less sensitive; broadband phase coherence was more sensitive to either narrow-band phase coherence or that calculated in 'multiples' of phase frequencies (i.e. integer multiples $n:m = 1:1, 1:2, 1:3, 2:3$). They found that the narrow band MPC measure could lead to inconsistent results in finding synchrony that was not also demonstrated by

their other methods.

In Netoff and Schiff's study [137], correlation length across the network decreased during the initiation of seizures, while it increased at seizure abatement. They also studied cortical microelectrode data prior to seizures, finding that mean phase coherence is increased prior to bursts, but decreased prior to seizures. In a contrasting study of the behaviour of two coupled neurons, Elsom[65] found stronger coupling with synchronisation at slower time scales such as one would find during bursting behaviour, whereas asynchronous behaviour was found at at faster timescales.

In summary, the question of how synchronisation occurs may depend on which of multiple timescales are measured, or whether broadband or narrowband measures are used to infer the presence of synchrony in the network. In absence epilepsy one would suspect that the strongly reverberating thalamocortical loop, with its dominant low-frequency component, and widespread reciprocal connections to much of cortex would give rise to more widespread synchrony. In one of Dominguez's [58] four patients with absence epilepsy, more widespread global synchrony was seen.

Perez-velaquez (2007) investigated the difference mean phase coherence between limbic areas during 'typical' or 'atypical' absence seizures, using a narrow band MPC measure. To do this he analysed mean phase coherence in the frequency ranges 5 - 30 Hz in increments of $\pm$ 2 Hz and a sliding window of 1 second with overlap of 0.3 seconds. He did not analyse the MPC leading up to seizures but he did show that hippocampal MPC was bilaterally increased during cortical SWDs. He showed that there is increased network synchronisation in regions outside the thalamocortical networks during SWDs.

Chavez used empirical mode decomposition to find what intrinsic timescales were involved in synchronisation, finding an increase in fast time scale synchrony at seizure onset. Chavez also studied amplitude versus phase coherence prior to neocortical seizures. He found focally increased coupling around the area of the seizure focus in focal epilepsy, and decoupling from more distant cortical areas[42].

Other authors have suggested that the presence of altered synchrony may be an epiphenomenon of other physiological changes relevant to seizures. Whilst many authors have

concentrated on synchrony as a measure of coupling in epilepsy, Majumdar and colleagues [121] investigated the problem of synchrony in epileptic seizures as one of cause or effect. After all, the causes of seizure initiation or termination are likely quite diverse and may not necessarily be synchrony related. They analysed 87 seizures from 21 patients, finding that phase synchronisation increases towards the termination of seizures. They suggested that acidosis and the breakdown of heterogenous neuronal firing patterns may be more relevant than the synchrony changes themselves.

Cross frequency coherence

Cross frequency coherence has attracted increasing interest only comparatively recently. As already discussed it has been proposed as a particularly elegant solution to neural binding in which local neural assemblies share higher frequencies, and lower frequencies to bind different brain regions together [95].

It has been studied in the context of cognitive tasks, in Parkinson's disease and in social anxiety and other mental health disorders. It has also been studied in epilepsy comparatively recently.

Ibrahim [91] studied cross frequency phase-amplitude coupling (PAC) in relation to 9 seizures in two patients undergoing DBS surgery for intractable epilepsy. They studied the presence of cross frequency PAC and also phase synchrony in anterior thalamic nuclei of both hemispheres, finding that there was greater PAC on the nuclei on the side of the epileptogenic hemisphere. Interestingly they reported a different phase of preferred coupling in the lower frequency cycle between the epileptogenic and non-epileptogenic hemisphere, and that this was consistent. There was a greater degree of phase locking in the nuclei on the epileptogenic hemisphere, especially at lower frequencies.

Fitzgerald and co-workers have also studied both PAC and amplitude - amplitude cross frequency coupling in the centromedian anterior thalamus and prefrontal cortex subdural electrodes in three patients who underwent both subdural grid electrode monitoring and DBS surgery for intractable epilepsy[69]. They found significant, but variable patterns in both measures, perhaps in part relating to different recording locations or also different

cognitive states or demands at the time of recording. However, strengths and patterns of cross frequency coupling seen between cortex and thalamus did tend to correlate in their study.

Guirgis and colleagues investigated cross-frequency coupling in the intracranial EEG of 7 patients with extratemporal lobe epilepsy[118], using an automated approach to identifying regions of influence. They studied modulation between theta (4-8 Hz), delta (0.5 - 4 Hz) and higher frequency oscillations between 30 and 450 Hz, using surrogate analysis to minimise statistically less significant detections, and an eigenvalue decomposition on the mean MI values found. They noted a significant increase in the likelihood of a poor post-operative outcome, in seizure frequency, correlating with increasing numbers of eigenvalue decomposition channels identified.

Measures of cross frequency coupling have been used as part of seizure detection algorithms in expert systems such as support vector machines for detection of both seizures and the pre-ictal state.

One confounding issue pointed out by Ibrahim [91]which is especially relevant to epilepsy is concurrent increases in synchrony near the seizure onset zone, potentially making it difficult to determine CFC from third-party common driving influence at different frequencies. A second problem, explored by [2] is the potential for 'edge effects' if higher frequency components are present in the signal, for example during SWDs.

Assessing causal relationships between brain regions

In disentangling interactions between different brain networks it is very helpful to know what regions may influence the behaviour of others. In estimating 'driving' as opposed to 'responding' networks many different methods have been proposed to tackle this problem [154]. For example, information theoretic approaches such as transfer entropy estimate the direction of information flow. A major way of approaching this problem is a temporal argument, in that cause should precede effect [142],[141] : if the 'driving' contains information about the recipient's future, not contained in the recipient's past, and comes before the recipient of a system, then this provides evidence of effect.

Granger Causality

As introduced by Clive Granger in 1969[83], the basis of Granger Causality is testing for asymmetry in the accuracy in prediction between one time series and another. If one time series aids in the prediction of the other's future states, but not vice versa, then one may consider that the first time series is the driver, and has some causal influence on the receiver.

Stated mathematically, given two time series X and Y, if the variance of the prediction error of X is improved given information from Y, as compared with prior information about X's past only, then it could be said that Y has some causal influence on X.

Granger causality has been extensively used in neuroscience to analyse data from a multitude of time and spatial (i.e. from single cell to whole brain network analysis) scales, across a number of different modalities (e.g. EEG, MEG, fMRI, local field potentials), in a number of different variations (e.g. adaptations of the technique for the frequency domain or point processes) and also across a number of experimental conditions (for example, consciousness, cognitive tasks, pathological brain states, or stimuli presented). Given that brain oscillatory dynamics are studied as indications of the underlying organisation of neural activity, it is not surprising that frequency resolved GC is very popular as an analysis tool.

Granger originally formulated his definition of causality based on linear prediction of stochastic time series. As such it was designed for approximately linear, time invariant, stationary data, and requires a well approximated autoregressive model of parameters for further estimation of causality. Stokes [218] analysed criteria by which it may break down, finding that it can be biased severely or of high variance, and can be difficult to interpret or erroneously interpreted separate from the component part of the system model.

It also ignores components of the system dynamics, and has been shown to give inconsistent results in certain circumstances such as spiking activity, or in the cases of latent hidden variables, strongly inhibitory networks, or poorly approximated VAR models for the data. In this latter case negative causality estimates may be unreliable even in the setting of finite-VAR models of good fit[218].

As stated by Sugihara and May[78], a key component to the concept of Granger Causality is separability - that information relating to a causative factor is independently unique to the variable modelling or representing this factor. However, they argue that for weakly coupled dynamical systems, information about one variable is also likely to be redundantly present in other variables, and so cannot be separated out from them. Such systems would need to be considered as a whole, and Granger Causality has been demonstrated to fail in this instance. As above, another weakness of Granger causality is that it does not represent the system dynamics, so a number of variables may in fact cause similar effects giving rise to apparent synchrony (the so-called Moran effect).

nonlinear association analysis

This approach was developed by [242], and is further summarised in Section 4.1.3. Like Granger Causality, it relies on the fact that asymmetric interdependencies between two signals result in differences between unexplained variances found in each signal arising from the other. A significant difference is that it is a non parametric measure.

This unexplained variance is found by calculating the change in normalised conditional variance from the mean of one signal at successive time steps given the other signal. Knowing this variance, one can calculate the degree of asymmetry in driving influence in each signal and also a measure of the time delay for this one to reach a maximum. The combination of these measures over time allows a measure of driving influence between two time series. In contrast with Granger Causality, this variance is found directly from the data, rather than from autoregressive modelling.

Phase Slope Index

This measure was introduced by Nolte[142]. It uses the slope of the phase spectrum to estimate the direction of information flow in multvariate time series data. In Nolte's original paper describing this method, he demonstrated that it is insensitive to the superpositiion of independent sources (which can lead to falsely significant estimates in Granger Causality), and that it can give meaningful results from nonlinear phase spectra, and that it also properly statistically weights the contributions of different frequencies.

The slope of the phase spectrum is calculated from the complex coherences, $C_{ij}(f)$ of the cross spectra $S_{ij}(f)$ between channels i and j, in windows of data of length T. The

phase slope is defined from the complex coherencies

$$C_{ij}(f) = \frac{S_{ij}(f)}{\sqrt{S_{ij}(f)S_{ij}(f)}} \tag{1.6}$$

as

$$\Psi_{ij}(f) = \mathrm{Im}\Big(\sum_{\delta f \in f} C^*_{ij}(f)C_{ij}(f+\delta f)\Big) \tag{1.7}$$

where Im is the imaginary part of the complex coherencies, the star (*) denotes the complex conjugate, f the set of frequencies over which frequency contributions f are summed. Resolution between increments in frequencies $\delta f = 1/T$. To see that it does represent the phase spectrum slope, Nolte gives the example of a time delay between one signal $y(t)$ and another, $y'(t) = ay(t-\tau)$ (here a is an arbitrary constant). The Fourier transform of $y'(t)$ is $a\exp(-i2\pi f\tau)\hat{y}(f)$, so that the cross spectrum would be given by

$$S_{ij}(f) = \langle \hat{y}(f)\hat{y'}^*(f)\rangle \sim \exp(i2\pi f\tau) \tag{1.8}$$

so that the phase spectrum $\Phi(f)$ is $2\pi f\tau$. This is linear and proportional to the time delay τ, and will affect different frequencies differently. Further properties of this measure are detailed in section 4.1.3.

Methods based on nonlinear time series

Accurate inference behind causal relationships between neural populations are made more complex by the existence of interactions across multiple timescales; the likely mixture of linear and nonlinear interactions and also the nonstationary nature of EEG and ECoG signals[218]. If the underlying dynamics have a few dominant variables interacting in a lower dimensional space, then techniques used to analyse dynamical systems may offer an opportunity to model these interactions[154]. On the other hand if the interactions seem dominated by stochastic noise in a higher dimensional space then multivariate modelling may be more appropriate. A number of approaches have been proposed in the literature.

The EEG has been shown to have varying degrees of nonlinearity, but this appears to differ depending on the methods of measurement such as scalp vs. intracranial depth recordings[158] and sampling rates. The question then arises as to whether this irregularity

is due to noise, or chaos. On the one hand, if due to noise, it would be indistinguishable from random fluctuations, but on the other hand if due to chaos it would reflect the underlying properties of the attractor giving rise to the system dynamics.

Higher dimensional dynamics may be missed if one is only focussing on low-dimensional deterministic activity only, is present.

So, should we use linear or nonlinear methods to analyse causality in ECoG data?

Sugihara's methods have concentrated on causality from a dynamical systems approach. Their approach centres on the observation that variables are likely to share a causal relationship if they share the same attractor manifold that accurately describes their dynamics (Section 4.1.2). Their technique of Conformal Cross Mapping (CCM) estimates the extent to which one variable may allow estimation of the state of another.

If conditional information is present between variables we may infer causality. For example, considering two variables X and Y, both of whom share the same attractor, if information regarding X can be recovered from Y but not vice versa, we may conclude that X causes Y. A few groups have used Sugihara and May's methods to explore the EEG in Alzheimer's disease and also focal epilepsy. Intuitively one would expect that Sugihara's method should provide meaningful results since it uses the information contained in the system dynamics to demonstrate conditional influence.

The question of whether statistical modelling or deterministic parameter-free approaches best measure the associated activity between brain regions has been a subject of fierce debate. However, Perretti and colleagues[34] showed that dynamical methods give superior fit, even over properly fitted stochastic models. It would be expected that given the short timescales in the thalamocortical circuit, the nonlinear methods of Sugihara [78] should be the most accurate as suggested by Perretti's work. Another issue is that investigations of cellular[161] and network activity[242] suggest strongly that thalamcortical interactions are reciprocal, and at timescales between 9 and 20 msec[177]. So, any recording method must allow for analysis of short data epochs at those time scales. This is the dominant reason why Grainger Causality is most likely less suited to analysis of this data given autoregressive methods or entropy based methods generally require long data

sets.

To conclude, from a physical viewpoint, whenever oscillations are encountered, characteristics of (1) temporal association; (2) precedence of information flow; and (3) phase coupling are most often useful and easiest to interpret in a further understanding of the dynamics behind synchronous processes when their underlying dynamics are not known.

1.3.3 Theories of spike-wave generation

Is there a focus?

Apart from our earlier work[249], no one has really examined the differences between S1 vs S2 in seizure generation, and how seizure generation may vary between regions of somatosensory cortex in rats.

In 2012 we published results indicating that SWDs were preceded by 5 - 9 Hz physiological field potential oscillations detected first in the somatosensory cortex (S2 and insular cortical (IC) regions)[249]. In this study maximal suppression of SWDs occurred after injection of an endogenous neuropeptide NPY into S2, more than S1; pre ictal oscillations occurred first in S2/IC before S1 or motor cortex, in the one or two seconds before generalised SWDs; and SWDs could be triggered by lower intensity microstimulation in deep layers of S2 than S1. High frequency oscillations occurred earlier in S2, by more than 20 sec, a remarkably long lag considering the close proximity of the two paired recording regions (1 - 3 mm), this being the first time that HFOs had been described in absence seizures[249]. At the cellular level, it was found that the majority ($\sim$79%) of cells in deep cortical layers fired rhythmically at the SWD frequency of 5-9Hz before and after seizures using paired glass electrode recordings, suggesting that these cells may have been part of the 'rhythm generator' circuit, from which SWDs arise. The conclusion of this study was that the S2 somatosensory cortex also forms an important part of the seizure generating circuit, and that this region would also merit more study.

1.4 Evidence for criticality in seizure transitions in neuronal networks

Any attempt to unravel neural dynamics comes up against the problem of the complexity of the CNS itself. Over the last 20 years our ability to record from multiple cells simultaneously across separate brain areas has dramatically increased. Ultimately, no matter how many cells one can realistically record from, the system will be vastly under sampled in which much brain activity is still hidden. For example, one cubic millimetre of brain, containing as many as a billion neurons, is still dwarfed by the $\gg 10^{11}$ other neurons by a factor of more than 10^6. Additionally, the brain's recorded electrical activity underlies a vast complexity of other variables such as neurotransmitter activity, cellular messaging systems, the extracellular environment (such as metabolite, glucose or ion concentrations, oxygen, pH, etc), and on a longer term scale, gene expression, mitochondrial activity, circadian rhythms, immune activity, or external effects such as cognitive interactions with the environment around us.

It is hard to understand the larger scale behaviour of neural systems based on small samples, since the statistics at small samples may be substantially different. On the other hand, even if we could record from a substantially larger portion of neural activity, we would then be left with the mind boggling amount of data this produces, then having the same problem with the data as we do with the original system - what has been called the 'curse of dimensionality'[247].

One approach might be to examine the statistics of synchronous neural interactions, as has been done in [247],[144], or how neurons dynamically organise into individual networks (assemblies)[155]. Another approach, pursued in Chapter 3 of this thesis, is to examine the dynamics of neural interactions at different spatial and temporal scales.

A number of authors have examined the question of differences in the brain's EEG depending on the scales being investigated. Considering this for the case of epilepsy, Stead and coworkers [210] used microelectrode bundles set amongst the usual intracranial grid electrodes used for depth EEG studies prior to epilepsy surgery. They chose as control subjects patients who had intracranial electrodes inserted for the management of

intractable facial pain. They found that although seizures were seen to start abruptly at the macroscale level of clinical EEG recording, seizures were more often observed on microelectrodes, sporadically coalescing before evolving into clinical seizures. They also more rarely observed the same 'microseizures' occurring in the brains of control patients though these did not evolve into seizures.

Keller and colleagues observed markedly heterogenous firing patterns during interictal epileptiform dischargres in human cortex. Recording from up to 166 neurons in small patches of cortex in 20 patients with intractable epilepsy, they found firing patterns were heterogenous even in a small cortical region, both within and outside the seizures focus[100]. There was relatively sparse single neuron participation found, in that only half of recorded neurons changed their firing pattern at the commencement of seizures, and these same neurons were not necessarily involved in subsequent seizures. This is at odds with our previous findings[249] in the deep layer cortical neurons of the thalamocortical circuit, that a precursor physiological oscillation was found prior to seizures in the S2 region, and that almost all neurons were involved.

1.4.1 Self organisation and self organised criticality

Many aspects of the brain's functioning exemplify emergent collective dynamics. Its underlying ability to flexibly organise collectives of different neural groups across different spatial and temporal dimensions; its capacity for integrated and segregated functioning (eg divided attention); or the dynamic range of the senses beyond what is physiologically possible for individual neurons may illustrate this.

From a theoretical standpoint Chialvo [43] suggested that a brain which has evolved around emergent behaviours arising out of underlying collective dynamics would allow it to exploit a wide range of sensitivity to input (e.g. discriminating sound, light, to touch across a wide range of scales) and to adapt to, or learn from its environment. Beggs and Plenz [170] similarly suggested that this might explain the brains ability to segregate or integrate information as required, for example through the concept of dynamic 'cell assemblies' [74] and a number of authors [123] have shown how a brain poised at criticality optimises

information transfer. A number of authors, including Botcharova[28] and Meisel[132] suggest that the brain may be in a slightly subcritical state, to enhance stability.

Self organised criticality originated from studying the statistics of simpler systems such as sand piles, or events such as forest fires or earthquakes. Bak showed that the statistics of avalanches of sand piles follow a scale free pattern, and subsequently that many other natural phenomena such as population dynamics or earthquakes follow the same statistical distribution similar to the Gutenberg-Richter or Zipf law. Beggs and Plenz subsequently demonstrated the existence of neural avalanches, or a scale-free distribution of the statistics of spiking, which occur with extreme precision across long time frames of within milliseconds over up to 24 hours[18].

Such emergent features are a property of self organised systems. Many models of biological systems have revealed statistical evidence of being near a critical state (e.g. flocks of birds[23], frequency of words in language[93], natural images[213], or large sequences of amino acids. The question of whether the brain is an example of a system in a SOC state (or, in Mora and Bialek's words [134], "like the boundary between being nearly dead and fully epileptic") has been keenly debated.

Critical slowing

The phenomenon of critical slowing has been extensively studied in such wide-ranging fields as financial markets, medicine, ecology and atmospheric research. In any of these fields, abrupt changes in the behaviour of a system (*critical transitions*) can occur. Respective examples could be a stock market crash, asthma attack or epileptic seizure, sudden decline in species of an ecosystem, earthquakes, or climate change. In many instances, despite the suddenness of change there may be subtle features which warn of impending change[197].

Critical transitions are sudden, rapid changes in macroscopic system properties (behaviour), reflecting subtle changes in underlying system dynamics, which are possibly governed by parameters that may not be immediately apparent. A goal in recent years has been to uncover what factors govern these tipping points, when the underlying dynamics of the system can not be clearly known.

Analytical models which are developed to study this behaviour focus on tracking the behaviour of variables associated with the cause of the critical transition (control parameters), such as the temperature T in the ferromagnet. Other parameters may follow the behaviour of system properties (order parameters). A description of the system dynamics can be built up by plotting the trajectory of the observed behaviour of the system taken through successive points governed by the relationship between variables : the control parameters on the x axis, and the order parameters on the y axis.

In the example of the ferromagnet, the behaviour of order parameters allow us to study the interaction of this system with its environment. Increasing the temperature T, a proxy for the energy contained within the system, varies its magnetic properties. At a critical temperature T_c, a magnetic material suddenly loses it's magnetic properties. A famous model of this was developed by Ernst Ising in 1929[92] where individual domains of magnetism were modelled as 'spins' aligned either with an external magnetic field or against it. In this model, lower temperatures of the magnet are dominated by an 'orderly' phase where many domains are aligned with the external magnetic field, and large clusters of common magnetic domains form. Above the critical temperature, much smaller correlations are seen with much more disorder and less large-scale recognisable structure.

At the boundaries between clumps or domains of differently aligned magnetic spins, the individual alignments of constituent spins flip most quickly, creating a heirachy of levels of activity or disorder in this system. This model undergoes a phase transition at a critical temperature, manifested by a change in a number of macroscopic properties. The magnetisation disappears at this point, and the emergent statistics of many parameters become scale free. Correlation between sites also increases at this critical point.

At critical points in such a system's dynamics, fluctuations may be seen across all characteristic length scales or interaction sizes, such that interactions might occur at any scale. This fractal scale of interactions across multiple scales implies that interactions at any one part of the system may affect distant sites. Consider the example of neuronal avalanches occurring over a range of diverse spatial scales, the size and frequency of which follows a power law distribution where the probability of observing and avalanche of size s

is $P(s) \propto s^{\alpha}$.The relative occurrence of different avalanche sizes is constant : $P(ks)/P(s) = k^{\alpha}$. With an exponent $\alpha \approx -1.5$ large events are sufficiently probable that as the size of the system increases, a mean event size does not exist[170] :

$$E(s) = \int sP(s)ds = \int ss^{-1.5}ds = \int s^{-0.5}ds = \int \frac{1}{s^{0.5}}ds \to \infty. \tag{1.9}$$

In this way any site can engage any other site.

Such behaviour has been seen at the critical point in the dynamics, and has important implications. Perturbations might have either small effects in only the local neighbourhood to their occurrence, or long-range effects. One characteristic consequence of this is scale free distribution of responses which can be also described by power laws.

Many natural systems have been found to have scale-free behaviour of signficant statistics governing their behaviour. For example, Per Bak's 1987 description of changing dynamics of sand piles, the size and frequency of earthquakes, the distributions of words in English texts, or the populations of cities, have been shown to have long range, complex interactions. These are most prominent when the critical point in these dynamics are reached.

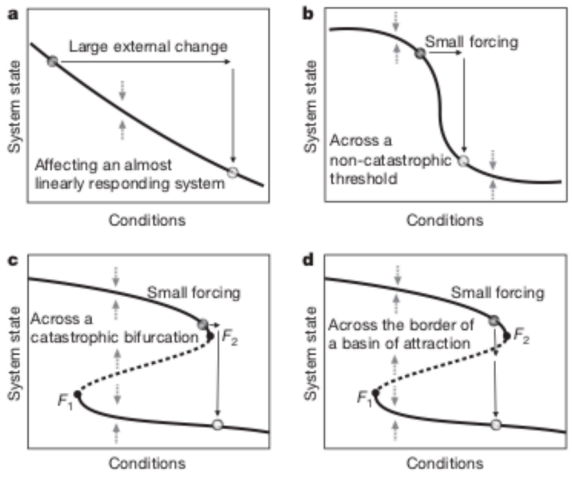

Figure 1.6: Example of the dynamics behind critical transitions. From [197]

To explore this further, researchers have looked for generic indicators of critical slowing which hint at changes in underlying dynamics as above. An intriguing feature in such

different systems is the potential to study dynamical changes even when the underlying dynamics governing system behaviour is not known. Such generic indicators seem to be applicable to a very large number of disparate types of systems [197].

Critical slowing has been characterised as a change in system intrinsic rate of change to perturbation [197],[198]. At the critical point, abrupt and extreme shifts in system behaviour may manifest because of a change in underlying system dynamics and its response to perturbation (e.g. noise).

Indicators of this may be an increased variance in system fluctuations which may reflect an exaggerated response to perturbations. To see that the response to perturbation increases, consider a 1D model $x(t)$ observed at some scale r, which is subject to a small perturbation ϵ. Suppose that it has a fixed point at x^* where $f(x^*, r) = 0$, such that a Taylor expansion around the small perturbation is valid. This expansion would read

$$\partial_t(x^* + \epsilon) = f(x^*, r) + \epsilon f'(x^*, r) + ..., \tag{1.10}$$

or, to first order and ignoring cross terms,

$$\partial_t(x^*) + \frac{\partial \epsilon}{\partial t} \approx f(x^*, r) + \epsilon f'(x^*, r) + ..., \tag{1.11}$$

which implies that $\frac{\partial \epsilon}{\partial t} = \lambda \epsilon$, with the solution $\epsilon(t) = Ce^{\lambda t}$ for small ϵ.

A similar mathematical argument also shows that the autocorrelation of the system's time series data is likely to increase as a system undergoes critical slowing and its dominant eigenvalues tend towards zero, as a natural consequence of the slowing of recovery from (small) perturbations. In the words of [197] an intuitive understanding of this is that the current state of the system $x(t)$ "becomes more like its past". This may also be reflected in an increase in longer range correlations. Possible underlying reasons for slowing may be because of a slow shift in system dynamics, or as a shift in attractor stable point as shown in the successive panels of Fig 1.6.

Close to the bifurcation point, the most unstable dimension in the system's phase space is given by the eigenvector corresponding to the dominant eigenvalue which will tend

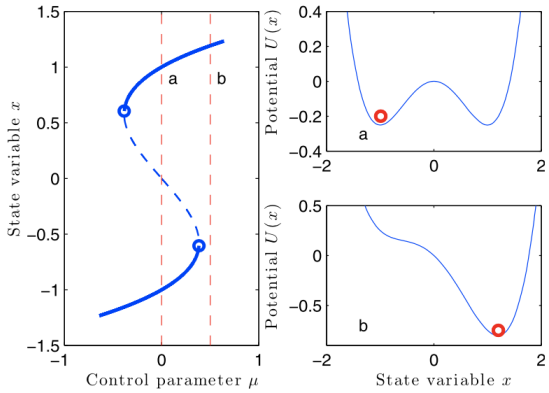

Figure 1.7: Example of the dynamics behind critical transitions. From [57]

towards zero or become positive. This will dominate the system's change in dynamics, and is shown as a shift in the saddle between points **a** and **b** in Fig 1.7. A consequence of the gradual shifting of these dynamics is that some transitions in system state will be more likely than others. This asymmetry in system fluctuations will be reflected in an asymmetry in the probability distribution of system states, measured as an increase in the skewness of this distribution, defined by Eq. 3.3.

'Flickering' is the phenomenon seen when a system oscillates between basins of attraction of two different attractors in response to stochastic forcing [57]. Statistical evidence of this may be an increase in variance, skewness, or a bimodal distribution [197].

There are a number of options for exploring the stability of this system. One approach suggested by Lade and Gross [105] was to use the eigenvalues of the linearised Jacobian[6], calculated from time series data, to provide information regarding fast and slow timescales of the system. If we suppose that we are near enough to a basin of attraction that the derivative of this system's Jacobian at equilibrium tends to zero, the system dynamics should be captured by the dominant eigenvector(s) in phase space. Changes in the eigenvalues associated with these eigenvectors from stable (real, negative in the case of differential equation models, or less than one in the case of discrete maps) to marginal or unstable coincided with alterations in the fast timescale dynamics, and a tipping point.

Alternativey, Suffczynski used a Langevin model to account for the dynamics that

[6]The Jacobian of some system $F(x)$ is given by $\mathsf{J}_{ij} \equiv \frac{\partial F(x)}{\partial x_i \partial x_j}$

could describe the statistics of the intervals between seizures of GAERS rats[220]. In this approach, he assumed the dynamics of the dominant variable x_i above can be modelled by a Langevin equation, like the problem of a potential in a well [7]. In this way he showed that the distributions of interictal and seizure events in humans and GAERS rats could be reproduced by a mathematical model with bistability properties.

In the language of statistical physics, it would be intuitive to regard a seizure as a phase transition, and that critical slowing is an indicator of an impending phase transition and hence seizure. The next question is what approaches best describe this, and what macroscopic variables best describe the parameters of the system.

Evidence for criticality in the brain

Previous research into criticality in neural systems have focussed on a number of main areas, such as evidence of critical transitions in altered brain states such as anaesthesia[217], depression[228], sleep and altered consciousness[222], or altered scaling in the EEG correlated with altereations in cognition or behaviour [229].

In those studies focussing on experimental data, evidence has been sought regarding scale free statistics and behaviour or evidence of critical slowing. Meisel [132] studied the inverse of the variance in EEG time series data prior to seizures in patients undergoing epilepsy surgery for refractory seizures. He showed that the maxima of this quantity occurred before seizures, and reasoned that this corresponded to increases in variance expected with critical slowing.

Kramer and colleagues studied markers of criticality towards seizure termination at a number of different scales [103]. In this study, data was taken from EEG records, intracranial grid electrode recordings of the ECoG, and multi unit activity from depth electrodes in between five and eight patients who had secondarily generalised focal seizures. They found a decrease in the frequencies of peak average power and an increase in autocorrelation and

[7] In other words, if the potential for some variable x is given by $U(x)$, then the Langevin equation describing this would be $\partial x_i = \partial_x U(x) + \sigma_i \eta_i$. The statistics of U(x), such as changes in the data variance and autocorrelation, or the distribution of event durations can be studied by altering the value of σ and comparing modelled variance with the data from experiment

spatial correlations, in keeping with critical slowing prior to seizure termination. Interestingly, they also found that at smaller scales multiunit activity showed more variable patterns with less signatures of critical slowing being seen.

Expert systems such as the NeuroVista device [47] have achieved a significant degree of success in predicting increased probability of seizures using subtle spectral changes before seizures, a result made possible because of the large amount of data available from the implantable device, unique to each patient. Similarly, there is active research on individual seizure prediction by stratifying additional patient specific factors such as circadian rhythm and seizure history [15].

Linkenkaer-Hansen [112] showed the existence of very long range temporal correlations in 10 - 20 Hz cortical oscillations from simultaneous MEG and EEG studies in relaxed awake human subjects, and further demonstrated power-law scaling behaviour in the amplitude fluctuations of these correlations.

Kitzbichler et al [101] studied power law scaling of low frequency (using fMRI) and high frequency (using MEG) oscillations in human brain activity. The basis for Kitzbichler's analysis was the averaged Hilbert wavelet transform, $\vec{C}_{ij}(t)$. It is defined as in Eq. 1.2 but using a 'sliding window' technique

$$\vec{C}^{k}_{ij}(t) = \frac{\langle \mathcal{W}_k(F_i)^{\dagger} \mathcal{W}_k(F_j) \rangle}{\langle |\mathcal{W}_k(F_i)|^2 \rangle \langle |\mathcal{W}_k(F_j)|^2 \rangle} \tag{1.12}$$

where $\langle . \rangle$ indicates an average over the time interval [t,t+Δt] and $|\Delta t$ equal to 2^k times the window size, expressed in units of the wavelet scale used.

Kitzbichler defined the phase-lock interval,

$$\Delta\phi_{ij}(t) = \arg(\vec{C}_{ij})$$

and global lability of synchronisation index,

$$\Delta^2(t, \Delta t) \equiv |N(t + \Delta t) - N(t)|^2$$

where N, the number of phase-locked pairs at any point in time, is defined by $N(t) =$

$\sum_{i<j} |\Delta\phi_{ij}(t)| < \pi/4$. They demonstrated that these measures show a power law scale dependence of synchronisation in both the 2D Ising model and the Kuramoto model at critical temperatures. They went on to find a similar power law dependence in MEG and fMRI signals from human resting brain subjects, and concluded that a 'broadband' critical regime may exist in the brain across these frequency ranges.

This conclusion has been challenged by Botcharova and colleagues [28]. They showed that pooled pairwise phase locking intervals from a Kuramoto model in the non critical regime can also give rise to a power law statistic, perhaps as a consequence of superposition of a number of competing phase relationships in the model.

Many previous studies have identified scaling behaviours suggestive of criticality, for example in the size or duration of neuronal avalanches. However, comparatively fewer studies have identified how this may correlate with dynamical behaviour at different scales. One exception is El Boustani and Destexhe, who found higher dimensional chaos at the neuronal network level (studied with an asynchronous irregular neuronal network model), scaling to heirachically lower dimensional chaos found in the EEG in different levels of consciousness in humans, and in different disease states.

Bornholdt has proposed that an Ising - like spin model governed by a Hebbian-like wiring rule can account for burst behaviour and avalanches in dissociated cultures of rat hippocampal neurons and Leech ganglion cells[190]. Previous authors have analysed avalanches using the theory of branching processes ([18], [87]). Apart from this a current limitation of much of the literature is, in main, its reliance on analysis of power - law like analysis methods in determining criticality. For example, Bedard [16] has shown that a 1/f scaling in power spectra is not sufficient evidence of criticality.

In a larger scale study Friedman [71] used micro electrode array recordings of rat cortical cultures to study higher resolution LFP data. He fitted avalanche size and duration to power law distractions to find critical exponents for the avalanche behaviour.

However it has also been pointed out that power law distributions are ubiquitous in nature, and that it is often difficult to reliably fit power laws especially in the case of limited data, and that 1/f scaling can arise from stochastic processes and is not necessarily

evidence of criticality [16].

There have been some papers fitting characteristics of distributions such as the intensity of natural images [213] or neural data [248] to thermodynamic quantities such as specific heat after assuming a Boltzmann distributed sample. Other authors have stressed that such analogies need to be made cautiously, and in the context of the dynamics underlying the generation of data. In response to the analysis of [213], Saremi and Sejnowski showed that an independently distributed, non-critical model can spuriously give rise to seemingly critical behaviour [194]. They followed this observation with very elegant alternative analysis showing that when mapped to binary bit planes or image layers, creating a heirachy of image intensities from a natural image, that there is scaling behaviour like that seen in a second order phase transition in image layers closest to the point of maximal intensity changes [194].

1.4.2 Complexity

The French philosopher Edgar Morin distinguished between a complicated system (or state), composed of a large number of components, and a complex system, comprising a large degree of entanglement between components and multiple layers of interactions between them [53]. For complicated systems, one might deduce overall functioning from a detailed knowledge of the components. However, for complex systems, essential macroscopic behaviour or function emerge from interactions in the network.

Further understanding of the nature of these interactions in time or space might be found from the scaling behaviour of the system, where fluctuations may indicate details behind any altered function. Complexity can be studied from a number of perspectives : self similarity, to focus on scaling and fractal behaviour; nonlinear methods which quantify the phase space of an attractor giving rise to the system dynamics; or by studying disorder - for example with stochastic methods, or entropy. There is also the added problem of what different time and spatial scales most appropriately reflect altered dynamics in brain activity, or indeed, appreciating the limitations to the scales of data that can be currently collected.

Apart from the viewpoint of self similarity (in which the presence of fractal or multfractal behaviour is studied) one can view complexity from a number of other angles. One could consider complexity as a measure of disorder - in which methods of entropy analysis could be used. Alternatively, one could consider measures of multiscale correlations in the data. From a dynamical viewpoint, one could assess the dimension of the phase space in which the data can be represented. This also allows the application of methods from nonlinear systems [78],[128],[127].

There are natural mathematical links between these approaches. For example, when considering multscale correlations, the method of wavelet scaling and stochastic methods analysing the joint probability at different scales have a natural link.

For example, Equation 3.6 describes a Morlet wavelet, $\psi(t)$, which can define a scale shifted to location k and dilated by a 'width' factor a. Scaling behaviour can be assessed across a number of successive scales $a = 2^j$, $j = 1...n$. A 'poor man's' wavelet can be constructed to illustrate the same scaling, centred at some point x_N, using the difference between a pair of Dirac δ functions as $\psi_{r_i,x_N}(x) = \delta(x_N - x) - \delta(x_N - r_i - x)$ [152]. Scaling increments are then given by

$$\xi(x_n, r_i) = \int_{-\infty}^{\infty} \psi_{x_n,r_i}(x)dx \tag{1.13}$$

The behaviour of correlations between different scales can then be explored in a number of different ways : for example, graphically, through a log-log plot of the wavelet coefficients; the behaviour of probability density functions of $x(t)$ at different scales. The structure function defined in Equation 3.5 is also closely linked to the classical correlation function, and the wavelet spectrum via the Wiener-Kinchin theorem.

For scaling which follow a self similar structure at some scales r and r_1, from equations 3.4 and 3.5,

$$\langle \Delta x_r^n \rangle = \left(\frac{r}{r_1}\right)^{\zeta(q)} \langle \Delta x_1^n \rangle. \tag{1.14}$$

Alternatively, scale invariance would be present for those scales r_i if, for some values λ

$$\mathcal{S}_n(\lambda r_0 | r_1, ..., r_n) = \lambda^{\zeta(q)} \mathcal{S}_n(r_0 | r_1, ..., r_n), \tag{1.15}$$

the function $\zeta(q)$ was linear, whereas multifractal scaling would be present if $\zeta(q)$ was nonlinear. Such scale invariance would be revealed by a power law between structure functions $\mathcal{S}_n$. Intermittent dynamics would show departures from such self similar scaling relations.

One can also study scaling behaviour over time at different time scales. Suppose that the behaviour of "fused" correlations $\mathcal{F}$ at multiple scales $r_i \sim r$ with a separation by an intermediate scale R, $r \ll R$ was of interest. The multiscale correlations $\mathcal{F}_{p+q}(r, R) \equiv \langle [\mathcal{S}(r, R)]^p \mathcal{S}(r, R)]^q \rangle$, of structure functions $\mathcal{S}_q(x)$, corresponding to individual single-point correlations defined by Eq. 3.5 and are given by

$$\begin{aligned} \mathcal{F}_{p+q}(r, R) &\sim \left\langle \left[\mathcal{S}(\frac{r}{R})\right]^p \right\rangle \left\langle \left[\mathcal{S}(\frac{r}{R})\right]^q \right\rangle \\ &\sim S_p(r) S_{p+q}(R)/S_P(R). \end{aligned} \tag{1.16}$$

Dynamical measures of EEG complexity have also been studied to infer how this may change during different brain states (such as seizures), and whether these changes might be due to changes in underlying dynamics, arising from the properties of the underlying attractor, or noise (i.e. stochastic processes).

McSharry [128] found increased EEG time series variance in the minutes before seizures; Martinerie [124] reported subtle decreases in the dimensionality of the EEG up to 25 minutes before a seizure.

Various authors have studied this question by using Grassberger and Procaccia's correlation dimension $C(r)$, given by Eq. 3.29, to quantify the complexity of brain activity. Quintao and colleagues [176] studied the onset of absense seizures with this measure, and tested for the presence of low dimensional chaos rather than noise using phase randomised surrogate data. They found mixed results. Out of 7 seizures, the EEG data displayed a reduction in $C(r)$ at seizure onset in two patients, and they found evidence for both low dimensional chaos and noise in the data sets of different patients.

Techniques for analysing nonlinear systems have also been applied to EEG analysis. Attempts were made to use the concept of correlation dimension to quantify the complexity of brain behaiovur [159], [160]. Pijn [159] documented a reduction of $C(r)$ at seizure onset,

and later studied [160] the interictal and ictal intracranial EEG from patients with TLE. Very interestingly, the brain activity as measured by high quality iEEG from regions outside of the seizure focus were indistinguishable from randomised data regardless of brain state, whereas brain areas within the seizure focus did show evidence of determinism, suggesting that in this case tools from the analysis of chaotic signals could have a helpful role.

Alterations in synchrony, as seen with seizures, could be expected to affect the complexity of the EEG, and alternatively, increased irregularity (or disorder) should be associated with an increase in complexity [204]. A number of entropy-based measures have been proposed to study EEG complexity. Examples include Approximate Entropy, introduced by [168], as a measure of the irregularity of the time series data. Regularity was measured by computing the log likelihood that sequential patterns in the data remain close in successive sequences, but this was found to have the drawbacks of dependence on record length of the data used and bias introduced by self matches. A refinement, Sample Entropy, was suggested by Richman[182], based on a measure of the conditional probability that two similar sequences, represented as m-point vectors remain similar at further points in time. Fuzzy Entropy, an attempt to improve Sample Entropy based on the concept of Fuzzy sets[204], has seen a number of implementations in neuroscience.

Stochastic methods

Another option for assessing interdependencies between different components of the EEG is to use stochastic methods. Since Siegert and Friedrich's paper [73] describing how stochastic methods may be used to separate deterministic and random (noise-related) components of experimental data, this technique has been applied in many different areas.

The advantage of stochastic methods are that they are independent of explicit modelling assumptions, except to initially ascertain that the data is appropriate for stochastic analysis. They can offer ways to separate time varying stochastic behaviour from deterministic processes found in the data. Separating dynamical and measurement noise processes allows one to approximate the deterministic dynamics of the underlying dynam-

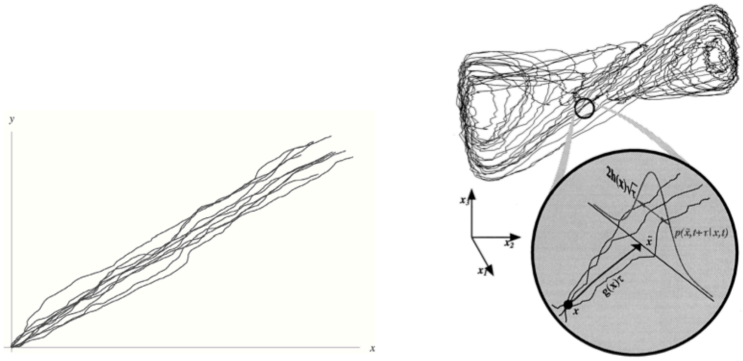

(a) (b)

Figure 1.8: Illustration of the Langevin equation, Eq. 4.6. Illustration of the effects of noise on subsequent realisations of deterministic behaviour, (a) seen in one dimension. From [7]. (b) seen in phase space around an attractor. From [73].

ical system which can then be analysed using traditional methods of nonlinear time series analysis[72].

Prusseit and colleagues[175] used a one dimensional Fokker-Planck equation to explore the dynamics of the EEG. They studied 8 patients who had focal epilepsy and who were undergoing intracranial grid monitoring to better determine the siezure focus. these patients provided multichannel recordings acquired at 200Hz across 20 - 60 recording locations in relevant brain structures over 5 to 12 days. All patients went on to have surgery and were seizure free at the time of their publication (2007), so it is reasonable to assume that the identified seizure focus used in their analysis was accurate. EEG signals were bandpass filtered between 0.5 and 85 Hz, and fitted to a Fokker-Planck equation. They first verified that this type of analysis was appropriate, in that the assumption of Markov properties was true. EEG signals from within the focus were found to have MArkov Einstein timescale of 1, in the units of their data sampling.

The fitted coefficients showed some very interesting properties. The first Kramers Moyal coefficient $D^{(1)}$ displayed overall linear damping behaviour and could be fitted with a low order polynomial; $D^{(2)}$ showed evidence of nonlinearities indicating the multiplicative effects of noise, and $D^{(4)}$ showed evidence of nonlinearities suggesting that the driving noise $\Gamma(t)$ modelled by the Langevin analysis deviated from a Gaussian distribution. $D^{(4)}$ was negligible and slightly above zero in distant brain regions, whereas within the seizure focus

it was more clearly nonzero. Integrating the Langevin equation with the experimentally found drift coefficients truncated to second order, $D^{(1)}$ and $D^{(2)}$ coincided well with results from distant brain regions, but again there were deviations from areas within the seizure focus.

They concluded that this method of analysis allowed them to differentiate physiological EEG states from pathological states, and that this also was a valid approach to EEG data.

They defined the quantity $R_{1,2}$ for each of the determined drift or diffusion coefficients as

$$R_{1,2} = |\max D^{(1,2)} - \min D^{(1,2)}|,$$

using a moving window of at least 1000 data points at a time available with a 50% window overlap. the highest R_2 value was seen close to the seizure focus, and interestingly in their study was associated with only small changes in variance over time. Averaging over all constants from either side of the brain allowed them to identify which side contained the seizure focus.

Kramers-Moyal coefficients have been applied to establish the theta-gamma dependence in the EEG[12], but has not been explicitly been applied to explore different scaling properties of different cortical areas in EEG analysis. Tabar and colleagues have applied similar analysis to the statistics of ECG variability. They found that both a Fokker-Planck analysis and scaling differences using structure functions allowed ways of discriminating the patterns of ECG variability in patients with heart failure from healthy volunteers.

Studies involving Lyapunov exponents

Given that neurons themselves are nonlinear, its perhaps not surprising to intuitively expect that networks of neurons behave in nonlinear ways, especially prior to seizures where the EEG characteristics in phase space change markedly. From the appearance of SWDs, one would imagine that these EEG dynamics have become low-dimensional. On that basis many groups have looked to pickup changes in nonlinear characteristics prior to seizures. Two main ways of investigating this have been changes in dimension, most often investigating by measuring a window-shifted correlation dimension, or changes in

the Lyapunov exponent calculated from EEG data.

Wolff's[243], Rosenstein's[188], Ruelle's[62], Abarbanel and Brown's[31], Sato's[196], or Sano and Sawada's[192] algorithms for finding the largest Liapunov exponent are to some extent all based on the need to find divergent trajectories in the flow of the attractor giving rise to the system dynamics. For example, Wolff's is based on searching for successive nearest neighbours from some original starting point in time-delay embedded data. After finding this point, the system dynamics are evolved forwards some 'time' (i.e. distance in state space, or in the language of his algorithm called the evolution time) l, and a new estimate of the distance l' calculated. This process is repeated for each nearest neighbour found near the original point x_0.

Iasemidis [90] has investigated the largest Lyapunov exponent, and found lower values of this during seizures whilst remaining positive, suggesting that it retains some properties of a chaotic attractor. He based his own measure of this quantity on Wolff's celebrated algorithm[243], in later works modifying this to deal with short data fragments. Iasemidis's group has published results finding that this measure predicts impending seizures in 85% of seizures [41]; it also agrees with the literature finding changes in $C(r)$ minutes before seizures also.

However, there is disagreement as to whether these changes are truly due to changes in the attractor underlying the system dynamics, or whether they may reflect other changing properties of the EEG signal such as the time-frequency signal energy changes and bursts, as found by Litt and coworkers[113]. If one accepts that Lyapunov exponents are meaningful quantities in limited data context, with noise, then one would tend to believe this reflects some reduction in dimension prior to seizures. However, Lai and colleagues challenge this view with an opposing view that the EEG instead is more similar to stochastic systems resembling a high-to-infinite dimensional dynamical system, where Lyapunov exponents become very difficult to quantify[106]. As pointed out by Aberbanel and Brown[31], Lyapunov exponents arising from higher dimensions are much harder to accurately compute, and distinguish from spurious exponents, because the higher dimensional spaces tend to have less points for embedding available data.

Lai [106] reanalysed EcoG data from 20 patients with treatment refractory epilepsy

undergoing intracranial grid recordings, studying the accuracy of $C(r)$ changes leading to seizures. However, when Theiler's method [225] was used to remove spurious correlations from the data, correlations $C(m, d)$ for $m = 5...30$ did not plateau with increasing m, suggesting an absence of low dimensional chaos in this case. Similarly, using Theiler's method of surrogates to generate shuffled data preserving the original frequency spectrum and autocorrelation properties of the original data, the surrogate data showed *better* prediction for seizures. This suggests that the time-frequency energy properties of the data are more useful predictors than dynamical quantities.

Parameters such as the embedding dimension m, the data length, delay τ (usually reliably calculated as either the first zero of the data's autocorrelation function) can affect the accuracy of the Lyapunov exponent, as will measurement noise.

Work from the study of very well known low dimensional chaotic systems such as the Lorentz attractor, for which the system equations and hence the theoretical Lyapunov spectrum are known, attest to the difficulty of accurately calculating the numerical exponents from limited data even in the presence of minimal noise[127]. This debate has sharpened in the context of seizure prediction, where it has been found that other indices such as spectral changes are of more benefit.

1.4.3 Statistical Identifiability of criticality in neural networks

As above there have been many studies exploring the similarity of large-scale correlation behaviour, or scaling behaviour using power law distributions. But it is really possible to identify critical behaviour with statistical arguments?

A number of lines of argument suggest that the problem of *reliably* statistically identifying criticality in complex networks with many degrees of freedom is inherently difficult. This is partly because the system's number of possible states will greatly exceed the number of samples available to characterise it. A number of recent authors have identified that the statistical properties of such models are degenerate, with arguments that could be summarised as follows.

Mastromatteo[125] has studied the problem of inferring probability distributions of binary variables in the setting of under-sampled data from a complex system. To do this, he derived the space of probability distributions and considered the distinguishability of two very close solutions from the same data. The key to his argument was to consider the behaviour of the Fisher Information matrix (inverse susceptibility) for two very close sets of inferred parameters for the same data.

In his notation, the argument is as follows. Consider two solutions drawn from i.i.d. of the same data given by $p(s_g|g)$ and $p(s_{g'}|g')$. The degree to which these two solutions with small changes in parameters could be distinguished is given by Sanov's theorem ,

$$p(s_g|s_{g'}) \simeq e^{-TD(g||g')}, \tag{1.17}$$

where $D(g||g')$ is the Kullback-Leibler divergence[8] between the two distributions. We need a minimum difference between the KL divergence of both models to be able to distinguish the solutions $p(s_g|g)$ and $p(s_{g'}|g')$.

To see this, Mastromatteo showed that the Fisher Information provided an invariant measure in the space of statistically distinguishable distributions. This space was not

[8]the Kullback-Leibler divergence is the distance between two probability distributions given by $D(g||g') = \left\langle \log \frac{p(s_g|g)}{p(s_{g'}|g')} \right\rangle$. The inverse susceptibility matrix for the inferred models is closely related to the Fisher information, which is also related to the KL divergences as the matrix χ of the second derivatives of $D(g||g')$.

uniform but instead concentrated on critical points where the inverse susceptibility was found to be largest. These models are likely to yield solutions close to the singular points of parameters, because at these points the system's response to perturbations is large. This suggests that inferred paramters from most models of the system are likely to suggest critical behaviour, because they are more likely to converge to these points in parameter space.

The above is a *very* similar observation to that of Cocco and Monasson's [46],[45], in deriving their selective cluster expansion of the entropy in their solution of the inverse Ising problem. Unfortunately, the main problem with inverse Ising inference as applied to neuroscience is over fitting of the data[9], because such a small part of the system can be observed. It would be expected that maximum entropy models perform better when correlations between elements are weak, and interactions are local, such as in data from retinal recordings (such as in the study by [144]). Unfortunately, cortical recordings are more likely characterised by sparser connections with intermittent, stronger correlations. These approaches are more likely to fail in such conditions, as they perform more badly with strongly correlated data as in that generated by a 'critical' Ising model.

Consider a solution for the inverse problem in which some couplings $\mathbf{J}$ have been found for some data $\mathbf{p}$. Cocco and Monasson asked what would happen if some values in a subset of the data is changed so that $\mathbf{p} \to \mathbf{p} + \delta\mathbf{p}$. There are a few possibilities. Observed couplings may reflect this, so that only the couplings of the new data change slightly, or alternatively all the inferred system couplings may change in an extended response. The response of the couplings δJ to this is

$$\frac{\delta \mathbf{J}}{\delta \mathbf{p}} = \frac{\partial^2 S(\mathbf{p})}{\partial \mathbf{p} \partial \mathbf{p}} = \chi^{-1}, \tag{1.18}$$

the inverse of the susceptibility matrix χ. χ^{-1} is generally sparser than χ, so even if strong correlations dominate the system, whether the inverse problem is 'well behaved' (i.e. has a localised response with small changes in the data) will depend on the eigenvalues of χ, so each inferred coupling may depend on only a mall range of frequencies $\mathbf{p}$.

[9] most likely in the case of observing the relationship between single cells. This concern might apply less to the observation of the ECoG, where the signal is more representative of network activity

Cocco and Monasson got around these problems by suggesting an algorithm for recursively building up a systematic cluster expansion of the cross entropy in the Ising model based on the data. In their approach the size of the clusters are not fixed a priori, but are data driven. Because the expansion is built from the data it addresses the problem of over fitting, and deals with noisy data from their simulations. Unlike other approaches for solving the equilibrium inverse Ising problem this method does not rely on computing the partition function for the system, so it was not limited to networks of less than 20 neurons.

It is based on the idea that there will be a difference (loss) in entropy between, say, an isolated given cluster of spins, constrained to take on separate variable values (e.g. shared correlations) and that system with combined statistics added together, as the system grows in size. They showed that truncating the expansion of the entropy also allowed them to set a threshold on the effects of noise.

For all of these reasons, and given the previous controversy regarding the application of equilibrium statistical measures to infer criticality arising from previous studies discussed in section 1.4.1, the phenomenon of critical slowing down will be studied from a stochastic and dynamical framework in this thesis.

1.5 Objectives of this thesis

The aim of this study is to explore the dynamics of seizure generation in a major model of absence epilepsy, the Genetic Absence Epilepsy Rats from Strasbourg (GAERS) model. It builds on our previous work that has shown that a focus of hyper excitability, predisposing to the onset of seizures exists[249], and in a slightly different location to that suggested by earlier research.

This study uses the technique of tetrode recordings which allows simultaneous recording of local populations of neurons, and also simultaneous depth electrode recordings of large areas of different parts of somatosensory cortex. This allows us to characterise the relationship between activity at the level of groups of single cells and the ECoG with seizure progression.

Alongside the aim of further detailing the origins of absence seizures in the somatosensory cortex of GAERS rats, the second aim of this thesis is to identify fruitful methods of analysing changes in dynamics underlying these, from EEG recordings. The objective of Chapter 3 is to study the scaling behaviour of cortical activity, evidence for critical slowing, associated dynamical changes using the Lyapunov spectrum, and how these change prior to seizures. Following this, in Chapter 4, the driving relationship between thalamus and different areas of somatosensory cortex is examined. Then, in Chapter 5, the question of what processes underly the resonance in these different areas of cortex is addressed. Moving from previous analyses of dynamics underlying such resonance, directions for further investigation of this phenomenon is proposed, based on the findings of Chapter 5.

Drawing from the fields of statistical physics and nonlinear systems a heirachical approach to data driven analysis is used throughout this thesis. Specific changes in network dynamics are examined prior to seizures at multiple spatial and temporal scales, related to thalamocortical coupling at different stages of seizures, and associated changes in cortical resonance and cortical synchrony with seizure onset.

1.5.1 Objectives of Chapter 3

In Chapter 3, the changes in neural dynamics prior to seizures are examined. A few studies have explored how critical dynamics may change in relation to seizures, such as [132] and [133]. Although this has been a subject of significant interest in recent times, the bulk of the literature has concentrated on equilibrium statistical measures. However, previous research also suggests that given the nonlinearity and nonstationarity of the EEG, statistical quantities such as power law scaling behaviour etc may be misleading. For this reason nonlinear measures are used, such as evidence of separation of time scales from the Lyapunov spectrum.

In Chapter 3, data driven methods are used to find evidence of criticality in cortical components of the thalamocortical network believed to be involved in seizure generation. The scaling behaviour in different regions of somatosensory cortex is also investigated at both the large scale level of multiple simultaneously recorded areas of cortex, and at the

single unit level of tetrode data from specific areas of somatosensory cortex.

1.5.2 Objectives of Chapter 4

In Chapter 4, coupling between a number cortical areas and thalamus is studied. Methods are chosen which are appropriate given the nonlinearity and the oscillatory nature of the EEG signal, and short data sets.

To quantify the degree of nonlinearity present in the measured ECoG signal at different scales, Sugihara's methods of simplex projection are used. Then, the measures of nonlinear regression[158] and phase slope index[142] are used to assess causal influence between thalamus and cortex as seizures occur. The results of analysis at both coarse and fine temporal scales are discussed.

1.5.3 Objectives of Chapter 5

If there is a cortical focus, it is then relevant to ask what evidence is present of increased resonance, and what mechanisms underlie this.

To answer this question, the characteristics of spectral power, amplitude and phase coherence and also cross frequency coupling and comodulation, high frequency oscillations, and measures of phase dispersion are used to compare network behaviour in different areas of cortex in relation to seizure onset and termination. Because resonance could also be the result of underlying changes in dynamics [52], markers of change in dynamics such as finite time and scale dependant Lyapunov exponents are computed. To further understand dynamical changes, alterations in complexity are also measured with seizure onset.

The network's sensitivity to perturbation is analysed by its response to electrical microstimulation in different cortical regions as performed by Zheng[249], and a graphical method to enable tracking changes in phase space trajectory in response to perturbation is introduced.

Chapter 2

Methods

As discussed in section 1.2.2, GAERS are an inbred Wistar rat strain that exhibits spontaneous absence-like seizures with spike and wave discharges on EEG recordings, as well as behavioural phenotypes and responses to antiepileptic drugs which closely follow those of patients with absence epilepsy. Non-epileptic control rats of the same strain will be used as a control in the experiments described in this thesis.

Two different types of experiments were performed. The first experiment was designed to study multiple cortical areas simultaneously and involved chronic implantation of multisite depth EEG electrodes. The second type of experiment was designed to study very small regions of cortex, or thalamus, at a time. For this purpose tetrodes were used to obtain dual recordings between selected areas of cortex and thalamus simultaneously. For these tetrode experiments three GAERS rats and two NEC rats were used.

2.1 Tetrode experiments

All stages of these experiments and surgical protocols complied with animal ethics guidelines of the Australian National Health and Medical Research council regarding the use of animals in scientific research, and had ethics approval through the University of Melbourne and the Howard Florey Institute.

Surgical procedures were performed in rats under general anaesthesia. Anaesthesia was induced with a mixture of ketamine and xylazine. A craniotomy (described below) was required to expose the brain surface for insertion of either recording electrodes (tetrodes)

or depth electrodes. Once surgeries were completed, electrophysiological recordings commenced under neuroleptic analgesia (haloperidol/fentanyl/tubocurarine).

Adult rats of 14 weeks of age or older were used, as absence seizures fully develop in these rats by that time. Male rats were used because of the requirement for dorsal penile vein catheterisation for the neuroleptic analgesia infusion. At the end of the experiments, the animals were euthanised without regaining consciousness. The entire experimental procedure for tetrode recordings consisted of three parts, which are summarised below.

Surgical procedure

Anaesthetic induction was completed with ketamine (50mg/kg)/xylazine (150mg/kg) given i.p. using a 26G needle. Once adequately anaesthetised, eye gel was applied to the eyes to prevent drying during anaesthesia, a pulse-oximeter connected to the animals foot, and the animal placed on a heat pad. Padding was placed under the rat's extremities which were not on the heat pad to minimise external stimuli. Rats underwent dorsal penile vein catheterisation so a neurolept infusion could be maintained for the duration of electrophysiology recordings. This included carefully isolating the penile vein and making a lose knot with ligatures around the vein. A small incision was made in this vein and a catheter inserted which was then secured in place by tightening the ligatures to minimise displacement during the experiments. Once fixed in position, the cannula was flushed through with 0.2ml heparinised normal saline and connected to a saline-filled syringe until ready for use. The purpose of this is to facilitate the IV neurolept infusion.

Rats then underwent tracheostomy in preparation for ventilation. The trachea was carefully isolated by making a 1 cm incision and dividing the pectoral muscle layers. A plastic cannula was inserted in the trachea as an endotracheal tube and again secured in position. Positive pressure artificial ventilation was initiated with oxygen (8 - 12 cm H_2O, 60 breaths per minute). Ventilation is necessary because of the use of tubocurarine, a neuromuscular blocking agent which prevents the animal from breathing unassisted.

Rats were then gently positioned in a stereotaxic frame, and a rectal thermometer inserted. An incision was made in the skin over the scalp, and 2 small burr holes made

over the frontoparietal region. Screw electrodes were gently positioned in these to allow for epidural EEG recordings. These EEG recordings allowed continual monitoring of the depth of anaesthesia during the experiments.

The rats then underwent craniotomy and durotomy. The target location of the craniotomy is calculated from Paxinos and Watson's atlas [77] based on the location being recorded (i.e. thalamus or somatosensory cortex) and the calculated stereotactic guidance trajectory of the electrode. A 2 - 2.5 mm diameter craniotomy was performed by drilling the skull carefully under view using a surgical microscope until a thin layer of bone was left. This bone layer was then carefully peeled off to expose the dura. To perform the durotomy, a small incision was then made on dura using a bent 26 gauge needle under the microscope to allow for a small opening to the brain ($\lesssim$1mm) for insertion of recording electrodes (tetrodes).

The final procedure was the insertion of tetrodes into the brain. This was done by stereotaxic guidance into the brain regions relevant for the particular experiment. These were lowered through the opening in the dura and then lowered into the brain using automated stereo microdrives, capable of controlled position changes of from 200 μm down to 1 μm at a time. The electrodes remained fixed to the frame/stereodrives at the required position for recordings to commence.

During these surgical procedures, animals were monitored for depth of anaesthesia by several methods. These included the toe pinch test, EEG, core temperature, blood oxygen saturation and heart rate.

Cellular recordings

Cellular recordings using the inserted tetrodes were acquired under neurolept analgesia delivered as an intravenous infusion at a flow rate of 0.5 ml/hr. The neuroleptic cocktail consisted of: d- tubocurarine chloride (2mg/ml), fentanyl (2 μg/ml), haloperidol (0.2 mg/ml) and glucose 25 mg/ml. Haloperidol provides the tranquilisation effects with fentanyl providing analgesic effects. A non-depolarising neuromuscular block (D-tubocurarine) was also administered to prevent muscle contractions induced by the haloperidol.

Under this anaesthesia, local field potential and single cell recordings can be acquired in vivo while rats experience intermittent absence seizures. The primary benefit of this cocktail is that it does not suppress spike and wave discharges, the seizure hallmark of absence epilepsy, whereas other agents, such as ketamine + xylazine, halothane or isoflurane, or barbiturates, all inhibit spike-wave discharges. Monitoring of the depth of anaesthesia continued while animals remained under neuroleptic analgesia.

Recordings commenced when the animal was stably under the influence of the neuroleptic analgesia. This was estimated based on the appearance of a desynchronised EEG, with only rare slow waves, but prominent theta rhythm and appearance of spontaneous seizures. The tetrodes which were stereotactically inserted into the brain are connected to amplifiers. Under neuroleptic analgesia, the tetrodes were slowly lowered using microdrivers capable of step movements down to 1 μm to reach either single neurons or groups of cells in the regions of interest. Once either single cells or groups of cells were identified by their spike morphology, recordings of this neuron were then acquired for several minutes. After this, the tetrode was then lowered again in search of another cell.

Termination of the experiment

Following the completion of the recordings, rats were euthanised without regaining consciousness by an i.v. injection of sodium pentobarbitone (0.5 mls), as standard ASCART procedure.

Analysis of the electrode position and track through the brain in sequential recordings using an injected marker dye is unfortunately not possible with tetrodes, as it is in the case of glass electrode recordings.

2.2 Depth Electrode Experiments

Rats were chronically implanted with 127 μm stainless steel electrodes bundles in which each electrode bundle consisted of insulated wires where the insulation was stripped at 0, 1.0, 3.0 and 5.0 mm from the end, enabling recording simultaneously at four different

locations in cortex. Electrodes were implanted bilaterally into S1Ul and S1Fl, S2 and IC (insular cortex), and a separate electrode was implanted into motor cortex, later in this chapter labeled M1. Extradural reference electrodes were implanted into parietal bone. These experiments were performed by Zheng[249], and rats were allowed to recover for 7 days before recording sessions.

In the case of depth electrode data, electrodes were placed in two regions of S1 - associated with the forelimb homunculus, as determined by the Paxinos and Watson stereotactic rat brain atlas [77], here called S1Fl, and perioral area, called S1Ul. Other regions were the insular cortex (IC), S2 somatosensory cortex, and M1 motor cortex.

2.3 Data collection summary

The numbers of rats required for experiments were calculated based on statistical significance of our previous results [249]. Based on this experience we estimated that recordings from 6 GAERS rats vs control rats should yield sufficient data to provide statistically significant results.

For example in one experiment which contributed to that work, we studied high frequency oscillations in different areas of somatosensory cortex - either primary (S1) or secondary somatosensory cortex (S2). In those experiments these oscillations were found to occur 20 msec earlier in the S2 region compared with S1 for n = 7 rats (range -66.4 $\pm$ 2.8 msec for S2, 40.7 msec $\pm$ 2.4 msec for S1 giving $p < 0.001$).

The success rate for obtaining multi unit tetrode recordings is approximately 80% of rats studied. For the current work it was therefore estimated 10 GAERS rats and 10 NEC rats would be required to allow a meaningful assessment of neuronal properties in the three regions of interest in somatosensory cortex.

For this thesis, seven tetrode experiments were performed in total (5 GAERS rats and 3 non epileptic control (NEC) rats). Four of these experiments were performed to evaluate the performance of different types of tetrodes, and to perfect experiment conditions including the signal to noise ratio of obtained data.

To start with home made tetrodes were fabricated with platinum-iridium wire, as well as commercial tetrodes manufactured by Neuronexus Inc. and FHC. We experimented with platinum-iridium wire at a number of different diameters (12.7μm, 17μm and 25μm) and electrode tip coatings (including gold and platinum black plating), and altering the sharpness of the platinum-iridium tip by etching with calcium chloride[1], in an attempt to optimise the reliability of the fabricated tetrodes and also SNR of data obtained.

Signal to noise ratio was calculated for each electrode type. The best noise figure was obtained with the commercial FHC tetrodes, manufactured to an impedance of 4MΩ. Although the literature suggests that low impedance, plated microelectrodes have superior SNR especially for chronically implanted EEG recordings, we found the high impedance electrodes vastly superior.

The time of seizure onset were determined by visual inspection for all seizures. For both types of experimental data the start of seizures was taken to coincide with the first SWD. This was distinguished from coarse somatosensory rhythms that are sometimes seen in GAERS by their morphology and amplitude (greater than 400mV peak to peak, as defined by Pinault [161],[166]). When visually inspecting data, if any artifacts were present this seizure was not included in further analysis.

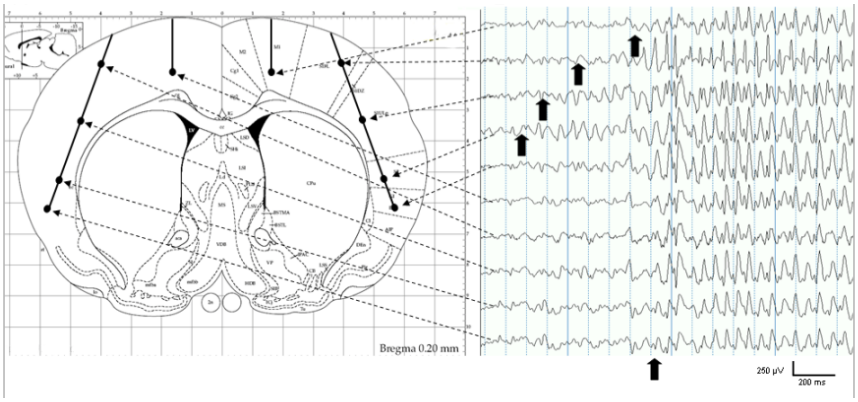

Figure 2.1: Example of tetrode advancement through cortex showing the method for successive ECoG recordings through S1, S2 cortex and the junction region "S12". From [249]

Tetrode data was obtained from three GAERS rats for analysis. Further experiments

[1]Given the that 10% Pt-Ir electrode material has a similar composition to that used for atomic force microscopy we reasoned that calcium etching would be a controllable and suitable process to clean electrode tips by etching. We found the amount of electrode removal hard to control in practice though

Tetrode data : duration, number of seiziures				
Cortical region	Quantity	Expt. 1	Expt. 2	Total
S1	Time (minutes)	20	29	49
	Seizures (n)	69	73	142
S12	Time (minutes)	24	32	56
	Seizures (n)	62	56	118
S2	Time (minutes)	23	34	57
	Seizures (n)	70	58	128

Table 2.1: Summary of tetrode data used for analysis

Depth eletrode data : duration, number of seiziures				
Rat	Recording type	Duration	Seziures (n)	Comments
1	NEC	47	0	left electrodes faulty
2	NEC	46	0	
3	NEC	42	0	
4	GAERS	30	2	
5	GAERS	11	4	
6	GAERS	58	23	intermittent dropout R S2 electrode
7	GAERS	91	95	

Table 2.2: Summary of tetrode data used for analysis

were not added because this data already provided statistically significant results. The number of seizures and recording times per rat for each somatosensory cortical region is summarised in Table 2.2.

From these three experiments approximately 460 seizures were recorded, with between three and nine seizures per minute in each recording location. Interictal discharges ('bursts') were discounted from analysis, as were seizures which commenced either within one second (25000 samples) of commencement of the recording, or terminating within one second of the end of the recording. The reason for this was that many instances of analysis required analysis prior to the first SWD. In the case of tetrode data three different areas of somatosensory cortex, S1, S2, and the junction region between these, 'S12' are analysed. In S1 there were a total of 142 seizures; in S12, 118; and in S2, 128 seizures.

2.4 Data analysis

Data was sampled at 250Hz, for at least two 60 minute recording sessions for each rat. Both the GAERS and NEC control strain of GAERS rats used in these experiments were at least 13 weeks old, and weighed between 250 and 350 grams. Recordings were taken from different cortical areas in 5 GAERS and 3 non epileptic control (NEC) rats.

Data was sampled at 25 kHz using an Intan RHD2116 amplifier system (Intan Technologies, LLC[2]), unfiltered, before being imported into Matlab for subsequent analysis. Data was initially unfiltered during collection to allow for spike sorting if needed later (even very low frequency filtering will distort spike waveforms and can affect the accuracy of spike classification). However, the analysis methods presented in this chapter are concentrated on ECoG and EEG data only and do not require spike sorting. Data was subsequently digitally filtered in Matlab for further analysis and specific details of the filtering procedures will be given where these occurred.

Unless otherwise stated in what follows, before further analysis the unfiltered tetrode data was low pass filtered up to 600Hz using the built in elliptic filtering function in Matlab.

[2] www.intantach.com

Chapter 3

Evidence for Critical Slowing from a Dynamical Perspective

3.1 Prior evidence for critical brain dynamics

It would be natural to anticipate that seizures might represent an underlying change in dynamics governing the brain's behaviour and function. An important goal in the understanding of seizure transitions is an understanding of how underlying brain dynamics change with the onset of seizures, and what factors underlie these changes. One approach is to conceptualise seizures as a phase transition. In this case, it would be natural to search for changes in dynamics which are associated with this. It would also be of significant interest is how these changes may correlate with dynamical parameters of stability and complexity.

Self-organised criticality is a property of complex systems[1] operating near a critical point[2] in their dynamics and which generates scale free characteristics across space and time. This critical point may be marked by a number of unique characteristics, discussed in Section 1.4.1 such as an abrupt change in the behaviour of the system (e.g., emergent order or synchrony from chaotic behaviour, or Bénard instabilities shown in Fig. 1.1), its macroscopic properties (e.g.. the disappearance of magnetism when a ferromagnetic material is heated) or appearance (such as the change of state from liquid to gas).

Ashby [9] was one of the first theorists to emphasise the fundamental influence of

[1] discussed in Section 1.4.2

[2] The critical point in a system, discussed in Section 1.4.1, is one at which the dynamics which govern it's behaviour undergoes a shift, and which may be heralded by a tipping point in system characteristics

self-organisation in brain functioning. The property of self-organisation may play a role in explaining some of the brain's underlying abilities, such as flexible organisation of collectives of different neural groups across different spatial and temporal dimensions; the capacity for integrated *and* segregated functioning (e.g., divided attention), or the dynamic range of the senses beyond that physiologically possible for individual neurons. Another property of self-organised systems is that of emergent collective dynamics.

There has been marked interest in early warning signs of impending critical transitions, reflected in subtle changes in the underlying dynamics to cause such abrupt macroscopic changes. The problem is, these underlying dynamics are often not known.

The objective of this chapter is to extend previous work on the dynamics of seizure generation, by examining a rat model of absence epilepsy, the Genetic Absence Epilepsy Rats from Strasbourg (GAERS) model.

To achieve this objective, changes in scaling behaviour (i.e., the interactions between relevant variables describing the state of a system at different scales of interaction), and evidence for critical slowing are examined at the onset of seizures. This scaling behaviour is also used to derive approximate dynamics of the inter-ictal state.

The phenomenon of critical slowing[3] has been extensively studied in many fields, ranging from financial markets, medicine, ecology and atmospheric research.

Critical slowing has been characterised as a change in system intrinsic rate of change to perturbation [198]. In this scenario, Scheffer [198] showed how abrupt and extreme shifts in system behaviour may manifest because of a change in underlying system dynamics and its response to perturbation (e.g., noise). Indicators of this may be an increased variance in system fluctuations (e.g., because of exaggerated perturbation response); longer autocorrelation time as a marker of longer range correlations; increased skewness (e.g., because of an asymmetry in system fluctuations). 'Flickering' can be evidence of a system's response to stochastic forcing, which causes it to move between basins of attraction [57]. Possible reasons for slowing may be because of a slow shift in system dynamics (as considered by [220]) or as a shift in an attractor stable point.

[3] discussed in Section 1.4.1

The question of critical slowing in neural models and human epileptic networks has been studied previously by Meisel [132] who examined the EEG prior to seizures in patients undergoing epilepsy surgery for refractory seizures. He studied the inverse of the time series variance, showing that maxima of this quantity occurred before seizures, and reasoned that this provided evidence of increases in variance expected with critical slowing.

One problem in demonstrating the often subtle critical threshold changes ("tipping points") which lead to such large abrupt macroscopic behaviour change, in the midst of noise, is the high dimensionality of the system itself, secondary to the number of degrees of freedom possible in brain dynamics. To manage this, researchers have looked for 'generic' indicators of tipping points in dynamics and large-scale behaviour, such as critical slowing, which seem to be applicable to a very large number of disparate types of systems.

Available experimental data is only able to represent activity of a vastly under-sampled representation of a much more complex system. Epileptic seizures are traditionally characterised as the result of hyper synchronous neural activity arising from unbalanced excitation, but recent evidence suggests a much more complex picture. In the first analysis of single neuron dynamics in human focal epilepsy, Truccolo [227] found heterogenous spiking activity in different regions, suggesting interactions among different neural groups in seizure production is complex, even down to the scale of small cortical patches.

3.1.1 Statistical measures of criticality

The most studied markers of criticality have been statistically based, as a proxy for an underlying complex system dynamics which might give rise to these. A classic model of criticality and phase transitions is the Ising model, initially developed by Ernst Ising [92] as a one dimensional model of magnetism. Subsequent two dimensional models, such as that solved by Onsager in 1944 [145], exhibited phase transitions even if the one dimensional model did not.

In the Ising model of magnetic interactions, individual spins (i.e., dipoles, or elements) are positioned on a lattice and are able to take a value of $+1$ if they are aligned with the external magnetic field, H, or -1 if oriented in the opposite direction. Each spin ϕ can

interact with the effect (described as a 'field') produced by other spins in its vicinity, with the strongest effects felt from closer neighbours. In this way, the energy, E, of the configuration of spins in the lattice can be expressed as the sum of two terms, the first being the direct effect of an external magnetic field, H, and the second that of interactions between neighbouring spins:

$$E = -H \sum_i \phi_i - J \sum_{\langle ij \rangle} \phi_i \phi_j \qquad , \tag{3.1}$$

where the sum of neighbouring states $\langle ij \rangle$ is taken over spin pairs. Energy is lowest if all spins are aligned with each other and oriented to the prevailing field H. However, this is balanced by the effects of random disorder on the system. When considering the terms in Eq. 3.1 one can see the competing forces of entropy[4], dominant when the effects of disorder are less, in which neighbouring spins tend to align with each other and the prevailing magnetic field, and thermal energy which results in increasing disorder, and which 'over rides' entropic tendencies. This produces *frustration* where local spins cannot completely align (by analogy with the common definition of frustration, an unresolved tension between terms in Eq. 3.1 governing interactions between neighbouring spins in an energy sense, so the system cannot minimise its potential energy). The amount of disorder is quantified by the entropy, related to the *temperature*, a control parameter[5] defined through the statistics of the distribution of all possible states in the system.

There are clearly multiple configurations of possible spins for this system. To examine more macroscopic or large scale properties of this system we move to a *mean-field* picture where individual spin variables can be replaced by their population averages, since all spins are equivalent. This allows the calculation of the probabilities of any particular spin configuration, and macroscopic measurable quantities such as *magnetisation* $M = \sum_i \langle \phi_i \rangle = N \langle \phi_i \rangle$[6].

[4]Entropy could be conceptualised as a measure of disorder in a system, or alternatively a measure of uncertainty or the multiplicity of states in the system; or from thermodynamics sense, a measure of irreversible changes in the system

[5]Discussed in Section 1.4, page 41

[6]here, the square brackets indicate an ensemble average as a 'mean' of that particular combination of micro-states $\phi_i, i = 1....N$ of the system, to contrast with an average of the state of that one spin, ϕ_i, in time

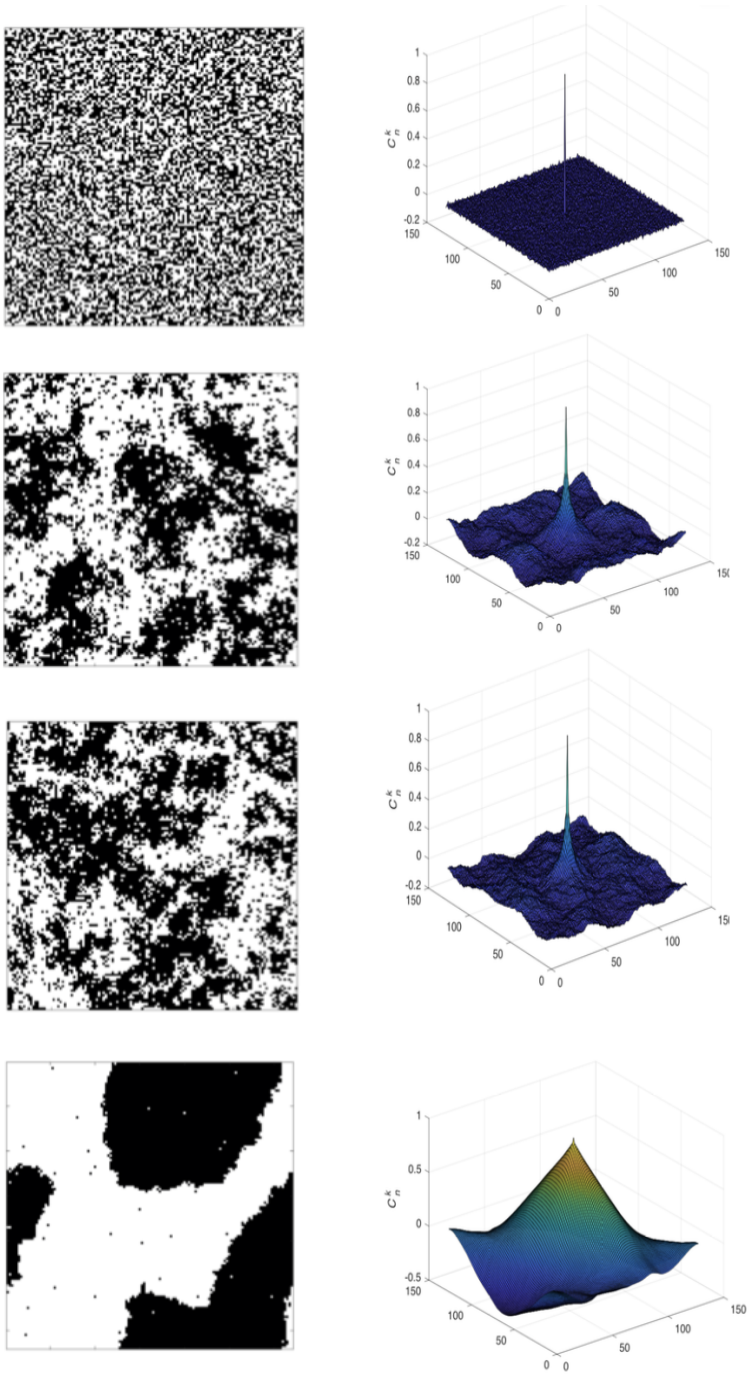

(a) **(b)**

Figure 3.1: Simulations of 2 dimensional Ising model, lattice size $N = 128 \times 128$, showing: (a), distribution of spins, and (b), spatial correlation between spins, C_n^k given by Eq. 3.2, at different temperatures, as a function of spacing from lattice position n by distance k. From top to bottom - $T/T_c = 5.0$, 1.00, 0.99, and 0.01

This model undergoes a phase transition at the critical temperature, T_c, manifested by a change in a number of macroscopic properties. The magnetisation disappears at this point (a phenomenon widely observed when ferromagnetic material is heated). Correlation between sites, given by

$$C_n^k = \langle \Delta x_{k+n} \Delta x_k \rangle = \frac{1}{N-n} \sum_{k=0} x_{k+n} x_k, \qquad n = 1, 2, ..., N, \tag{3.2}$$

also increases at the critical temperature T_c as shown in Fig 3.1.

Many studies have considered the ways by which the brain processes information on different spatial and temporal scales. Beggs and Plenz [18] first described rapidly propagating patterns of local neuronal synchrony, occurring spontaneously across a variety of spatial and temporal scales, which they called neuronal avalanches. A particular topic of debate has been around the dynamics underlying these.

A number of studies have found that their size distribution $P(s)$ decays as a power law $P(s) \sim As^{-\alpha}$, with typical values of α around 1.5 [18],[17]. By analogy with theories of self organised criticality, this suggests that the brain may operate at a 'critical' state [43], since this power law distribution of avalanche sizes is scale invariant (i.e. the relative likelihood of two different avalanches $P(ks)/P(s) \sim k^{-\alpha}$ is independent of s). This finding has been replicated in cortical slices [18] and the behaving animal [156]. In a very elegant data driven study, Fraiman [70] and colleagues investigated the distribution of clustering in fMRI resting brain networks in five human subjects. They found node-to-node temporal correlations directly from the fMRI data, and then studied the network statistical properties of the frequencies of network node average degree (i.e. number of connections) for both positively and negatively correlated networks. They found a power law distribution of average degree frequency appearing to be poised at criticality, strikingly similar in form to what might be found in an Ising model at a critical temperature.

Chialvo [43] suggested that a brain which has evolved around emergent behaviours arising out of underlying collective dynamics would allow it to exploit a wide range of sensitivity to input (e.g. discriminating sound, light, to touch across a wide range of scales) and to adapt to, or learn from its environment. Beggs and Plenz [18, 170] similarly

suggested that this might explain the brains ability to segregate or integrate information as required, for example through the concept of dynamic 'cell assemblies' [74] and a number of authors have shown how a brain poised at criticality optimises information transfer [123]. Many authors [28],[132] suggest that the brain may be in a slightly subcritical state so as to enhance stability.

Some authors have fitted characteristics of distributions to neural data to thermodynamic quantities such as specific heat after assuming a Boltzmann distributed sample [246]. However, others have stressed that such analogies need to be made cautiously. In response to Stephen's analysis of the scaling behaviour found in natural images [213], Saremi and Sejnowski showed that an independently distributed, non-critical model can spuriously give rise to seemingly 'critical' behaviour[194], and then re-analysed this same problem to show how critical scaling behaviour actually arises in that instance [193].

Many studies have identified scaling behaviours suggestive of criticality, for example in the size or duration of neuronal avalanches. However, comparatively fewer studies have identified how this may correlate with dynamical behaviour at different scales. One exception is El Boustani and Destexhe [64], who found higher dimensional chaos at the neuronal network level (studied with an asynchronous irregular neuronal network model), scaling to heirachically lower dimensional chaos found in the EEG in different levels of consciousness in humans, and in different disease states. The approach most often used in the literature on criticality in neural networks has previously been to measure power law relationships in avalanche size directly [244].

Many authors have pointed out that power law distributions are ubiquitous in nature, that it is often difficult to reliably fit power laws especially for limited data (as discussed for example, in the works of Sornette and colleagues [147]), and that $1/f^{\beta}$ scaling can arise from stochastic processes and is not necessarily evidence of criticality [16] One example is that of the statistics seen to arise from fractional Brownian processes [79].

3.1.2 Complex synchronous activity and criticality

Given that long range correlations are a defining feature of critical systems, one approach is to investigate whether there is a 'fractal scale' of correlations in cortex. Linkenkaer-Hansen [112] showed the existence of very long range temporal correlations in 10 - 20 Hz cortical oscillations from simultaneous MEG and EEG studies in relaxed awake human subjects, and further demonstrated power-law scaling behaviour in the amplitude fluctuations of these correlations. Kitzbichler et al [101] also studied power law scaling of low frequency (using fMRI) and high frequency (using MEG) oscillations in human brain activity.

However, this is not necessarily a marker of criticality either: Botcharova [28] showed that pooled pairwise phase locking intervals from a Kuramoto model in the *non* critical regime can also give rise to a power law statistic, perhaps as a consequence of superposition of a number of competing phase relationships in the model.

3.1.3 Dynamical measures of criticality

While the majority of studies have concentrated on neural avalanches, a number of others have analysed the dynamics of phase transitions using neural mass models [186].

McSharry [127] found increased EEG time series variance in the minutes before seizures; Worrell reported subtle decreases in the dimensionality of the EEG up to 25 minutes before a seizure [244].

Suffrzynski investigated the distributions of inter-ictal and seizure events in humans and GAERS rats, and showed that these durations could be reproduced by a mathematical model with bistability properties [220]. Most recently it has been proposed that an Ising - like spin model governed by a Hebbian-like wiring rule can account for burst behaviour and avalanches in dissociated cultures of rat hippocampal neurons and Leech ganglion cells [190]. Previous authors have analysed avalanches using the theory of branching processes [18], [87]. However, a potential limitation of relying on analysis of power - law like analysis methods in determining criticality is that a $1/f$ scaling in power spectra is not sufficient evidence of criticality [16].

Hence, if we want to more rigorously explore if the brain operates at a critical point, we need to find approaches outside of the statistics of power laws. One approach is to examine EEG dynamics directly, as has been done in some model studies such as Haghighi and colleagues [208]. A few studies have explored how critical dynamics may change in epilepsy (e.g. Meisel's study [132]). With the notable exception of Milanowski and Suffczynski [133], very few studies have examined dynamical markers of critical slowing at the levels of networks of individual neurones in the behaving animal. It is interesting that in Milanowski's study, the transitions to seizures did show some evidence of a critical transition in the animal model, but that these were absent in the EEG studies of human subjects.

Here, data from the GAERS rat at the levels of simultaneous depth electrode recordings from multiple areas of somatosensory and motor cortex and tetrode recordings in specific areas of somatosensory cortex and thalamus is used to explore evidence of criticality in the thalamocortical network, in the transition to seizures. Alongside this, the statistics of critical slowing such as EEG variance and scaling behaviour are analysed in the transition to seizures.

3.2 Hypotheses

In this chapter the following hypotheses will be investigated using data from the GAERS rat :

Hypothesis 1 That the onset of seizures is accompanied by a separation of dynamic timescales, with an emerging dominant dynamic driving the system into marginal stability (i.e., SWDs).

Hypothesis 2 That these changes are accompanied by a change in scaling of the EEG, and that this change in scaling represents a departure from inter-ictal scaling behaviour.

In the sections that follow, the methods used to investigate these hypotheses are presented.

To start with, the statistics which commonly accompany critical slowing are analysed in relation to seizures in Section 3.3.2. To quantify scaling behaviour with seizures both wavelet methods and structure function methods are used (Section 3.3.2), and the results of there are compared with a Fokker-Planck analysis in Section 3.3.3.

To find evidence of alteration in dynamics during the transition to seizures the Lyapunov spectrum is analysed (Section 3.3.4). To investigate whether these changes in scaling behaviour might be related to deterministic dynamics or by stochastic forcing, the deterministic contribution to the dynamics are derived from the drift coefficient of the Fokker-Planck equation.

3.3 Analysis Methods and Data Processing

3.3.1 Data collection

Details of surgery and electrode implantation techniques are explained in more detail in Chapter 2. Here, the salient features of data collection are briefly summarised in the context of the analysis which follows. Details of relevant ethics approval are also listed in Chapter 2.

Briefly, two different types of experiments were performed. The first experiment was designed to study multiple cortical areas simultaneously and involved chronic implantation of multisite depth EEG electrodes. The second type of experiment was designed to study very small regions of cortex, or thalamus, at a time. For this purpose tetrodes were used to obtain dual recordings between selected areas of cortex and thalamus simultaneously. For these tetrode experiments three GAERS rats and two NEC rats were used.

Depth electrode experiments

Rats were chronically implanted with 127 μm stainless steel electrodes bundles in which each electrode bundle consisted of insulated wires where the insulation was stripped at 0, 1.0, 3.0 and 5.0 mm from the end, enabling recording simultaneously at four different

locations in cortex. Electrodes were implanted bilaterally into S1Ul and S1Fl, S2 and IC (insular cortex), and a separate electrode was implanted into motor cortex, later in this chapter labeled M1. Extradural reference electrodes were implanted into parietal bone. These experiments were performed by Zheng[249], and rats were allowed to recover for 7 days before recording sessions.

Data was sampled at 250 Hz, for at least two 60 minute recording sessions for each rat. Both the GAERS and NEC control strain of GAERS rats used in these experiments were at least 13 weeks old, and weighed between 250 and 350 grams. Recordings were taken from different cortical areas in 5 GAERS and 3 non epileptic control (NEC) rats.

Tetrode experiments

For tetrode recordings, neuroleptanalgesia was used after induction with ketamine and xylazine, intravenous catheterisation through the penile vein and ventilation. A craniotomy and durotomy was performed prior to stereotactically guided tetrode insertion into the brain. Micro-stepper motors allowed graded electrode advancement right down to increments of 1 μm at a time. The advantage of neuroleptanalgesia is that the animal remains in a pain free quiet awake state in which seizures occur spontaneously. One disadvantage of tetrode recordings is that it is not possible to histologically confirm electrode placement, so as to clearly identify which layer of cortex the electrode was in; however stereotactic guidance allowed placement in each of S1, S2 and intermediate areas, and ventroposterior - medial (VPM) and ventrobasilar (VB) thalamus to a sufficient level of precision as to be confident in the sub region of each cortical area. These experiments were performed by Zheng [249] and the author.

Data was sampled at 25 kHz using an Intan RHD2116 amplifier system (Intan Technologies, LLC[7]), unfiltered, before being imported into Matlab for subsequent analysis. Data was initially unfiltered during collection to allow for spike sorting if needed later (even very low frequency filtering will distort spike waveforms and can affect the accuracy of spike classification). However, the analysis methods presented in this chapter are

[7] www.intantach.com

concentrated on ECoG and EEG data only and do not require spike sorting. Data was subsequently digitally filtered in Matlab for further analysis and specific details of the filtering procedures will be given where these occurred.

Unless otherwise stated in what follows, before further analysis the unfiltered tetrode data was low pass filtered up to 600 Hz using the built in elliptic filtering function in Matlab.

Seizure time stamps were determined by visual inspection. For both types of experimental data the start of seizures was taken to coincide with the first SWD. This was distinguished from coarse somatosensory rhythms that are sometimes seen in GAERS by their morphology and amplitude (greater than 400mV peak to peak, as defined by Pinault [161],[166]). When visually inspecting data, if any artifacts were present this seizure was not included in further analysis.

As discussed in Chapter 2, two of the three rats had seizures but recordings from the third rat showed only bursting behaviour between cortex and thalamus without seizures, so this data is not included in the comparisons that follow. From these first two experiments approximately 460 seizures were recorded, with between three and nine seizures per minute in each recording location. In the case of tetrode data three different areas of somatosensory cortex, S1, S2, and the junction region between these, 'S12' are analysed. In S1 there were a total of 142 seizures; in S12, 110; and in S2, 130 seizures.

In the case of depth electrode data, electrodes were placed in two regions of S1 - associated with the forelimb homunculus, as determined by the Paxinos and Watson stereotactic rat brain atlas [77], here called S1Fl, and perioral area, called S1Ul. Other regions were the insular cortex (IC), S2 somatosensory cortex, and M1 motor cortex.

3.3.2 Scaling behaviour of the data prior to seizures

Multi fractal scaling has been described in EEG analysis previously, and correlated with fMRI for behavioural tasks [229].

Statistical evidence of critical slowing

To start with, relevant statistics of the GAERS data is calculated using a moving window for the length of the data to calculate the skewness, γ, and kurtosis, κ,

$$\gamma = \langle x^3 \rangle; \qquad \kappa = \frac{\langle x^4 \rangle}{\langle x^2 \rangle^2}; \tag{3.3}$$

and the autocorrelation function at first lag i.e. Equation 3.2 for the case $k = 1$.

Structure functions and Extended Self Similarity

The concept of Extended Self Similarity was first introduced by Kolmogorov in the study of turbulence, where it was used to demonstrate the existence of scale invariance over finite but limited timescales.

The approach is to analyse the scaling between increments i.e. $\Delta x = x(t + \tau) - x(t)$. The aim is to uncover the form of its dependence on τ is - for example, evidence of a power law such as $S_q(\tau) \sim \tau^{\eta(q)}$, or in other words

$$\langle |\Delta x|^q \rangle \sim \langle |\Delta x|^3 \rangle^{\zeta(q)}. \tag{3.4}$$

It is a more effective approach than analysing correlations if one is unsure of the stationarity of the data [201], however the question of data stationarity is addressed in the results of analysis described in Section 3.3.2. As found by Benzi and colleagues [19] it can reveal scaling relations in data increments even when this is not originally apparent in the data initially. Incremental data may have a Gaussian distribution even when the original data departs from this (i.e having a heavy tailed distribution), and structure functions provide a useful way of checking for this. For the case of Gaussian distributed processes the scaling should obey $\zeta_q = q/3$.

The starting point is with the definition of a *structure function*

$$S_q(\tau) = \langle |x(t + \tau) - x(t)|^q \rangle \tag{3.5}$$

averaged over all possible pairs $(x(t+\tau), x(t))$. To find evidence of a power law such as $S_q(\tau) \sim \tau^{\zeta(q)}$, successive powers of the moments of $S_q(\tau)$ are plotted against $S_3(\tau)$. Negative and positive values of q would indicate smaller and larger increments of $x(t)$ at each time step respectively.

Consider the example of a random walk, illustrated in Fig 3.2a. This was generated as the cumulative sum of a random sample from a Gaussian process using Matlab's `rand` function. The quality of the distribution generated is shown in the inset of Fig 3.2a, fitted to a normal distribution. Fig 3.2b shows power law scaling when the ratios of $S_q(\tau)$ are plotted against $S_3(\tau)$, $q = 2, 3, 4, 5, 6$. As expected, the fit of these functions $S_q(\tau)$ is a linear function of q, with slope almost exactly (to precision of 10^{-9}) -1, equivalent to a Hurst exponent of 0.5.

The Hurst exponent H provides some information on the temporal range such that $0 \leq 0.5$ suggests mainly short range and $0.5 \leq 1.0$ suggests long range temporal dependency. Monofractal processes may show a linear fit to describe a power law $S(q) = C_q 2^{2H+1}$; multi fractal processes may show a more complex dependence $S(d, j, q) = C_q 2^{\zeta(q)}$, for some polynomial $\zeta(q) = \sum_{p=1} c_p q^n / p!$.

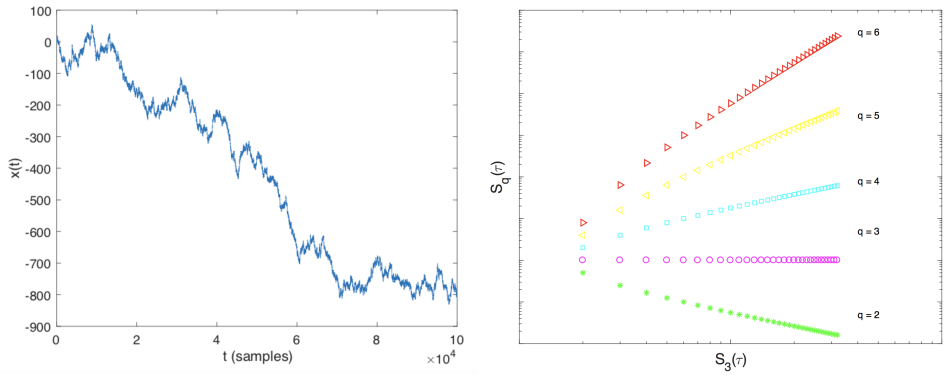

(a) **(b)**

Figure 3.2: (a)Simulation of Brownian motion, for 10^5 steps (b)Plot of the quantity $S_q(\tau) = \langle |x(t+\tau) - x(t)| \rangle$ vs. $S_3(\tau)$ for this data.

Wavelet analysis offers a way of analysing the scaling in the data. Wavelets are attractive for this purpose because of the natural 'scale invariance' of the wavelet basis function, constructed across successive scales, and again their ability to deal with non-

stationary data. Here, the Morlet wavelet, $\psi(t)$, across n successive scales $a = 2^j$, $j = 1...n$, is used. The wavelet scale shifted to position k and dilated by a factor a is

$$d_x(a,k) = \frac{1}{a}\int X(t)\psi(\frac{t}{a} - k)dt \tag{3.6}$$

Self similar or scale free behaviour will have a logarithmic relationship between the energy of wavelet coefficients and their scale, so that $x(t)$ and $\tau^H x(t)$ (or$X(t)$, if the data $x(t)$ is considered as a stochastic process) will have similar distributions. A scaling function can be defined as

$$S(d,j,q) = \frac{1}{n_j}\sum_{k=1}^{n_j} |d_x(2^j,k)|^q, \tag{3.7}$$

to describe the scaling behaviour of the wavelet spectrum, where

- As before monofractal processes may show a linear fit to describe a power law $S(d,j,q) = C_q 2^{jqH}$; multi fractal processes may show a more complex dependence $S(d,j,q) = C_q 2^{j\zeta(q)}$, where ζ is some polynomial $\zeta(q) = \sum_{p=1} c_p q^n/p!$.

- a structure function, computed from the wavelet coefficients, is defined,

$$S(d_x,j,q) = \frac{1}{n_j}\sum_{k=1}^{n_j} |d_x(2^j,k)|^q, \tag{3.8}$$

  where n_j is the number of coefficients at scale j, q is the power exponent to be found, and d_x is the wavelet coefficient defined for the Morlet wavelet above. In a piecewise linear sense, successive scales of q are added to approximate $\zeta(q)$ above.

In practice this is computed in Matlab as the sum of the n_j wavelet coefficients at each wavelet scale j. One would expect power law scaling for this model at the critical temperature as it has been shown that the eigenvalues of the coefficients arranged by scale have been shown to have a power law distribution for the Ising model at T_c[174]. In Fig D.1 one can see the intrusion of finite size effects : given the small lattice size of 128×128, boundary conditions interfere with cluster formation distributions because of their large edges compared with the relatively small grid size, visible in Fig 3.1. These effects can be seen in Fig D.1 as uneven scaling towards towards smaller scales, coinciding with the

larger cluster sizes in Fig 3.1.

3.3.3 Stochastic analysis - multiscale correlations and Fokker-Planck analysis

Another way to characterise scale-dependent fluctuations and correlations in the ECoG data is through the analysis of the joint statistics present in the data. In theory, if a general n-point description of the statistics in the data were known, the behaviour of increments in this data at different scales would allow a description of the fluctuations in the system from large to small scales and so identify scale - dependent processes giving rise to these.

The way of achieving this is through heirachically ordering suitable scales for analysis in the data, and solving a Fokker-Planck Equation across these scales. The "suitable" timescales are found as those for which the data satisfies criteria for a Markov process of either the Chapman-Kolmogorov equation (Eq 3.27), or having the 'memoryless' quality of exponentially decaying autocorrelation, or a minimum in the calculated mutual information for the time series. The steps in analysis are to characterise the joint multi scale statistics for the ECoG data via their joint probability functions, found from the joint moments calculated directly from the data. From these one can deduce the scaling behaviour of *increments* in the data. To achieve this, the approach used here is to verify that this analysis is statistically valid for the given data and then to model the drift and diffusion of probability density functions found from the moments of the data.

It might seem that the existence of long range correlations in the data arising from self similarity may rule out the possibility that a Fokker-Planck analysis could be valid. The necessary condition of having a Markov property instead implies that correlations exponentially decay, so that the data does not have long range memory, or equivalently that long range correlations cannot exist. However, even if these long range correlations are present, the Markov property may be satisfied by *increments* of the data. To show that this is indeed the case, it is sufficient to show that these increments satisfy a Chapman-Kolmogorov equation.

The algorithm for studying the scale invariance of these increments follows directly

from the derivation of the Kramers-Moyal expansion from *jump moments*. A brief recap of the derivation of the KM expansion clarifies the physical interpretation of jump moments, and is given in Appendix A.

The necessary $P(.)$ terms in Equation A.6 are found as the conditional average of the binned increments of the stochastic variable Y. These are found from the PMF distributed from the time series data, i.e. the integral in the above equation is the conditional average $\langle [y(t+\tau)-y(t)]^m \rangle$ evaluated for the instances of the spatial increments $y(t)$ equal to some value $t = T$.

In practice, to calculate the Kramers-Moyal coefficients directly from the data :

- after determining which scales are relevant for analysis[8], the data is binned. The choice of how many bins are appropriate is in part determined by the amount of data available, required to capture less prevalent transitions between values found in the data
- A conditional PDF is calculated between state transitions in the data increments
- The most direct way to calculate the conditional PDF is through Baye's theorem, from the normalised joint PDF (in one dimension, found using Matlab's `crosstab` command; in two dimensions one could either use for loops to count ocurrences, or the `reshape` command from a multidimensional histogram)
- in one dimension, the "prior probability" is the frequency of binned data at the initial scale

After finding the Markov-Einstein timescale, the one dimensional Kramers Moyal coefficients are calculated after verifying the Chapman-Kolmogorov equation is satisfied for that data. In two dimensions, to explore what relation may exist between θ and γ bands, the two dimensional Kramers Moyal coefficients that would satisfy the coupled Langevin equations

$$\partial_t \mathbf{x}_i\big|_{i\in\{\theta,\gamma\}} = D_i^{(1)}(\mathbf{x},t) + \sum_j \sqrt{D_{ij}^{(2)}(\mathbf{x},t)}\Gamma(t), \tag{3.9}$$

[8] in practise, this is known after the Markov Einstein timescale (Section 3.4.3) is determined

are found, where $\mathbf{q}(t) \equiv [\theta(t), \gamma(t)]$ is a vector of the Θ and γ passband filtered data; $i, j \equiv \{\Theta, \gamma\}$ and $\Gamma(t)$ is a Gaussian white noise term to approximate the small scale fluctuations in the data. The conditional moments are calculated directly from the data such that the moments

$$M_i^{(k)} = \frac{1}{\Delta\tau} \int d\mathbf{x}'(\mathbf{x}' - x)^k P(\mathbf{x}', t + \Delta t | x, t), \tag{3.10}$$

are approximated respectively as

$$\begin{aligned} M_i^{(1)}(P_1, P_2, \tau, \Delta\tau) &= \frac{1}{\Delta\tau} \sum_{P_i'} \Delta P_i p \\ M_{ij}^{(2)}(P_1, P_2, \tau, \Delta\tau) &= \frac{1}{\Delta\tau} \sum_{P_i', P_j'} \Delta P_i \Delta P_j p, \end{aligned} \tag{3.11}$$

where $\Delta P_i' = P_i'(t+\Delta\tau) - P_i'(t)$ and the sum is over the PDF of discretised bins forming the PDF $P_{i,j}(t + \Delta\tau)$, and p is the conditional probability of observing the data $\mathbf{q} = [q_\theta, q_\gamma]$ at time $(t + \tau)$ knowing the values at time t. To assist with writing the Matlab code for data analysis, I used the R package and documentation of [184]. This was of great assistance for debugging the Matlab code, and I also used their package for the two-dimensional analysis.

What dynamics underlie the Fokker-Planck terms found?

Here the goal is to extract a quantitative measure of dynamic changes which may underlie the different drift and diffusion characteristics we may find.

Two ways of doing this have previously been proposed : (1) following the method of Prusseit [175], and (2) following the method of Bahraminasab [12]. This latter method was applied to our GAERS data.

They showed that their rats' EEG data was able to be modelled by a Langevin equation, and found the drift and diffusion coefficients. From this they then found the flows of this system in phase space using the following reasoning. They assumed that the dynamics could be separated into deterministic and stochastic components, $\partial_t \xi = \partial_t^D \xi + \partial_t^S \xi$,

where the deterministic component is given by $\partial_t^D \xi = D^{(1)}$ and the stochastic component is $\partial_t \xi = \sqrt{2D^{(2)}\xi}\Gamma(t)$. They ignored this second term, computing the dynamics only from the effects of the drift term.

In one dimension, this amounts to solving $\partial_t^D \xi = D^{(1)}$. To explore the dynamics further between the theta and gamma bands in the data, they solved the coupled differential equation

$$\partial_t \mathbf{x}_\theta = \partial_t D_\theta^{(1)}(\theta, \gamma), \partial_t \mathbf{x}_\gamma = \partial_t D_\gamma^{(1)}(\theta, \gamma). \tag{3.12}$$

This system of equations could either be solved iteratively using coupled ODE solvers. Alternatively, one could think of the combined solution to these coupled equations as describing the phase space of interactions between the theta and gamma bands. Since there is no time dependence in the right hand side drift coefficient terms of Eq 3.12 then to first approximation

$$\frac{\partial \theta}{\partial \gamma} \sim \frac{\partial_t D_\theta^{(1)}(\theta, \gamma)}{\partial_t D_\gamma^{(1)}(\theta, \gamma)}. \tag{3.13}$$

This approach would only be valid if the data was quasi-stationary.

Another question of interest is whether there are clear changes in scaling behaviour with seizures. These are found by measuring the gradient of the one dimensional drift coefficients To solve this I used Matlab's `ode23` for this purpose, and also its built in linear curve fit functions `fitoptions`() to estimate the gradient of $D^{(1)}$.

3.3.4 Methods for establishing timescale separation in critical networks

Only a few previous studies have attempted to analyse changes in dynamical timescales in epilepsy. El Boustani and Destexte [64] related altereations in EEG dynamics found in neurodenerative diseases such as Alzheimer's disease and Creutzfeldt-Jakob disease, and also investigated stochastic dynamics in model networks relating to the dynamics of EEG changes seen across different disease states in humans.

The starting point here is to calculate the Lyapunov spectrum directly from time series data to obtain information about the different dynamic timescales which are present.

Embedding dimension of the data

One of the hallmarks of famously studied chaotic systems such as the Lorenz system of equations is that very complex system behaviour might be described by a only few variables, with marked sensitivity to initial conditions. Here we have the opposite problem: that of complex dynamics, potentially explained by an unknown subset of variables to find.

Taken's theorem[223] provides a principled way of estimating an appropriate embedding dimension in phase space for some time series data $x(t)$. The number of relevant variables describing the underlying dynamics (such that $\partial_t V = f(V)$, $V = v_1, ...v_n$) are given by the dimension of the embedding, m.

Gao (2007) [79] suggests some general considerations for choosing appropriate variables to find a suitable time delay embedding. For a dynamical system that can be described by a set of n differential equations, we can equivalently represent this system by one ODE comprising terms ∂_t^n, ∂_t^{n-1}, and so on. If we form vectors of $V_i = [x(i), x(i+L), ..., x(i+(m-1)L)]$, where m is the embedding dimension, and L is the delay time of this system, with Δt the sampling interval, this produces a mapping (i.e. dynamics) [79]

$$V_{n+1} = \mathcal{M} V_n \quad . \tag{3.14}$$

The problem of 'optimal embedding' involves the correct choice of delay time $\tau = L\Delta t$ and m, forming the embedding window $(m-1)\tau$ spanned by the reconstructed vectors V. If m is too small, the reconstructed trajectory may incorrectly intersect itself, violating the uniqueness of the embedding [37]. Below are two related methods for determining m and τ

- The *false nearest neighbours* (FNN) method[5]. This is a geometrical method that relies on the fact that there will be no self intersections when the correct embedding dimension is found. When comparing the reconstructed delay embedding vectors some dimension $(m-1)$, which is not an embedding, to m, which is, there should be a sharp reduction in the number of nearest neighbours. More precisely [79], consider the reconstructed vectors V_i^m, where m is the current embedding dimension. For

each V_i at that dimension m we then find V_j, its nearest neighbour in phase space. If we pass from m to $m+1$ these vectors are $V_i^{(m+1)} = [x(t_i)x(t_i+\tau)....x(t_i+(m-1)\tau x(t_i+m\tau)] = [V_i^{(m)}x(_i+m\tau)]$ and $V_j^{(m+1)} = [V_j^{(m)}x(_j+m\tau)]$ will now not be close together.

This gives a criterion for optimal embedding. After finding the distance between all nearest neighbours in m dimensional Euclidean space as

$$a(i,m) = \frac{||x(t_i+m\tau) - x(t_j+m\tau)||}{||V_i^{(m)} - V_j^{(m)}||}, \tag{3.15}$$

and choose m such that this is greater than some threshold value. Most agree that this is a reliable method, but Gao [79] points out that it is less reliable in the presence of noise.

- Another method, of ensuring consistent reconstructed vector norms in subsequent embedding dimensions, was suggested by Cao [37]. It is based on the same ideas as that of Abarbanel and colleagues above[5]. The difference with his method is that he defines a mean value of all the distances between reconstructed vectors in the time series of length L, in his notation $E(m) = \langle a(i,m)\rangle = \frac{1}{L-m\tau}\sum a(i,m)$. To see how this varies from $m-1$ to m, we plot the quantity $E1(m) = \langle E(m+1)/E(m)\rangle$. He also defines another measure, used to distinguish stochastic from deterministic signals, E2. If, for each x_i, we have found the nearest neighbours (in his notation) $x_{n(i,m)}$ of x_i, the measure

$$E2(m) = \langle E^*(m+1)/E^*(m)\rangle, \quad \text{for} \quad E^*(m) = \langle |x_{i+d\tau} - x_{n(i,m)+d\tau}|\rangle. \tag{3.16}$$

The choice of τ can appear to be more arbitrary, because it is mathematically independent from the choice of m. In the limit of the absence of noise, or infinite data lengths, it would be arbitrary and should not influence results. However, too small values of τ will lead to increased correlation between successive points in the embedded data, and too large values of τ would lead to large, uncorrelated, separated points in phase space. Guides to choosing τ are (1) the first zero of the autocorrelation function of the data; (2)

the first minimum of the mutual information in the data; or (3) by inspection, a fraction such as 1/4 of the known period of the data[31],[5].

Lyapunov Spectrum

To calculate the Lyapunov spectrum we used the approach of Eckmann and Ruelle [62],[63], with extensions of this idea based on Brown and colleagues [31] and Yao [245]. The background to Eckmann and Ruelle's method relies on calculating the linearised Jacobian matrices of the flow[9] to calculate local Lyapunov vectors and exponents, orthonormalised periodically to prevent numerical overflow. We assume that the dynamics of the GAERS rat ECoG generating our data can be described by a map, for the discrete case, $x(n+1) = F(x(n))$, for a variable x that varies over the phase space M. Lets first assume this space is linear, then question this assumption once we come to analyse the timescales in the data. We first want to find the matrix

$$D_f^k = D(f^{n-1})...D_x(f(x)), \tag{3.17}$$

the matrix of partial derivatives of the m components of F(x) with respect to the m components of x.

Taking small steps along the orbit at successive times T_2, a small perturbation $\delta\mathbf{x}$ will propagate according to a relation satisfying $\delta\mathbf{x}(t+T_2) = D_f(\mathbf{x}(t))\delta\mathbf{x}(t)$. If we evaluate the product of successive Jacobian matrices for K steps along the orbit, then

$$D_f^k = D(fk) \cdot D(f(k-1) \cdot ... \cdot D(f(1)), \tag{3.18}$$

and Oseledec's multiplicative ergodic theorem suggests that the Lyapunov exponents are given by the (log of the) eigenvalues of the matrix

$$\lim_{L\to\infty} [(D_f^K)^T (D_f^K)]^{\frac{1}{2K}}, \tag{3.19}$$

[9] that is to quote their description (p. 2787), and their third equation, in that they are really calculating $J^T J$, where T is the transpose

where ^{T} is the matrix transpose.

Given that we have experimental data represented by a scalar time series $x(n), n = 1, ..., L$ rather than model equations for our system we need to find an estimate of D_f from the data. Even before starting there are problems. If the dynamical system which adequately produces our data is embedded in high dimensions and/or noisy, numerical instabilities will be magnified when multiplying these matrices together, leading to an ill conditioned final matrix above and errors in the eigenvalues. Opposing problems in practically calculating the Lyapunov spectrum using this approach also arise because (1) positive exponents by their definition suggest exponentially divergent trajectories, so multiplying these together may quickly lead to numerical overflow - this is dealt with by frequent orthonormalisation; and (2) the attractor may be 'thin' in places with relatively few trajectories covering it, leading to singular matrices of rank less than the dimension required to embed the data. The ways around these various problems are detailed below.

The task for calculating D_f amounts to that of finding local maps $\mathbf{F}$ of the local trajectory in phase space. To represent the scalar time series data as a series of vectors describing an orbit in phase space I used Takens' theorem, the method of time delays to represent this scalar time series data $x(n)$ as a series of vectors in phase space.

$$\mathbf{y}(n) = [x(n)x(n+T), ..., x(n+(d-1)T] \quad . \tag{3.20}$$

This is based on Whitney's theorem, which states that any smooth manifold of D dimensions can be embedded in a Euclidean $2D+1$ dimensional space, and we accept that this theorem is proved only for integer values of D. Further, Taken's theorem suggests that an attractor can be reconstructed from the method of time delays to be have the same topological properties (i.e. similar dynamics). However, it will vary in appearance depending on the time delay chosen, and since the dimension m is not directly observable it can only be either estimated or inferred from the sufficiency condition of Taken's theorem above.

Assuming that the $y(k)$ evolves according to some map $y(k) \rightarrow y(k+T) \equiv \mathbf{F}(y(k))$, we want to find a *local linear map* of nearest neighbours around a point $y(k)$, to the next

point $y(K+T)$. Consider the rth nearest neighbour of $x(n+T)$,

$$x^r(n+T) = \mathbf{F}(n+T) = [F_1(\mathbf{x}^r(n)), F_2(\mathbf{x}^r(n)), ..., F_m(\mathbf{x}^r(n))] \quad . \tag{3.21}$$

Consider the αth component of $\mathbf{x}^r(n)$, i.e. $\mathbf{x}^r_\alpha(n)$ and $\mathbf{x}^r_\alpha(n+1)$ respectively. The tangential map of the dynamics linking $\mathbf{x}^r_\alpha(n)$ to $\mathbf{x}^r_\alpha(n+1))$ can be represented by $F_\alpha(\mathbf{x}^r(n))$, found by a Taylor expansion

$$x^r_\alpha(n+T) = F_\alpha(\mathbf{x}^r(n)) = a_\alpha + \sum_{i=1}^{m} b_{\alpha i} x^r_i(n) + \sum_{j,k=1}^{m} c_{\alpha jk} x^r_j(n) x^r_k(n) + ... \quad . \tag{3.22}$$

Now the task is to find the coefficients a_α, $b_{\alpha i}$, and $c_{\alpha jk}$.

To accomplish this we construct a matrix equation $\mathsf{V}^\alpha = \mathsf{X}\mathsf{B}^\alpha$, where B^α is the matrix of linear mapping connecting local neighourhoods of nearest neighbours at time n, X, to local neighbourhoods at time $n+1$, V.

Consider first the case where we truncate this expansion to first order. In the case of $T = \tau, x^r_\alpha(n+1) = x^r_{\alpha+1}(n)$ for $\alpha = 1, 2, ..., m-1$, we find, after a lot of algebra leads to a matrix equation for the Jacobian matrix for this time step, $\mathsf{J} \equiv \frac{\partial F_p}{\partial x_q}|_{x^r_q(n)}$ as

$$\begin{bmatrix} 0 & 1 & 0 & \dots & 0 \\ 0 & 0 & 1 & \dots & 0 \\ \vdots & \vdots & \vdots & \ddots & \vdots \\ 0 & 0 & 0 & \dots & 1 \\ a_1 & a_2 & a_3 & \dots & a_m \end{bmatrix}, \tag{3.23}$$

allowing us to find the a_k's by a least squares fit of the term

$$\min\Big(\sum_{j \in \mathsf{S}_i(r)} \Big[\sum_{k=0}^{m-1} a_{k+1}(x_{j+k} - x_{i+k}) - (x_{j+m} - x_{i+m}) \Big]^2 \Big), \tag{3.24}$$

where $\mathsf{S}_{i(r)}$ is the set of neighbours $\mathbf{x}_j$ within a radius r of $\mathbf{x}_i$. To calculate the least squares fit the Matlab backslash operator was used i.e. `B = V/X` since this uses a least

squares fit to invert the B matrix giving less error than the alternative `lsqlin` command.

Once the local neighbourhood mappings B have been found, a QR factorisation (using the `qr` command in Matlab) was used to calculate the L's.

Now that the Lyapunov spectrum is known, information about relevant timescales of dynamical processes can be found. Information about timescale separation in a system described by a mapping of its dynamics can be calculated, providing this mapping is known. The background and proof of this is given from a differential geometric perspective in [129] and summarised here.

Let's say we have found the local Jacobians, described by the product of transition matrices described by Eq. 3.18 governing the map. From this, the Lyapunov spectrum is also known. The Lyapunov vectors, and timescales, can be equivalently found either using a singular value decomposition approach, or QR factorisation.

The local Lyapunov exponents and vectors describe how a sphere of initial conditions evolves into a m-dimensional ellipsoid, depending on the different timescales present in the dynamics of the system. We can use this to analyse what these timescales are. Mease (2003) [129] provides a theoretical framework for this, in which the steps are as follows. Consider a nonlinear system in which a mapping Φ is known such that some vector $\mathbf{v}$ in a compact region of phase space evolves into $\mathbf{v_T} = \Phi(T, x)\mathbf{v}$ after some time T along the orbit ϕ. Then:

- the singular value decomposition of the transition matrix Φ is $\Phi = N\Sigma L$, where N and L are $m \times m$ orthogonal matrices and Σ is a diagonal matrix. Rearranging terms, we have

$$\Phi L = N\Sigma. \tag{3.25}$$

  From Oseledec's theorem, if the SVD of Φ has m distinct values, these values then describe a filtration of nested subspaces of χ [129], and one representation of these subspaces is in terms of the column vectors of L :

$$L_1 = \text{span}\mathbf{l_1}; L_2 = \text{span}\mathbf{l_1}, \mathbf{l_2}; ...; L_m = \text{span}\mathbf{l_1}, \mathbf{l_2}, ..., \mathbf{l_m}. \tag{3.26}$$

If we view the columns of L as vectors in our phase space (χ), then the principal axes of the ellipsoid of evolution is described by the column vectors of N, and the degree of expansion or contraction by the diagonal elements σ, such that $\Phi l_i = \sigma_i n_i$.

- The spectrum of Σ is the spectrum of Lyapunov exponents. A spectral gap in the Lyapunov exponents which persists over some time frame T_2, $\Delta\sigma$ indicates suggests a splitting in subspaces e.g. L_j and L_{j+1} that can be resolved[129].

Coherent structures

When considering the strength of driving network activity (in Ch 4), and changes in resonance as an expression of these changes in dynamics (in Ch 5), it would be interesting to see if any elements were common to multiple channels at a time. To see how common elements of coherence and ECoG spectral energy change between cortex and thalamus with the evolution of seizures, the coherent structures that exist in the tetrode sampled data were analysed.

In terminology borrowed from the turbulence literature, coherent structures can be described as "persistent macroscopic structures amidst small scale activity" [31]. The singular value decomposition approach, summarised in Appendix B was used to examine the temporal evolution of dominant coherent structures participating between cortex and thalamus.

3.4 Results

3.4.1 Statistical measures of criticality

To start with the statistical moments in the data were examined to see if there was any change in these prior to seizures. The first four moments were calculated, with the skewness and kurtosis defined by Eq 3.3. Figure 3.3 shows an example of how these quantities vary over a one minute recording (Rat 1, recording # 202207) containing four seizures. This example shows a stable but lower mean outside of seizures, some increase in kurtosis and

variance with a reduction of the inverse coefficient of variation at the commencement of seizures.

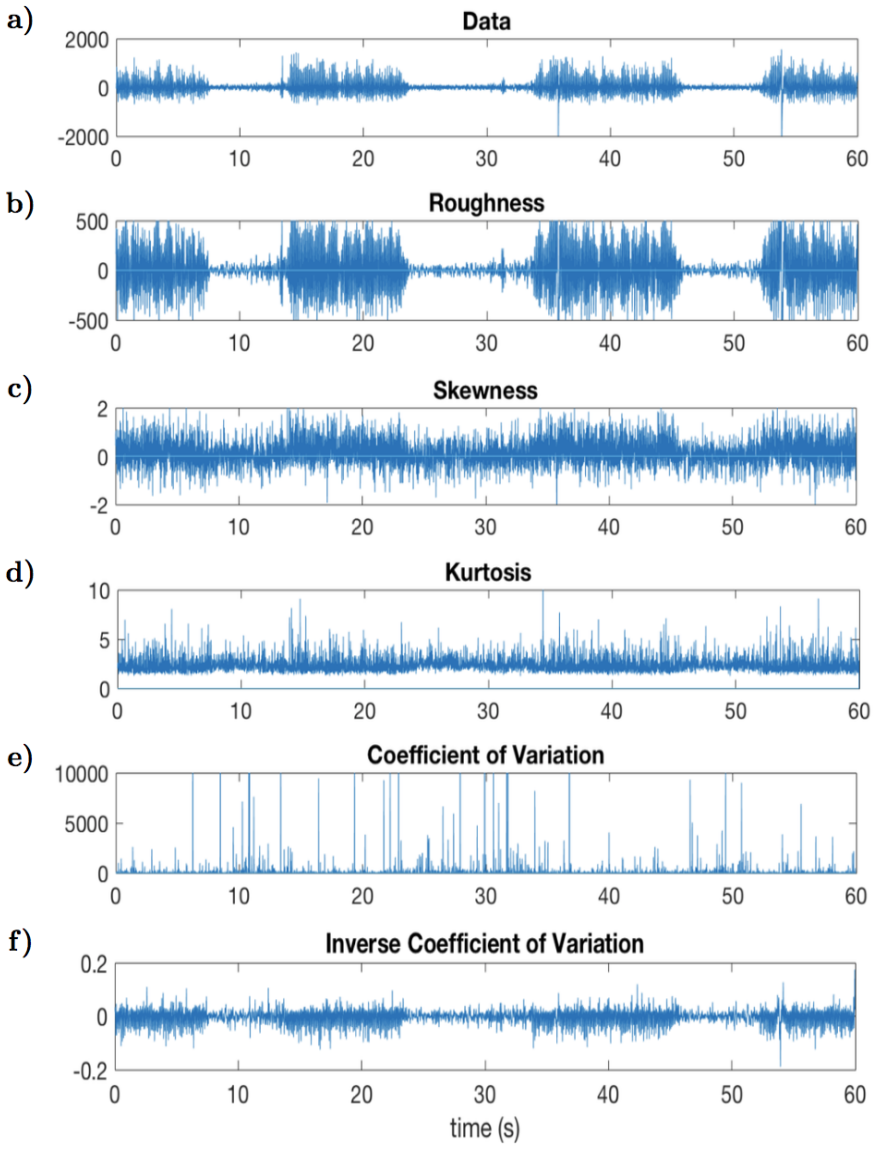

Figure 3.3: Statistical changes in tetrode data with seizures. From top to bottom : (a) the data itself, bandpass filtered between 1 - 600 Hz; (b) mean; (c) skewness; (d) kurtosis; (e)coefficient of variation and (f) inverse coefficient of variation

To see if this indicated a wider trend, the skewness, kurtosis, and coefficient of variation was calculated at specific time points for all of the available tetrode data and is shown below in Fig 3.4. For generating the results shown in this figure, a sliding window of

1000 points with 50% overlap was used for each of six arbitrary time points (the midpoint between seizures in the inter ictal period; four, three, two, and one second before; and the first second of the seizure). For each given second-long segment of analysis, 47 overlapping windows were generated, giving 2632 samples for each timepoint apart from the mid seizure point. This point resulted in only 1645 samples being available for analysis because of the requirement of an inter-ictal period greater than 11 seconds which excluded shorter inter-ictal periods between seizures from further analysis. Mean, variance, skewness and kurtosis were calculated using proprietary Matlab commands. The error bars in Fig 3.4 were calculated from the confidence interval found from the mean and standard deviation of the data, using Eq. 5.23.

Theses results show that the mean, variance, skewness and kurtosis are relatively stable prior to seizure onset, but after this there is a marked change in these parameters.

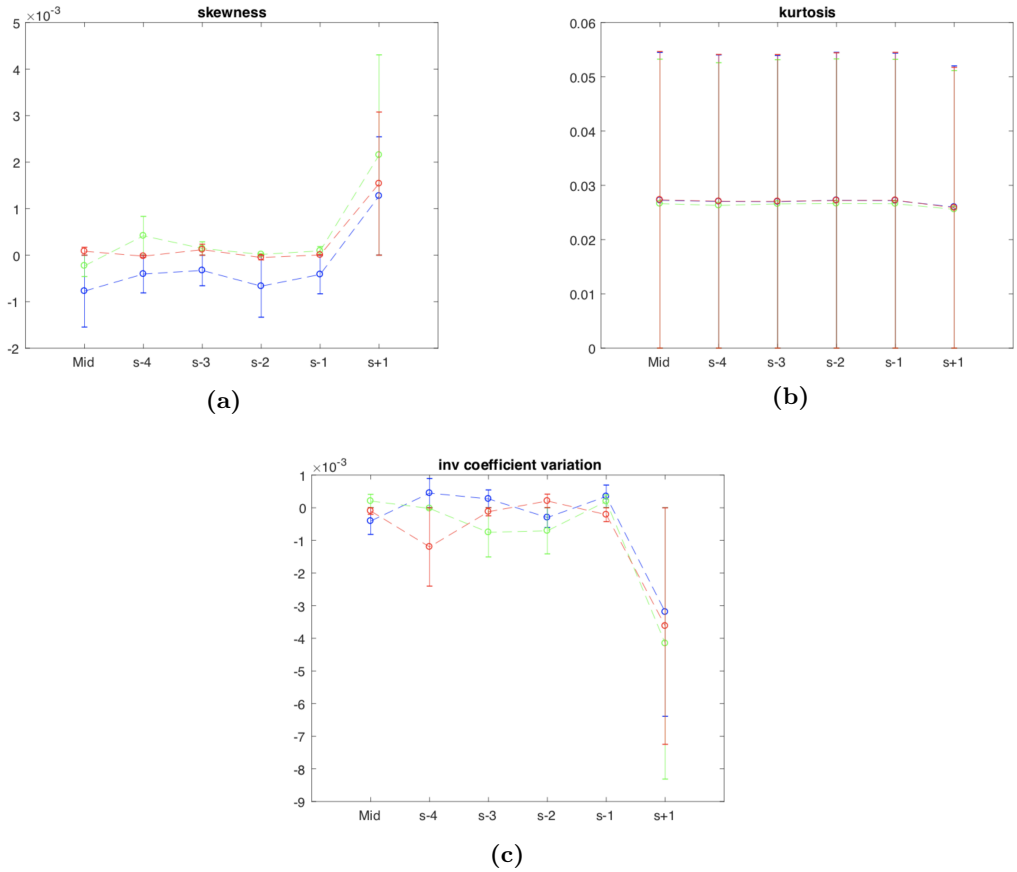

Figure 3.4: Statistics of (a) skewness, (b) kurtosis, and (c) inverse coefficient of variation for all available tetrode data

3.4.2 Evidence of multfractal scaling and its change with seizures

Analysis by Extended Self Similarity, shown in Fig 3.5, naturally gives some intuition into the scaling behaviour of the EEG in relation to seizures. To start with, the scaling relation $S_3(\tau)$, defined by Eq. 3.5 and calculated for values of τ between 5 and 800 samples, in increments of 4 samples at a time, i.e. increments Δt are defined as the differences in increments separated by time τ, given by $\Delta t = x(t+\tau) - x(t)$. This range was chosen so as also to encompass the small scaling region expected to be dominated by 'noise' at $q \ll 1$, the valid region of scaling for Fokker-Planck analysis discussed in Section 3.4.3 where the Markov-Einstein timescale was found at ~ 0.03 seconds, and the scaling behaviour seen at larger scales of $q > 1$.

The behaviour of the structure function $S_3(\tau)$ is shown in 3.5a. Interestingly, this shows a type of 'devil's staircase' behaviour at values of τ between 30 and 200, and when plotted against other powers of q, linear relations can be seen, as clear evidence of extended self similarity for the values of τ investigated here, as shown in Fig 3.5b.

To find the scaling behaviour, $S_q(\tau) \sim \tau^{\zeta(q)}$, successive powers of the moments of $S_q(\tau)$ are plotted against $S_3(\tau)$ (note that these are plotted for all values of τ). The straight lines seen are characteristic of ESS. The scaling exponents ζ_q are calculated by finding the gradient of the fit for each curve $q = 2, 3, 4, 5, 6$ in fig. 3.5b. This is shown in Figure 3.5c as a progressive curve for each epoch of data at seizure termination, just prior to seizure onset, and for inter-ictal data each of two seconds' duration (i.e. 50 000 samples). In figure 3.5d, one can see the departure from multifractal scaling inter-ictally in the pre seizure period, which is also seen in the results of wavelet scaling analysis presented in the next section. From this figure one can also see deviation from Gaussian statistics, suggestive of long-tailed increments in the data, demonstrated when ζ_q deviates from 1/3 as in Fig 3.5c.

Figure 3.6 shows an example of changes in wavelet scaling behaviour with seizures in the S2 region of a GAERS rat (recording # 200813). One can clearly see that there is a breakdown of scaling in the immediate pre-ictal period, approaching a flat gradient. The predominance of lower frequency change is consistent with the observation of an increase

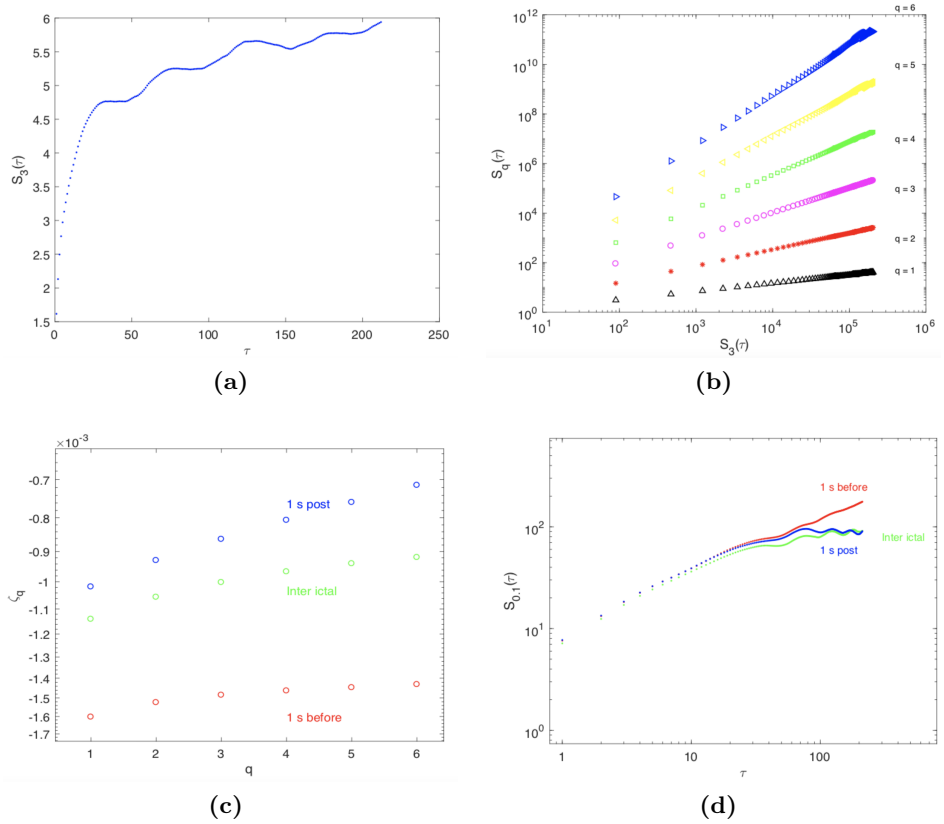

Figure 3.5: Extended Self Similarity scaling for tetrode data. (a) Example of analysis of scaling based on the concept of Extended Self Similarity showing $S_3(\tau)$ calculated for τ using Eq. 3.5 b) Scaling relations between $q = 2, 3, 4, 5, 6$ shown by plotting these against $S_3(\tau)$. (c) Exponents ζ_q extracted as gradients of the straight lines fitted for $q = 2, 3, 4, 5, 6$, for segments of data immediately after a seizure (green), inter-ictal (blue), and immediately prior to a seizure (red); (d) differences in small scales, seen for $S_{0.1}(\tau)$, each of the three time periods shown in (c).

in lower frequencies of the power spectrum just prior to seizures as found in Ch 5, and also demonstrated by other authors, e.g., [206]. Although this is not direct evidence of critical slowing it is consistent with the phenomenon of 'red shift' which is often associated with this, and also the Lyapunov spectrum changes reported later in this chapter.

To see whether there are any differences in scaling between regions For the analysis shown in Fig 3.7 Morlet wavelets were used. Parameters of Eq. 3.6 were chosen for 64 wavelet coefficients to resolve down to a scale corresponding to 0.2 seconds temporal resolution, so the minimum resolvable frequency component for one second's worth of data was 2 Hz. To generate Fig 3.7a, scale coefficients were summed and the gradient for the

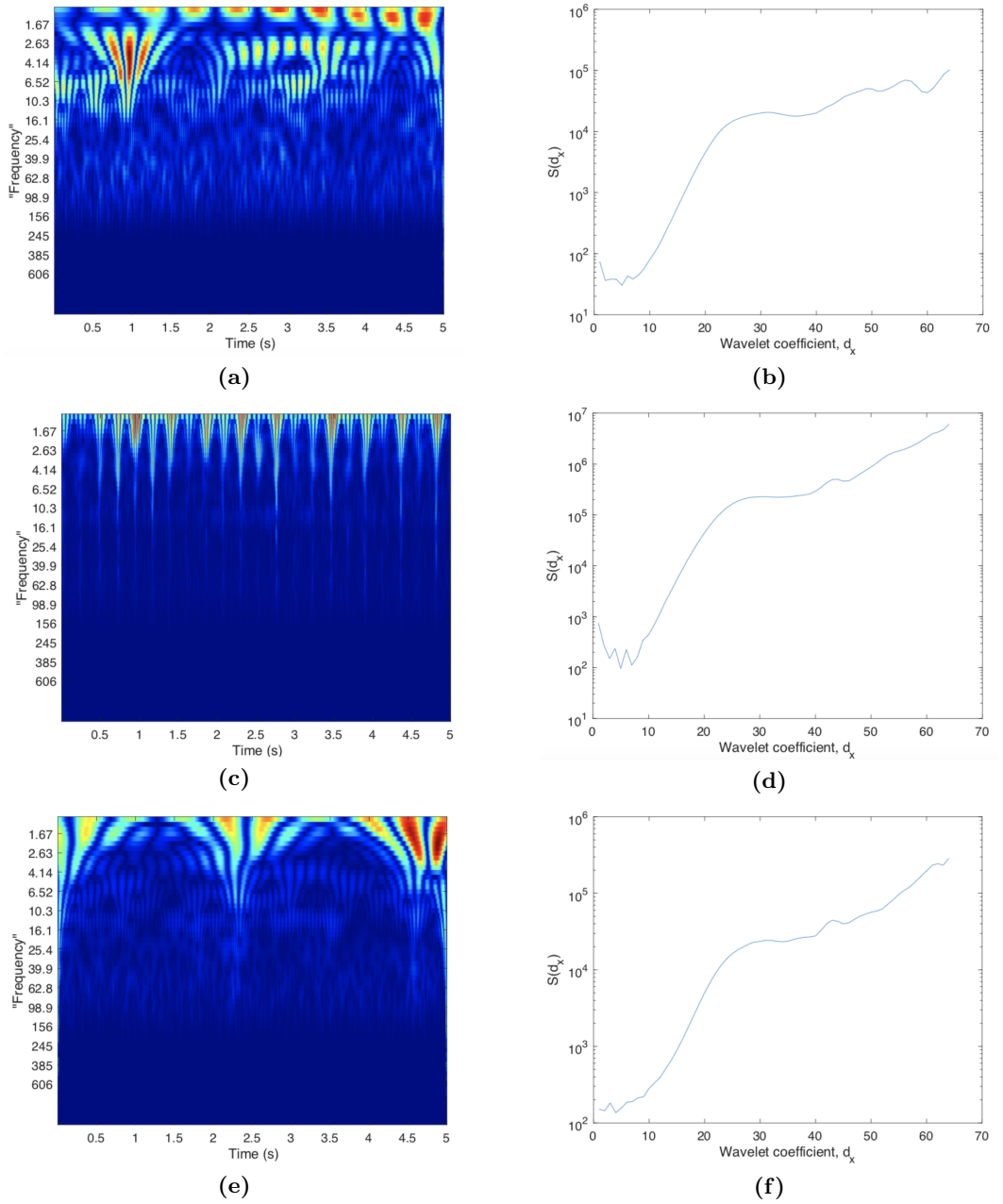

Figure 3.6: wavelet scaling analysis for a GAERS rat in S2 region, from tetrode data. Plots on the left, show contour plots of the wavelet spectrum for data of 4 seconds' duration for a) pre-ictal, c) ictal; and e) post-ictal periods. Here the vertical axis show "frequencies" calculated from the wavelet scales as a function of time (horizontal axis). Data was sampled at a rate of 25 kHz, and lowpass filtered to 600 Hz prior to analysis. Plots on the right show the scaling function given by Eq. 3.7 for b) pre-ictal, d) ictal; and f) post-ictal periods respectively

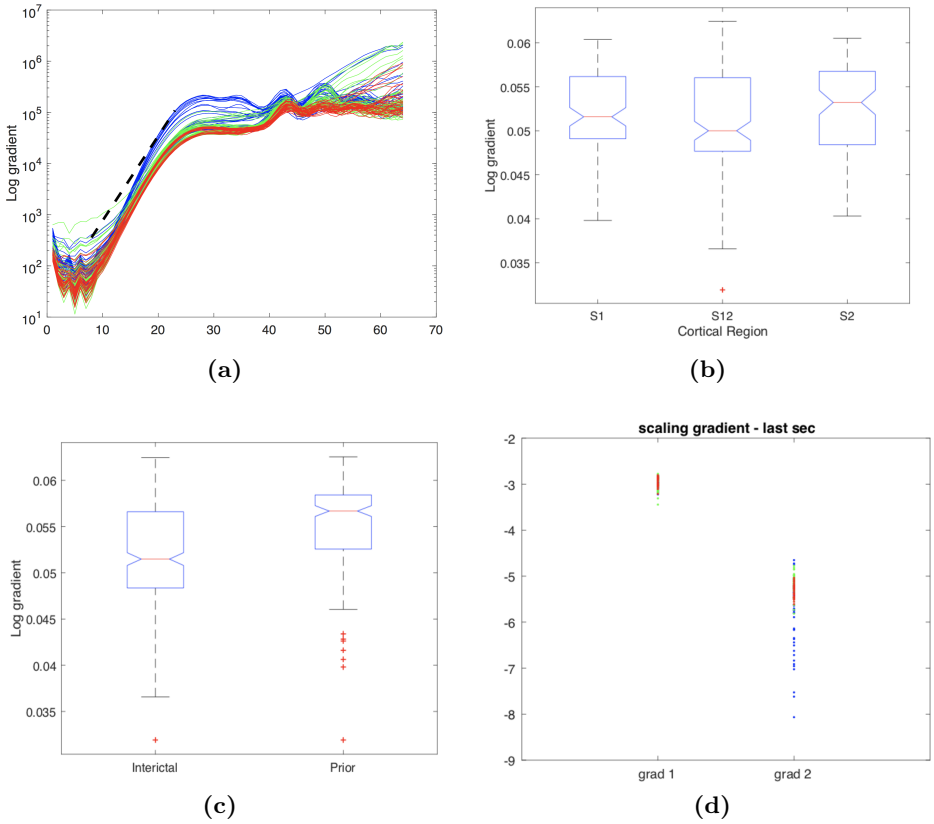

Figure 3.7: Top: Statistics of wavelet scaling for tetrode data. (a) Distribution of scaling for three cortical regions S1 (blue), S2 (red), and the junction region S12 (green) and b) distribution of gradients fitted for these regions. (c) Difference in scaling between inter-ictal and in the last second prior to seizures, for all regions and (d) The 'spread' of scaling seen from the data

two linear segments seen on the semilog plot estimated with Matlab's `fit` command using the `exp1` option. The statistics of changes in gradient of these segments were analysed using an ANOVA with results shown in Figs 3.7a - Fig 3.7d. For this, the gradient of the 15 coefficients comprising the black dotted line inset in Fig 3.7a were calculated for all available seizures found in the tetrode data. The inter-ictal data chosen for analysis was at the midpoint between seizures given the variable amount of time between seizures. Analysis for inter-ictal data was restricted to those intervals between seizures of more than 11 seconds.

From these results, some important features emerge. Firstly, there was a change in scaling gradient between inter-ictal data and in the second immediately prior to seizures

for the S2 ($p < 2 \times 10^{-13}$) and the S12 ($p < 10^{-7}$) regions, but not S1. The difference in gradient was not statistically significant for the S1 region at $p = 0.616$. The scaling between cortical regions was also significantly different from each other at $p < 0.0009$. Qualitatively, one can see that the S12 region show a much wider range of scaling with almost a 'scale free' linear character, whereas the S2 region is more tightly consistent from all the available tetrode data analysed.

3.4.3 Fokker-Planck analysis

If critical slowing is present prior to seizures, one might also expect to see an increase in non-local, longer range correlations and heavier tailed distributions, as suggested in the preceding scaling analysis of Section 3.4.2. If longer range correlations are present, it might seem at first glance that Fokker Planck analysis should not be valid as the data deviates from Markovian "memoryless" properties, making this analysis approach inappropriate. However it is possible that increments in the data still retain their Markovian qualities despite this, as demonstrated by [12]. This implies that a Fokker-Planck equation can still meaningfully approximate the statistics of the data.

Validity of the Markov assumption and Fokker Planck approximation

A starting point is to show that the data is quasistationary, with stable values for the first four statistical moments. To calculate the mean and variance, the usual definition is used[10], and the skewness and kurtosis are defined by Eq 3.3.

To verify the Markov assumption is valid it is necessary to show that the Chapman-Kolmogorov (CK) equation,

$$p(x_2, t_2|x_1, t_1) = \int dx_3 p(x_2, t_2|x_3, t_3) p(x_3, t_3|x_1, t_1), \tag{3.27}$$

holds for some times $t_2 > t_3 > t_1$. In the top rows of Figure 3.8 the LHS of the CK

[10] i.e. the mean, $\langle x \rangle$, of a set of N observations x_i is $\frac{1}{N}\sum_N x_i$; the variance of these same observations is given by $\frac{1}{N-1}\sum_N |x_i - \langle x \rangle|^2$

equation is calculated directly from the data, and the RHS is calculated numerically by multiplying the conditional probabilities at the respective timescales $t_2 \rightarrow t_3$ and $t_3 \rightarrow t_1$ together. The results are clearly congruent for $\tau = 5$ (Fig 3.8a) and $\tau = 10$ (Fig 3.8b).

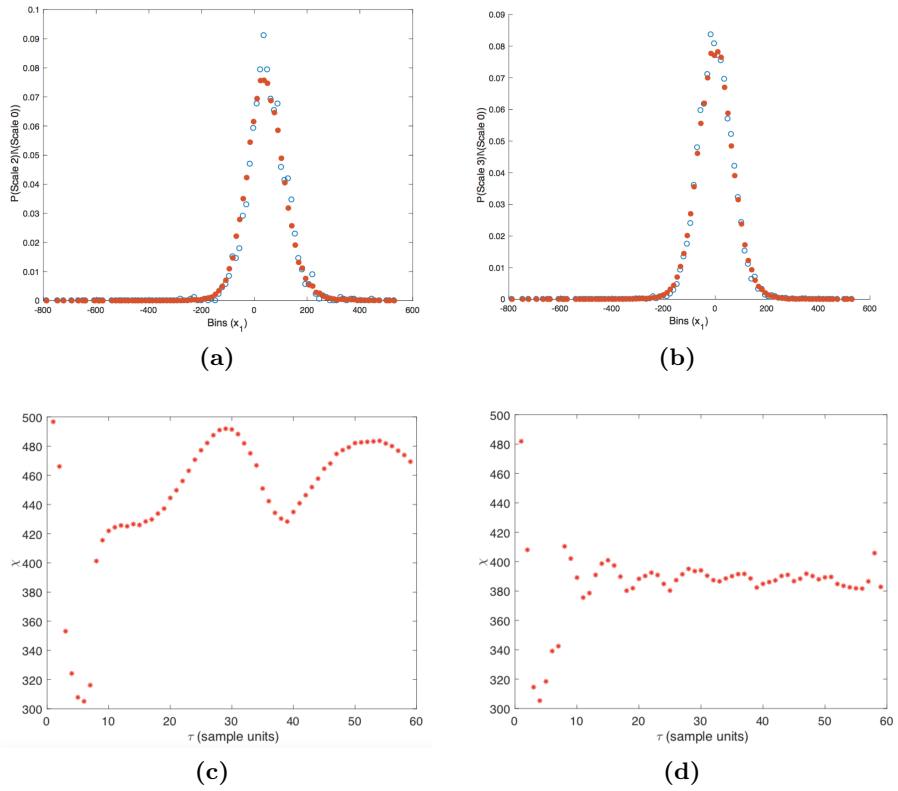

Figure 3.8: Top : Numerical verification of the Chapman-Kolmogorov equation from unfiltered data, at 'timescales' (a) $\tau = 5$ and (b) $\tau = 10$. Open circles are the PDF calculated directly from data, and closed circles are integrated Bottom : calculated Markov-Einstein timescale τ_M, estimated from Eq 3.28

Markov Einstein time scale

The interpretation of the Chapman-Kolmogorov Equation, Eq. 3.27, is that the data retains a 'memoryless' quality, that only more recent conditional probabilities of a system's previous states account most for finding it in it's current state at that time.

A relatively direct approach is to find the time scales $t_3 - t_1$ at which the discrepancy between the LHS and the RHS of Eq 3.27 is minimised. To clarify this a useful approach

is to calculate the quantity

$$\chi^2 = \int \Big(\prod_{i=1}^{3} dx_i \Big) \frac{[p(x_3, t_3; x_2, t_2; x_1, t_1) - p(x_3, t_3|x_2, t_2)p(x_2, t_2|x_1, t_1)]^2}{\sigma_j^2 + \sigma_k^2}, \tag{3.28}$$

as a function of the timescale τ. Here σ_j^2 and σ_k^2 are the variances of $p(x_3, x_2, x_1)$ and $p(x_3, x_2)p(x_2, x_1)$ respectively. The Markov condition is fulfilled when this quantity approaches zero. Bahraminasab and colleagues [12] calculated this to be just over 0.1 sec 3.8c. Here, a minimum is clearly seen at τ = six samples (i.e., $t = 0.025$ sec). This is in good agreement with the direct iteration of the Chapman-Kolmogorov equation, Eq 3.28, at the same timescales, where a good fit between probability distributions is seen in Figs 3.8a and 3.8b. In Fig 3.8d the same quantity is calculated for tetrode data, at timescales $\tau_1 = 250$ samples, and $\tau_2 = 400$ samples. Again this shows good agreement, as expected since these same timescales show a valid reconstruction of the Chapman-Kolmogorov equation (data not shown for brevity).

Another possible method for estimating appropriate timescales for analysis is to calculate the first minimum of the mutual information for the data (this data is not shown). This method gave a somewhat 'noisy' estimate of the Markov timescale of 11 ms. This method was not used further in this thesis.

To check that Pawula's theorem is satisfied, the ratio of the fourth and second Kramers-Moyal coefficients was calculated to ensure that this quantity was negligible (i.e. that KM4 was $\ll$ KM2^2, less than 0.05%). This criterion was valid, which means that the higher Kramers-Moyal coefficients above the first two could be ignored for the present analysis, and that a Fokker-Planck equation can approximate the statistics of moments found in the data.

Analysis by somatosensory cortical areas in one dimension

A comparison of Kramers-Moyal coefficients from the depth electrode data across different

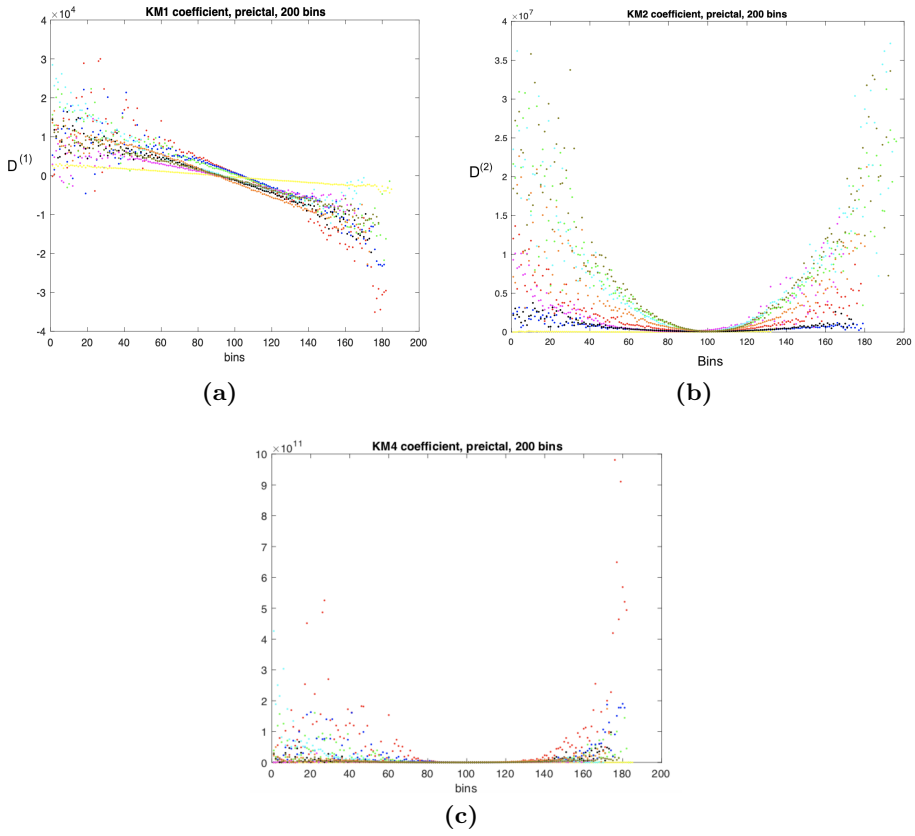

Figure 3.9: Kramers-Moyal coefficients for different cortical areas, bilaterally from depth electrode data, from a NEC rat: yellow, S2, orange and red, IC, green and blue, S1. a) KM1; b) KM2; and c) KM4.

cortical areas is shown in Figs 3.9, 3.10, and 3.12. To generate this result, 8 sec of continuous depth electrode data, sampled at 256 Hz, from a NEC rat (rat #1) was used. To see that this was a consistent finding over a long segment of data, analysis was also undertaken over further smaller snippets of data both within and outside a 40 second epoch of data (∼10000 data points), to ensure calculated drift coefficients were consistent over this longer data length. Altered scaling between different cortical areas was seen across all examples of data considered, as well as in GAERS rats. To test this, separate analyses of 20 seconds of continuous depth electrode data, sampled at 256 Hz, from GEARS rat # 7 was used (this data is not shown).

Figure 3.9 shows that different cortical areas have different scaling behaviour, as seen by the changing slope of $D^{(1)}$. Very interestingly, this observation is consistent with the observation of different fundamental frequencies of instantaneous theta rhythm oscillation, discussed in Chapter 5 (Section 5.3.2).

Analysis by somatosensory areas in two dimensions

Figure 3.10 shows that the two dimensional coefficients $D^{(1)}_{\theta\theta}$ and $D^{(1)}_{\gamma\gamma}$ are largely independent of each other, i.e. there is not strong dependence of the γ frequencies on the dominant θ frequency.

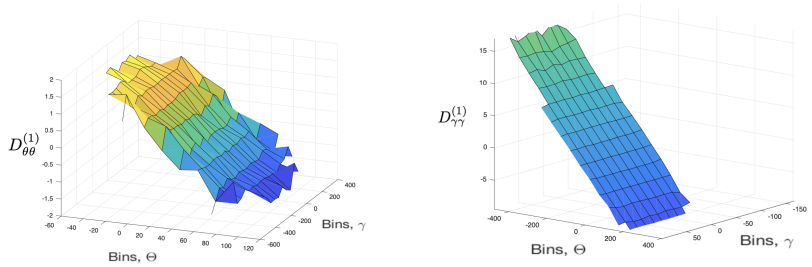

(a) **(b)**

Figure 3.10: 2 Dimensional Kramers-Moyal coefficients $D^{(1)}_{\theta\theta}$ and $D^{(1)}_{\gamma\gamma}$ for cortex in a NEC rat. (a) Two dimensional drift coefficients as a function of θ and γ frequencies, $D^{(1)}_{\theta\theta}$, for cortical area S1UL (b) $D^{(1)}_{\gamma\gamma}$ for the same cortical area in a). The horizontal axes in these plots represent bins

Looking at the bin limits shown in the horizontal axes of the plots in Figure 3.10, one can see that the data is not completely populated across the entire space of increments possible. The reason for this is shown in Figure 3.11, where not all conditional probabilities are present in the data.

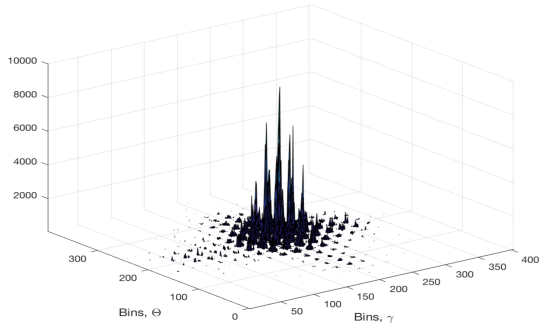

Figure 3.11: Plot of conditional moment $M^{(1)}_{\theta,\gamma}(P_\theta, P_\gamma, \tau, \Delta\tau)$, from Equation 3.11

Diffusion coefficients $D^{(2)}_{\theta\theta}$ and $D^{(2)}_{\gamma\gamma}$, shown in Figure 3.12, also did not show strong interdependence.

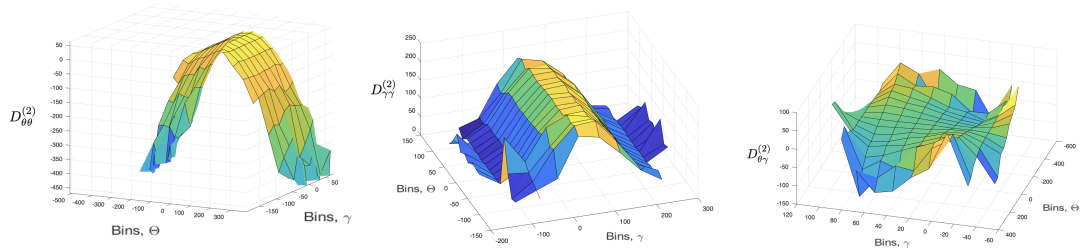

(a) **(b)** **(c)**

Figure 3.12: (a) $D^{(2)}_{\theta\theta}$ for cortical area S1UL, (b) $D^{(2)}_{\gamma\gamma}$ and (c)$D^{(2)}_{\theta\gamma}$ for the same cortical area in a). Horizontal axes denote bins, as in Fig 3.10

In agreement with this, from Fig 3.12c it can indeed be seen that the interdependence of the cross term $D^{(2)}_{\theta\gamma}$ was weak.

Change in drift coefficients prior to seizures

A plot of the change in the drift coefficient in the depth electrode data of a GAERS rat (# 7) is shown in Fig 3.13 between four seconds' interictal data (20 seconds prior to a seizure), and in the four seconds prior to the next seizure seizure which occurred 20 seconds later.

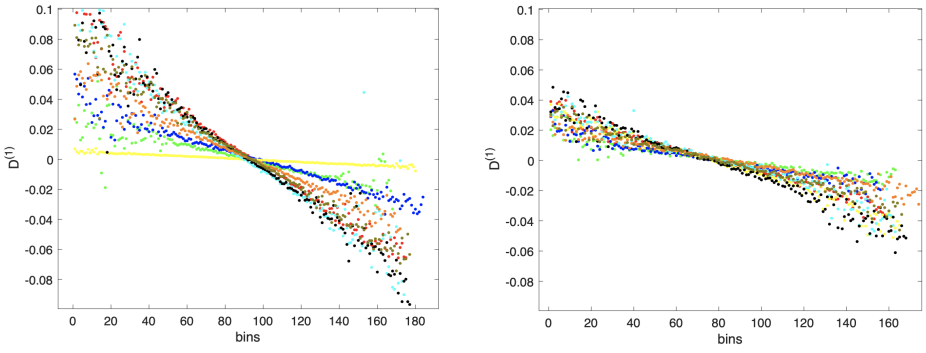

(a) **(b)**

Figure 3.13: Kramers-Moyal coefficients for different cortical areas from depth electrode data in rat #7. Colours, as in those shown for Fig. 3.9, are IC : yellow, S1Fl : red, S2 : green, S1Ul : blue, contralateral motor cortex for comparison : orange. a) KM1 in the inter ictal period; b) KM1 for the same rat in the four seconds prior to a seizure 20 seconds later

As also noted by [175] in their Fokker-Planck analysis of the intracranial EEG in

the context of seizures, the drift coefficient, $D^{(1)}$, shown in 3.9a showed linear damping behaviour in NEC rats[11]. This can be clearly seen in both the NEC rats of Fig. 3.9 and the GAERS rats of Fig. 3.13a. From the depth electrode data prior to siezures in Fig. 3.13, a breakdown in "differentiation" of scaling across the different areas of cortex can be clearly be seen. This implies that scaling breaks down prior to seizures, consistent with the breakdown in multifractal scaling seen in wavelet analysis.

To see if the drift coefficient changed prior to seizures, tetrode data was analysed for seizure intervals of > 8 seconds for all regions from our first experiment both for a two second interval 4 seconds before the first SWD and then in the last two seconds. Sample results for 61 seizures in both S1 and S2 are shown in Figs 3.14a-3.14c. Fig 3.14a shows a trend towards flattening in the gradient of $D^{(1)}$ just prior to seizures. It can be seen for a majority of the seizures in this limited example, there *are* different drift coefficient dynamics between these two time points but not exclusively. In the immediate pre-ictal period there is a greater diversity of drift coefficients and, again, some overlap between the differing scales, and even some seizures where the gradient pattern is reversed.

A scatter plot of 61 drift coefficient $D^{(1)}$ gradients obtained by linear fitting (using Matlab's `fitobject`() command) is shown in Fig 3.14b, where the horizontal axis is used to spread the data points consecutively by number $n = 1, 2, ..., 61$ for clarity. Here, as in Fig 3.14a it can be seen that there is no absolute separation between groups, but a one way ANOVA analysis shows that these populations are likely have different means with a p value of 0.029, again for $n = 61$, and the corresponding box plot is shown in Fig 3.14c.

From this it is concluded that there is a likely trend towards changes in drift dynamics prior to seizures, but that a larger sample is needed to demonstrate this more conclusively.

Deriving dynamics from Fokker-Planck analysis

Assuming the stochastic and deterministic components in the dynamics underlying seizure transitions are separable, it might be possible to reconstruct the dynamics between θ - γ interactions from the drift coefficients, as outlined in Eq. 3.12.

Since there is no time dependence in the right hand side of the coupled differential

[11] this same pattern was also seen in GAERS rats

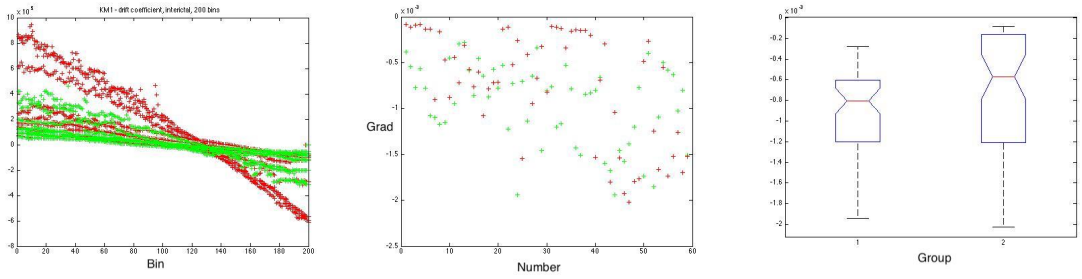

(a) **(b)** **(c)**

Figure 3.14: Kramers Moyal coefficients for different cortical regions in the GAERS rat tetrode data, showing changes in drift coefficient $D^{(1)}$. (a) Drift coefficients in the two seconds immediately prior to a seizure (green traces), and four seconds before (red traces). (b) Gradients fitted and plotted as single points for each of 61 pre-ictal periods. In this figure, the horizontal axis shows a spread of data for clarity. (c) Box plot suggesting the presence of separate means in the two distributions at p=0.0291

equations in Eq. 3.12, it is possible to describe the phase space of interactions between θ and γ components in the data to first order, using the approximation of Eq. 3.13. Figure 3.15 shows the form of this space, reconstructed from the two dimensional drift coeffients of inter-ictal tetrode data from rat # 3.

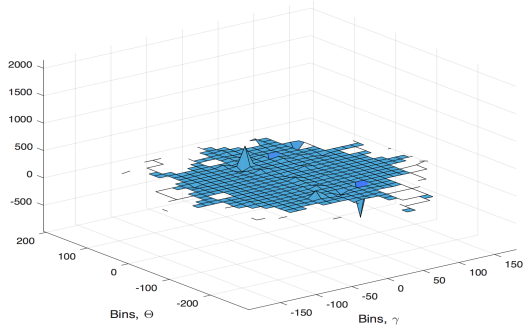

Figure 3.15: Plot of the θ - γ phase space found using Eq. 3.12

Not surprisingly, as seen in Figure 3.15 these interactions are relatively flat. One would expect this from the relative independence of the two dimensional Kramers Moyal coefficients $D^{(2)}_{\theta\theta}$ and $D^{(2)}_{\gamma\gamma}$, and the weakness of interactions between them seen, given by $D^{(2)}_{\theta\gamma}$.

3.4.4 Evidence for timescale separation in thalamocortical networks

Looking at a sample of tetrode data, Fig 3.16 shows the transition from a higher dimensional (Fig 3.16a) to a lower dimensional phase space (Fig 3.16b) in the first seconds of a seizure.

In calculating the Lyapunov spectrum the embedding dimension m used was $m = 3$ and $m = 4$, as indicated and the time delay is taken as $\tau = 16$msec for the NEC and GAERS rat tetrode data.

One can see from Fig 3.16b that the the choice of m and τ seems reasonable. The value of τ was calculated by finding the minimum of the mutual information of the data, and checked with the results of the autocorrelation of the data. Values of m and τ were checked using data from a number of cortical areas, and times in relation to seizures. This value of τ is also consistent with previous known estimates of the thalamocortical propogation delay of 8 - 60 msec[177]. To put this estimate range in the context od known electrophysiology results, Pinault found a delay of 12 msec for simultaneous firing of TRN and thalamic relay neurons after the SWD peak in his experiments[161].

The method used here to find the lyapunov spectrum was validated on a Lorenz system with parameters $a = 10$, $b = 8/3$, and $c = 28$. It underestimated the dominant Lyapunov exponent considerably, by around $30 - 40\%$, compared to a simulation of expected theoretical values for a Lorentz system with the same parameters (these exponents were calculated by numerically simulating the Jacobian matrix derived from the model equations starting from arbitrary initial conditions). It also markedly underestimates the negative exponents in this system (i.e. values around -3, compared to the correct value of -14). It is a well known problem that large negative exponents are more difficult to estimate with accuracy.

However, we can see from Fig 3.17 that the forward and reverse Lyapunov spectrum for depth electrode data from a NEC rat appear to agree reasonably well. Despite an occasional lag in numerical values at times the smaller peaks and troughs in each exponent was mirrored in both forwards and reverse directions reasonably well. To recall McSharry's observation on the difficulty of estimating dynamical quantities [127], and inferring pre-

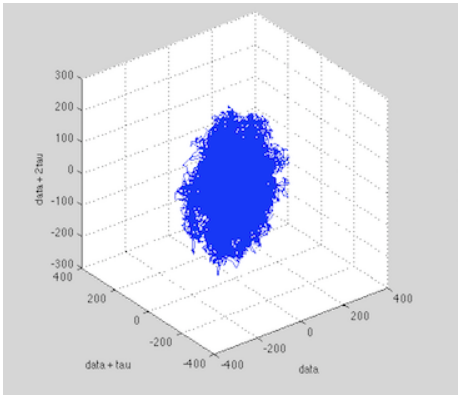

(a)

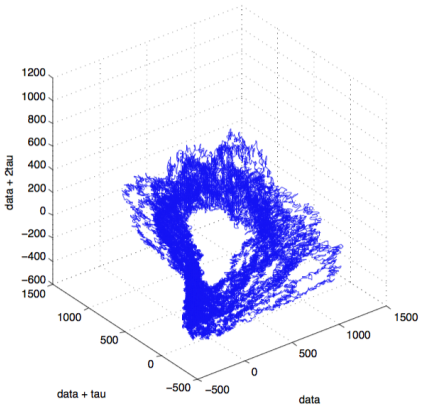

(b)

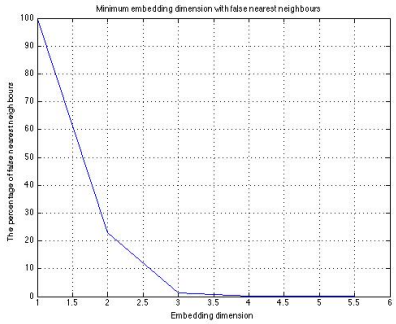

(c)

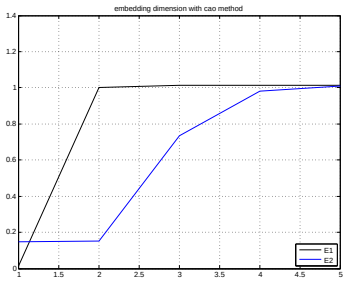

(d)

Figure 3.16: Reduction in dimension of phase space in the lead up to a seizure, showing the phase space for unfiltered tetrode data (a) inter-ictally, and (b) during a seizure. (c) Plot of percentage of false nearest neighbours vs. embedding dimension, for a threshold R_T of 15 (d) Plot for same data, now using Cao's method [37]. The quantities E1 and E2 are defined in Section 3.3.4.

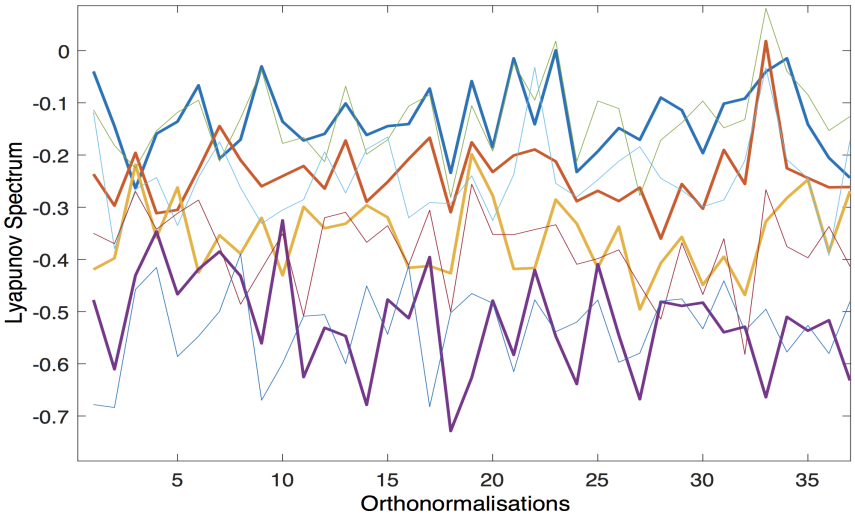

Figure 3.17: Bold lines : forward Lyapunov exponents and fainter lines : reverse Lyapunov spectrum plotted for a 60 sec EEG segment in an NEC rat from depth electrode data, using $m = 4$ and $\tau = 16$ msec.

cision into their numerical values, it is more appropriate in the case of the results that follow to observe the behaviour of the Lyapunov spectrum.

For example, consider the 'gap' between the first and second exponent, here called $\Delta\lambda_{12}$ rather than each exponent's numerical value. In what follows, the obtained spectrum is considered as a pseudo spectrum of Lyapunov exponents. if anything, the error in numerical values demonstrated above will lead to an underestimation of $\Delta\lambda_{12}$ when this gap is present. Such a separation in $\Delta\lambda_{12}$ is found for values of m from 3 and 4, up to $m = 7$. The results of analysis here for $m = 3$ are presented given this is the minimum embedding dimension appropriate for the data, but similar results were found for $m = 4$ as well. It is also important to note that higher values of m are more likely to lead to spurious exponents [31].

Data from the depth electrode experiments most clearly showed evidence of time scale separation (Fig 3.18), though the data from tetrode experiments in higher detail also show some evidence of this (Figs 3.19 and 3.20), indicating that $\Delta\lambda_{12}$ tended towards both wider variance and skewed towards a larger value of $\Delta\lambda_{12}$. Both of these tendencies can be seen in Fig 3.19. This appeared to occur throughout most of the distributed areas of the thalamocortical system (S1 and S2, as well as IC) but not as reliably in motor cortex

(Fig 3.18). This normalised after the termination of a seizure, and was not as marked in NEC rats (this data is not shown).

Figure 3.19 shows further detail in the Lyapunov spectrum in tetrode data. Because of the high sampling rate of the data, filtered to 600 Hz, we also see high frequency oscillations at the peak of the SWD. The Lyapunov spectrum appears to peak just prior to each SWD cycle, ramping up to positive values of λ_1 up to 0.5, at a time point of about 5000 data points *before* the SWD peak (in other words, $\sim$ 0.25 seconds). This observation is consistent with the results of Chapter 5 that the instantaneous power of higher frequencies was strongly phase locked to the theta rhythm, and also that high frequency oscillations were also time locked with theta peaks.

Coincident with these time points in the data it can be seen that the histograms of the distributions of $\Delta\lambda_{12}$ 'broaden' successively as a the seizure is approached to become distinctly heavier tailed, indicating (1) a divergence from Gaussian distribution, which implies that (2) the value of $\Delta\lambda_{12}$ more often widens at that point.

The appearance of these histograms prompted further investigation of the statistical qualities of $\Delta\lambda_{12}$, using a moving window of 200msec (of the order of between five and ten 'time constants' of the thalamocortical circuit in rats and humans [177]). I experimented with overlap of moving windows by up to 50%, but this did not appreciably change the result. Interestingly, a ramping quality somewhat reminiscent of a 'sawtooth' pattern is seen in the change in mean value of $\Delta\lambda_{12}$, falling after the initiation of SWDs in the next seizure. Not seen in this figure is that a next seizure is about to commence in the next two seconds, consistent with the rise in mean $\Delta\lambda_{12}$ and inverse coefficient of variation, and also the fall of all other statistical parameters.

3.4.5 Karhunen Loeve analysis

A Karhunen Loeve analysis was undertaken to examine an orthogonal decomposition of the dominant network modes during the progression to seizures. The main findings of this analysis were that the theta 5 - 9 Hz frequency oscillations persisted across all cortical and thalamic tetrode channels, independent of seizure on- or offset, and so these results

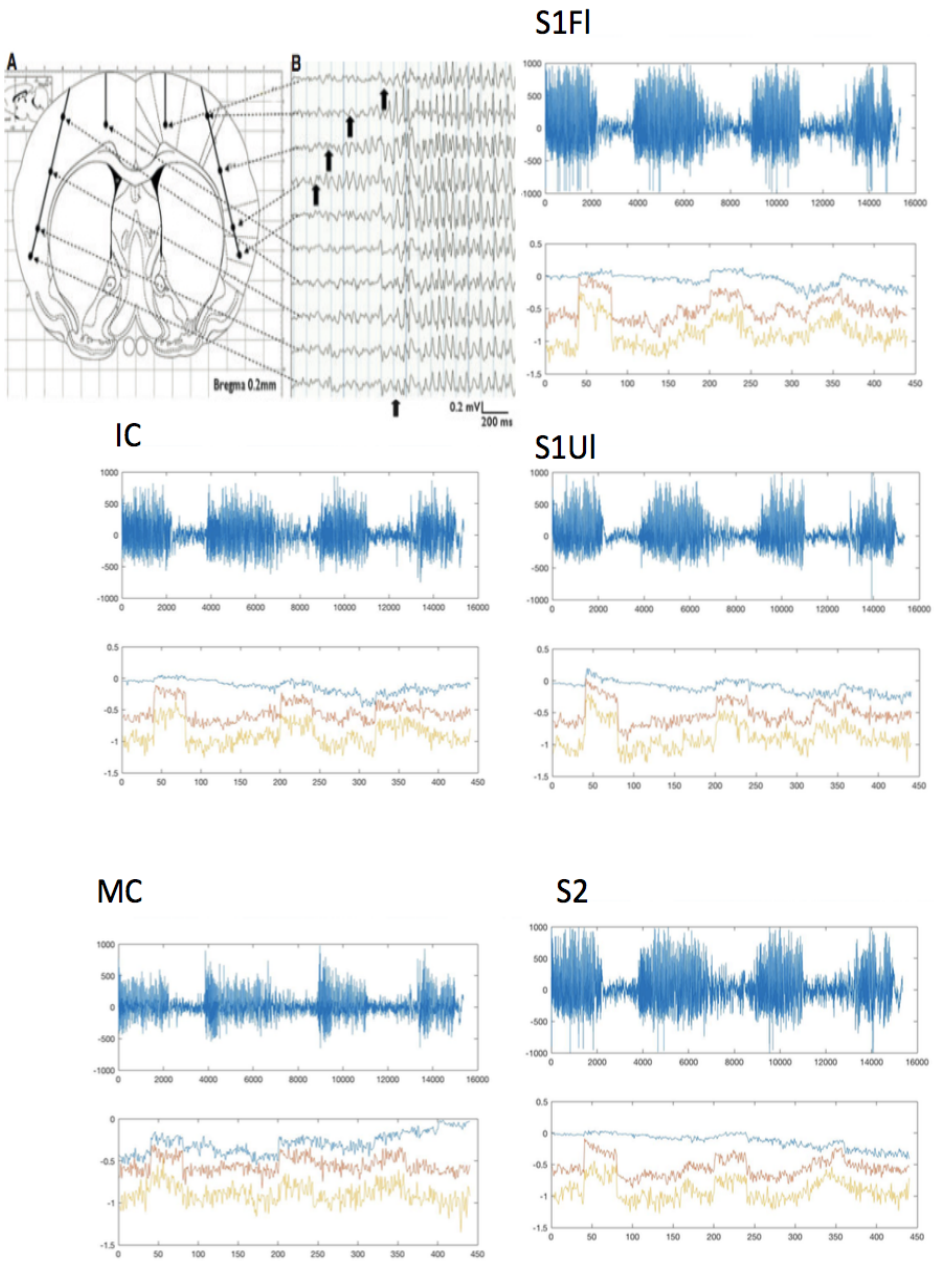

Figure 3.18: Plot of Lyapunov spectrum over a minute's duration of recordings, showing evidence of timescale separation. (a) schematic position of depth electrodes [249] and (b) EEG of all ten channels showing the start of seizures in S2/IC before S1 and M1 regions respectively. (c-f) upper : 60 sec EEG segment and lower : Lyapunov spectrum for each region

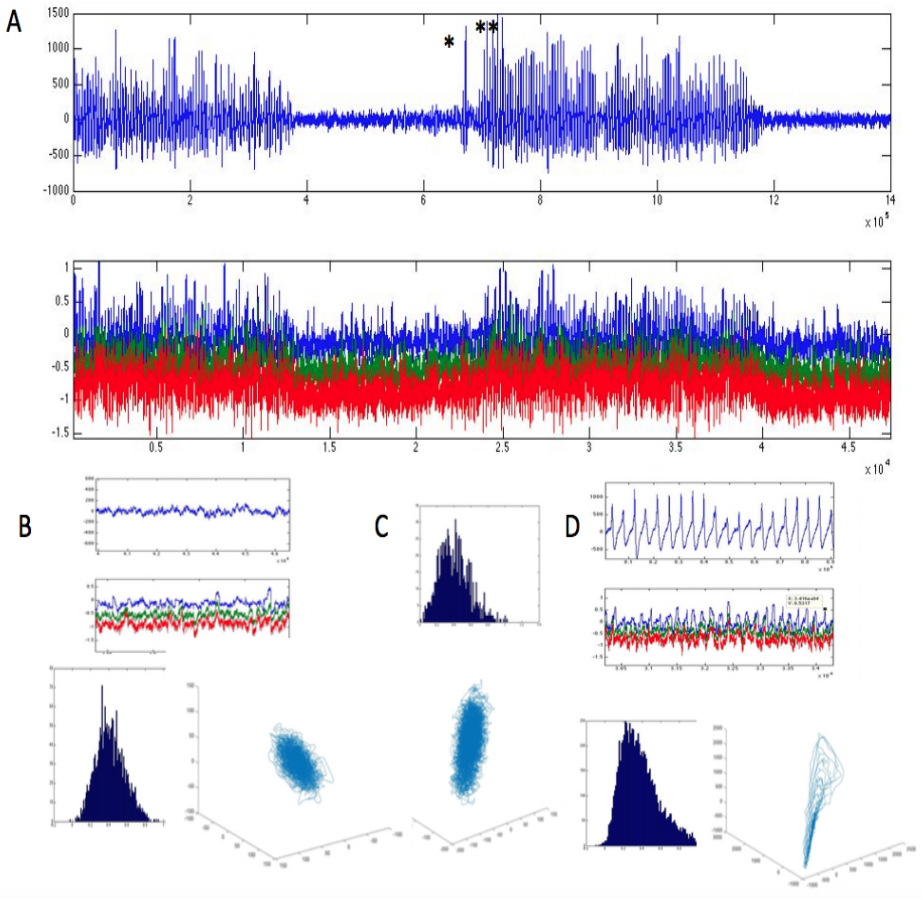

Figure 3.19: (a) Plot of Lyapunov spectrum for tetrode data, 1400000 data points or ~ 50 seconds duration. Below: snippets of data, histogram of $\Delta\lambda_{12}$, and phase space (b) inter-ictal; (c)at the 'hiccup' after discharge 1sec prior (exploded data view not shown); and (d) the first two seconds of the seizure

are not included in this thesis.

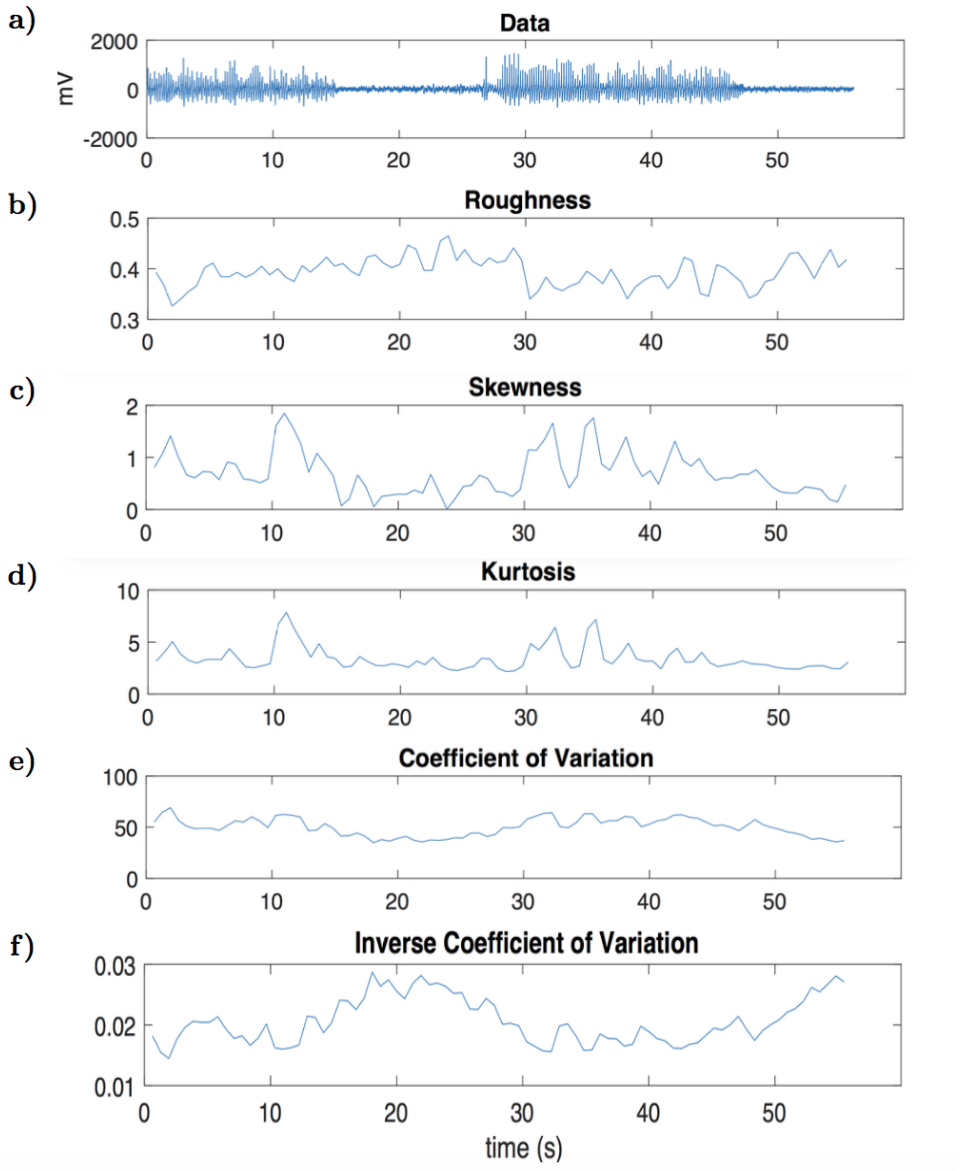

Figure 3.20: Plot of, from top to bottom : (a) the first 1400000 data points of recording # 202207, bandpass filtered between 1 - 600 Hz; (b) mean; (c) skewness; (d) kurtosis; (e)coefficient of variation and (f) inverse coefficient of variation in $\Delta\lambda_{12}$

3.5 Discussion

The goals of this chapter were to examine whether there was evidence to indicate altered dynamics prior to seizures, to ascertain if any altered dynamics may be consistent with critical slowing, and to document changes in scaling behaviour prior to seizures. A broader

question, in light of the significant recent interest in critical slowing from a neuroscience context [132], is to address which measures of critical slowing are most applicable to this data set, and how altered sensitivity to perturbation may be associated with changes in scaling, or dynamics.

Analysis of the structure functions defined by Eq 3.5 show evidence of power law scaling over a wide range of incremental displacement, τ, from values of $\tau \sim 20$ to 210. The scaling behaviour seen in Fig. 3.5b supports evidence published by previous authors suggesting power law scaling over five orders of magnitude [101],[28]. Although the Extended Self Similarity approach would be equivalent to fluctuation analysis in the special case of $q = 2$, fluctuation analysis is less robust to the effects of noise. Fig. 3.5c also shows that the scaling behaviour $S_q(\tau) \sim \tau^{\zeta(q)}$ of this data deviates from that expected in the 'pure' Gaussian case which would have resulted in linear scaling with $\zeta(q) = 1/3$. This would suggest the presence of long tailed increments, again in agreement with previous studies [185].

The results of Figures 3.5c and 3.5d also show subtle differences between the scaling of increments in the data from the post-ictal period, as compared with data from either inter-ictal or pre-ictal periods.

Scaling analysis using Morlet wavelets also supports this observation. Statistical analysis of changes in scaling behaviour with seizure onset shows that there were indeed changes between the inter-ictal and pre-ictal period for the S12 and S2 cortical regions. Although there were trends towards similar results for the S1 region these did not reach statistical significance. It is possible that this points to differences in scaling between regions; when scaling gradients were compared, there was statistically significant differences both between regions (at $p < 0.0009$), and in relation to changes prior to seizure onset. The flattening in the distribution of wavelet coeficient magnitude suggests a departure from power law scaling at higher wavelet scales (i.e. lower frequencies), and supports the phenomenon of 'red shift' documented by previous researchers [206]. The changes in wavelet lower frequency 'power' with time, as seen in Fig. 3.6c during seizures suggests the phenomenon of phase locking of higher frequency power with SWDs, which seems to occur at almost exactly the 5 Hz theta frequency in this particular example. In this case, it was

interesting to find that the fundamental frequency of SWD rhythms differed very slightly for different cortical regions from analysis of the depth electrode data (from rat #7) simultanously recorded in different parts of cortex, given the results to hand which show different scaling behaviour at this time.

Fokker-Planck analysis was demonstrated to be a valid approach for analysing increments of both depth electrode data and tetrode data using the Chapman-Kolmogorov Equation (Eq. 3.27, Section 3.4.3, and shown in Fig. 3.8), and quasi-stationarity of the data up until the time of SWD onset was checked by analysing the first four moments of the data. These two conditions, along with satisfying Pawula's theorem, suggest that Fokker-Planck analysis was a valid means of analysing this data. Qualitatively, the one dimensional drift coefficients $D^{(1)}$ revealed different scaling behaviour across the different areas of somatosensory cortex studied, as seen by the different gradients of this in Fig. 3.9. It is possible that the flatter gradient of the yellow curve corresponding to the S2 somatosensory region suggests a more uniform probability of state transitions across the space of all such increments observed in this data, perhaps making the transition to seizures more likely. This is speculative, since it is demonstrated only for this data and not necessarily present before all seizure transitions. However, such a change in drift coefficients was seen prior to seizures, as in the analysis presented in Fig. 3.13 for depth electrode data, or Fig. 3.14, for tetrode data. These changes are also consistent with the changes in scaling behaviour shown by the wavelet and structure function analysis of Section 3.4.2.

The one dimensional diffusion coefficients $D^{(2)}$ seen in Fig. 3.13b again point to a much flatter coefficient for the S2 region than elsewhere, possibly representing a more tightly bound change in state transitions across time in this cortical area.

The two dimensional Kramers-Moyal coefficients seen in Fig 3.10 show relative independence between the γ rhythm (analysed for frequencies of between 40 and 80 Hz) and the θ rhythm. The diffusion coefficients $D^{(2)}_{\theta\theta}$ and $D^{(2)}_{\gamma\gamma}$ did not show evidence of interdependence either, and to support this observsation, the cross term $D^{(2)}_{\theta\gamma}$ was weak. Again, this finding is consistent with that of previous work such as [12].

The collective θ-γ dynamics were inferred from the θ and γ drift coefficients, calcu-

lated from interictal GAERS tetrode data (rat # 3). This analysis showed that although the phase space of interactions inferred from this data was relatively flat, there were "non-linearities" seen in isolated peaks and troughs across the θ-γ phase space. It is entirely possible that the interactions between the two frequency ranges chosen (i.e., 5 - 9 Hz for the theta range, and 40 - 80 Hz for the low-gamma range) are not the most relevant to the dynamics. This data did contain inter-ictal discharges and some non-sustained runs of the theta physiological rhythm sometimes known to be a precursor to SWDs, though SWDs did not occur in the data used for this analysis. It would be interesting to compare data from different cortical regions, different combinations of frequency ranges, and with NEC rats to enable further understanding of the significance of this result.

An investigation of the statistical moments of the data in relation to seizure onset showed that there were significant changes in the skewness and inverse coefficient of variation just prior to seizure onset. With regard to the inverse coefficient of variation at least, this finding is in keeping with previous findings [132].

Taken together, these results all suggest that the scaling behaviour of the EEG change prior to seizures in both depth electrode and tetrode recordings in the GAERS rat. A number of these changes are at least in the second prior to seizures; a number of features are also suggestive of critical slowing, such as changes in the statistical distribution in the data; separation in timescales as suggested by a widening Lyapunov spectrum changes; and breakdown in scaling behaviour towards a predominance to low-frequency ranges suggestive of a "red-shift" in the data, seen with wavelet scaling, in the pre seizure period. Changes in scaling behaviour were also found through changes in the gradient of the first Kramers-Moyal coefficient $D^{(1)}$ prior to seizures, and the breakdown in "differentiation" of scaling between cortical regions prior to seizures seen in Fig 3.13.

One might postulate that this will be accompanied by a decrease in complexity, measured by a fall in permutation entropy in the pre seizure period, or in changes in the distributions of phase entrainment, called here 'phase entropy', prior to seizures and which are further explored in Chapter 5.

The most important indicators of timescale separation prior to seizures, are seen in the separation in the biggest two exponents of the Lyapunov spectrum, calculated using

Brown and Abarbanel's method, to first order[31]. The results obtained here suggest that this may be a consistent result across different cortical areas. Evidence for timescale separation was also consistent at the two different spatial and temporal data scales used - local field potential recordings sampled at 256 Hz simultaneously across somatosensory and motor cortex, and also the tetrode data from networks of neurons situated in deeper layers of cortex, and thalamus, sampled at 25 kHz.

Significantly, the Lyapunov spectrum obtained from depth electrode data of non epileptic control rats was also analysed for signs of timescale separation, and this was not found.

The method of using linearised Jacobian matrices to find local neighbourhood maps, and from these, the Lyapunov spectrum using Oseledec's theorem, is well established[31]. As such, the quantities found would be described as representing "local stability exponents", similar to the FSLE [10]. As mentioned by Brown[31] and, later, many others[127] the accuracy of this approach is often dependent on the data length available, and noise.

A relevant question is the correspondence between local Lyapunov exponents, as a measure of stability, and critical slowing. One could argue that the presence of changes in dynamics associated with critical slowing should instead be found from the behaviour of the Jacobian matrices themselves. However, a problem with using the behaviour of the Jacobian matrices directly, as observed by Letz[110], is that one cannot extrapolate later effects of a perturbation away from the local behaviour of the Jacobian matrix approximated to first order[12]. Instead, it is known that the Lyapunov spectrum is relevant in describing altered dynamics in certain kinds of tipping points, such as rate tipping. It has not been established here that rate tipping is relevant to the altered dynamics found, but this will be the subject of further study.

Evidence of timescale separation in underlying dynamics indicates an altered frequency response of the system at the point of seizures. Although it is not direct evidence of critical slowing, this finding is consistent with critical slowing, and consistent with statistical measures of critical slowing such as skewness and kurtosis in the collected data. It is also consistent with the observation that seizures could be electrically stimulated across

[12] for further discussion of this point, see Section 5.2.7

all somatosensory cortex and insular cortex, which are all parts of the thalamocortical network known to be important in absence seizure generation [249].

Multifractal scaling has been described in EEG analysis previously, and correlated with fMRI for behavioural tasks [229]. In this chapter, changes to the multifractal pattern of scaling was explored via a number of complementary methods. Results found from the method of Extended Self Similarity using structure functions was in agreement with those of changes in wavelet scaling, and also the measured change in drift coefficients at different times found from Fokker-Planck analysis.

In the wavelet scaling data at seizure onset it was found that higher frequency power seemed phase locked with theta peaks, suggesting that higher frequency oscillations are aligned with theta peaks. It is interesting that the Lapunov spectrum seems to reliably peak in the ramping phase to these theta oscillations and this possibility would merit further analysis. Whilst there is a possibility of 'edge effects' [102] causing spurious higher frequency components in the data, it is not clear how this would influence Lyapunov exponents.

To this end, another question is what meaning the local Lyapunov spectrum has at the level of local networks, where it is 'non-smooth'. This question has been studied by David Cai and colleagues in Leaky Integrate and Fire networks theoretically, but as yet not addressed elsewhere in animal or human studies.

Implications of changes in scaling behaviour for dynamical analysis

Consistent with the observed delay plots of SWD data in an appropriate embedded phase space, showing fixed oscillating behaviour in a limit cycle (Figure 3.16b), the largest Lyapunov exponent of zero was not found to vary during the transition to seizures. This is consistent also with the results of Chapter 5, where the Finite Scale Lyapunov Exponent was not found to change prior to seizure onset, and where perturbation techniques were presented and used to show that there was not divergence in the system phase space suggestive of a positive Lyapunov exponent at seizure onset.

However, changes in scale with seizure on- or offset raise the question of how stable the parameters of time constant τ, embedding dimension m, and dynamical dimension

actually are.

Here, the appropriateness of a 'fixed' value of embedding dimension was tested at both inter-ictal and pre-ictal periods for a limited sample of ten different recordings in each of S1, S12, and S2 data. This at least suggests that it was appropriate to use a value of $m = 3$, or to further minimise false neighbours in the embedding, $m = 4$. However, this does not rule out subtle variations in τ, which will be the subject of further studies. Interactions at different scales occur in chaotic attractors containing interwoven fractals in which each may have a different fractal dimension. It is not clear from the above analysis whether that is the case here. Demonstrating this would involve showing how the dimensionality of the data changes with time, or scale. However this properrty is not as simple as it may seem to prove [127].

For example, one approach is to calculate the dimension from the data on a number of different scales, using either approaches from fractal geometry, from analysis of wavelet scaling, or from the scale dependent Lyapunov exponent [79] (discussed in Chapter 5).

To illustrate the difficulties in this, consider the box counting dimension, estimated using the Grassberger Procaccia algorithm which produces an equivalent measure [79]. The algorithm is based on calculating the correlation integral

$$C(\epsilon) = \lim_{N\to\infty} \frac{1}{N^2} \sum_{i,j=1}^{N} H(\epsilon - ||V_i - V_j||) \tag{3.29}$$

where, for N randomly chosen points on the attractor, $C(\epsilon)$ represents the average number of points within a ball of radius ϵ.

The results in Fig. 3.21 show that while the correlation dimension does indeed change between seizures and inter-ictal periods, the meaning of such changes are less clear. McSharry [127] cautions against too much reliance on the absolute quantitative interpretation of Lyapunov exponents or the Grassberger Procaccia correlation integral, since these are prone to numerical error and incorrect interpretation of the dimensionality of the data. He comments that a main value of these measures is as a 'pseudo' spectrum given they are internally consistent, as they have been used here. Possible ways of getting around this problem are by using the scale dependent Lyapunov exponent and a Karhunen Loeve

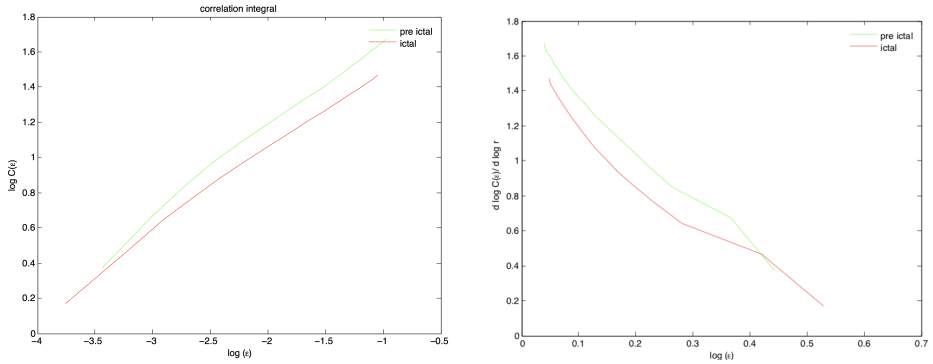

(a) **(b)**

Figure 3.21: (a) Grassberger Procaccia correlation integral and b) derivative of log C(ϵ), for embedding dimension 3 and τ 50 dt, for the same data shown in Fig 2.

analysis at short time scales, as done previously by Chavez and colleagues [42].

The estimated Lyapunov spectrum was found to first order approximation for the Ikeda map and also the Lorenz system with parameters 28, 8/3, 10, (i.e. the last three equations comprising the Lorenz equations in Equation 4.6). The results found using the method used in this thesis are in error when compared with the numerically iterated results obtained from the Jacobians found from these equations, with respect to the negative exponents.

To further investigate the algorithm's accuracy Rosenstein's method was also used[13] to verify the value of the largest exponent λ_1. The results from this method were also in error when tested on a Lorentz system with the same parameters, where the largest exponent was underestimated by approximately 30% and an underestimation for the most negative exponent (of -1.8 compared with a true value of almost -14).

These errors may lie in truncating the nearest neighbour fit to first order, but another problem is always that negative Lyapunov exponents are always harder to accurately determine using delay embedding approaches [127].

Possible refinements to this method so as to give more accurate estimates of the negative Lyapunov exponents could be using a higher order Taylor series expansion for the nonlinear fit of nearest neighbour trajectories, or averaging out for the effects of random noise when searching for nearest neighbours as described in Yao [245], as a natural

[13] this used the lyarosenstein.m routine, downloaded from the Matlab Central website, May 2017

extension of Brown et al's algorithm.

The problem with the first order expansion summarised above is that it will always be less accurate when estimating predominantly negative Lyapunov exponents, given there is less expansion of trajectories in this region of phase space, so they will not have the strength to overcome the influence of the first k positive exponents which define the Lyapunov dimension of the attractor and which help to define its character ([31], page 2791). This is overcome by extending the local neighbourhood to neighbourhood mapping to at least second order, which improves the estimated exponent. Yao also demonstrated that increasing the number of neighbours used to incorporate averaging for the effects of noise also improved the accuracy of negative exponents.

However it is again relevant that the reverse Lyapunov spectrum, seen in Figure 3.17, is at least qualitatively consistent when checked against the forward exponents, calculated from the same data.

Other extensions to the results presented in this chapter could be to analyse changes in the Lyapunov spectrum to perturbation by electrical stimulation, in keeping with the method of Section 5.2.7. To understand the utility of inferring the θ-γ phase space from drift coefficients, it would be important to pool data from more tetrode experiments to improve the statistical analysis of drift coefficients before a seizure. It may be useful to examine drift coefficients more remote than four seconds before a seizure since this may make differences between these states more marked.

Other ways to correlate any changes in coherence or synchrony with dynamics leading to seizures could be to recover the correlations from wavelet analysis of the power spectrum via the Wiener-Kinchin theorem. Evidence for critical slowing may again be found in a 'red shift' in spectral properties, showing an increase in lower frequency components, or the ratio between higher and lower frequencies, suggesting increasing long range correlations in the data. This has been also been demonstrated in some studies analysing tipping points in ecological systems [198], and also for canonical critical systems such as the Ising model [8].

Empirical Mode Decomposition approaches, as used by Chavez and colleagues may

shed light on the question of what are most relevant timescales for the generation of seizures or the stability of cortical oscillations in general.

3.6 Conclusion

In this chapter, markers of critical slowing were found in the GAERS rat model, as a separation in timescales indicated by a gap between the two largest Lyapunov exponents in the spectrum. This seemed to vary with seizure onset in depth electrode recordings. Supporting evidence for this variation was also found in the skewing of the statistics of this gap $\Delta\lambda_{12}$ in GAERS rat tetrode studies, which also varied with seizure on- and offset.

Consistent with this finding, the scaling behaviour of tetrode data, analysed by both wavelet methods and also stochastic methods, also varied with seizure onset. A Fokker Planck analysis found that the scaling of the theta band did not depend on higher frequency gamma band activity. The first Kramers Moyal coefficients were used to reconstruct a phase space of $\theta - \gamma$ activity, from which a description of the dynamics between these two bands was derived for inter-ictal data. However, changes in dynamics were not found when using either this method or when analysing the largest Lyapunov exponent alone. These results are also consistent with the null findings using the Finite Scale Lyapunov Exponent found in Chapter 5.

Chapter 4

Cortex Drives the Thalamus at the Initiation of Seizures

An important issue in the understanding and treatment of epilepsy is the longstanding debate about the extent to which generalised seizures have a focal origin. With reference to generalised absence seizures (Section 1.2), the concept of a 'focus' has been used to describe an identifiable localised area which is involved in generating seizures. If present, this might raise the prospect of focal intervention for absence seizures at the level of local cortical brain networks before they progress to bilaterally synchronous generalised seizures. If local treatment is possible this might greatly diminish the severity of seizures as well as alleviating systemic side effects and so improve the efficacy of available treatment.

Inherent in the hypothesis of a focus is that there is (1) a point in the thalamocortical circuit where seizures arise first; and (2) that this point is more 'excitable' than surrounding areas, to which seizures might spread at later times. One measure of whether a cortical focus is likely to exist is whether cortex leads the thalamus at seizure initiation, as suggested by evidence from studies of cellular characteristics and local network behaviour [167, 161, 166, 249].

There are a number of available ways to analyse the direction of information flow, or "driver" and "response" relationships, from multivariate data. In the brain of an awake, behaving animal it is difficult to directly perturb the system being studied, and direct knowledge of the underlying dynamical model is not available, so the mainstay has been to investigate temporal correlations between regions. A widely used way of approaching the problem of demonstrating causality between brain networks or regions has been Granger

Causality [83]. In this formalism, a time series responding to the causal effects of the influence from a driving time series might be distinguished from a non causal correlation if information about the recipient's 'future' is contained in the time series of the driver network, and not in its own past, whilst the converse is not true (Sec. 1.3.2).

However the role of Granger Causality can be controversial and can lead to inaccurate predictions under certain conditions, leaving the results from these analysis methods difficult to interpret. As pointed out by Nolte [142, 141] Granger Causality can break down in the presence of mixtures of source spectra, or nonlinear phase spectra, both of which are often present in ECoG data. Granger Causality results obtained are also vulnerable to the quality of fit of the underlying autoregressive model used to represent the statistics of the time series data. Sugihara and May [78] have noted that a key requirement of Granger Causality is separability, i.e., that a causative factor between the two time series is independently unique to one variable. If information in this case is not unique and present in other variables, as is often the case in weakly coupled dynamical systems (as examples, consider the predator-prey system governed by Eq 1.1 illustrated in Fig. 1.4 and discussed in Section 1.3.2, or the coupled Rossler-Lorenz system of Fig. 4.1, given by Eq. 4.6), they are not separable and Granger Causality will fail.

Stokes [218] has noted that Granger Causality has a number of weaknesses especially in the context of neuroscience. Estimates found with this method can be biased severely or of high variance, again making results difficult to interpret out of the context of the behaviours of individual system components, given that it is derived independently of, and so ignores, the underlying system dynamics. These difficulties are often especially pronounced in the presence of negative coupling, or strongly alternating dynamics. Despite this Granger Causality is widely used in neuroscience, and has been applied across a large magnitude of scales of brain behaviour and function.

In this Chapter, the objective is to characterise the driver-response relationships between somatosensory cortex and thalamus. Meeren's study [131] used a measure of nonlinear association to study this question, finding that in the first 500 msec of a seizure, cortex was leading the relevant thalamic nuclei, and that a 'focus' could be localised around the S1 cortex corresponding in their study to a homunculus representing the upper lip (S1Ul)

in their study. This area was found to lead the thalamus before other areas of cortex in the commencement of seizure activity (Sec. 1.3.1).

However, apart from Zheng and colleagues [249], no one has really examined the differences between S1 vs S2 in seizure generation, and how seizure generation may vary between regions of somatosensory cortex in rats. Zheng's study found that SWDs were preceded by 5 - 9 Hz physiological field potential oscillations detected first in the deep layers of somatosensory cortex (S2 and insular cortical (IC) regions) [249], and that maximal suppression of SWDs occurred after injection of an endogenous neuropeptide NPY into S2, more than S1; and that SWDs could be triggered by lower intensity microstimulation in deep layers of S2 than S1. At the cellular level, it was found that the majority (∼79%) of cells in deep cortical layers fired rhythmically at the SWD frequency of 5-9Hz before and after seizures using paired glass electrode recordings, suggesting that these cells may have been part of the 'rhythm generator' circuit from which SWDs arise. The conclusion of this study was that the S2 somatosensory cortex also forms an important part of the seizure generating circuit, and that this region would also merit more study.

The purpose of this Chapter is to build on that work by studying the driver / response relationships between cortex and thalamus in the GAERS rat in relation to seizure onset.

Hypothesis

The hypothesis investigated here is that the somatosensory cortex drives thalamus at the initiation of seizures in the GAERS rat.

The results of previous single cell electrophysiology recording studies and network studies cited above suggests that deep layers of cortex in the S2 region and junction region between S1 and S2 somatosensory regions are drivers in the initiation of seizures. Meeren's previous study showed that in the first 500ms cortex leads thalamus [131], however this study used surface EEG only. To investigate the activity of deep layers of cortex explicitly, depth ECoG recordings were obtained from the S1, S12, and S2 regions of the GAERS rat at both coarse and fine time scales.

Because of the strong oscillatory nature of the precursor rhythms found prior to SWDs and also the documented nonlinear nature of EEG signals, methods have been chosen that

have been shown to be robust in the inference of the direction of information flow, and which are appropriate for nonlinear data. The two measures of causal relations between time series used here - nonlinear association analysis [158, 242], and the phase slope index [142] are widely used and validated in such data. Prior to this analysis Sugihara's conformal cross mapping algorithm, the S-Map method, was used to quantify the nonlinearity of the data at the two different local scales of (1) tetrode sampling small regions of cortex (25kHz) and (2) depth electrode EEG, sampled at 250 Hz.

4.1 Analysis Methods and Data Processing

4.1.1 Data collection

Details of surgery and electrode implantation techniques are explained in more detail in Chapter 2. Here, the salient features of data collection are briefly summarised in the context of the analysis which follows. Details of relevant ethics approval are also listed in Chapter 2.

Briefly, two different types of experiments were performed. The first experiment was designed to study multiple cortical areas simultaneously and involved chronic implantation of multisite depth EEG electrodes. The second type of experiment was designed to study very small regions of cortex, or thalamus, at a time. For this purpose tetrodes were used to obtain dual recordings between selected areas of cortex and thalamus simultaneously. For these tetrode experiments three GAERS rats and two NEC rats were used.

Depth electrode experiments

Rats were chronically implanted with 127 μm stainless steel electrodes bundles in which each electrode bundle consisted of insulated wires where the insulation was stripped at 0, 1.0, 3.0 and 5.0 mm from the end, enabling recording simultaneously at four different locations in cortex. Electrodes were implanted bilaterally into S1Ul and S1Fl, S2 and IC (insular cortex), and a separate electrode was implanted into motor cortex, later in this chapter labeled M1. Extradural reference electrodes were implanted into parietal bone. These experiments were performed by Zheng[249], and rats were allowed to recover for 7 days before recording sessions.

Data was sampled at 256Hz, for at least two 60 minute recording sessions for each rat. Both the GAERS and NEC control strain of GAERS rats used in these experiments were at least 13 weeks old, and weighed between 250 and 350 grams. Recordings were taken from different cortical areas in 5 GAERS and 3 non epileptic control (NEC) rats.

Tetrode experiments

For tetrode recordings, neuroleptanalgesia was used after induction with ketamine and xylazine, intravenous catheterisation through the penile vein and ventilation. A craniotomy and durotomy was performed prior to stereotactically guided tetrode insertion into the brain. Micro-stepper motors allowed graded electrode advancement right down to increments of 1 μm at a time. The advantage of neuroleptanalgesia is that the animal remains in a pain free quiet awake state in which seizures occur spontaneously. One disadvantage of tetrode recordings is that it is not possible to histologically confirm electrode placement, so as to clearly identify which layer of cortex the electrode was in; however stereotactic guidance allowed placement in each of S1, S2 and intermediate areas, and ventroposterior - medial (VPM) and ventrobasilar (VB) thalamus to a sufficient level of precision as to be confident in the sub region of each cortical area.

Data was sampled at 25 kHz using an Intan RHD2116 amplifier system (Intan Technologies, LLC[1]), unfiltered, before being imported into MATLAB for subsequent analysis. Data was initially unfiltered during collection to allow for spike sorting if needed later (even very low frequency filtering will distort spike waveforms and can affect the accuracy of spike classification). However, the analysis methods presented in this chapter are concentrated on ECoG and EEG data only and do not require spike sorting. Data was subsequently digitally filtered in MATLAB for further analysis and specific details of the filtering procedures will be given where these occurred.

Seizure time stamps were determined by visual inspection of the EEG. For both types of experimental data the start of seizures was taken to coincide with the first SWD. This was distinguished from coarse somatosensory rhythms that are sometimes seen in GAERS by their morphology and amplitude (greater than 400mV peak to peak, as defined by Pinault [161, 166]). When visually inspecting data, if any artifacts were present [2] this seizure was not included in further analysis. Such artifacts were extremely rare in the tetrode data, occurring in less than a percent of all recorded seizures. In tetrode data, such events were also very (1%) rare in rat #7, but occurred much more frequently in rat

[1] www.intantach.com

[2] such as a spike which is much larger amplitude and clearly suggestive of an amplifier glitch

#6, where of the 23 seizures recorded, more than half of these had such artifacts.

As discussed in Chapter 2, two of the three rats had seizures but recordings from the third rat showed only bursting behaviour between cortex and thalamus without seizures, so this data is not included in the comparisons that follow. From these first two experiments approximately 460 seizures were recorded, with between three and nine seizures per minute in each recording location. In the case of tetrode data three different areas of somatosensory cortex, S1, S2, and the junction region between these, 'S12' are analysed. In S1 there were a total of 142 seizures; in S12, 110; and in S2, 130 seizures. In the tetrode recordings, all seizures were measured only in the cortical region being recorded.

In the case of depth electrode data, electrodes were placed in two regions of S1 - associated with the forelimb homunculus, as determined by the Paxinos and Watson stereotactic rat brain atlas [77], here called S1Fl, and perioral area, called S1Ul. Other regions were the insular cortex (IC), S2 somatosensory cortex, and M1 motor cortex.

4.1.2 Analysing nonlinearity of the EEG

There has been argument that linear measures of correlation can provide as meaningful information as nonlinear measures, but are easier to interpret. An example of one such linear measure is the cross correlogram, historically a stalwart of analysis in neuroscience. However, the preceding chapter provides evidence that the statistical properties of the ECoG data changes as the thalamocortical system progresses to seizures, which suggests the presence of nonlinearity. Given this, it makes sense to establish whether the measured ECoG data is indeed nonlinear before using techniques which are most appropriate to the analysis of nonlinear data.

Convergence Cross Mapping

Sugihara's method[78] of simplex projection and Conformal Cross mapping (CCM) was chosen to investigate nonlinearity of the ECoG in the transition to seizures. With the *S-map* (the authors' short-hand for *'Sequential locally wieghted global linear maps'*) method,

driver - response relationships in the thalamocortical network from a dynamical viewpoint could also be studied.

Granger Causality ignores the underlying dynamics of the network under study and can be prone to high variance or bias, especially in the case of negative causality [218]. By way of contrast, Sugihara's method is of interest because it can estimate causality from the reconstructed manifolds of the attractor giving rise to the time series by estimating the extent to which the state of one variable can be estimated from knowledge of the state of another[3].

From a dynamical systems viewpoint, there would be evidence of interaction between variables if they were from the same dynamical system, i.e., if they shared the same attractor manifold. 'Causation' between two putative variables of the system can be studied by analysing the way reconstructed manifolds of those variables representing the system correspond to the actual behaviour of the system observed through its time series data.

A causal (i.e., driver - response) relationship between two variables (say, X and Y) would then hold if information about X could be recovered from Y, in the form of forecasting information about X, but not vice versa. The degree of asymmetry of this forecasting will provide information regarding the direction of influence between the two time series. The degree to which the prediction converges with increasing lengths of data also provide further evidence of causality.

The starting point of the algorithm is to assume that the temporal 'flow' between successive states of the system generating our measured data can be represented by a dynamic process, ϕ, evolving through time in some E dimensional state space. As in Chapter 3, Taken's theorem of time delay embedding can be used to define the manifold (attractor) containing all trajectories of the system, such that if $\mathbf{m(t)}$ is a point on $\mathcal{M}$ then

$$\phi : \mathcal{M} \rightarrow \mathcal{M}; \mathbf{m(t+1)} = \phi(\mathbf{m(t)}), \tag{4.1}$$

where $\mathbf{m(t+1)}$ is also a point on the same manifold.

[3] the temporal sense inherent in causation is inplicit in the phase space and embedding

Consider, in Sugihara and May's terminology [78], a 'library' of observations of the system arising from the dynamics ϕ. This mapping of $\mathcal{M}$ gives rise to a real valued scalar time series X which tracks the trajectory of points in $\mathcal{M}$. In their notation, X is an observable function of the system governed by some dynamic process ϕ, from which we can measure a time series of observations evolving over time X_t. This observable function of the system X might in turn be a function (such as a transformation, or combination) of the E variables describing the dynamics $X : \mathcal{M} \to \mathbb{R}$. Lagged coordinate embedding of successive points in X form a shadow, or reconstructed, manifold $\mathcal{M}_X$ such that points on this manifold are given by the vector $x(t)$, on $\mathcal{M}_X$ comprising the state of the system at time t,

$$x(t) = [X(t)X(t-\tau)...X(t-(E-1)\tau], \tag{4.2}$$

which should correspond via some transformation or map 1:1 to points $m(t)$ on $\mathcal{M}$, i.e., $\mathcal{M}_X$ is a diffeomorphic reconstruction of $\mathcal{M}$.

May makes use of this to show that a subset of points in X can be used to forecast further points on X outside the original sample (library L). For fully deterministic, noise free systems this would converge towards perfect predictability as $L \to \infty$. In practice this convergence will be limited and $\mathcal{M}_X$ will instead converge to some point determined by the stochastic or process noise in the system, data length, or observer error (e.g., sampling effects, etc.).

Sugihara and May's *Convergence Cross Mapping* uses this property of reconstructed manifolds as a means for estimating causality. If two observed time series X and Y are dynamically coupled in some way, then the local neighbourhoods of $\mathcal{M}_X$ and $\mathcal{M}_Y$ will also have some mapping between each other. Measuring how correlated this mapping is can give a measure of what influence exists between the two processes.

Sugihara and May [78] make the distinction between the required dimension of the state space E, the number of fundamental variables required to unambiguously define the system, and that required to define the manifolds d.

Peretti [34] showed that state space reconstruction predictive methods outperformed mechanistic parameterised statistical models for predicting fluctuations in ecological data,

and so Sugihara's S-Map method of nonlinear time series prediction is used here to estimate the nonlinearity of EEG data at different scales.

Sugihara and May's[78] concept of S-maps allow us to estimate the amount of nonlinearity in the signals. The core idea in this method is to quantify what degree of nonlinear filter θ is needed as a weighting function to ensure that the phase space is accurately reconstructed, as summarised in [78]. These authors have shown that this method and the CCM method can also be used to assess the accuracy of the inferred causality and also quantify how this is affected by noise.

Using Sugihara's outlined algorithm, their sample code[4] for the CCM method was modified and implemented in MATLAB as follows.

Two delay embedded time series, x (say, from cortex) and y (from thalamus) of length L are used to form the reconstructed manifolds $\mathcal{M}_X$ and $\mathcal{M}_Y$ using Taken's theorem.

For the time point $x(t)$ the k nearest neighbours, $k = E + 1$, is found, being the minimum number of points required to form a bounding simplex, for a given embedding dimension E.

These time points are ordered $t_1, ..., t_{E+1}$, and their time indices can be used to identify corresponding time points in the time series Y in the following way :

- The Euclidean distance between $X(t)$ and its ith nearest neighbours is used to calculate a locally weighted mean of the corresponding points in Y. Weights w_i are determined from neighbours of $x(t)$ by

$$u_i = \frac{e^{-||x(t)-x(t_i)||}}{||x(t) - x(t_i)||}, \tag{4.3}$$

$$x_i = \frac{u_i}{\sum u_j}; \qquad j = 1, ..., E + 1. \tag{4.4}$$

- The corresponding point $y(t)$ is estimated from the locally weighted mean of the corresponding $E + 1$ points near $y(t)$, the $y(t_i)$ values. Successive points $y(t_i)$ form

[4] this code is made available on their website, accessed May 2018

a conditional estimate

$$\hat{Y}(t)|\mathcal{M}_X = \sum_{I=1}^{E+1} w_i Y(t_i), . \tag{4.5}$$

If X and Y are dynamically coupled they are from the same attractor, and indices of neighbourhoods from $\mathcal{M}_X$ should identify corresponding neighbourhoods of $\mathcal{M}_Y$. With increasing library length L, the manifolds $\mathcal{M}_X$ and $\mathcal{M}_Y$ become more densely populated. Then, $\hat{Y(t)}|\mathcal{M}_X$ should converge to $Y(t)$, and $\hat{X(t)}|\mathcal{M}_Y$ should converge to $X(t)$.

This convergence is illustrated with the model system introduced by Le van Quyen and colleagues [107], and also discussed by Sugihara and May [78]. This system consists of a Lorentz attractor driven by a Rossler system as follows, and shown in Fig. 4.1 :

$$\begin{aligned}
\frac{du}{dt} &= -\alpha(v+w) \\
\frac{dv}{dt} &= \alpha(u+0.2v) \\
\frac{dw}{dt} &= \alpha(0.2+w(u-5.7)) \\
\frac{dx}{dt} &= 10(-x+y) \\
\frac{dy}{dt} &= 28x - y - xz + Cv^2 \\
\frac{dz}{dt} &= xy - 8/3z
\end{aligned} \tag{4.6}$$

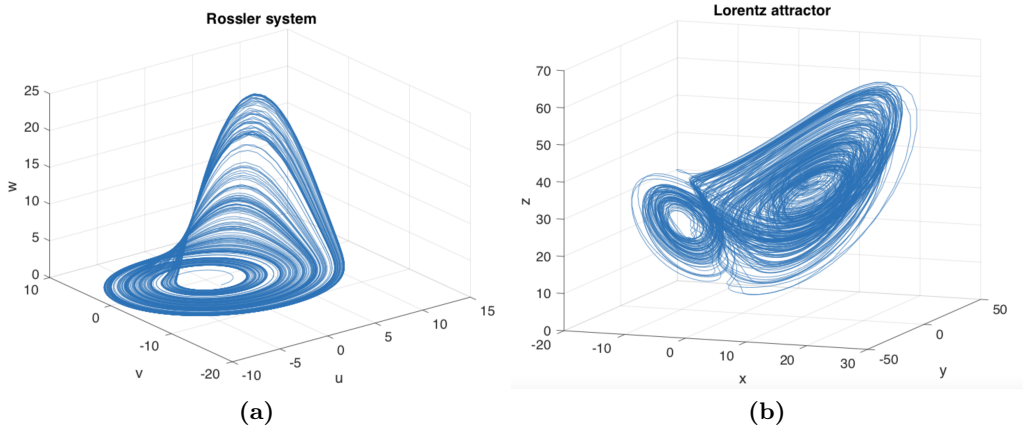

(a) **(b)**

Figure 4.1: (a) Rossler system described by Eq. 4.6. Following the example of [107] the Lorenz system, in (b), is driven by the Rossler system, in (a) with parameters $\alpha = 6$ and $C = 2$

To study convergence behaviour of Sugihara's simplex projection procedure, the Mean Absolute Error between the projected next point found by the algorithm and the known next data point was calculated, for ten library lengths between $L = 25$ and $L = 5000$. As can be seen in Fig. 4.1 prediction error decreases with increasing L as expected.

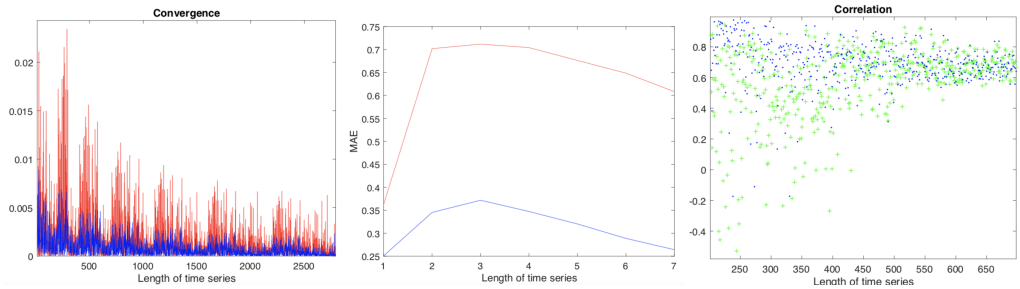

(a) **(b)** **(c)**

Figure 4.2: Example of the convergence and predictive power of Sugihara's Convergence Cross Mapping technique for different 'library' lengths L. (a) convergence, (b) Mean Absolute Error (MAE) and (c) correlation with time series length L.

The algorithm for this is as follows : First, the time series data is time-lag embedded using Taken's theorem (Section 3.3.4), such that there is a trajectory of states $\mathbf{X}_t \in R^{E+1}$. The optimal embedding can be checked using a number of methods described in Section 3.3.4, or alternatively, self consistent checks in the predictions are that excessive embedding dimensions often increases noise and decreases predictive power.

The embedded time series is then taken forwards some number Tp of time points, by following ALL k trajectories in the phase space of 'library' data, and a weighted average of these calculated.

$$w(d) = e^{-\theta d/\bar{d}}, \tag{4.7}$$

where $\bar{d}$ is the average distance for each of the k trajectories, and θ is a tuning parameter which changes the mapping from a global, linear map at $\theta = 0$ (i.e., all trajectories weighted equally) to increasingly local, nonlinear maps up to $\theta = 1$.

Given this background, the MATLAB code of this algorithm proceeded as follows:

1. find the k nearest neighbour trajectories after optimally embedding the data[5]

[5]the embedding procedure is described in Section 3.3.4

2. calculate the distances of each trajectory from the predictee's trajectory y, $d = \frac{1}{k}\sum_i ||X_{N_i} - y||$.

3. for all k trajectories calculate individual weights $w_i = e^{-\theta||X_{N_i}-y||/\bar{d}}$ using an arbitrary choice of θ

4. for the library data $\mathbf{X}$, a matrix of trajectories, A, is organised in the following way

$$\begin{bmatrix} 1 & X_{N_1} & X_{N_1-1} & \dots & X_{N_1-E-1} \\ 1 & X_{N_2} & X_{N_2-1} & \dots & X_{N_2-E-1} \\ \vdots & \vdots & \vdots & \ddots & \vdots \\ 1 & X_{N_i} & X_{N_i-1} & \dots & X_{N_i-E-1} \end{bmatrix}. \tag{4.8}$$

5. The matrix at time Tp points forward, b, of points, is calculated as

$$\begin{bmatrix} X_{N_1+Tp} \\ X_{N_2+Tp} \\ \vdots \\ X_{N_i+Tp} \end{bmatrix}. \tag{4.9}$$

6. Using singular value decomposition the coefficients of the average trajectory is solved as a minimisation with respect to c, against the matrix of forward time points Tp, weighted by their distance from the trajectory y,

$$\hat{c} = \arg\min||Ac - Wb||^2, \tag{4.10}$$

where W is again the matrix of weights.

7. $\hat{y} = \hat{c_0} + \sum_k \hat{c}_i y_i$ gives our found 'predictee' $\hat{y}$.

Consider a famous example of chaotic dynamics shown in Fig. 4.3, the tent map defined by

$$\begin{aligned} x_{t+1} &= 2x_t & 0 < x_t < 0.5, \\ x_{t+1} &= 2 - 2x_t & 0.5 < x_t < 1. \end{aligned} \tag{4.11}$$

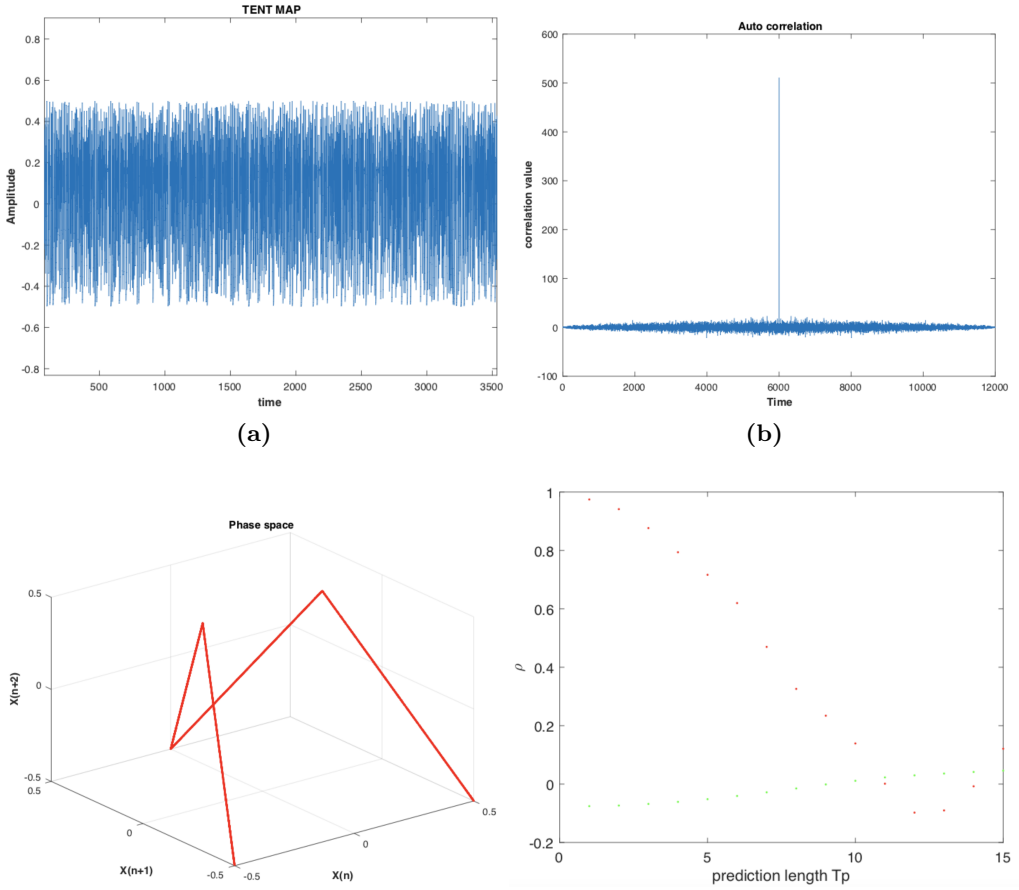

Figure 4.3: Data generated by the tent map given by Eq 4.11, and it's autocorrelation function (b), showing that it seems indistinguishable from noise. However, it's phase space when plotted in R^3 shows its deterministic structure. (d) S-Map predictions (in red) vs. AR(5) predictions (shown in green) for the data in (a)

As can be seen the data seems very random, and it's autocorrelation function very similar to that for noise. However, plotting some point x_n against its immediate preceding neighbour reveals the familiar tent mapping (not shown), or alternatively it's phase space reveals its deterministic structure. Fig 4.3d shows that a S-Map predicts the course of the next 7 or so points well for a mildly nonlinear map $\theta = 0.2$ whereas the autoregression predictor inbuilt in MATLAB's `lpc` function of order 5, does not even predict the next points at all well.

4.1.3 Directional analysis of influence between thalamus and cortex

Two different methods are chosen to investigate this question. Firstly, the nonlinear association index [154, 242] is well validated and robust to nonlinearity. It is appropriate to describe interactions between the cortex and thalamus at time scales smaller than the time constant of this system of between 10 and 40 msec. Secondly, the phase slope index is chosen because of the dominant oscillatory nature of the data, especially at theta frequencies prior to seizures [249].

Nonlinear association index

The approach used here is based on that developed by [242]. At its core, it utilises the fact that asymmetric interdependencies between two signals (say, x and y) will result in differences between the unexplained variances in each signal arising from the other, and also that this difference can be calculated.

It is a non parametric measure of the change in normalised conditional variance from the mean of y at successive time steps τ, $y(t+\tau)$, given knowledge of x, as follows. In contrast with Granger Causality, this variance is found directly from the data, rather than from autoregressive modelling.

Let x be time series data from cortex, and y that from thalamus. The expected value of y given x from the data would be [242]

$$\mu_{y|x} = \int_{-\infty}^{\infty} y f(y|x) dy. \tag{4.12}$$

This can be calculated from the data using piecewise linear regression, following the method of [158]. The nonlinear association between these two signals, $h^2_{y|x}$, is then given by

$$h^2_{y|x} = \frac{\sum_{k=1}^{N}(y(k+\tau) - \langle y \rangle)^2}{\sum_{k=1}^{N}(y(k+\tau) - \langle y \rangle)^2 - \sum_{k=1}^{N}(y(k) - \mu_{y|x}(x(k)))^2}. \tag{4.13}$$

In a similar way to the interpretation of linear cross correlograms, the time $\tau_{x|y}$ is found as the time for h^2 to reach it's maximum. $\tau_{y|x}$ and $\tau_{x|y}$ are used to calculate the delay

time,

$$\Delta\tau = \tau_{y|x} - \tau_{x|y}, \tag{4.14}$$

The degree in asymmetry of the coupling is given by

$$\Delta h^2 = h^2_{y|x}(\tau_{y|x}) - h^2_{x|y}(\tau_{x|y}). \tag{4.15}$$

For example, if $h^2_{y|x}$ is stronger this implies an influence of x on y [177], [242], this leads to the definition of a *Direction Index D*

$$D = \frac{1}{2}(\text{sign}(\Delta h^2) + \text{sign}(\Delta\tau)). \tag{4.16}$$

if D is +1 this implies a temporal relationship $x \rightarrow y$ and similarly, for D= -1, $y \rightarrow x$. From the behaviour of D the ratio of cortical to thalamic drive can be calculated.

The first step in the calculation of nonlinear association is the calculation of the conditional variance for y given x, $h^2_{y|x}$ using Eq. 4.13. This requires knowledge of $\mu_{y|x}$, which is found using piecewise linear regression [177], [158]. Originally Pijn described a method for calculating this curve using the average y value at the midpoint of each bin j, however the method used here[6] utilises the MATLAB command `interp1` for this function. Next, the deviation of each sample in the time series y_i from this curve, $f(x)$, is found, so the unexplained variance for each point in the time series within the bin is

$$\text{var} = \sum_i (y - f(x_i))^2, \tag{4.17}$$

$h^2_{y|x}(\tau)$ is then calculated using equation 4.13 above. Compared with the linear correlation function, $h^2_{y|x}(\tau)$ can be asymmetric. Pijn [158] has also suggested using this as a way of characterising nonlinearity between the two signals.

[6] the code for this routine was modified from original MATLAB code written by Dr Alan Lai

Phase Slope Index

The Phase Slope Index (PSI) is a bivariate measure designed to resolve direction of information flow in oscillatory components of each signal. Nolte's Phase slope index, $\tilde{\Psi_{ij}}$ is defined as [142]

$$\tilde{\Psi_{ij}} = \mathrm{Im}(\sum_{f \in F} C_{ij}(f) C_{ij}(f + \delta f)), \tag{4.18}$$

where Im is the imaginary part, f is a frequency band within the set F of frequencies over which the PSI is to be calculated and C_{ij} is the complex coherence

$$C_{ij} = \frac{S_{ij}(f)}{\sqrt{C_{ij}(f) C_{ij}(f)}}. \tag{4.19}$$

As summarised in [142], this measure is relatively insensitive to mixtures of independent sources in the signal since in this case, excluding discontiguous jumps in phase $0 \to \pm\pi$, Ψ fluctuates around zero. It can cope with nonlinear phase relationships (Sec. 1.3.2).

To first approximation the PSI properly weights contributions from different frequencies according to their contribution to the coherence phase spectrum because, by its definition

$$\Phi_{ij} = \sum_{f \in F} a_{ij}(f) a_{ij}(f + \delta f) \mathrm{sin}(\phi(f + \delta f) - \phi(f)), \tag{4.20}$$

so, to first order for smooth phase spectra, $\mathrm{sin}(\phi(f + \delta f) - \phi(f)) \sim (\phi(f + \delta f) - \phi(f))$, then [142]

$$\sum_{f \in F} a_{ij}(f) a_{ij}(f + \delta f)(\phi(f + \delta f) - \phi(f)) \sim \sum_{f \in F} a_{ij}(f)^2 (\phi(f + \delta f) - \phi(f)). \tag{4.21}$$

This shows that the phase slope index is a meaningful estimate of the average phase slope between the two signals across all frequencies of interest. In contrast, note that the frequency resolved Granger Causality can lead to erroneous results in the case of mixtures of sources or nonlinear phase relationships since these sources can have nontrivial spectral properties [142].

4.2 Results

Data from all available seizures in two of the three GAERS rats that had seizures during tetrode recordings was analysed in MATLAB using the methods described above. There were a total of approximately 460 seizures analysed with a total of 142 seizures in S1; 110 in the junction region S12; and 130 seizures in S2 (Section 4.1.1).

4.2.1 Nonlinearity of the EEG at different scales

It has previously been demonstrated that the EEG is nonlinear by a number of authors (Section 1.3.2). Quite apart from the effects of underlying changes the brain's resting state such as those found in the pre ictal period, the degree of nonlinearity found in EEG signals might depend on how they were acquired [158]. A number of authors have investigated how the EEG complexity changes with proximity to seizure focus, or temporally, in the transition to seizures. The goal here is to quantify how the ECoG nonlinearity changes with the onset of seizures, since further analysis of the data may be affected by this.

To quantify the degree of nonlinearity in the EEG during the inter ictal period, the S-Map method, an extension of the simplex projection method, was used. The difficulty in distinguishing chaos from either nonlinear or linear stochastic processes, to noise, is a well known problem. However Sugihara and May[78] proposed an approach to analysing this problem which is again based on the accuracy of prediction using dynamical methods : chaotic signals are complex but because they may arise from a few variables contributing to the majority of the dynamics of the system, they are still predictable. If this is the case, the EEG dynamics will still be predictable and distinguishable from higher dimensional processes such as stochastic processes or noise if the dynamics are accurately reflected by the attractor described by the lower dimensional embedding (i.e., few chosen variables/degrees of freedom). The S-Map technique allows us to use nonlinear methods to predict data whilst 'tuning' the degree of nonlinear mapping used. The accuracy of prediction using linear autoregressive techniques is used as a comparison.

This method will not provide accurate future prediction if the main dynamics arise

from high dimensional processes such as high dimensional chaos, or stochastic forcing, or noise.

Figs 4.4 and 4.5 shows an application of the S-Map nonlinearity analysis to to quantify the presence of nonlinearity in both EEG and ECoG data. Fig 4.4 shows EEG data from a GEARS rat which was sampled at 256 Hz. Data predictions (shown in red) fitted to θ of 0.3 (Fig 4.4a) or 0.4 (Fig 4.4b) best fit the real subsequent data points better than a correlation $\rho = 0.5$ for up to five data samples ahead, or 2 milliseconds in time. A fifth order linear autoregressive prediction filter, shown by the green squares, failed, indicating that a linear prediction will not be able to fit this data. When this test was applied to the ECoG data from tetrode recordings sampled at 25 kHz (Fig 4.5), its prediction accuracy was valid to a precision of $\rho > 0.5$ for up to 15 predictions. This greater longevity of accuracy may reflect the higher sampling rate of this second data set.

The ability to reliably predict the tetrode data at a level $\rho > 0.5$ for up to 15 samples ahead would suggest that a 4 dimensional embedding reveals some deterministic qualities in this data irrespective of higher dimensional stochastic processes, or noise.

Of note, an embedding of $\tau = 11$ msec was used for the embedding prior to applying the S-Map method. It is unknown whether τ may change during the progression to seizures, but this was not seen in the results from tetrode recordings in this thesis.

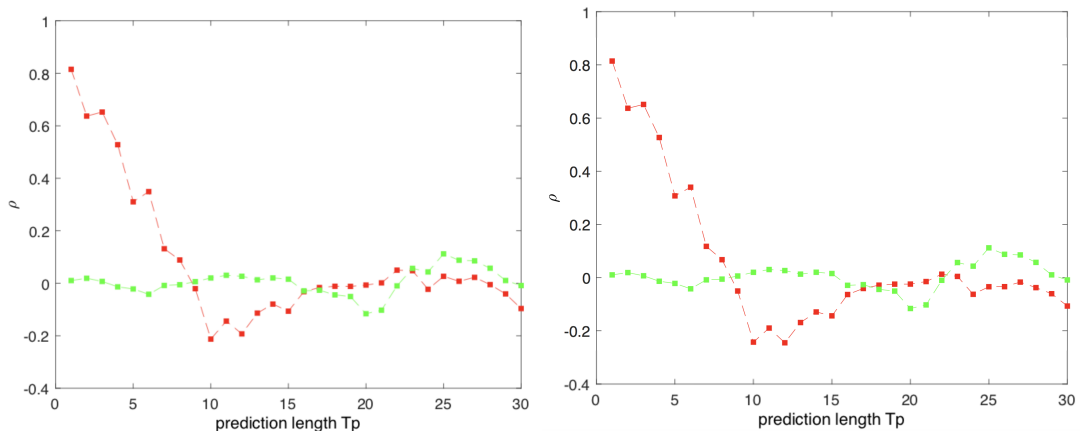

Figure 4.4: Application of nonlinearity analysis to EEG data from a GEARS rat which was sampled at 256 Hz. Prediction accuracy as a function of the number of data points ahead (prediction length), with a nonlinear filter of (a) $\theta = 0.3$; and (b) $\theta = 0.4$

4.2.2 Coupling between Thalamus and Cortex at Fine and Coarse Scales

To see that the inter dependencies between two ECoG signals is not symmetric graphically, consider the nonlinear association curves used to estimate the quantity $\mu_{y|x}$ given by Eq. 4.12. Fig. 4.6 shows the binned data (red crosses) and the piecewise regression curves in black for $\mu_{y|x}$ and $\mu_{x|y}$ where the same data x and y has been used for each subfigure. The asymmetry between $\mu_{y|x}$ and $\mu_{x|y}$ is indicated by the differences in the black curves in each figure.

Interdependency between cortex and thalamus at fine timescales

To start with, consider the interdependence between thalamus and cortex at fine scales. To generate the results that follow, data from tetrode recordings sampled at 25 kHz are used. For the nonlinear association calculation a sliding window technique with a window length of 1250 consecutive data points (i.e., 50 msec) and a window advancement of 2 msec was used. To calculate the piecewise regression curves 50 bins at 2 msec each were used to allow us to calculate correlation behaviour between $\pm$ 50msec at a time with a resolution τ of 2 msec, keeping in mind that the time scale of the thalamocortical circuit

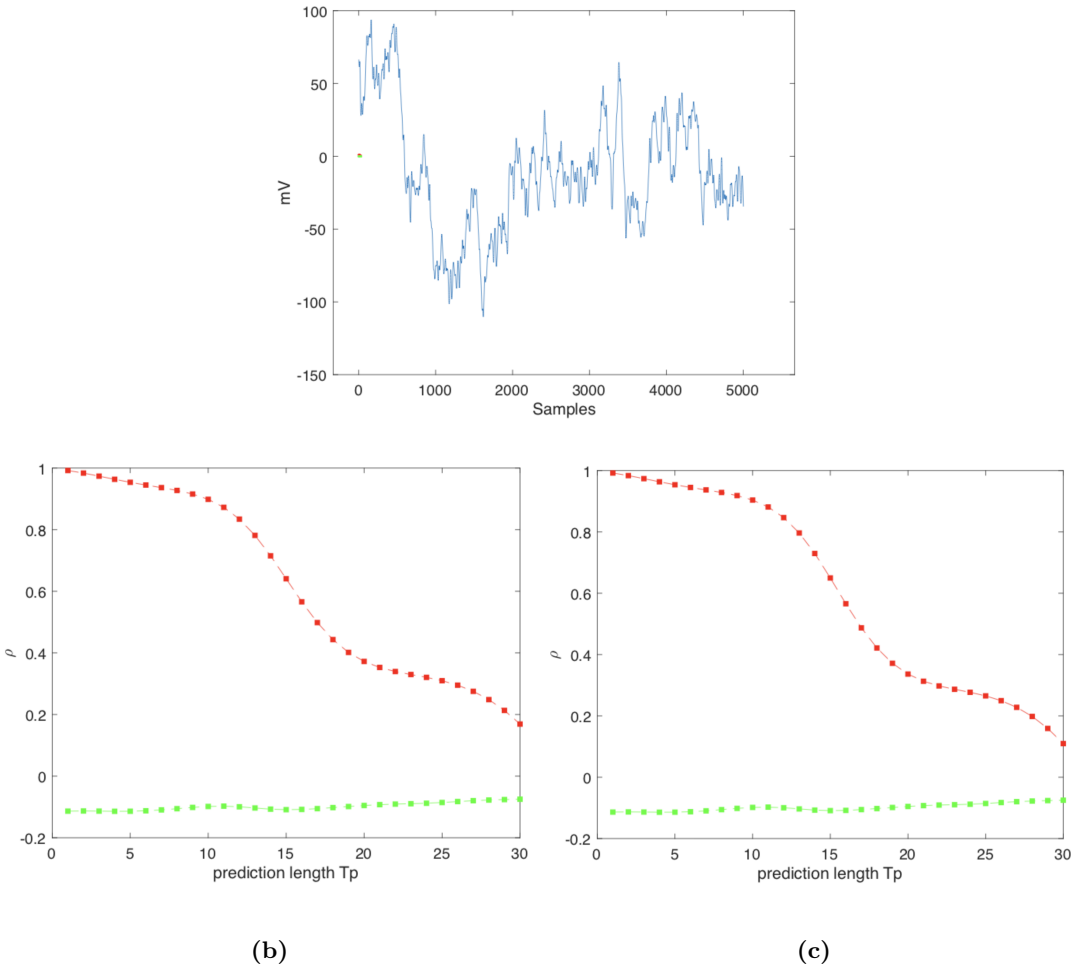

(b) **(c)**

Figure 4.5: Application of nonlinearity analysis to ECoG data from a GEARS rat (recording #200457) which was sampled at 25 kHz (a) the 5000 samples of the data used, (b) nonlinear prediction accuracy for a nonlinear fitting coefficient $\theta = 0.8$, and (c) nonlinear prediction accuracy for a nonlinear fitting coefficient $\theta = 0.7$

is variously estimated at between 10 - 40 msec. The reason for choosing these bin widths was to ensure more than 100 data points in each bin so as to improve the accuracy of the regression calculation. A data length of 0.1 seconds total overlapping windows was used for calculating correlations.

Similarly, in calculating the phase slope index a sliding window technique with time increments of 10 msec was used to ensure appropriate resolution for capturing the changes in driving behaviour between thalamus and cortex at fine timescales. Because the frequency range of interest is wide (between 4 and 80 Hz) a longer window length is necessary.

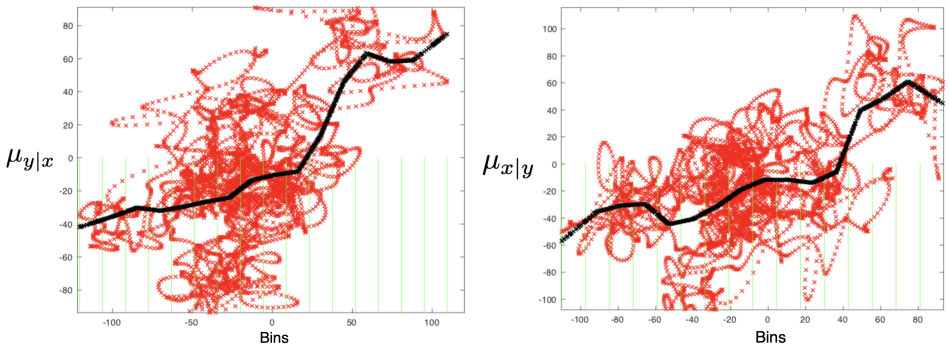

(a) (b)

Figure 4.6: Plot showing piecewise interpolation to calculate the quantity $\mu_{y|x}$, defined by eq. 4.12, (shown in black), from the data points (shown in red) used in the the calculation of the nonlinear association measure $h^2_{y|x}$, which is then calculated using Eq. 4.13. Here, examples of μ are calculated for 5000 data points, shown in red, (a) $\mu_{y|x}$, between cortex and thalamus and (b) $\mu_{x|y}$, between thalamus and cortex, for the same data. Green vertical lines indicate the bins for calculating each piecewise linear midpoint q_j

Fig 4.7 shows a clear oscillation in driving behaviour between thalamus and cortex. Coinciding with the peak of each SWD complex is a peak in nonlinear association between cortex and thalamus. In the example shown in Fig 4.7, the delay D is positive for the first seconds of the seizure, showing that cortex leads thalamus temporally at these times.

Aggregate analysis of all available data from tetrode experiments in the three rats suggest that the patterns found in Figs. 4.7 and 4.8 occur with seizure onset in most seizures recorded. In Figs. D.7a and D.7c the average fluctuations in drive across the first second after SWD occurrence is shown, again supporting this observation. Boxplots show a higher peak drive for the S12 region, followed by S2 in these examples. These support the examples of Figs. 4.8 and 4.7 for the same sample data which showing an alternating pattern of driving influence between thalamus and cortex during SWDs at fine time scales. No frequency dependent behaviour is revealed in the Phase Slope Index measure since this includes a weighted average / aggregate in the calculation of interaction strength, as given by Eq. 4.21.

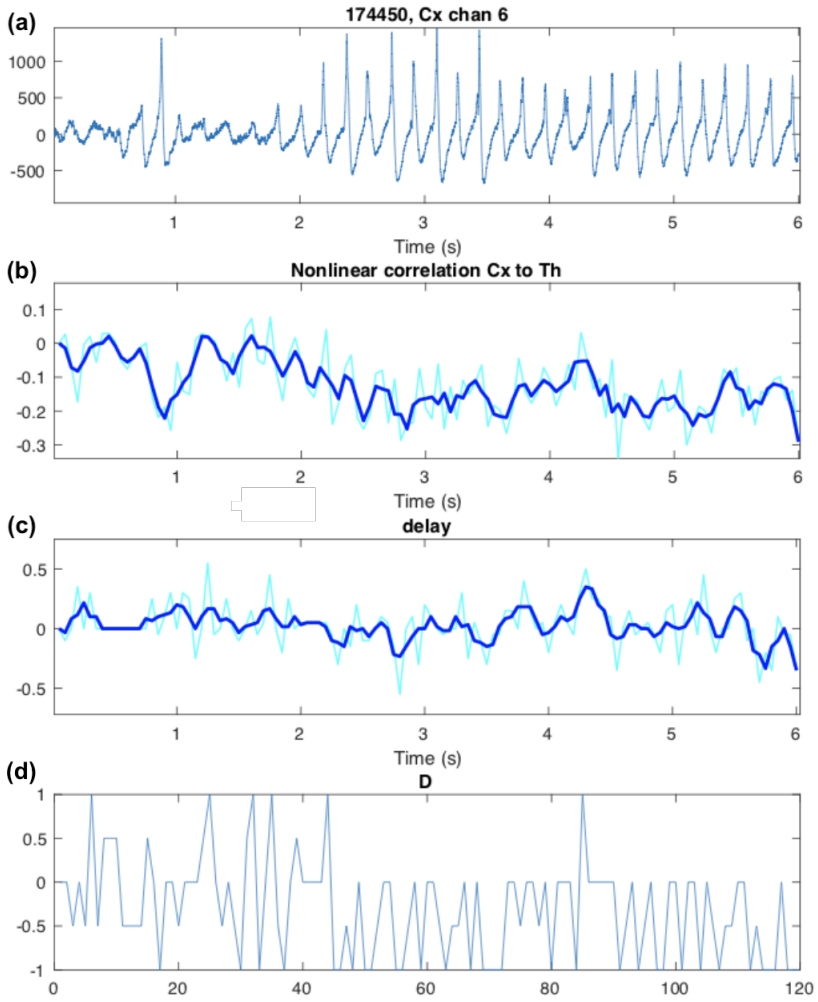

Figure 4.7: Example of nonlinear association analysis for the first 6 seconds of a seizure in a GAERS rat. (a) The recorded data; (b) nonlinear association $h^2_{y|x}$, using Eq. 4.13; (c) delay $\tau_{x|y}$ calculated using Eq. 4.14; (d) the quantity D calculated using 4.16. In both (b) and (c), the cyan trace is the original calculated value, and the darker blue trace shows a moving average calculated over three values of $\tau_{y|x}$ and $h^2_{y|x}$ respectively

Interdependency between cortex and thalamus at coarse timescales

Results for the driving behaviour between cortex and thalamus at the time of seizure onset were found to have grossly similar and consistent patterns using both nonlinear association and PSI methods. However there were some subtle differences in results which reflect the differences in the ways these two methods infer causality.

Fig 4.9 shows the result of nonlinear association analysis for eight consecutive seizures

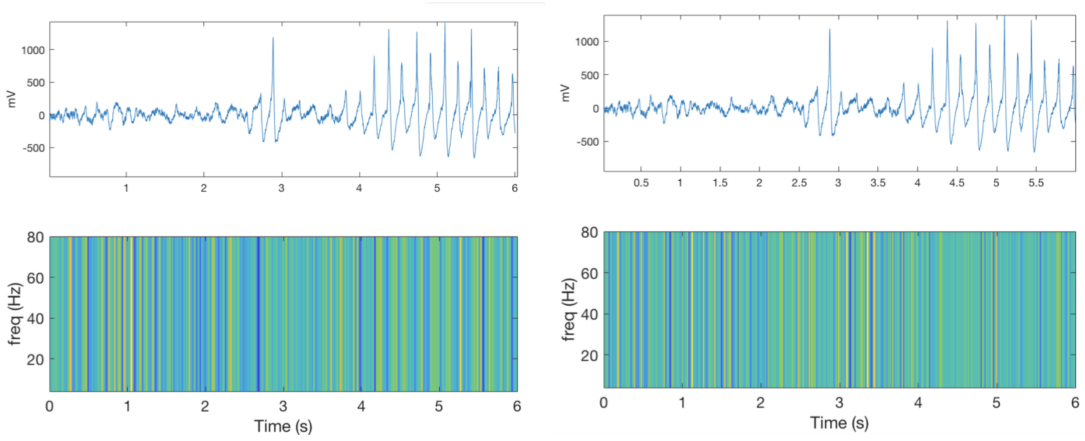

Figure 4.8: Example Phase Slope Index calculated for frequencies between 4 and 80 Hz, just before the onset of a seizure. Top panels show the data, and bottom panels, the Phase Slope Index (a) between thalamus and cortex and (b) between two cortical channels. In both cases the colour map used to show intensity of coupling is blue : strongly negative coupling → yellow : strongly positive coupling.

across a continuous two minute recording. Here it can be seen that the positive drive between cortex and thalamus at the beginning of a seizure. The delay D fluctuates, but appears to become positive at the beginning of some seizures. The Direction Index D is postive during seizures but then becomes negative during interictal periods, again indicating a driving direction in the nonlinear association measure $h_{x\to y}$ of cortex leading the VB thalamus at the start of seizures. The raw data obtained from the sliding windows of 0.1 seconds width is shown in light blue, and the smoothed data (using a moving average of five consecutive data points, shown in dark blue) shows a reduced positive drive but still in the same direction as the raw data. These trends appeared preserved across most seizure data inspected.

To quantify the robustness of the observed trends in the data, all available data for seizures across all rats for each of the three areas of cortex was pooled for further analysis. This resulted in 76 seizures in the S1 region, 84 seizures in the junction region S12, and 56 seizures in S2. To gain a sense of what trends may be present in the data, both the nonlinear association and phase slope index were calculated at the commencement of seizures as shown in Fig. D.7a. Fig. D.7b shows a three way ANOVA from the first

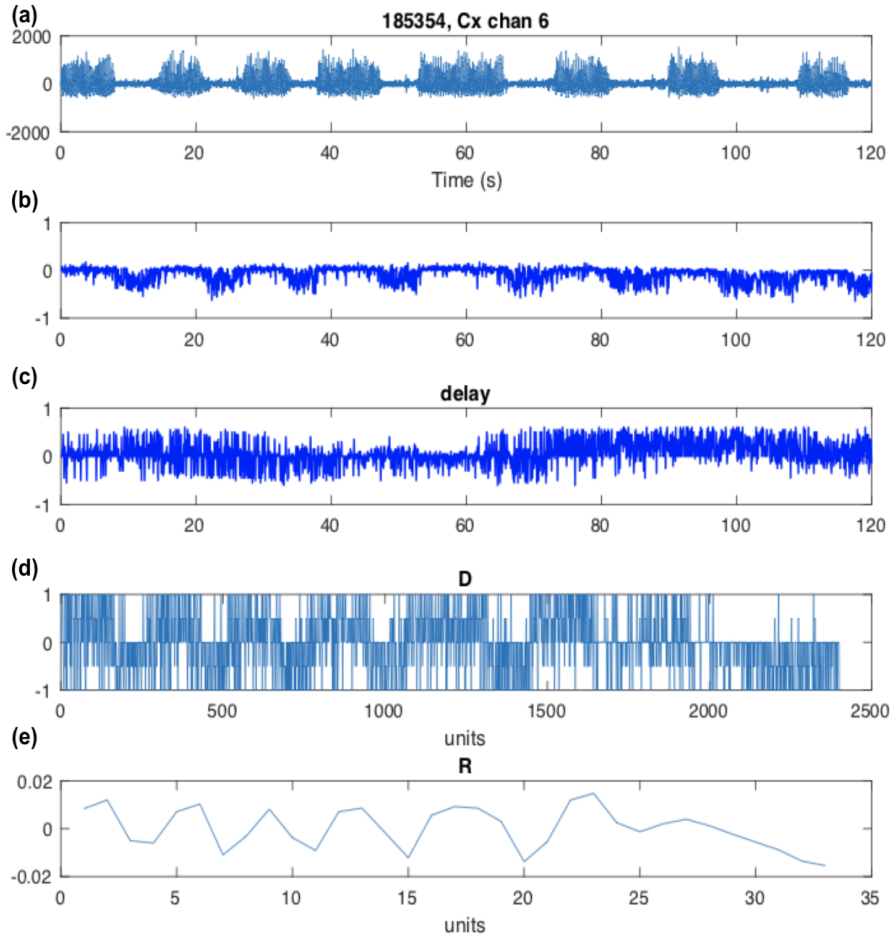

Figure 4.9: Example of nonlinear association analysis over the course of 8 seizures, in 120 seconds, in a GAERS rat (recording #185354). The fluctuation in drive from cortex to thalamus can clearly be seen. (a) The recorded data; (b) nonlinear association $h^2_{y|x}$, using Eq. 4.13; (c) delay $\tau_{x|y}$ calculated using Eq. 4.14; (d) the quantity D calculated using 4.16; and (e) the quantity R, a moving average of 80 consecutive values of D.

second of all seizures, using the FieldTrip plugin script `nonlinearassociation.m` in which there was a statistical difference between the three means[7]. While the boxplot of this figure suggests statistically significant differences, the nonlinear association analysis written independently using Eqs. 4.13 to 4.16 shows a less markedly positive association.

The further analysis in Fig 4.12 and 4.13 demonstrate some reasons for this apparent discrepancy. In Fig 4.13, the quantity Δh^2, defined by Eq. 4.15, is calculated by stage or seizure development or termination. However, the quantity D, which can be seen as

[7]This FieldTrip routine was not used for the analysis of this chapter.

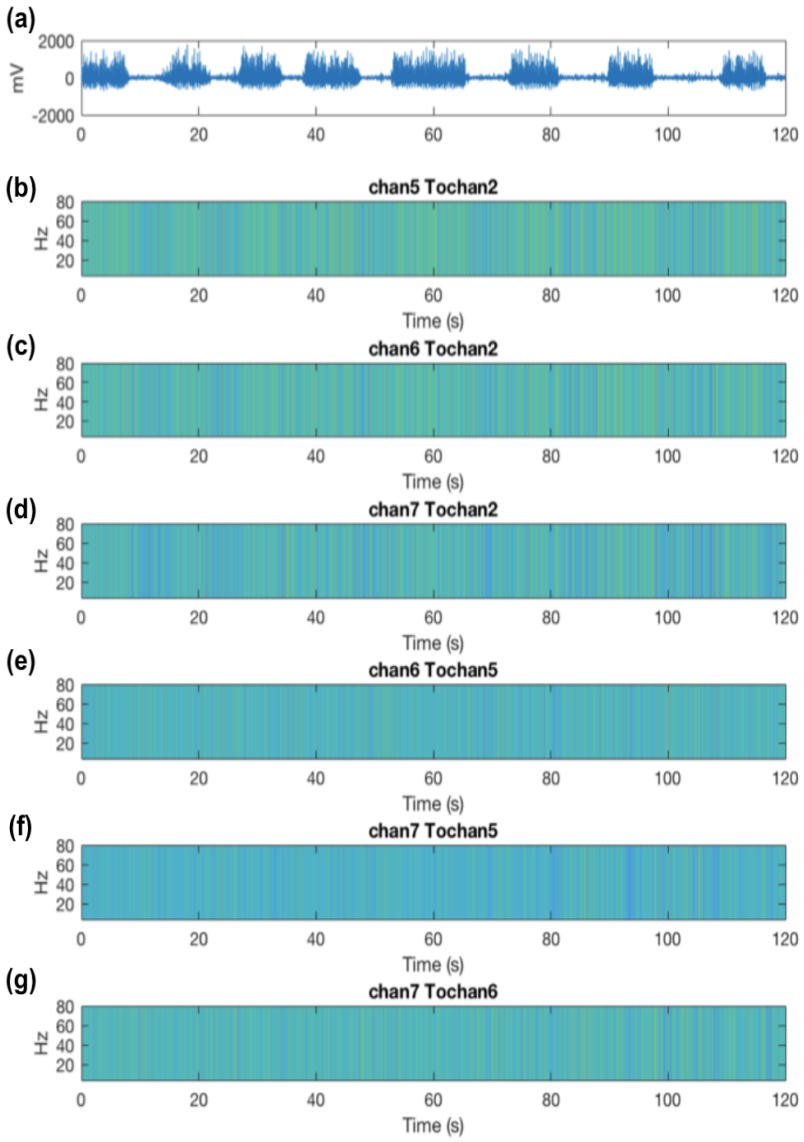

Figure 4.10: Example of PSI over 8 seizures over 2 minutes in a GAERS rat. (a) the data as in Fig 4.9. (b)-(d) Corticothalamic coupling strength and (e)-(g) Cortico-cortical coupling strength. The tendency for increased positive drive from cortex to thalamus can clearly be seen. As in Fig. 4.8, in all cases the colour map used to show intensity of coupling is blue : strongly negative coupling → yellow : strongly positive coupling.

an averaged 'composite' measure of both Δh^2 and $\Delta\tau$ given by Eq. 4.16 suggests that a predominantly leading cortex at seizure initiation is more likely from the data. This was calculated by finding the maximum and minimum of the SWD cycle after seizures had commenced, as illustrated by example from some SWD data, in Fig 4.11a. The magenta

asterisks show the calculated position of SWD peaks and troughs respectively. The reason for a slight lag in these respective positions is that I found it more accurate to calculate the maxima from 5 - 9 Hz bandpass filtered data so as to eradicate the possibility of double maxima being found and also to minimise noise. A sample of 3000 data points were taken from either behind or in front of this maxima from either cortex or thalamus.

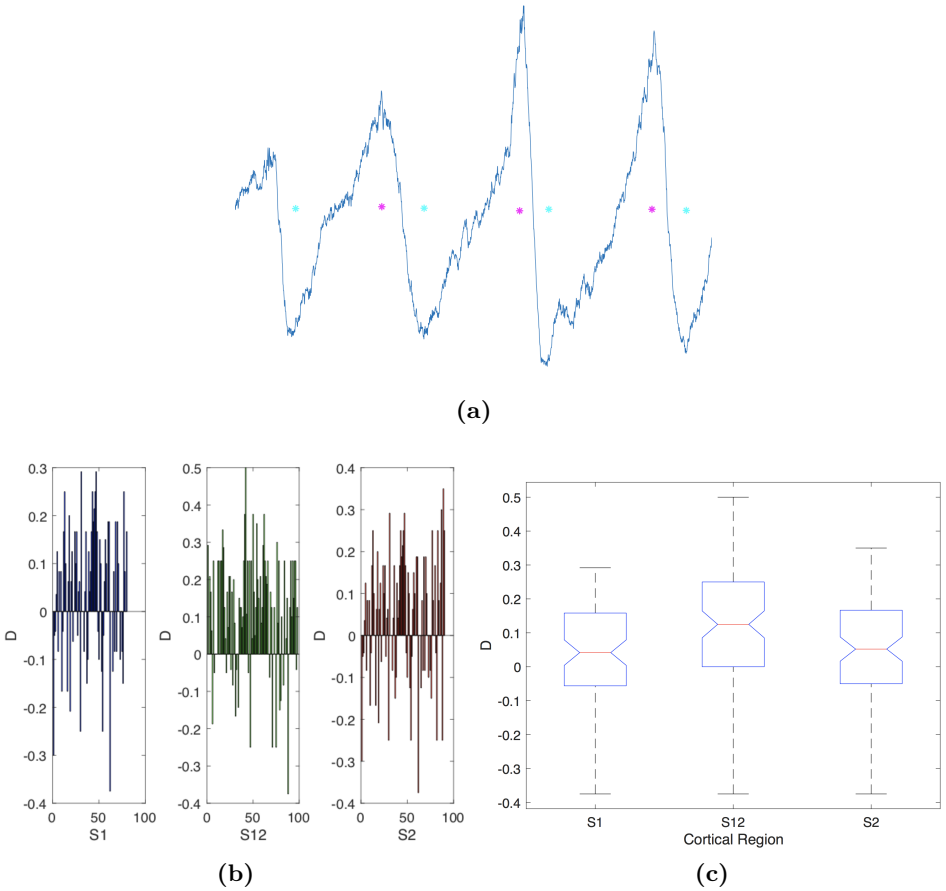

Figure 4.11: Mean values of D, defined by Eq. 4.16 found using samples of 3000 data points, prior to each SWD peak or trough, shown in magenta or cyan stars respectively : (a) Representative segment of SWDs; (b) Histogram of D values for all available seizures in the second after seizures commence; (c) Boxplot from ANOVA analysis of the histograms in (b) showing a statistically significant difference in means, $p < 0.013$.

In subsequent analysis, the statistics generated from ANOVA analysis such as quantiles, or mean and standard variation, were used to calculate the statistics for error bars also.

To show how drive fluctuates across all pooled tetrode data for all regions and seizures,

an ANOVA of coupling strength and delay was done. The results are summarised for each of the main time points before and after seizures in Fig. 4.12 and 4.13. Time points chosen for analysis as 'inter' - interictal (calculated as the midpoint between termination of the last seizure and the start of the next; 's - 4' - four seconds prior to seizure onset; 's + 2' - two seconds after seizure onset; and 't - 4' - four seconds prior to seizure termination, etc. The midpoint of seizures 'mid' was calculated for each seizure individually as all seizures had differing lengths. To ensure the mid seizure timepoint was a valid concept and different from other time points, seizures of less than ten seconds' duration were excluded from this analysis.

For the Phase Slope Index computations, the frequency range 4 to 120 Hz was used. Fig. 4.12 and 4.13 show the standard deviation (dotted lines) and mean (bold lines) of driving influence from cortex to thalamus by seizure stage. Here, the main result is that pooled drive between cortex and thalamus was positive at the start of seizures, for both PSI and nonlinear association measures. When comparing the cortico-cortical drive between closely adjacent regions in deeper layers of cortex, it can be seen that the S2 area had higher driving intensity at the commencement of seizures.

Inspection shows that the S12 region has higher coupling with thalamus than S2 or S1 immediately before a seizure. ANOVA analysis shows a statistically significant difference between means for these comparisons between averages at $p < 10^{-7}$.

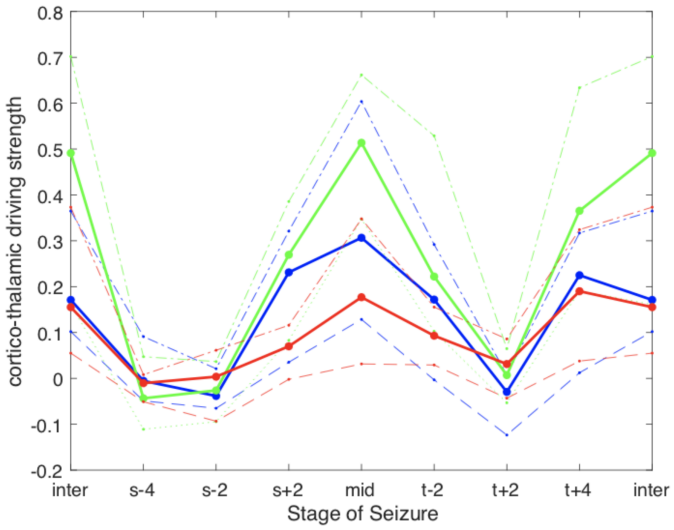

(a)

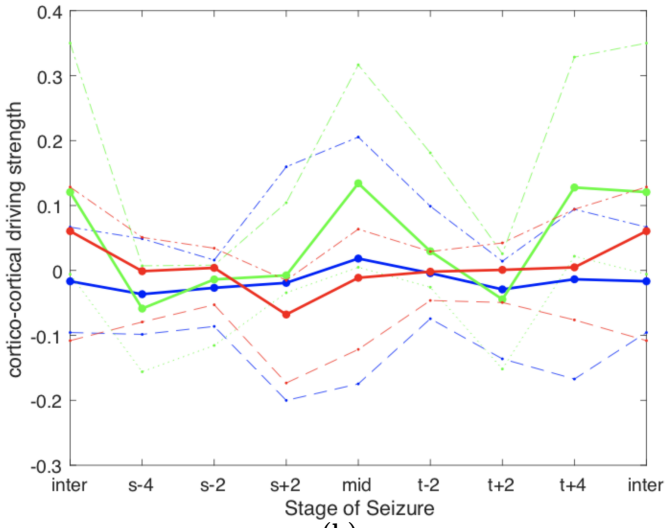

(b)

Figure 4.12: Cumulative plot showing mean and quartiles in direction and strength of drive (a) between cortex and thalamus in relation to initiation and termination of seizures, at ictal and interictal time points. Pooled data, analysed with the Phase Slope Index is shown for each of the three cortical regions. The x axis labels refer to the time in relation to seizures starting and terminating, respectively : s -, prior to seizure onset; s +, after onset, t -, prior to termination, etc. (b) As above, but for cortico-cortical channels. Solid lines denote the mean calculated values with dashed lines the 25th and 75th quartiles in range of calculated values at each stage. Colour code is S1 (blue), S12 (green), S2 (red).

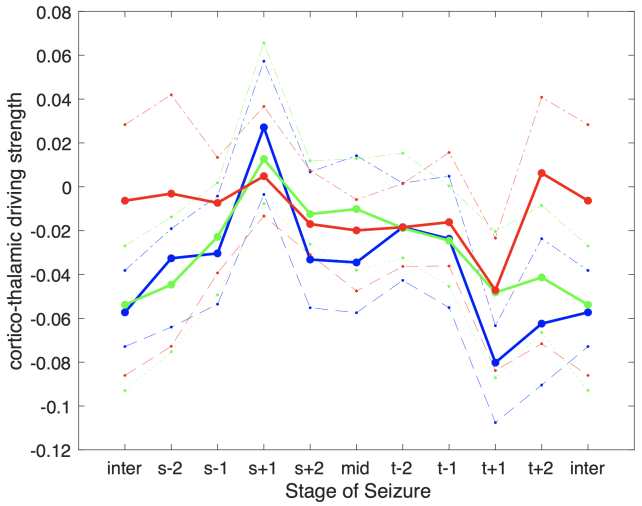

(a)

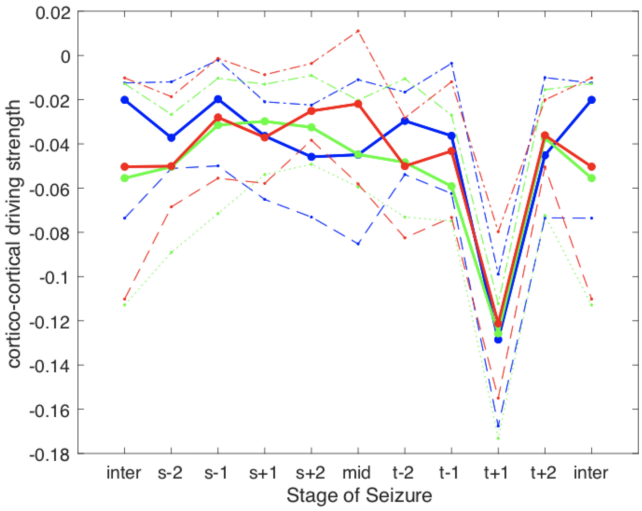

(b)

Figure 4.13: Cumulative plot showing mean and quartiles in direction and strength of drive (a) between cortex and thalamus in relation to initiation and termination of seizures, at ictal and interictal time points. Pooled data for all nonlinear association analysis, showing Δh^2 as given by Eq. 4.15 for each of the three cortical regions. X axis labels refer to the time in relation to seizures starting and terminating, respectively : s -, prior to seizure onset; s +, after onset, t -, prior to termination, etc. (b) As above, but for cortico-cortical channels. Solid lines denote the mean calculated values with dashed lines the 25th and 75th quartiles in range of calculated values at each stage. Colour code is S1 (blue), S12 (green), S2 (red).

4.3 Discussion

4.3.1 Comparision with previous studies

Nonlinearities in EEG signal analysis

The studies outlined in this Chapter were designed to infer the directional influence of drive between different areas of somatosensory cortex (S1, S2, and the junction between these, here called 'S12') and thalamus. It is known that the normal action of thalamus is to facilitate synchronisation between disparate brain regions through modulation of the membrane potential of thalamic nuclei [98], and that the thalamocortical circuit can display altered modes of activity between different brain states such as sleep and wakefulness [214], which are integral to normal brain function 1.2.1. The mechanisms behind the alterations in the functioning of this network, which result in a pathologically high degree of hypersynchrony between cortical and thalamic areas, and bilaterally, in seizures is investigated separately in Chapter 5.

Oscillations are presumed to reflect synchronised action potentials between areas of cells recorded at a finer level of resolution, and seen in the studies of Pinault [161, 166], and our previous work [249]. It makes sense, then, to utilise methods that arise from a framework which allows inference of temporal imformation flow, and that also take into account the oscillatory properties of the data. It also makes sense to account for the time constant of the thalamocortical circuit, so that any directional activity is interpreted within this context, or spurious effects such as 'edge effects' [102] which can give rise to spurious higher frequency components not present in the data.

The methods used in this study were chosen because they are non parametric and also well validated in the study of EEG data. The phase slope index was chosen because it allows inference of the consistency of drive across a number of frequencies present in the data, weighting these appropriately [142]. The Pairwise Phase Consistency measure of Vinck and colleagues [238] has been used in other work studying thalamocortical mutual influence in the WAG/Rij rat model [3] was considered. This measure is calculated from the distribution of pairwise relative phase interactions, so it would require segmented anal-

ysis at different times of the thalamocortical 'cycle', given that the results of this chapter indicate that driving influence fluctuates between thalamus and cortex when analysed at fine time scales of the order of the thalamocortical time constant. This would complicate the analysis, especially at low frequencies, and given that each frequency range would need to be analysed separately with this measure, offsetting its advantage of being statistically robust for differences in sample size. Instead, statistical analysis based on uneven samples was performed with the phase slope index, and should be similarly statistically robust. Another issue is that the phase slope is estimated as an average across all frequencies in a statistically meaningful way. None of the measures used here assume a linear relationship between the two time series.

The results of S-Map analysis of ECoG and depth electrode data indicate that the degree of nonlinearity varies with the spatial scales of cortex sampled. This is not surprising given that neurons are highly nonlinear devices, yet when summed over great distances the degree of nonlinearity may change. This has implications for the applicability of the wide variety of different available inference measures used in neuroscience, of which at least 42 have been proposed [14].

These results are in agreement with previous studies by Pijn [158], and Lopes da Silva [242]. They point to different degrees of nonlinearity at finer scales of data collection, which is not unsurprising given the highly nonlinear nature of spikes. What is less studied is the way in which that may affect analysis.

A potential oversight in the analysis presented in this chapter is the possible confounding issue of time-dependent coherence changes in the data common to both thalamus and cortex. Coherence measures do not generally separate shared amplitude increases (Section 5.2.3) from increased phase consistency, and can then lead to ambiguous results in the setting of increased cortical population recruitment. This issue is specifically addressed in Chapter 5.

4.3.2 A Cortical or Thalamic Focus, or Both?

The objective of this chapter was to document the strength and direction of interactions in the cortex and thalamus at both coarse and fine timescales in the course of development of SWDs in GAERS rats. A novel aspect of this study was to investigate both depth electrode data sampled at 256 Hz and 25 kHz tetrode data for characterising deep layer cortical networks. This is also the first study of directional influence in corticothalamic networks for different areas of somatosensory cortex in the rat.

The main finding of this chapter is that the thalamocortical network displays reciprocal driving behaviour both before and during SWDs. Cortex was found to drive thalamus at the beginning of seizures, a finding that is consistent with previously published literature such as Meeren's study finding that the S1 cortex leads thalamus in the first 500 msec of seizure activity [131]. However here it was found that the S12 and S2 cortex have different characteristics to S1, and that S12 was slightly stronger in cortical drive. Whether this may arise from increased cortical resonance with thalamus or from changing dynamics is explored in Chapter 5.

At both fine and coarse timescales, very similar trends in the oscillation of coupling direction between thalamus and cortex were found using either nonlinear association analysis or using the Phase Slope Index. The change to positive lead by cortex during the start of seizures would be consistent with the loss of normal inhibition by thalamus in the thalamocortical loop at that time.

From Fig 4.9, it can be seen from the calculation of R that this swings between positive values coinciding with seizure onset, to negative values interictally. There is inherently some 'lag' in the measure since it is an aggregate average of 80 consecutive calculations of the signed-interaction measure D, and D itself is a summed measure over 50 msec chunks of data at a time. D itself strongly trends towards the positive at the commencement of seizures and there is supporting evidence of a similar trend this using the PSI measure a shown in Fig 4.10.

Changes in the Phase Slope Index measuring cortcothalamic drive shown in Fig. 4.11c suggest this is slightly stronger for the S12 region in the first second of seizures significant

at the start of seizures. From the analysis this trend is statistically significant at $p < 0.0133$ for all available seizures in three animals, a conclusion which is supported by the Phase Slope Index analysis shown in Fig. 4.12. PSI ratios also move from a predominantly negative yet balanced interaction interictally to a more cortex-predominant driving picture during seizures.

Examination of interactions at fine timescales explains why the strength of these interactions overall is weak when analysed at 'coarser' time and spatial scales as this would represent an averaging over smaller time frames, given a thalamocortical time constant of between 10 and 40 seconds [177], even though peak interactions are strong. From the results of this chapter it appears that oscillations between the thalamus and cortex are coincident in timing with the dominant thalamocortical rhythm.

These results were consistent between analysis methods used and also in agreement with previous studies. In our previous work, we also found rhythmic layer VI cells more dominant in S2 cortex [249].

One difference between the experiments summarised here and Mereen's study was that he utilised surface EEG recordings. These results extend those previous studies using high density depth recordings, and also by including a comparison of different areas of somatosensory cortex. These results also point to the importance of method selection in the interpretation of results found, because of the nonlinearity of EEG data.

Before using the Phase Slope Index, Granger Causality was also investigated. This did not obtain consistent results either from surrogate data generated from the coupled Rossler-Lorentz system shown in Fig. 4.1 or from tetrode data. Approximately half the time, the conditions for using Grainger Causality were not met because it was not possible to generate an appropriate autoregressive model. This could be because the alternating drive between cortex and thalamus will cause difficulty fitting an appropriate autoregressive model. Here, it is relevant to mention a method developed by Sysoeva and colleagues, based on instead inferring Granger Causality on the time delay mapping between local neighbourhoods in the phase space of the data [221]. The inference in this method is then based on an autoregressive fitting of this trajectory. While it would be interesting to see if this method could accommodate the alternation in drive between cortex and thalamus,

it may be likely that Sugihara's S-Map method may be more applicable as it eliminates the need for an autoregressive model. However, both of these methods would require an accurate determination, from the phase space embedding, of 'library' segments which are accurately aligned with the progression in drive between relevant structures. These analyses are the subject of further work, and not included in this thesis.

4.4 Conclusion

In this Chapter the presence of nonlinearity in the depth recordings obtained from GAERS rats is confirmed. This was measured with both depth EEG recordings in somatosensory cortex, sampled at 256 Hz, and in tetrode recordings sampled at 25 kHz. At the much finer spatiotemporal resolution present in the tetrode recordings, the degree of nonlinearity appeared higher, as measured with the goodness of fit of predictions using Sugihara's S-Map alogrithm with increasingly nonlinear weighting functions θ.

The interdependencies between thalamus and different areas of somatosensory cortex were also studied. In agreement with previous literature, it was found that cortex does lead thalamus at the onset of seizures, and also at various times in the inter ictal period. Following termination of seizures there is a period of reduced drive in both thalamus and cortex, with a tendency of the thalamus to drive cortex. All areas of somatosensory cortex showed positive drive at the onset of seizures, but this drive appeared highest in the S12 region. This region also showed the highest degree of coupling between adjacent cortical regions.

Using an ANOVA analysis the differences between means was shown to be significant, but with only two rats studied the differences in confidence intervals between cortical regions still overlap. To see that the strong trend for increased drive in the S12 region is consistent, further experiments are planned.

Chapter 5

Evidence for the Cortical Focus Theory, and mapping resonance

5.1 Introduction

The term *resonance*, derived from the Latin 'resonantia', echo, and 'resonare', meaning to resound[1], is a phenomenon observed in many natural systems when oscillatory activity may produce a larger amplitude response after input from certain frequencies rather than others, termed *natural frequencies*. Familiar examples might include the 'wolf notes' well know to players of stringed or brass instruments, electrical resonance in electronic circuits such as radio receivers, the 'singing' of wires under certain wind conditions, or the shattering of glass in response to a high-pitched note.

Oscillations are an inherent property of the thalamocortical loop, and a consequence of the oscillatory membrane behaviour of thalamic nuclei ([98], and Section 1.2.1). They are believed to underlie our brains' ability to synchronise different cortical regions[32]. A central question, then, is how and why naturally occuring somatosensory rhythms sometimes transform into pathological oscillations, given that both arise from the same brain networks.

One may suppose that network resonance has some part in this process, and the investigation of this phenomenon is the subject of this chapter. The focus here is (1) whether changes in resonance can be demonstrated in the thalamocortical network prior to and during seizures; (2) in which parts of the thalamocortical loop and somatosensory

[1] From Wikipaedia, accessed June 2019

cortex this actually occurs, and (3) what mechanisms may underlie this resonance.

Absence epilepsy is characterised by recurrent, generalised non convulsive seizures manifesting in brief episodes of altered consciousness, often commencing in childhood, with or without accompanying automatisms. Patients are often not aware of these events while witnesses can observe multiple episodes, up to hundreds in a day. It is often treatment resistant in that anti epileptic drugs (AEDs) will fail to attain seizure freedom in up to 50% of patients either because of intolerable side effects to the patient or inadequate seizure control [49],[68](Section 1.2). Apart from being an important clinical problem, the study of generalised absence seizures also offers the opportunity to understand the neurobiology behind other types of generalised seizure occurrence as well as the process of epileptogenesis and its treatment. Invasive electrophysiological studies of the origins and dynamics behind these seizures in humans are not usually possible in human patients for ethical reasons, as most generalised idiopathic epilepsies are not usually amenable to surgical treatment. Consequently, we must turn to appropriate animal models instead.

In contrast with many models of 'seizures' such as in vitro slice preparations or induced seizure models such as the tetanus toxin, GHB, or penicillin induced post status epilepticus models reviewed in Section 1.2, the Genetic Absence Epilepsy Rats from Strasbourg (GAERS) model has many advantages[54]. Chiefly among these, this model resembles human absence epilepsy from the behavioural, pharmacological and electrophysiological perspectives, and can also be studied in the awake, behaving animal. Most importantly, bilaterally synchronous spike and wave discharges (SWDs - Fig 1.2, Section 1.2.1) - the hallmarks of absence epilepsy - seem to arise from a normal, desynchronised, background EEG, and also cease abruptly, without postictal slowing or depression (compared with other partial or generalised epilepsies involving convulsive seizures). As in humans, seizures most commonly arise from quiet resting wakefulness, often following or preceding slow wave sleep, and are less common in states of high arousal or other stages of sleep. Drugs that can be effective in suppressing human absence seizures such as ethosuxamide or sodium valproate are also effective in suppressing SWDs in GAERS rats, and medications known to aggravate absence seizures in humans such as carbamazepine or oxcarbazepine also have this effect on the SWDs in this rat model. Blumenfeld and colleagues showed that early

treatment with AEDs can impede later SWD development [26], and there is accumulating evidence that this also treats the analogues of common neuropsychiatric symptoms seen in humans such as anxiety and depression.

Most agree that absence seizures arise from the thalamocortical system, and require intact connections within this for generalised bilateral seizures, but there has been wide debate around what relative contributions of these regions generate these seizures, and how interactions between them lead up to SWDs. Gloor [81] introduced the 'cortico-reticular theory', postulating that the thalamus acted as a rhythm generator, and an excitable cortex transformed sleep spindles generated from the thalamic reticular nucleus and thalamocortical relay cells into SWDs. Meeren [131] found that seizures started locally mainly from perioral somatosensory cortex in surface EEG recordings from WAG/Rij rats. Polack [171] recorded from layers V and VI in the S1 region in GAERS rats, finding that pharmacological deactivation of neurons in deep layers of this region suppressed SWDs, and suggested that this may be a focus of absence seizures.

In 2012 Zheng and colleagues published results indicating that SWDs were preceded by 5 - 9 Hz physiological field potential oscillations detected first in the S2 and insular cortical (IC) regions of somatosensory cortex [249]. In this study maximal suppression of SWDs occurred after injection of an endogenous neuropeptide NPY into S2, more than S1; pre ictal oscillations occurred first in S2/IC before S1 or motor cortex in the one or two seconds before generalised SWDs; and SWDs could be triggered by lower intensity microstimulation in deep layers of S2 than S1. High frequency oscillations occurred earlier in S2, by more than 20 msec, a remarkably long lag considering the close proximity of the two paired recording regions (1 - 3 mm). This was also the first time that HFOs had been described in absence seizures[249]. At the cellular level, it was found that the majority (∼79%) of cells in deep cortical layers fired rhythmically at the SWD frequency of 5-9Hz before and after seizures using paired glass electrode recordings, suggesting that these cells may have been part of the 'rhythm generator' circuit, from which SWDs arise. The conclusion of this study was that the S2 somatosensory cortex and associated insular cortex also forms an important part of the seizure generating circuit, and that this region should also merit more study.

A relevant question, debated from different viewpoints in the literature, is of what mechanism leads to increased resonance and seizures when they occur. In other words, is there evidence of a change in system dynamics leading to more instability (in the line of works such as [94],[52],[89], and their cited literature), or is this phenomenon of increased resonance the result of increased synchrony and recruitment in greater areas in deep cortical neurons, in line with the single cell electrophysiology studies cited above?

To uncover details of the changes in large-scale behaviour of thalamocortical networks, there have been a number of studies of the direction of coupling and changes in coherence between thalamus and cortex. These have focused almost exclusively on primary somatosensory cortex and its behaviour in relation to anterior thalamic nuclei ([3], [161], [165], [166], [54]). Apart from Zheng's study discussed above, detailed examination of other relevant areas of cortex mentioned above such as S2 or insular cortex in relation to absence seizure generation has been rare. Many studies now accept that primary somatosensory cortex has many properties suggestive of a cortical 'focus' for absence seizures (for example [1], [3],[116],[230], [54], [131]) although studies of the phenomena underlying cortical resonance which may underlie this are, to quote Luttjohan and colleagues, "surprisingly rare"[115] (for background see Section 1.3.1). This chapter addresses this omission.

A number of authors have studied the behaviour of network phase coherence in epilepsy, but different studies have utilised different methods for obtaining this measure in different experimental conditions and epilepsy syndromes, so a unifying conclusion around the significance of phase coherence in the maintainence of synchrony is difficult to obtain. Netoff and Schiff found an increased synchrony before bursts from micro electrode data, and comparative desynchronisation prior to seizures[137]. Majumdar and colleagues [121] found decreased synchrony prior to seizures which increased before seizure termination, and suggested that the increased synchrony noted by early authors may in fact be an epiphenomenon of other changes such as acidosis[121]. Perez-Velasquez, Dominguez and colleagues [58] studied recruitment of distant brain regions such as bilateral hippocampi and dentate gyrus to the thalamocortical circuits involved in absence epilepsy using the Mean Phase Coherence measure of Mormann and colleagues [67],[135]. Their method was

to divide frequency bands of interest from 5 - 63 Hz into narrow bands of 4Hz. Whilst they did not consider pre-ictal synchrony changes in thalamocortical regions, they found increased synchrony between hippocampi during SWDs.

Previous studies have found some evidence for increased resonance in S1 cortex prior to seizures such as harmonics at 10 Hz optical stimulation [241], increased sensitivity to electrical stimulation[1], or increased amplitude coherence[59] in S1 cortex at similar frequencies.

Given the evidence presented in Chapter 4 that cortex has some increased driving influence on the the thalamus at the time of seizure onset, that this increase is in the first second of seizures, and also that this appears higher in S1, S12 and in S2 cortex in GAERS rats, it is natural to ask whether there is evidence of increased resonance in these relevant cortical areas which occurs at seizure onset. If this is the case, the next question is that of what the process generating this increased resonance is.

Resonance might arise from a number of different processes, which may not necessarily be mutually exclusive. For example, these may include increased recruitment of cortical areas which would be indicated by increased amplitude power in specific frequency bands and / or their harmonics. Increased amplitude coherence may indicate higher reciprocal connectivity between thalamus and cortex. Alternatively higher resonance may result from more complex patterns of synchronisation and phase entrainment. This may include similar phase angles across harmonic components or other frequencies which achieve resonance through a kind of 'coherent' addition without necessarily any increased spectral power in the signal, or cross frequency coupling. On the other hand, if resonance is associated with more dynamical instability it is likely to be accompanied by increased oscillatory components indicating Lyapunov exponents moving closer to zero, or indications of increased sensitivity to perturbation.

The hypotheses of this Chapter are :

1. That cortical resonance is present and accompanied by amplitude and phase coherence changes temporally with seizure development, and termination;

2. That this resonance is highest in the S12 and S2 regions, as measured by increased

phase and amplitude coherence, harmonic power, or coupling between the dominant theta rhythm and other frequencies of the local ECoG signal in deep layers of cortex

3. This will be accompanied by changes in dynamical stability, measured by differences in the Lyapunov exponent in the cortical ECoG signal

In what follows, the analysis approach of this chapter to test these hypotheses is to :

- Measure any changes in the power spectrum and both intra-cortical and corticothalamic coherence (Section 5.2.2) in relation to seizure onset and termination;

- Assess changes in harmonic power at seizure onset (Section 5.2.2);

- Assess changes in the synchrony of networks between different cortical areas and thalamus, at both the level of local networks (i.e. between tetrode channels) and global level (i.e. intracortical synchrony between simultaneous depth electrode channels in different cortical areas).

- To better understand the relative role of phase versus amplitude coupling prior to seizures (Hypotheses 1 and 2), phase coherence, and cross frequency coupling (Section 5.2.5) is also analysed in the different cortical regions.

- To further investigate the characteristics of phase entrainment, the amount of phase clustering or dispersion is also quantified (Section 5.2.4).

- Determine if there is evidence of a change in system dynamics, as might be assumed on the basis of different scaling behaviour (as discussed in Chapter 3), or as suggested by [220], [94]. To investigate changes in network dynamics with seizure onset permutation entropy (Section 5.2.4) is used to quantify relative signal complexity. The sensitivity of the system to perturbation is quantified using nonlinear analysis methods (Section 5.2.7) and also by the Finite Scale Lyapunov Exponent (Section 5.2.7).

This chapter focusses specifically on the thalamocortical networks believed to be the focus of absence seizures - not only S1 somatosensory cortex, but also the neighbouring

regions of S2 and insular cortex and also the VB thalamic nuclei which are known to be functionally connected. It also analyses the network changes accompanying absence seizures in the GAERS rats. The aims are to identify what mechanisms are involved in seizure generation, what the progression of changes are prior to seizures, and to what extent seizures originate in a stereotyped way.

5.2 Analysis Methods and Data Processing

5.2.1 Data collection

Details of surgery and electrode implantation techniques are explained in more detail in Chapter 2. Here, the salient features of data collection are briefly summarised in the context of the analysis which follows. Details of relevant ethics approval are also listed in Chapter 2.

Briefly, two different types of experiments were performed. The first experiment was designed to study multiple cortical areas simultaneously and involved chronic implantation of multisite depth EEG electrodes. The second type of experiment was designed to study very small regions of cortex, or thalamus, at a time. For this purpose tetrodes were used to obtain dual recordings between selected areas of cortex and thalamus simultaneously. For these tetrode experiments three GAERS rats and two NEC rats were used.

Depth electrode experiments

Rats were chronically implanted with 127 μm stainless steel electrodes bundles in which each electrode bundle consisted of insulated wires where the insulation was stripped at 0, 1.0, 3.0 and 5.0 mm from the end, enabling recording simultaneously at four different locations in cortex. Electrodes were implanted bilaterally into S1Ul and S1Fl, S2 and IC (insular cortex), and a separate electrode was implanted into motor cortex, later in this chapter labeled M1. Extradural reference electrodes were implanted into parietal bone. These experiments were performed by Zheng[249], and rats were allowed to recover for 7 days before recording sessions.

Data was sampled at 250Hz, for at least two 60 minute recording sessions for each rat. Both the GAERS and NEC control strain of GAERS rats used in these experiments were at least 13 weeks old, and weighed between 250 and 350 grams. Recordings were taken from different cortical areas in 5 GAERS and 3 non epileptic control (NEC) rats.

Tetrode experiments

For tetrode recordings, neuroleptanalgesia was used after induction with ketamine and xylazine, intravenous catheterisation through the penile vein and ventilation. A craniotomy and durotomy was performed prior to stereotactically guided tetrode insertion into the brain. Micro-stepper motors allowed graded electrode advancement right down to increments of 1 μm at a time. The advantage of neuroleptanalgesia is that the animal remains in a pain free quiet awake state in which seizures occur spontaneously. One disadvantage of tetrode recordings is that it is not possible to histologically confirm electrode placement, so as to clearly identify which layer of cortex the electrode was in; however stereotactic guidance allowed placement in each of S1, S2 and intermediate areas, and ventroposterior - medial (VPM) and ventrobasilar (VB) thalamus to a sufficient level of precision as to be confident in the sub region of each cortical area.

Data was sampled at 25 kHz using an Intan RHD2116 amplifier system (Intan Technologies, LLC[2]), unfiltered, before being imported into Matlab for subsequent analysis. Data was initially unfiltered during collection to allow for spike sorting if needed later (even very low frequency filtering will distort spike waveforms and can affect the accuracy of spike classification). However, the analysis methods presented in this chapter are concentrated on ECoG and EEG data only and do not require spike sorting. Data was subsequently digitally filtered in Matlab for further analysis and specific details of the filtering procedures will be given where these occurred.

Seizure time stamps were determined by visual inspection. For both types of experimental data the start of seizures was taken to coincide with the first SWD. This was distinguished from coarse somatosensory rhythms that are sometimes seen in GAERS by their morphology and amplitude (greater than 400mV peak to peak, as defined by Pinault [161],[166]). When visually inspecting data, if any artifacts were present this seizure was not included in further analysis.

As discussed in Chapter 2, two of the three rats had seizures but recordings from the third rat showed only bursting behaviour between cortex and thalamus without seizures,

[2] www.intantach.com

so this data is not included in the comparisons that follow. From these first two experiments approximately 460 seizures were recorded, with between three and nine seizures per minute in each recording location. In the case of tetrode data three different areas of somatosensory cortex, S1, S2, and the junction region between these, 'S12' are analysed. In S1 there were a total of 142 seizures; in S12, 110; and in S2, 130 seizures.

In the case of depth electrode data, electrodes were placed in two regions of S1 - associated with the forelimb homunculus, as determined by the Paxinos and Watson stereotactic rat brain atlas [77], here called S1Fl, and perioral area, called S1Ul. Other regions were the insular cortex (IC), S2 somatosensory cortex, and M1 motor cortex.

5.2.2 Power spectrum and harmonics

Power Spectrum

Resonance can be accompanied by increasing spectral power before seizures or increased coherence in dominant frequency bands. To disentangle these scenarios both are computed and compared. Under the hypothesis of a likely focus in somatosensory cortex, either S1, S2, or the junction between them, the power spectra, cross spectra and coherence markers in these regions was examined in each of the two seconds preceding the first cortical SWD and also at seizure termination.

The starting point is examining the power spectrum changes both prior to and after seizures. To do this custom written Matlab software was used. Where indicated individually in further sections, this in turn made use of the Chronux package [3][85], using a multi taper technique (Appendix C). For example, the power spectrum was calculated using the Matlab functions `mtspecgramc.m` prior to seizures. For the analyses shown a time-bandwith product TW=5, number of tapers K = 3, and a sliding window of 0.8 seconds with overlap of 0.4 seconds was used.

Epochs of data 1 second long prior to seizures and after seizure termination are analysed. For data preprocessing, an elliptic low pass filter is used so as to minimise phase

[3] www.chronux.org, accessed February 2015

distortion up to a frequency range of 450 Hz before any further spectral analysis.

Harmonics

The power spectrum of the tetrode ECoG data was analysed to investigate the presence of harmonics and to find indications of how they change prior to seizures. The Chronux package and the Matlab functions `mtspecgramc.m` were used to compute the multi taper spectrogram, with a time-bandwith product TW=5, and a number of tapers K = 3, and a sliding window of 0.8 seconds with an overlap of 0.4 seconds.

Statistical significance of differences either between regions or between inter- and pre-ictal periods was assessed using an ANOVA analysis in Matlab (the `anova1` function).

Phase entrainment in harmonics

Resonance might occur because of higher harmonic power at particular frequencies, or alternatively because of phase entrainment (that is, alignment), which would result in a type of coherent amplification effect, even in the event of lower harmonic power [99]. The goal of this section is to investigate whether there is phase clustering of harmonics of the theta rhythm, if these are found. It is based on the concept of the phase clustering index (PCI) defined by Kalitzin et al [99] and described below. His analysis centres around the discrete Fourier transform of the data at frequency bands which are multiples of a 'fundamental' or stimulation frequency. He defined a measure of phase dispersion for each frequency component to quantify the degree of alignment of phase in higher harmonics. In his notation, for the nth harmonic found in a signal this is

$$C^n = \frac{1}{N^n} |\sum_k F_k^n| \quad , \tag{5.1}$$

where N^n is the sum over k weighting factors found from the amplitude envelope of the Fourier mode F_n at frequency n.

To calculate this measure, the phase angles are obtained from the Hilbert transform of bandpass filtered data for the second before a seizure in the different cortical regions, and

plotted. If there is a high degree of phase entrainment one might see a collectively highly preserved phase angle. However, if there is not a large concentration in phase angle, and instead large amplitude harmonics in the power spectrum and spreading of phase angles in the data, there would be preserved variability in phase distribution but increased power (as seen with longer amplitude of vectors in the polar plots).

Relationship between the theta rhythm and higher frequency power

Cellular physiology studies by Pinault and colleagues [161, 166] have demonstrated the presence of synchronous precursor activity leading up to seizures in deep layers of cortex, centred mainly in S2 and insular cortex but also in S1 cortex. Whilst Truccolo and colleagures [227] found a great heterogeneity of single cell participation prior to and during neocortical seizures, Zheng's study [249] showed that the majority of cells in these areas of the corticothalamic circuit are rhythmic, and this rhythm appears to occur at the dominant 5 - 9 Hz rhythm in the GAERS rat.

To see whether higher frequency activity is linked to the theta waveform, the following procedure, based on a method used by Canolty and colleagues[36], was used. The basic idea was to plot the normalised instantaneous power at bandpass frequencies in intervals of 10Hz, and then superimpose the theta passband in the time leading up to a seizure.

In more detail, the raw signal is bandpass-filtered with centres from 10 Hz up to 400 Hz and bandwidth 5Hz; these were then normalised by subtracting each signal mean and dividing by the signal (temporal) standard deviation at that frequency band. The normalised instantaneous power was found at each time-frequency point by taking the Hilbert transform to get the amplitude envelope of each signal. These were finally squared element-wise to find the power at each frequency band.

5.2.3 Coherence

Amplitude coherence

Coherence is often defined as a measure of linear correlation between two signals as a function of frequency[154]. It is derived from the cross spectral density function which itself is a Fourier transform of the correlation of the two signals. Because it is an amplitude dependent measure it is normalised by the autospectra of each signal component. The coherence $C_{xy}(f)$ between two signals $x(t)$ and $y(t)$ is defined either as a frequency dependent function or as a magnitude squared value as follows

$$C_{xy}(f) = \frac{|\langle S_{xy}(f)\rangle|^2}{|\langle S_{xx}(f)\rangle||\langle S_{yy}(f)\rangle|}, \tag{5.2}$$

where $S_{xy}(f)$ is the cross-spectrum between signal x and signal y. A myriad of variants have been proposed to deal with the problem of artifacts induced by finite data length and the effects of windowing either by smoothing or averaging repeated epochs of data collected from similar trial conditions. Here, the multitaper method [85] was used, which breaks up the data window into orthogonal discrete prolate slepian sequences to minimise this problem as summarised in Appendix C.

The concept of coherence brings connotations of entrained phase. However the amplitude coherence measure defined by Eq. 5.2 does not disambiguate phase or amplitude relationships in the data [104], [233]. This is the rationale behind separately investigating phase coherence in the next section.

To analyse amplitude and phase coherence changes between thalamus and cortex, and also between very local cortico-cortical regions, tetrode data was used. To examine cortico-cortical interactions between much more widespread regions of different cortex simultaneously, depth electrode data was used. Tetrode tips are approximately 140 μm apart, and the tetrode path is presumed to travel along deeper layers of cortex, i.e., layers IV to VI. This tetrode placement unfortunately cannot be clearly verified histologically as one would with glass electrode recordings, so it is not possible to directly plot the electrode positions.

Phase coherence

The interpretation of phase coherence used in this analysis follows the discussion of Fig 1.5 in the Introduction (Section 1.3.2). Both amplitude and phase coherence have been studied in the context of a number of neocortical and temporal lobe epilepsy syndromes (Sec. 1.3.2). Matlab code was written to calculate mean phase coherence within specified frequency bands as defined by Mormann [136], [135] and using Morlet wavelets (defined in chapter 3, Eq 3.6). The starting point is calculating the instantaneous phase difference between two time series $x(t)$ and $y(t)$ using Hilbert transform wavelet coefficients.

A number of questions arise regarding the meaning of instantaneous phase and are handled differently by a number of authors. Breakspear (2002) makes the point that one can calculate the instantaneous phase of a wide band signal but that this is more likely to be affected by noise; however the physical meaning of wide band instantaneous phase is less clear than that of a narrow band signal [27]. The approach used here is similar to Perez-Velasquez (2007), with phase coherence calculated between successive passbands of 4 Hz between 1 and 200Hz for tetrode data, and between 1 and 120 Hz for depth electrode data between distant cortical areas.

In the notation of Kitzbichler et al[101], the Hilbert wavelet transform of the time series F_i and F_j in the frequency band defined by the kth wavelet scale is $\mathcal{W}_k(F_i)$, and the instantaneous phase difference $C_{ij}(t)$ over that frequency interval is

$$C_{ij}^k(t) = \frac{\langle \mathcal{W}_k(F_i)^\dagger \mathcal{W}_k(F_j) \rangle}{|\mathcal{W}_k(F_i)^\dagger||\mathcal{W}_k(F_j)|} \quad . \tag{5.3}$$

This is based on the "analytic signal approach" of Gabor (1946), also summarised in Hurtado [88] and Mormann [136]. The starting point of this method is to use a Hilbert transform to extract the instantaneous phase $x(t)$ from the time series F_i.

$$H(x) = \frac{1}{\pi} \text{p.v.} \int_{-\infty}^{\infty} \frac{x(\tau)}{t-\tau} d\tau, \tag{5.4}$$

(where p.v. is the Cauchy principal value of the integral) returns the instantaneous phase of the time series, with the same power spectrum of the original data, phase shifted by

$-\frac{\pi}{2}$. Following Hurtado [88] and Mormann [136] the Hilbert transform is taken in practice by taking the discrete Fourier transform of the signal, setting negative frequencies to zero, and then taking the inverse Fourier transform of the result.

One then obtains a 'phase series' by taking the argument of complex analytic signal $s(t)$ projected onto the unit circle: If $s(t) = x(t) + iy(t)$ where x(t) is the real part of the filtered signal and $y(t)$ is the imaginary (Hilbert transformed) component, then the phase, $\phi(t)$, is given by

$$\phi(t) = \arg(s(t)) = \arctan \frac{y(t)}{s(t)} \quad . \tag{5.5}$$

Mormann [135] makes the point that for noisy data like ECoG signals or chaotic time series, where phase discontinuities occur, an instantaneous "relative frequency" $\omega_{m,n} \equiv n\langle\omega_n\rangle - m\langle\omega_m\rangle$, for some integer combinations $m, n = 1, 2, 3, ...$, where $m \neq n$, is inadequate because it is strongly affected by noise. In the results that follow his definition of "phase entrainment"

$$|\varphi_{n,m}| = |n\phi_n(t) - m\phi_m(t)| < \texttt{const} \tag{5.6}$$

is used. This can be found through the trigonometric addition theorem, for example, in the case where $n = m = 1$

$$\varphi_{1,1}(t) = \phi_i(t) - \phi_j(t) = \arctan[\frac{\vec{s_i}(t)s_j(t) - s_i(t)\vec{s_j}(t)}{s_i(t)s_j(t) + \vec{s_i}(t)\vec{s_j}(t)}] \quad . \tag{5.7}$$

In what follows we take n = m = 1 as we don't know *a priori* what ratios of synchronisation may be present in the data. This renders the relative phase to be naturally bounded to [0,2π].

5.2.4 Entropy, statistical and probability measures

Changes in data complexity with seizure onset

The aim of this analysis is to determine if synchrony changes accompany the decrease in dimensionality of the data, and quantify this. To accomplish this the permutation entropy is used as a measure of the complexity in a time series using depth electrode recordings.

Permutation entropy is then analysed during the pre ictal period.

Permutation Entropy (PE) was introduced by Bandt and Pompe in 2002[13] as a means of quantifying the complexity of a time series. It uses an embedding technique to map the time series into a series of consecutive symbolic sequences of some length n, and it is defined in the following way.

Suppose we have a time series, $x(t)$, of length T. 'Symbols' (i.e. each possibility in a library of possible progressions of the series) of length n are formed using the time delay embedding technique (Section 3.3.4) with a time delay τ, so that $X = [X_t, X_{t+\tau}, \ldots, X_{t+(n-1)\tau}]$. For some choice n of the embedding dimension there are then $n!$ different possible sequences, or patterns, that might be formed. If each of the permutations π_j, $j = 1 \ldots n!$ has a frequency of $f(\pi_j)$ counted over the total number of embedded observations $L = T - (n-1)\tau$, then the permutation entropy H_p is given by

$$H_p(n) = \sum_{j}^{n!} p(\pi_j) log(p(\pi_j) \quad , \tag{5.8}$$

where $p(\pi_j)$ is the probability of finding the particular sequence permutation π_j.

In this way the PE is a measure of the regularity of a time series, bounded by a value of 1 for completely random series where each sequence is equally likely, to 0 for a completely regular time series.

The calculation of PE in Matlab follows the definition above. It strongly depends on the choice of parameters n and τ [183]. Higher orders permit better resolution of the complexity of the time series, but because of the rapidly divergent number of combinations ($n!$) to survey, these can lead to computational difficulties with memory needed. A survey of the literature using permutation entropy in EEG analysis favours values of τ between 1 and 2, and order n between 3 and 7[183].

Entropy measures of phase difference

If phase alignment in harmonics before seizures is a mechanism behind resonance and cortical excitability, this may affect only certain frequencies or Fourier modes in the EEG

and not others. At those frequencies, increased phase coherence would lead to an amplification of resonance as found by the phase clustering index above [99], and we would see a breakdown in the distribution of scaling in phase angles to a more unimodal distribution. However, more complex forms of phase clustering may not occur in linear combinations of harmonic frequencies, and then would be missed by that measure.

One solution to this problem is to examine the phase plots in certain frequency ranges from the data directly. The phase difference entropy measure helps to quantify phase entrainment and differentiate the possibilities mentioned above, along with the harmonic power and phase angle distributions. It was introduced by Hurtado [88] and allows a measure of 'clumpedness' of phases in the data. It is calculated by generating a histogram of the phase differences in data. It is derived from the mutual information between the two distributions of phase angles, and measures how tightly associated these distributions are. In more detail, histograms of phase angles ϕ_i and ϕ_j are found from two time series of length L, and the probabilities associated with each phase difference p_i can be calculated. The phase difference entropy is then [88] :

$$H_N = \sum_{i=1}^{L} \sum_{j=1}^{L} p_{ij} \log \frac{p_{ij}}{p_i p_j} \quad . \tag{5.9}$$

The physical interpretation of the mutual information defined by equation 5.9 is that it is a comparison between the joint histogram of phases in each of the two signals $p_{ij} \equiv p(\phi_{i,j})$, compared with the distribution which would be found if the two time series were independent of each other, i.e. $p_i p_j \equiv p(\phi_i)p(\phi_j)$.This quantity was calculated for the three cortical regions prior to seizures, and compared with the inter-ictal period.

5.2.5 Frequency comodulation, and cross frequency coupling

Frequency comodulation is the phenomenon of correlated changes in a signal across different frequencies, or 'nesting' of frequency bands in a signal[2]. Two approaches are used to quantify the presence of frequency comodulation in this chapter.

The first, cross frequency coherence, used later in this chapter (Sec. 5.2.5) is a measure

of phase-amplitude coupling as introduced in Section 1.3.2 and Fig 1.5. The second is a measure of how the frequencies between different spectra are correlated with each other and is here termed comodulation. A physical interpretation of this comodulation index is that it allows a measure of the degree of covariation in power cross spectral density across channels as a function of frequency, which gives an indication of which frequencies coexist together across those channels measured [178]. In this sense it is not only accounting for phase-amplitude coupling, but would also provide a measure of amplitude cross frequency coupling as well. This is calculated by finding the correlations between frequency bands of each cross spectrum, $S_{xy}(f)$, of two time series (channels) x and y, which in turn is found from a multitaper spectrogram of the signals.

Both measures are investigated here because it is plausible that phase- and amplitude-coupling may be distinct, separate processes in different parts of the seizure generating network. Closely related concepts of bicoherence or synchrograms, where in Eq 5.6, 1:2 or 1:3 synchronisation is also considered, are covered in the Discussion section of this chapter.

In more detail, the steps in calculating the comodulation index are

1. the between channel cross spectral density is calculated as a ratio of cross spectral power to auto-spectral power using the Chronux package;

2. the "cross frequency power correlations" as defined by Buszaki and colleagues [75] are computed. This is done by defining a two dimensional array of frequency intervals into bins bounded by the frequency ranges of interest. Then a 2d correlation is taken between the cross spectral power at one frequency in the first waveform with every other frequency bin of the second.

The Matlab code written for the comodulation analysis in this chapter used at its 'core' a method modified from that used by [75].

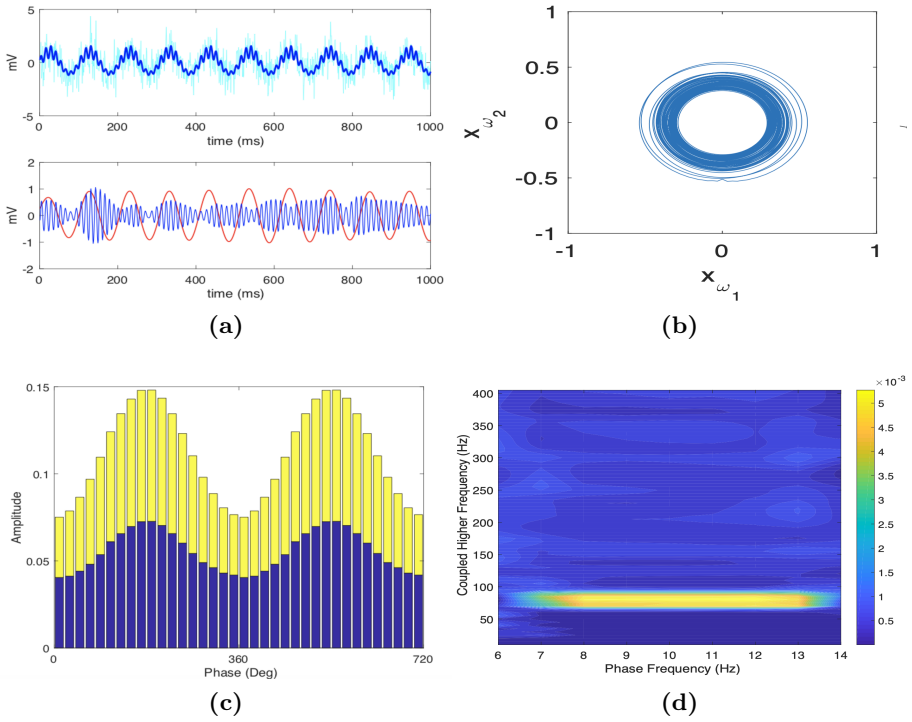

Figure 5.1: Illustration of phase-amplitude cross frequency coupling using surrogate data generated using Eq. 5.13 (a) Top panel: data with added noise (cyan), and without noise (overlaid in blue); the bottom panel shows the signal filtered at the base frequency of 10 Hz, and 80 Hz, confirming cross-frequency coupling (b) left panel: phase plot, and right panel: plot showing that base signal and it's high frequency components have the same origin in the complex plane; (c) histogram of amplitude $\langle A_{f_A} \rangle_{\phi_j}$ in higher frequency f_A waveform versus binned phase angle of base waveform f_B, Eq. 5.10, (d) Contour plot of MI values calculated from Eq. 5.12 for all base and higher frequency combinations

Cross frequency coupling

This phenomenon has attracted intense interest in the last few years but to date has not been applied to study differences between seizure periods within thalamcortical networks in absence epilepsy, nor between different cortical regions to our knowledge.

The method used here follows that outlined in the study by Tort and colleagues ([226] and his Supporting Information), which is in turn based on ideas from [88]. Their method is to derive an index of comodulation between the phase of one signal, which we will call the base signal, and the amplitude of others at varying frequencies of interest, to demonstrate whether cross frequency coupling occurs. The steps in their analysis are as follows :

1. It is important to check that both the base signal and it's high frequency components, have the same origin in the complex plane.

2. Successive pairs of separate frequencies for each signal, called here A and B after the notation of [226], are chosen. The raw signal is bandpass filtered at these two frequencies of interest f_A and f_B

3. Using the Hilbert transform (Eq. 5.5 and Sections 5.2.3 and 1.3.2) two time series for the phase and amplitude envelope of each signal are found.

4. The phase time series $\phi_{f_A}(t)$ is binned into eighteen 20° intervals and a histogram of the mean amplitude for the second time series is computed for each phase bin ϕ_j, j=1,...,18. In the notation of [226], $\langle A_{f_A}\rangle_{\phi_j}$ is the average amplitude of the f_A time series at phase bin j. From this histogram, the probability, p_j, for each amplitude at that phase bin can be estimated :

$$p_j = \frac{\langle A_{f_A}\rangle_{\phi_j}}{\sum_j \langle A_{f_A}\rangle_{\phi_j}}. \tag{5.10}$$

5. The entropy, H, of each of these phase - amplitude couplets is calculated as

$$H = -\sum_{j=1}^{N} p_j \log p_j \tag{5.11}$$

. Tort's modulation index for these two frequencies of interest is the normalised entropy, as calculated from the phase-amplitude histogram. A maximum value for this entropy H_{max} would arise from a uniform distribution, over all phase bins, of $\langle A_{f_A}\rangle_{\phi_j}$ = constant and p = 1/N, giving a normalised Modulation Index H_{MI} of zero[4]:

$$H_{MI} = \frac{H_{max} - H}{H_{max}}. \tag{5.12}$$

The phenomenon of phase-amplitude coupling was introduced conceptually in Section

[4]There will be an argument that the normalised H_{MI} should be $\frac{H}{H_{max}}$, but I followed the convention of [226] and his supplemental information, who used the normalisation given in Eq. 5.12

1.3.2. To illustrate this method consider the surrogate data shown in Fig 5.1. This data was generated by multiplying two sinusoids,

$$x(t) = A_1 sin((2\pi\omega_1 t) + A_2) sin(2\pi\omega_2 t) + \text{noise}, \tag{5.13}$$

with values of $A_1 = 0.2$ and $A_2 = 0.1$ and frequencies $\omega_1 = 10$ Hz to approximate a dominant theta rhythm, and $\omega_2 = 80$ Hz for a gamma rhythm. In Fig 5.1a approximately one seconds' data is shown at a sampling rate of 1024 data points / second; the lighter cyan trace shows data with added noise, and overlaid in blue is the modulated sinusoidal signal without noise, simulating 'filtered' data and also showing the existing of phase-amplitude coupling of the two signals more clearly. Inspection of the filtered data reveals that the amplitude of the 80 Hz signal reaches a predictable maximum at the $\pi/2$ maximum of the sinusoidal base ("theta") frequency waveform. As shown in Fig 5.1d, the only significant coupling between frequencies in this example is within the frequencies of 10 and 80 Hz, as expected.

An illustration of Broselec's theorem is shown in Fig 5.1b for the same surrogate data. Just as the bottom panel of Fig 5.1a illustrates the coupling between the two frequencies visually, Fig 5.1c shows a histogram of the quantity $\langle A_{f_A} \rangle_{\phi_j}$, or the variation in amplitude of the higher frequency signal filtered at 80 Hz versus the binned phase angle of of the 10 Hz signal, used via Eq. 5.10 to calculate H_{MI}. In this figure, it is important to note that in this example added noise, shown in the overlaid blue histogram, decreases the value of H_{MI}, compared with no noise (the yellow histogram). This illustrates the importance of testing for statistical significance in coupling.

One of the issues with all techniques used for assessing phase-amplitude coupling is the possibility that a common 'third party' driving influence co-modulates both frequencies. This could give rise to the erroneous conclusion of cross frequency coherence (Sec 1.3.2), especially in epilepsy where it may be anticipated that synchrony and driving influence across cortical channels within the seizure focus will increase with seizure onset (as found in chapter 4), and that during SWDs sharp 'edge effects' may lead to increased high frequency components, again leading to erroneous interpretation of cross frequency coupling [2].

To show that results are statistically significant, two measures are required : (1) that cross-frequency comodulation is significant beyond that may occur by chance; and (2) significant difference exists between measures for each part of cortex. To address the first possibility a surrogate data set of interictal and preictal snippets was generated to set a 95% confidence interval with a lower bound for significant at $p < 0.025$. This was done after the method described by Tort and colleagues [226] to produce 200 surrogate 'trial shuffled' MI distributions, generated from 90 two second long snippets of data by shuffling phase time series $\phi_{f_A}(t)$ and amplitude time series $\langle A_{\phi_j} \rangle_{\phi_j}$ randomly. Assuming a normal distribution of fluctuation in MI values, a threshold for signiifcance can be calculated directly from the distribution of surrogate MI values obtained. To assess between group differences in histograms of MI values obtained a one-way ANOVA, or T test was used.

The Matlab routine used to calculate the modulation index for this analysis was modified from code generously provided by Tort[226].

5.2.6 Analysis of synchrony clustering by eigenvalue decomposition

The aim here is to quantify the number of synchronous processes and whether this varies in the lead up to a seizure - for example, whether they fragment or coalesce as found by Kramer and colleagues [102], with an increase in synchrony prior to seizures (for further background on this result discussion see Sec 1.3.2).

The method used to quantify the number of clusters of synchronised modes of oscillations within tetrode data channels is an eigenvalue decomposition method developed by Allefield [6]. This is an eigenvalue decomposition of the matrix of instantaneous phases R_{ij}, i.e. the matrix of phase series for each channel i and j. The first step is to find the N eigenvalues λ_k and eigenvectors $\vec{v}_k$, $k = 1$ .... N for N channels,

$$\mathsf{R}\vec{v}_k = \lambda_k \vec{v}_k \quad . \tag{5.14}$$

For a decomposition based on matrices with entries $R_{ij} \in [-1, 1]$, the eigenvectors and eigenvalues are real and non negative so that the trace of eigenvalues should be invariant under a transformation to an orthogonal vector basis [6] (i.e. $\sum_k \lambda_k = N$, and the trace

of the correlation matrix will always be N since $C_{ii} = 1$). This allows us to order the contribution of strengths of different clusters based on the distribution of eigenvalues, of significant synchrony clusters with $\lambda_k > 1$, whilst those eigenvalues not contributing to that cluster are less than 1. A trivial example of the limits of distributions in this would be all channels independent, having each $\lambda_k = 1$, compared with one largest dominant mode independent of others in a decoupled system of oscillators having a largest eigenvalue $\lambda_1 \to N$ whilst $\lambda_{2...k} \to 0$.

The relationships between oscillators can be seen in the behaviour of corresponding eigenvectors. Since $\sum_i v_{ik}^2 = 1$, this implies that v_{ik}^2 gives a measure of the relative involvement of "channel" i in the cluster k [6]. Taken together, we can then define a measure quantifying the involvement "channel" i in cluster k , following Allefeld's notation, as the "participation index"

$$p = \lambda_k v_{ik}^2 \quad . \tag{5.15}$$

To analyse changes in p with time a sliding window technique was used, with windows of 0.2 s and overlap of 0.1s.

There is a caveat in interpreting the meaning of "channels", as pointed out in Allefield's original description of this measure [6]. The mean phase coherence is not a linear measure, unlike correlation, so it may not be possible to identify individual data channels from the decomposition of synchronous components from their time series. It would also be possible to use an Empirical Mode Decomposition approach instead, as in [42], and which was discussed in Section 3.4.5. Another potential problem with these approaches is that they can be degraded by noise and again that it can be difficult to interpret the physical meaning of individual modes.

5.2.7 Dynamical analysis

The first step in this analysis is finding the appropriate delay embedding parameters, as discussed in Section 3.3.4. Following this, the next task is to choose which Lyapunov exponents are of most interest in describing the behaviour of the dynamical system generated by the embedding used, and at which temporal or spatial scales.

Finite Scale, and Scale Dependent, Lyapunov Exponents

The Scale Dependent Lyapunov Exponent (here abbreviated 'SDLE') was introduced by Gao (2007) [79]. It is based on Wolff's algorithm for estimating the finite size Lyapunov exponent, but a drawback in Wolff's algorithm is the requirement for large data sets to define a reference and perturbed trajectory. Should the perturbed trajectory move far away from its reference trajectory, a reorthonormalisation procedure is needed, requiring large amounts of computing time and data.

Gao's algorithm uses a slightly different procedure, instead finding all pairs of trajectories close to each other (within a distance, say, ϵ), then calculating their distance at time t. Consider two trajectories, initially at time t_0 separated by distance ϵ_0, then at points represented by ϵ_t and $\epsilon_{t+\Delta t}$ at times t and $t + \Delta t$. As $t \to 0$,

$$\epsilon_{t+\Delta t} = \epsilon_t exp^{A(\epsilon_t)\Delta t} \tag{5.16}$$

or

$$\lambda_{\epsilon_t} = \frac{\log\epsilon_{t+\Delta t} - \log\epsilon_t}{\Delta t} \tag{5.17}$$

In their algorithm, they introduce the idea of a 'shell' in phase space, indicated by the subscript k, of radius ϵ_k. The work of the algorithm is to find as many of the reconstructed vectors V_i , V_j such that

$$\epsilon_k \leq ||V_i - V_j|| \leq \epsilon_k + \Delta\epsilon_k \tag{5.18}$$

where $\Delta\epsilon_k$ is an arbitrarily small distance.

Characterising sensitivity to finite perturbations from a dynamical perspective

The title of this section comes almost entirely from a paper by Tobias Letz and Holger Kantz[110]. Their approach is a variation of the concept of Finite Scale Lyapunov Exponent of Eric Aurell [10]. In this method they return to the definition of the Lyapunov exponent for systems in discrete time, which can be considered as maps of flows in phase

space : for a dynamical system $x_{n+1} = f(x_n)$ under the influence of some perturbation ε,

$$\lambda = \lim_{t\to\infty} \frac{1}{t} \frac{f_i(x_0) - f_i(x_0 + \varepsilon)}{\|\varepsilon\|} = \lim_{t\to\infty} \prod_{n=1}^{i} J(x_i) \frac{\varepsilon}{|\varepsilon|} \quad , \tag{5.19}$$

where $J(x_n)$ is the Jacobian matrix of the map f at x_n. They make the point that it is difficult to use this property to characterise the effects of finite perturbations at any point t using higher order terms in the expansion of ε because "the effects of these perturbations cannot be characterised by the local properties of f at the position of the unperturbed solution" [110]. Instead they use a technique of averaging over the distances between a reference trajectory, x_n in the direction of the maximal Lyapunov exponent (this being the largest vector in the tangent space) and two neighbouring trajectories close by (more specifically at a distance ε further in the direction of the maximal Lyapunov vector). They used a function $S(\varepsilon, t)$ of all such trajectories found for some distance ε and time t

$$S(\varepsilon, t) = \frac{1}{N} \sum_{n=1}^{N} \ln \left(\frac{1}{2} \sum_{k=+,-} \left| f_i(x_n) - f_i(y_n, k) \right| \right) \quad \text{for} \quad y_{n,k} = x_n \pm \varepsilon u_n, \tag{5.20}$$

for the unit vector u_n in the direction of the maximal Lyapunov exponent.

The divergence behaviour of $S(\varepsilon, t)$ gives information about local dynamical properties of the system. For chaotic systems the slope of S should be the maximal Lyapunov exponent of the system, for sufficiently small ε. They define the "scale dependent stability number" as

$$s(\varepsilon) \equiv \partial_t S(\varepsilon, t) \Big|_{t=t_c} \quad , \tag{5.21}$$

for, in their words, "some suitable t_c".

This quantity is then found numerically by estimating the slope of $s(\varepsilon)$ at suitably chosen arbitrary times t_1 and t_2.

The approach has similarities to both the Finite Scale Lyapunov Exponent, and Gao's assertion that the slope of the SDLE may indicate stochastic forcing. The reason, as explained by Gao [79], is that the Scale Dependent Lyapunov exponent can be related to

the FSLE by

$$\lambda_\varepsilon = \int_0^{\varepsilon'} \lambda(\varepsilon) p(\varepsilon) d\varepsilon, \tag{5.22}$$

where the probability density function at some scale ε, $p(\varepsilon)$ is proportional to the derivative of the correlation integral $C(\varepsilon)$ given by Eq 3.29, and the limit of integration ε' signifies scale as the point of renormalising parameter[79].

Given they share the same dynamics, the analysis of flows from the deterministic part of the Fokker Planck analysis in the method of [12] should also agree. If this is the case, this will be a fruitful way of linking the three concepts with the harmonics analysis above, however this analysis is not included in this Chapter. When done, this may provide a natural link back to Kalitzin's approach [99] above.

5.3 Results

Recordings were made with tetrodes and a reanalysis of simultaneous multisite depth recordings with tungsten electrodes from experiments described in [249]. These will be discussed in more detail below.

5.3.1 Seizure onset lags between regions

From visual inspection of all the seizures the 5 - 9 Hz physiological oscillations noted by Pinault [167] and in our previous work [249] were more common in the S1 and S12 regions than in S2. Interictal discharges (which are defined here as isolated discharges of 5 SWDs or less which rapidly self terminated) were also seen more commonly in the S12 region.

However, there was no statistically significant difference in thalamic and cortical onset times of the first SWD, measured in each of S1, S12, and S2 cortical regions.

5.3.2 Power spectrum and harmonics

Fig 5.2 shows the power spectrum changes in S1 and S2 cortex in each of the immediate 2 seconds prior, and also the first second after seizures. These plots are generated by averaging the spectral power obtained in each one second block preceding all of the seizures in that recording location. This number of seizures varied between 1 and 9 seizures in one minute's recording and the duration of recordings in each location were either 60 or 120 seconds. On the left of Fig 5.2 are superimposed plots for all seizures available, and on the right side, the average across all seizures by regions. These regions are divided into 'proximal' and 'distal' S1 (blue and cyan respectively), 'proximal' and 'distal' S12 (i.e. the edge of S1, and the edge of S2 - magenta and green respectively), and 'proximal' and 'distal' S2 - red and black.

Similarly Fig 5.3 shows spectral power in the three thalamic channels in each of the first two seconds prior to and the first second after seizures. For the thalamic power spectrum there is no significant difference, but the S1 region has significantly increased power in the higher-gamma frequencies, which did not decline with frequency. This was a

stable finding over all recordings. These findings agree with Sitnikova's findings [59] that a combination of theta and delta power is increased leading to a seizure in this region, however there were no changes in power observed with seizure onset in this data.

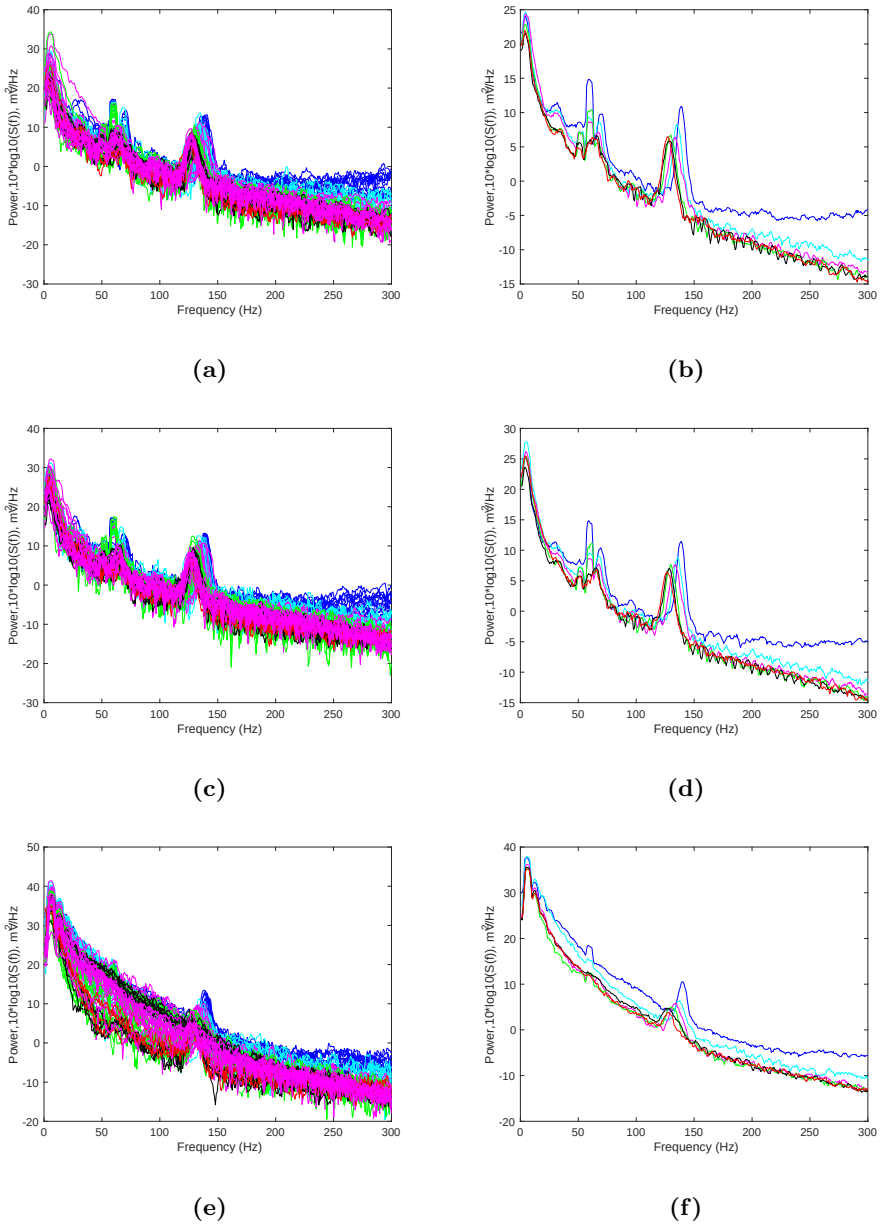

Figure 5.2: Power spectrum for each cortical region. From top : (a) two seconds before; (c) one second prior to the first SWD; and (e) in the first second after seizure termination. Plots on the left i.e., (a),(c),(e) are superimposed plots for all seizures, whereas the right-hand plots of (b),(d),(f) show the average taken over all data. Different cortical regions are denoted as : S1 (blue and cyan); S12 (magenta and green); and S2 (red and black)

Harmonics

Fig 5.4 shows the power in the first five harmonics of the 5 - 9 Hz theta frequency across the S1, S12 and S2 regions of cortex in the immediate second prior to seizures (i.e., the first SWD). As one can see in Fig 5.4, there is no significant difference in harmonic power between regions. A very slight difference can be seen in the first harmonic, which is not statistically significant.

Similarly, plots of phase entrainment in harmonics prior to seizures is not increased (this data is not shown).

Higher frequency power is linked to theta peaks

To see that higher frequency activity is linked to the theta rhythm consider the plot of the normalised instantaneous power with time, shown in Fig 5.5. To generate this figure, the normalised instantaneous power is plotted at each time-frequency point is calculated from the amplitude envelope of each signal at bandpass intervals of 5 Hz. These were finally squared element-wise to find the power at each of these frequency bands. Overlaid on this plot in bold red is the theta rhythm, found as the envelope of the 5 - 9 Hz bandpass filtered data.

In Fig 5.5, one can see that outside of seizures, higher frequency activity is not clearly phase locked to the theta rhythm. However, approximately one second after seizure onset, and *not* before the first SWD, higher frequency now becomes locked to the peak of the theta rhythm. This time locking behaviour not seen to the same degree in the pre ictal period. It continues, diminished into the post ictal phase.

This provides evidence that phase entrainment increases after seizure onset. Alongside the findings that harmonic power and phase entrainment is not increased prior to seizures, this suggests that the behaviour of phase coherence rather than amplitude power or coherence may be a more important mechanism for generating resonance in cortical structures at seizure onset.

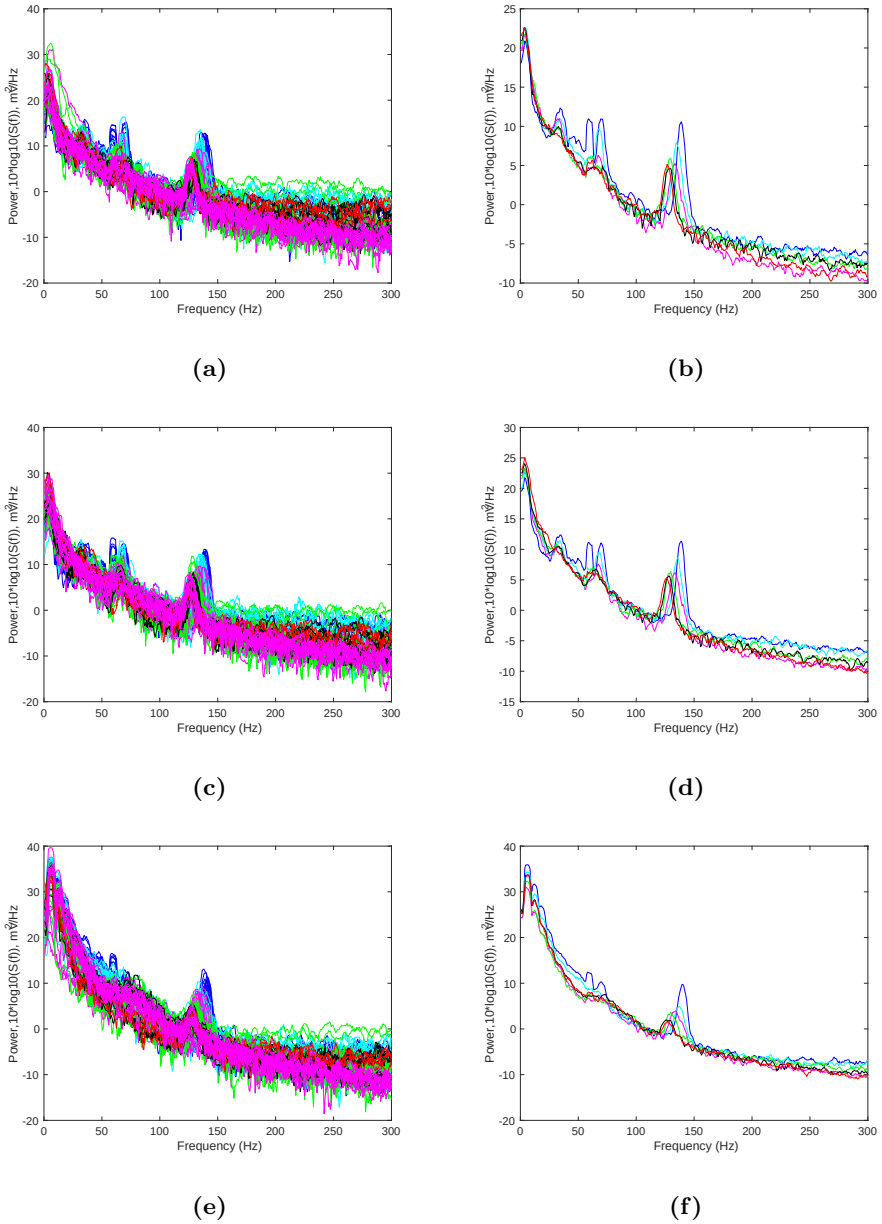

Figure 5.3: Power spectrum for thalamic nuclei associated with cortical areas during seizures. From top : (a) two seconds before; (c) one second prior to the first SWD; and (e) in the first second after seizure termination. Plots on the left i.e., (a),(c),(e) are superimposed plots for all seizures, whereas the right-hand plots of (b),(d),(f) show the average taken over all data. Different cortical regions recorded at the time of these thalamic recordings are denoted as : S1 (blue and cyan); S12 (magenta and green); and S2 (red and black)

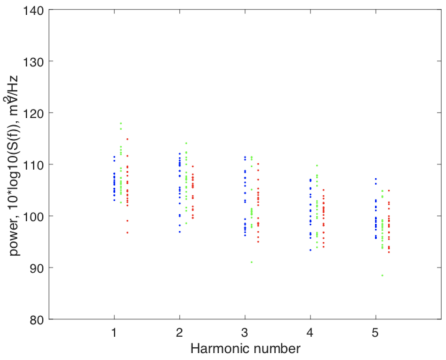

Figure 5.4: Power of the first five harmonics of the 5 - 7 Hz frequency in the first second before a seizure. Cortical regions are : S1 (blue); S12 (greem); S2 (red)

5.3.3 Coherence

Amplitude coherence

An analysis of amplitude coherence prior to or after seizures did not reveal statistically significant differences between regions. The cross spectra showed an increase in high frequency cross-coherence in cortical channels during seizures. In the immediate post ictal period higher frequency power content diminishes. This was a reliable pattern across all visual data inspected.

Phase coherence

Fig 5.6 illustrates by example the difference between 'broadband' mean phase coherence (MPC) and 'narrowband' MPC. The top panel of this figure shows a plot of cumulative 'narrowband' MPC spectrum which was obtained by calculating the MPC individually for 4 Hz bands spanning all frequencies between 4 and 120 Hz for tetrode data (sample rate 25 kHz, window size 16 msec, window overlap 50 %). An abrupt entrainment of lower gamma and theta coherence, which only occurs after seizure start, can clearly be seen. This pattern was observed across all seizures and all recorded locations. There was no difference if frequencies up to 250 Hz were also included when these were investigated (data not shown). The middle panel of Fig 5.6 shows 'broadband' MPC for the same data, obtained by calculating the MPC after filtering with a low pass elliptic filter to 450

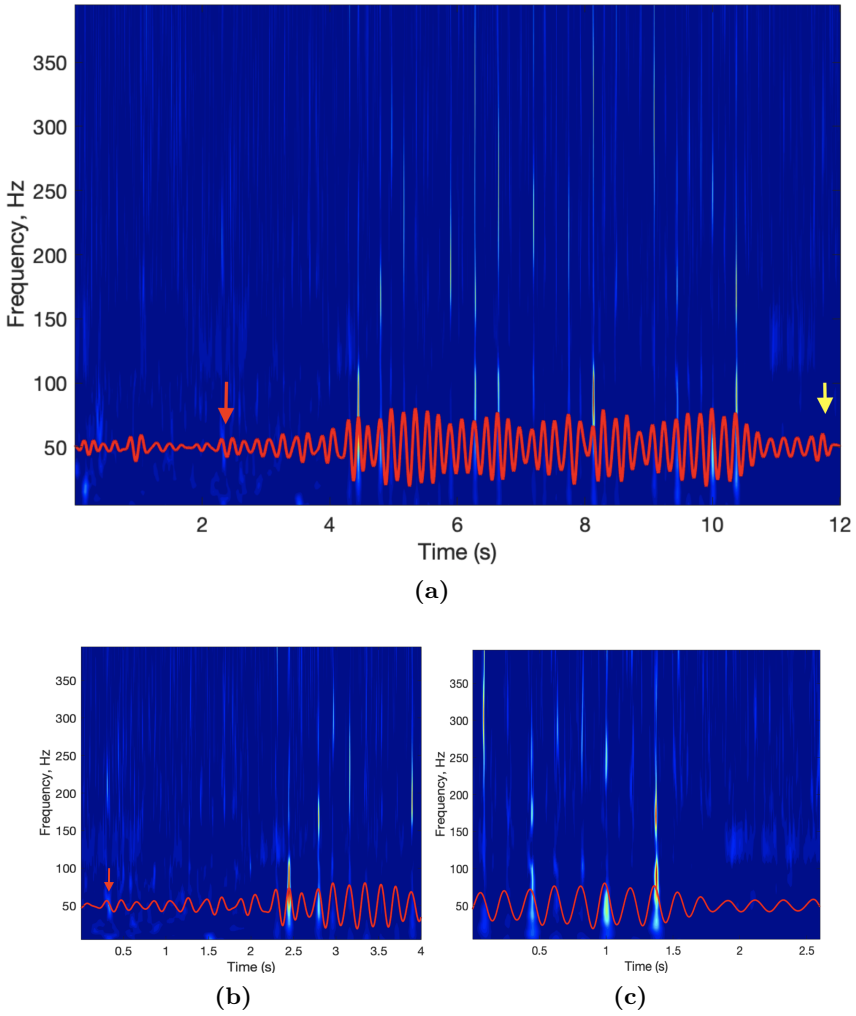

Figure 5.5: Plot of instantaneous power in the lead up to a seizure (recording #175536, Rat #1). The 5 - 9 Hz bandpass filtered theta waveform is overlaid in red (this theta rhythm was reduced in scale by a factor of 140 and shifted vertically for clarity).(a) Plot of the entire seizure, with the start of SWDs shown by the red arrow, and last SWD denoted by the yellow arrow. (b) Closer detail of the same seizure as in (a). (c) detail showing the last 3.5 seconds of the seizure. The actual seizure endpoint is just at the end of this plot

Hz. For nearly all seizures in all areas inspected the broadband MPC tended to gradually increase in the interictal period after a minimum at seizure termination as seen in the figure, whereas the narrow band MPC showed an abrupt change at seizure onset in lower frequencies only.

Fig 5.7 shows the broadband MPC for depth electrode data, between cortical regions plotted over the course of 1 minute. Here the same parameters of 16 msec window size

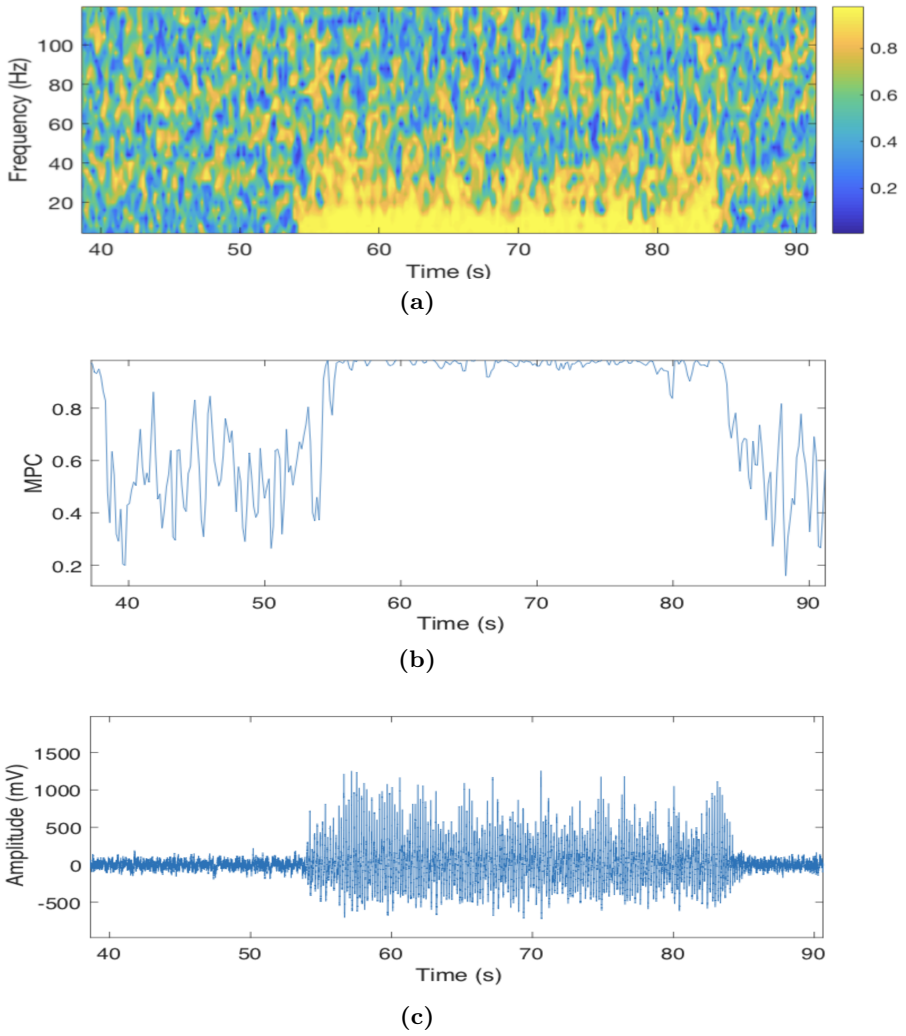

Figure 5.6: Sample Mean Phase Coherence (Eq 5.7) from tetrode data between thalamus and cortex from the S2 region in GAERS (Rat 1, recording #201456) : (a)Spectrogram plot of 'Narrowband' MPC consisting of bandpass filtered data from 4 Hz to 120 Hz in 4 Hz passbands using an elliptic filter, and (b) Line plot of 'Broadband' MPC of the same data as in (a), low pass filtered between 0 and 450 Hz using an elliptic filter. (c) Data from one cortical channel for comparison showing the commencement and termination of SWDs. In all MPC calculations window size is 16 msec with a window overlap of 50%

with 50% overlap is used. The upper panel of this figure shows MPC between each of S1Ul, S1Fl, IC and S2 and motor cortex, with the start of each seizure marked by a magenta asterisk (first SWD). In contrast, the lower panel shows a plot of MPC over the course of one minute for a NEC rat between the same regions (in this recording, the S1Ul electrode was not working). During seizures, IC and S2 regions tended to have higher values of

phase coherence. Contrasting with the higher MPC between IC and S2 cortex and M1 cortex during seizures, this was lower than S1Fl interictally, as is also seen in the NEC recording (Fig 5.7b).

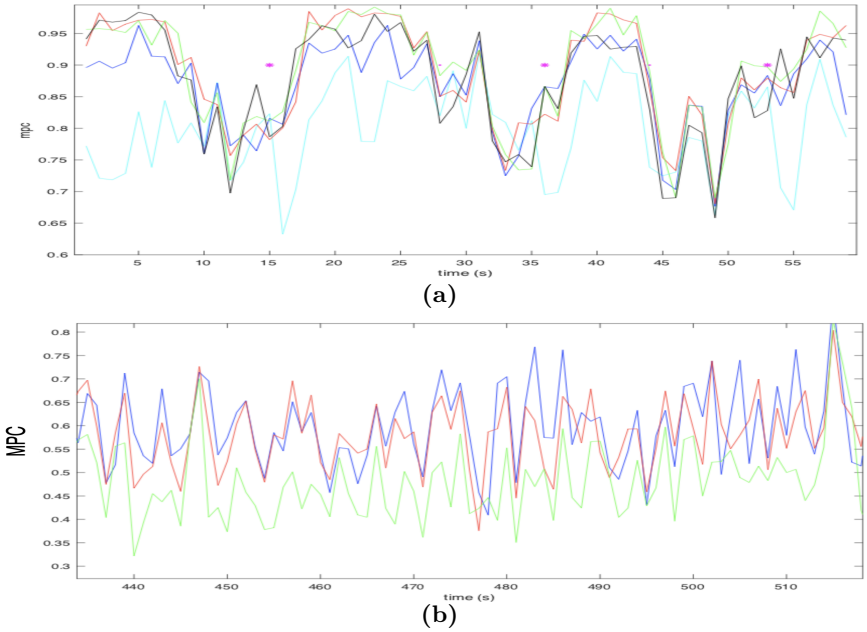

Figure 5.7: Combined analysis for Mean Phase coherence (Eq. 5.7) between different cortical regions, for depth electrode data acquired at a 256 Hz sampling rate, across one minute of recording. (a) data from a GAERS rat (rat # 7), showing each of S1fl (blue), S1ul (cyan), S2 (red), and IC (green) versus ipsilateral M1 cortex; and (b) Mean phase coherence between the same regions, now for a NEC rat, with S1fl (blue), IC (green), and S2 (red)

To investigate MPC across whole cortical regions in GAERS rats prior to seizures as compared to NEC rats, consider Fig 5.10. This data was generated by calculating the average values of 'broadband' MPC in the second prior to the first SWD in 85 consecutive seizures from rat #7, and results are compared with the same number snippets of data chosen at random times from an NEC rat. Here it can be clearly seen that mean phase coherences between all cortical region and motor cortex are increased, with the S1Fl region having a much greater spread of values prior to seizures. In comparison the S2 region has a more tightly bounded spread of MPC, with a higher mean. Compared to NEC rats, the GAERS rats have also higher S2 and IC phase coherence prior to seizures. Statistical comparisons between Fig 5.10b and 5.10d for S2 and IC regions reveals that this result reaches statistical significance at $p < 0.001$. (Can include confidence interval if needed).

The MPC was also analysed across the major frequency bands historically considered in EEG analysis and is shown in Fig D.3. Here, average mean phase coherence was obtained between thalamic and cortical tetrode channels for all seizures in each recording location. In this analysis window parameters and filtering are the same as those used for Fig 5.6. MPC was analysed prior to seizures in eight frequency bands ranging from 1 - 4 Hz up to the high gamma bands of 120 - 250 Hz and 250 - 450 Hz. The most striking result is that spread in mean phase coherence tends to be larger for S12 at theta and gamma frequencies up to 120 Hz, which is also shown in the ANOVA analysis seen in Fig 5.8. This reaches statistical significance for those frequency ranges.

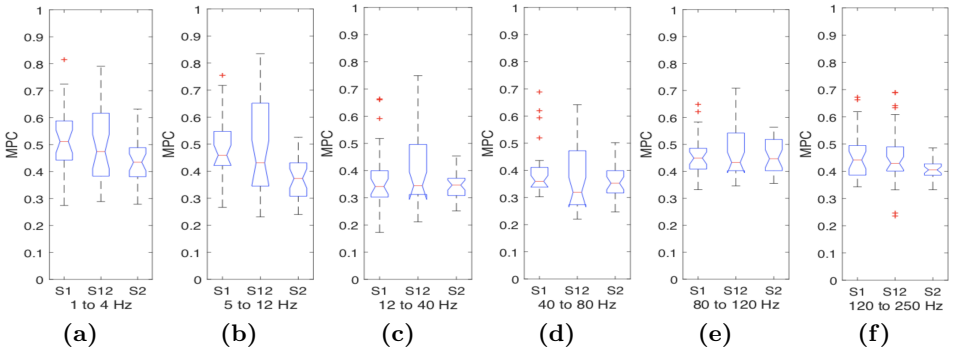

Figure 5.8: Combined ANOVA analysis of Mean Phase Coherence (Eq. 5.7) immediately before a seizure, between thalamus and each of three regions of cortex for bandpass filtered data from all seizures in tetrode data from GAERS rats. Data is in the consecutive frequency ranges shown over a two second window (a) 1 - 4 Hz , (b) 5 -12 Hz; (c) 12 - 40 Hz, (d) 40 - 80 Hz, (e) 80 - 120 Hz, (f)120 - 250 Hz

The mean change in thalamocortical MPC in the second prior to seizures from those levels seen during interictal periods is shown in Fig. 5.9. To generate this data, interictal MPC was calculated at times at least 10 seconds prior to seizures. The standard deviations of the data needed to calculate the confidence interval for the difference between means in this data was found using the Matlab `multicompare` command. To generate the error bars for this figure, the means $\mu_{1,2}$ and standard deviations $\sigma_{1,2}$ of both inter ictal and pre ictal data is found from the original ANOVA analysis in Fig 5.8 and also for interictal data, so that the confidence interval is then given by

$$(\mu_1 - \mu_2) \pm S_z \sqrt{\frac{\sigma_1}{n_1} + \frac{\sigma_2}{n_2}}, \tag{5.23}$$

where n_1 and n_2 are the sample sizes respectively and the z-score S_z of 1.96 corresponds to a 95% confidence interval. For the preictal data, n_i was 88 for S1, 81 for S12, and 67 for S2 which were then analyses across four frequency ranges of 40 to 80 Hz, 80 to 120 Hz, 120 to 250 Hz, and 250 to 450 Hz. For the interictal data, the constraint of a 20 second interictal period meant fewer data points of between 28 and 31 for each region.

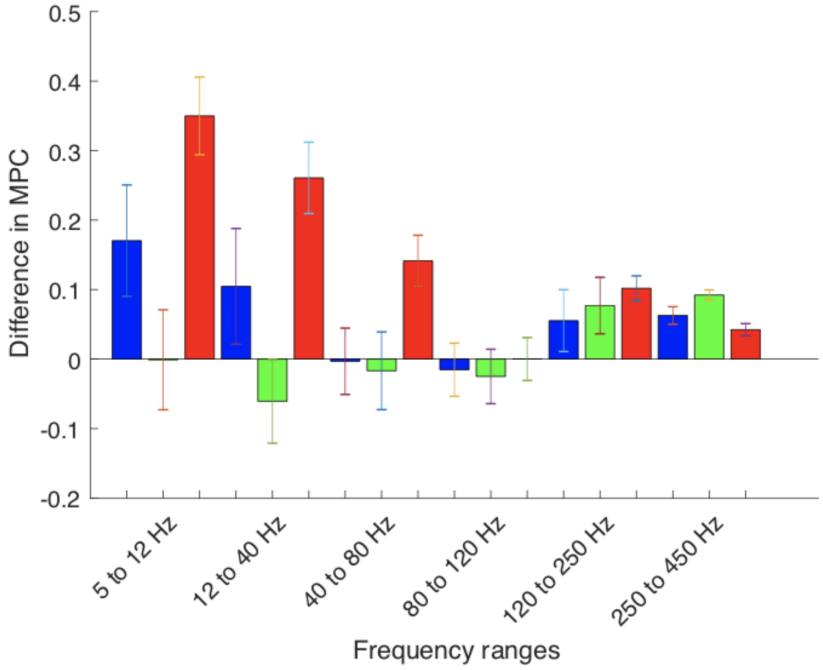

Figure 5.9: Difference in thalamocortical Mean Phase Coherence (Eq. 5.7), at various frequency ranges, between the average MPC calculated in the last second before a seizure, and the average MPC in the inter ictal period. Colour code is blue : S1, green : S12, and red : S2. Error bars are calculated using Eq 5.23

To explain the wide spread of MPC values in the data shown in Fig 5.8, consider Fig D.2 which shows an example of the variability in mean phase coherence between three thalamic tetrode channels and three corresponding cortical channels from one recording location, during three consecutive seizures. In that figure, each of the three colours shows a the phase coherence between one thalamic region and each of the three cortical channels, for each of S1, S12, and S2. From this we note

- there is marked variation between each thalamic channel (represented with different colours in each graph), but quite striking congruence within the three cortical

channels is preserved;

- From the tetrode data at the level of individual channels, individual thalamic and cortex single units show a wide variety in phase coupling, even for adjacent areas. For example, consider the case of cortico-cortical MPC in which tetrode channels are 140μm apart, in the same region leading to the same seizure, as well as between successive seizures. These plots show that some channels remain strongly coupled; some channels only weakly coupled; and some peak in coherence at different stages before a seizure.

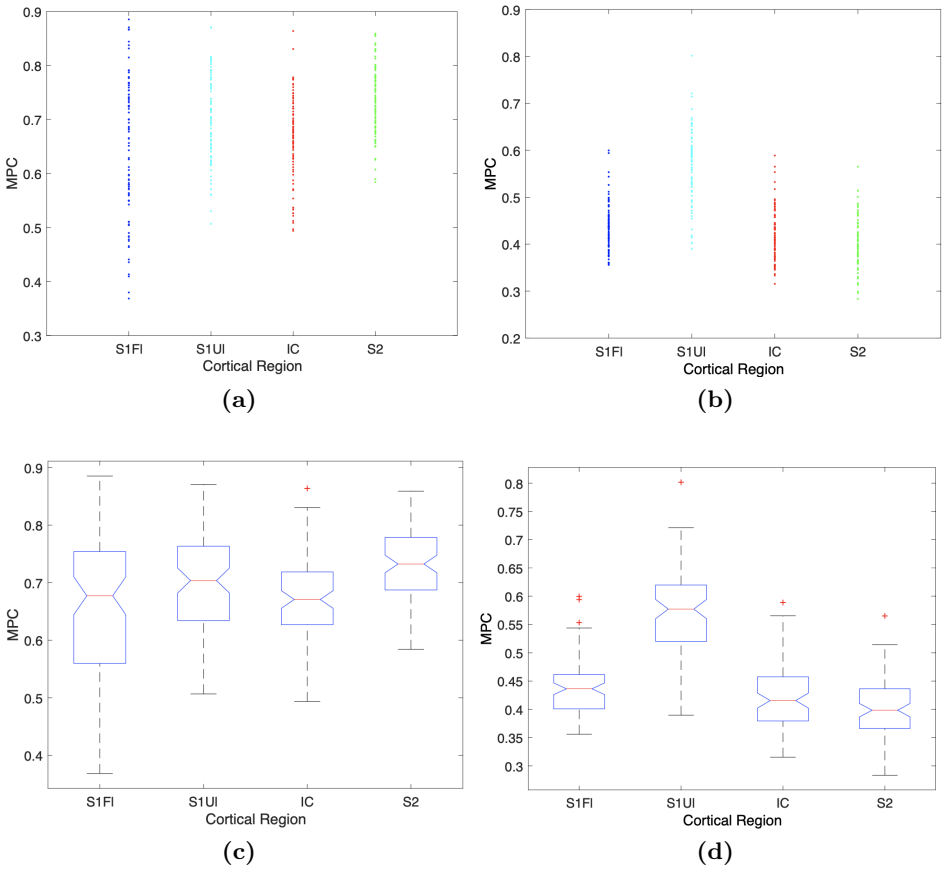

Figure 5.10: Plots of mean phase coherence (Eq 5.7) in the four seconds prior to seizure onset in GAERS rat #1, for 85 consecutive seizures and boxplot. S1FL (blue), S1Ul (cyan), IC (green) and S2 (red). Comparison plot of 85 four second intervals between the same regions in a NEC rat

5.3.4 Entropy, statistical and probability measures

Changes in cortical signal complexity prior to seizures

To quantify changes in ECoG complexity, its permutation entropy was analysed. Depth electrode data was used for this analysis because its lower sampling rate minimised noise and memory constraints. The other reasons for choosing this data rather than the tetrode data are that the latter is sampled at 25kHz and would have required an extremely large ordinal dimension for embedding m, and downsampling, which complicates the interpretation of results obtained. Simultaneous comparisons for widely spaced areas of cortex also give more meaningful results for this measure. Ordinal dimension of $m = 5$ and a delay parameter $\tau = 1$ were used for the analysis, which was performed for 87 consecutive spontaneous seizures for rat # 7.

From Fig 5.11 one can see clear changes in complexity across the different cortical areas, and that these also change as seizures develop. S1Ul had greatest ECoG complexity 4 seconds prior to each seizure, whereas S2 the lowest. One second prior to the impending seizure, S1Fl and S2 had lowest complexity, perhaps indicating the greatest oscillatory component in the signal. An ANOVA for the four groups show a statistically significant difference in means, shown in Fig 5.11c. Fig 5.11a shows the change in PE between interictal periods and the two seconds prior to seizures, for 87 consecutive seizures. In both this figure, and in 5.11b, the IC region has the greatest reduction in PE, though the S1Ul region also shows a significant reduction.

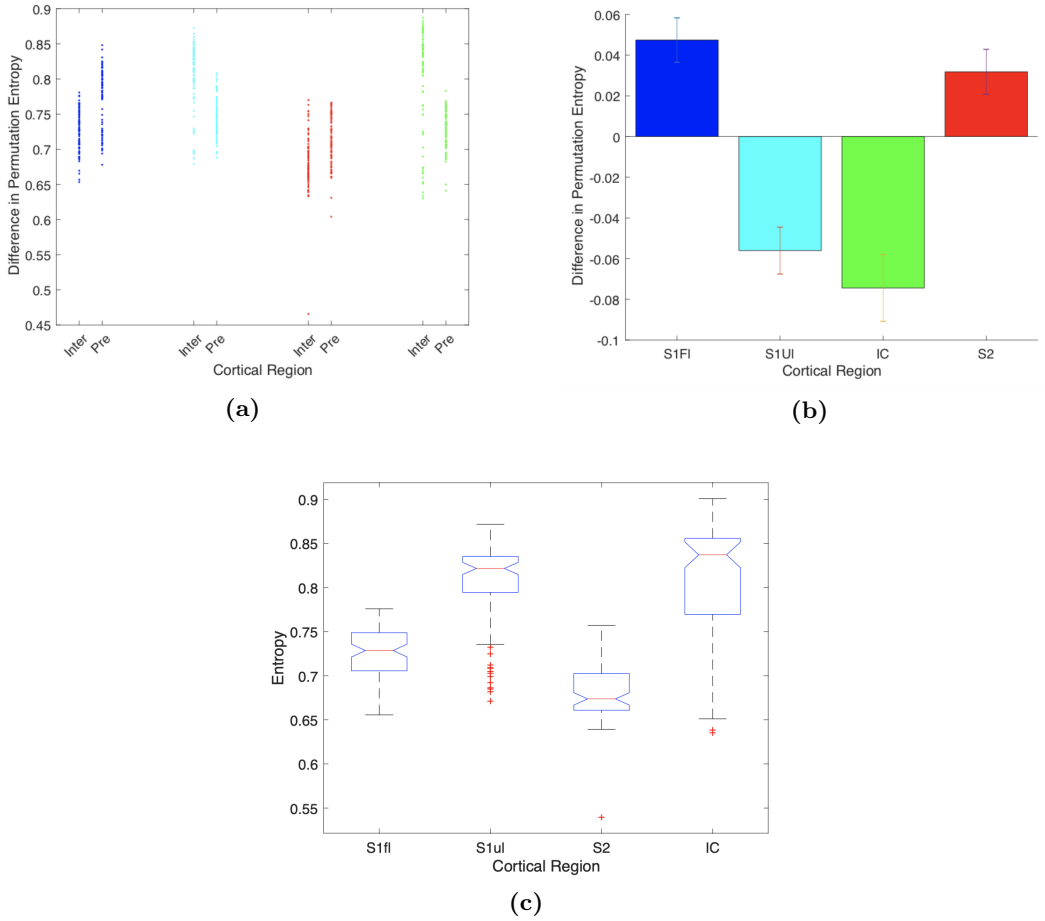

Figure 5.11: Permutation entropy calculated from depth electrode data showing changes in complexity prior to 87 consecutive seizures : red, S2, green, IC, blue, S1UL and cyan S1Fl. a) Permutation entropy 4 seconds prior for all seizures; b) two seconds prior ; and c) ANOVA for the data four seconds prior, with difference in means for the four groups at $p = 10^{-7}$

Mean phase difference entropy

Fig 5.12 provides a visual interpretation of the phase difference entropy measure, as a way of quantifying differences in phase clustering. The left side of this figure shows the phase plots each for 1 second of tetrode data recordings before seizures, with the right side showing a histogram of the difference $\phi_2 - \phi_1$, where ϕ_2 and ϕ_1 are the reconstructed 'instantaneous phases' found by Hilbert transform for a tetrode channel in cortex (Eq. 5.5) and thalamus respectively. The entropy is found using Eq. 5.9.

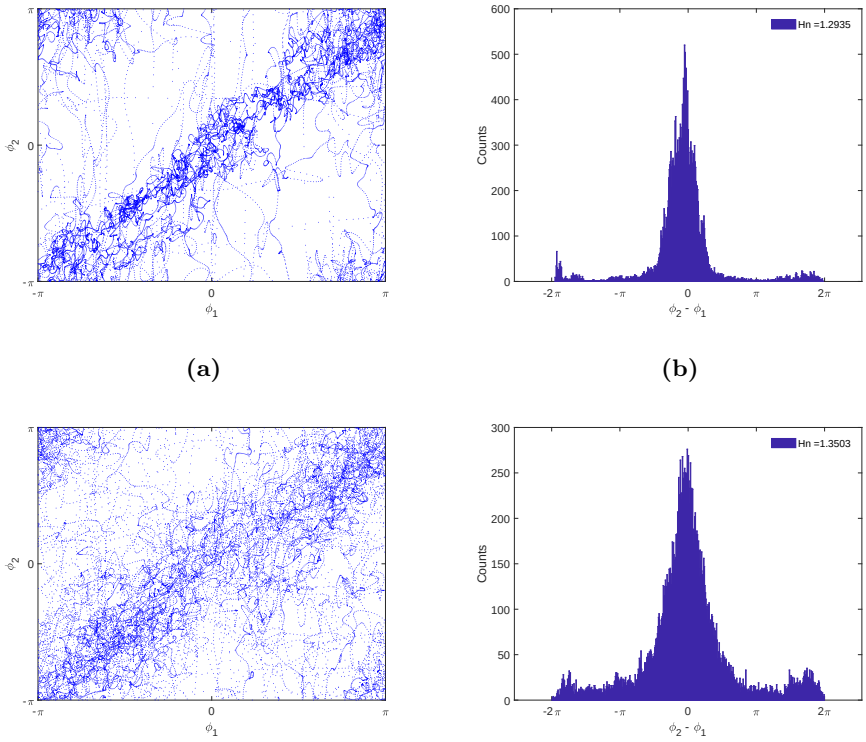

(a) **(b)**

(c) **(d)**

Figure 5.12: Plots showing two examples of phase distributions and their histograms, to illustrate the physical interpretation of numerical values calculated for phase difference entropy (Eq. 5.9). (a) Phase plot and (b) histogram showing an entropy of 1.29; (c) corresponding phase plot and (d) histogram showing an entropy of 1.35

One can see that this measure is sensitive to changes in the histogram distribution

and also the degree of clustering of phases seen in the phase plots. The example of 5.12b shows a number of smaller peaks to the side of the main peak and one can also see in the phase plot a number of parrallel valleys to the main valley running diagonally near the central $\phi_1 = \phi_2$ region. A synchrogram would uncover regimes of synchronisation other than the case of $n = m = 1$ covered by Eq, 5.6.

To see how phase clustering changes with seizures consider the analysis of both corticothalamic phase difference entropy and that between adjacent tetrode channels as shown in Fig D.4 inter ictally, and D.5 in the last second before seizures. Each data point in these figures is a cumulative average of all values calculated for all channels and seizures for that recording location. The duration of recordings is either one or two minutes, in which the number of seizures ranged from one to 11, across two rats (total : 460 seizures). This gave in total 88 data points for S1, 81 data points for S12, and 67 data points for S2 which were then analyses across four frequency ranges of 40 to 80 Hz, 80 to 120 Hz, 120 to 250 Hz, and 250 to 450 Hz. Inspection of shows that the S12 region (shown in green) generally has a larger range of phase difference entropy and a longer 'tail' tending to lower values for nearly all of the frequency ranges studied, reaching statistically significant difference between cortical regions by ANOVA.

In the immediate second prior to a seizure, this trend continued (Fig D.5), with higher phase difference entropy values for S12 and S2 in the lower gamma frequency range, and a wider spread of corticocortical values across most frequency ranges studied.

Comparing Figs D.4 and D.5, the greatest change in distributions is in the S12 region, with a lower mean and much greater heterogeneity of distributions of phase difference in this region prior to seizures. This region also had the greatest tendency towards lower values of this measure, especially for the cortico-cortical channels seen in Fig D.5. Statistically significant differences between means of S1 and S12 were present in the lower gamma frequency ranges (40 - 80 Hz), at $p < 0.0003$, and in the 250 - 450 Hz range, at $p < 0.0008$. The p values discussed here are listed for three way comparisons in each frequency range and listed in Table D.1.

These results suggest that a tighter 'clumping' of phase entrainment exists for these areas, within small cortical regions, and also between cortex and thalamus as well.

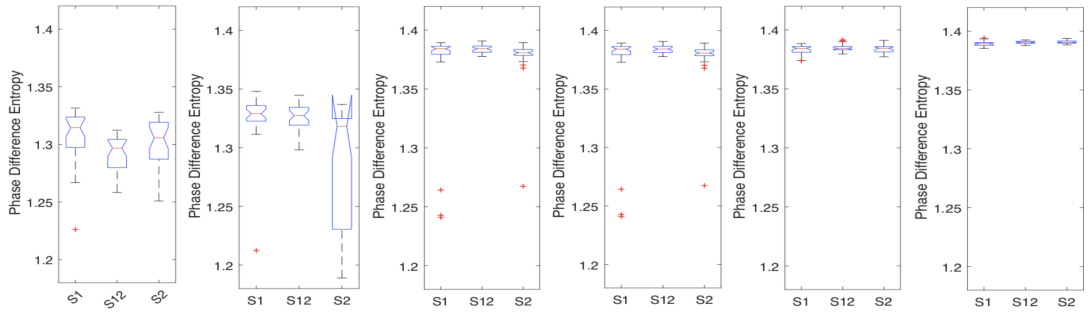

Figure 5.13: Mean Phase difference entropy (Eq. 5.9) as a measure of the "clumpedness" of phases distributed inter ictally between cortical tetrode channels for each of S1, S12, and S2 regions, in the frequency bands (a) 5 to 12 Hz (b) 12 to 40 Hz, (c) 40 to 80 Hz, (d) 80 to 120 Hz, (e) 120 to 250 Hz, and (f) 250 to 450 Hz

To see that this is indeed the case, consider the change between interictal mean phase clustering (Fig 5.13) and that prior to seizures (Fig 5.13). There is a spreading of phase clustering reflected in a greater range of phase clustering entropy, and also an overall reduction in this value as well. Error bars and 95% confidence intervals were generated in the same manner as that used for Fig 5.9, using Eq. 5.23.

Comparison of the differences in mean phase clustering entropy between interictal and preictal data for cortical channel pairs (in Fig 5.14a) or for corticothalamic channel pairs (in Fig 5.14b). Inspection of Figs 5.14a and 5.14b shows a greater, statistically significant reduction in this measure for the S12 region in most frequency ranges studied[5]. This confirms the impression seen from the group data, and that the 'clumping' of phase distributions in the S12 region increases much more markedly than in other regions prior to seizures.

5.3.5 Frequency comodulation, and cross frequency coupling

Cross channel frequency comodulation

Plotting amplitude coherence or mean phase coherence between individual cells, or mico-networks, in thalamus and cortex using tetrode recordings shows marked variation between

[5]error bars in these figures are again calculated using Eq. 5.23

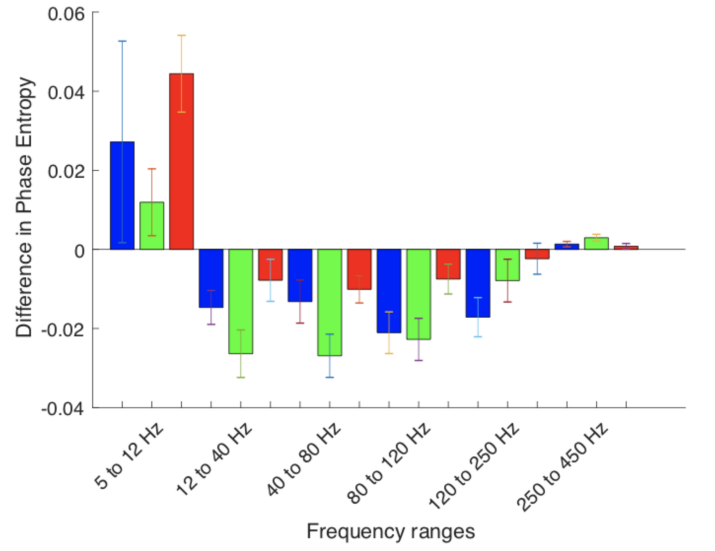

(a)

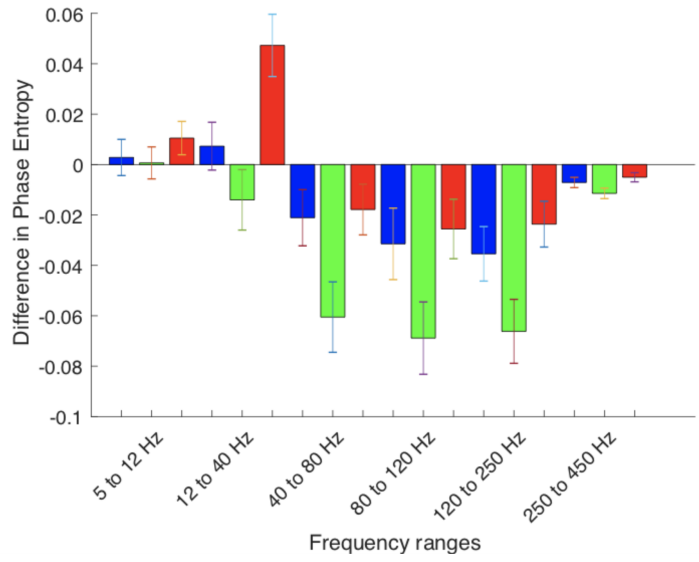

(b)

Figure 5.14: Change in Mean Phase difference entropy (Eq. 5.9) in the last second before a seizure and that measured inter ictally (a) between thalamus and cortex, and (b) between adjacent tetrode cortical channels. Colour code is blue : S1, green : S12, and red : S2. Error bars are calculated using Eq 5.23.

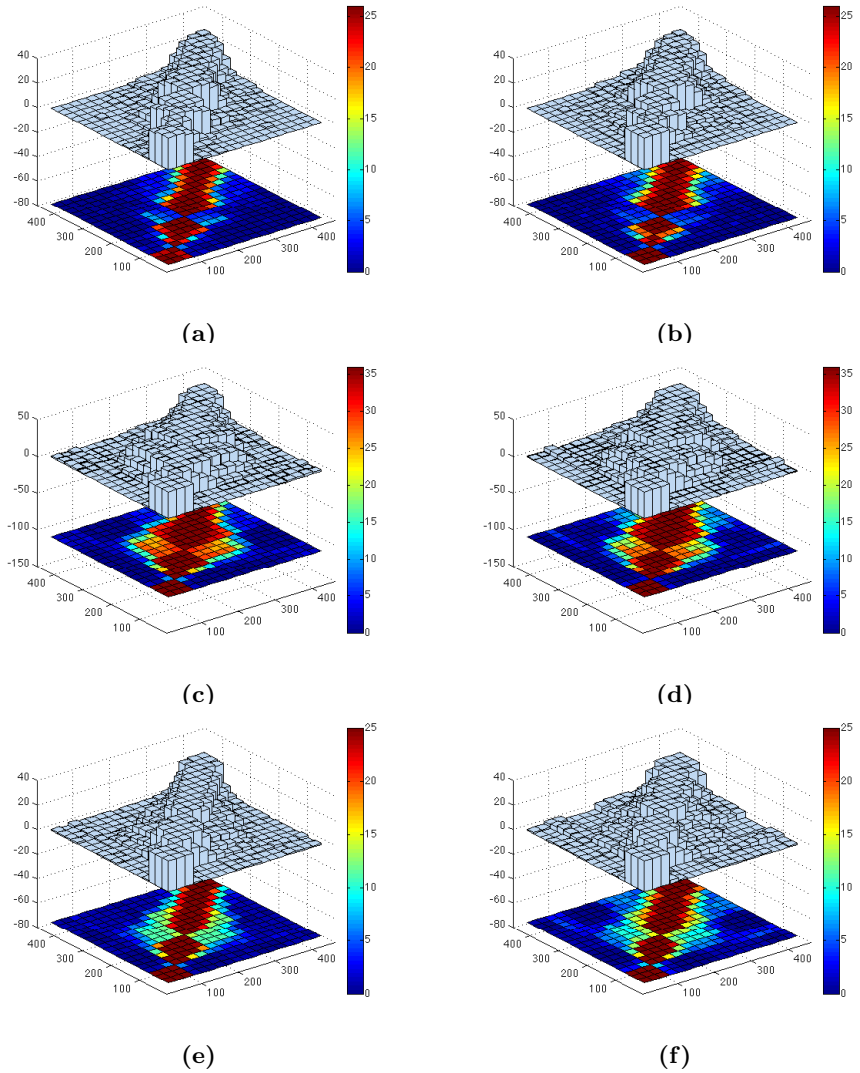

Figure 5.15: Histogram plots of mean comodulation between frequencies in all cortical tetrode channels in relation to seizure commencement for all seizures[6]. (a) S1, (c) S12, and (e) S2 for data 2 seconds before seizure onset, and (b) S1, (d) S12, and (f) S2 for data one second before seizure onset. Plots were generated by taking an average over all cortical channels and all seizures, and all recordings pooled together

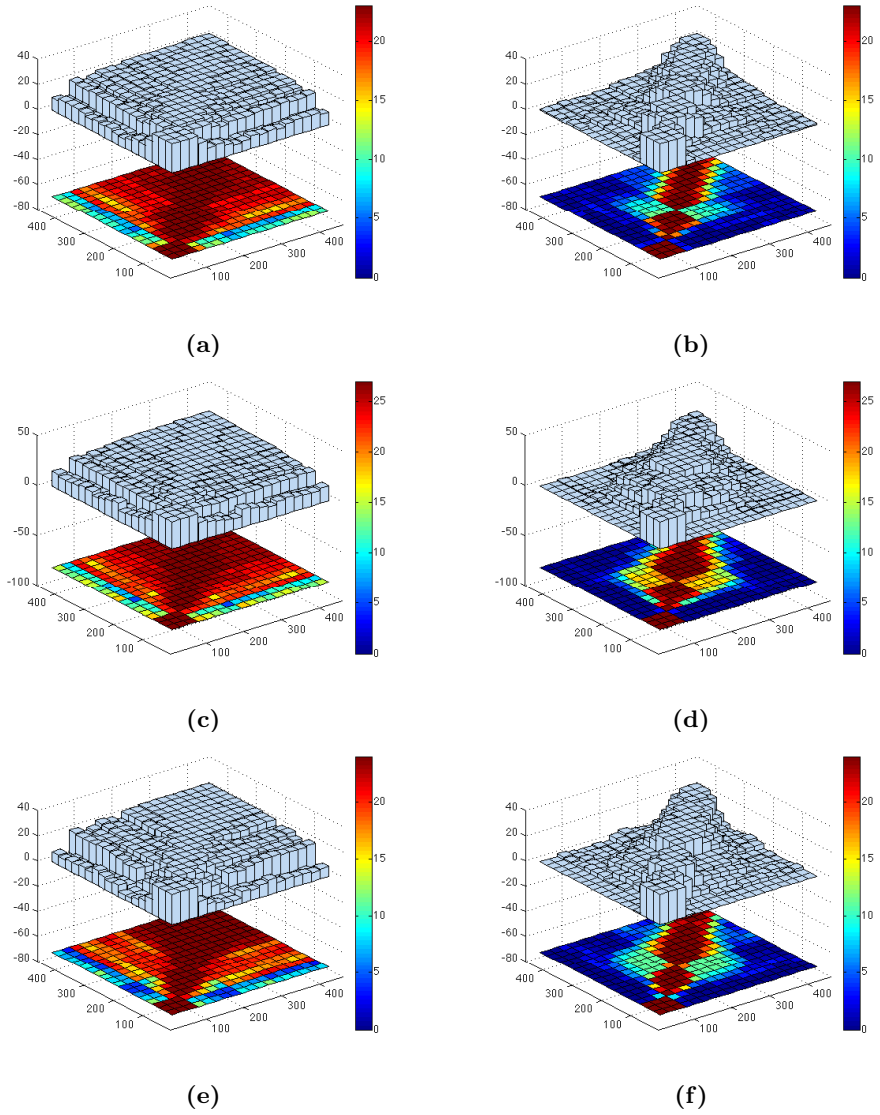

Figure 5.16: Histogram plots of average comodulation between frequencies in all cortical tetrode channels in relation to seizure termination for all seizures. (a) S1, (c) S12, and (e) S2 in the last second before seizure termination, and (b) S1, (d) S12, and (f) S2 in the first second after seizure termination. Method of generating these results is the same as in Fig 5.15

successive seizures, even in the same recording location. To see an example of this, consider the MPC results shown in Fig D.2. In order to see trends despite this variability, the previous results have focused on either average MPC over specific parts of many seizures for each part of cortex.

To overcome this variability in frequency comodulation, a similar approach was used by taking a histogram of comodulation between channel cross spectra above the median value. This is shown in Figs 5.15 and 5.16. This was calculated using a multi taper estimation of cross spectral density for each pair of channels, and then correlating each to form a measure of 'comodulation' between channels. This provides a measure of the degree to which changes in coherence are comodulated across different frequency ranges as a persisting trend.

Figs 5.15 and 5.16 show a histogram of all comodulation changes seen before all seizures for each of the three cortical regions. From these pooled results, it can be seen that S1 cortex is consistently slower to increase comodulation prior to seizures. The S12 region demonstrates a higher comodulation of freqencies, and after seizure termination, both the S12 and S2 regions were the last to extinguish this increased frequency comodulation[7].

From this data, the strongest comodulated changes in coherence occur either in lower frequencies less than 50Hz or in the higher frequency range i.e. 200 - 450 Hz for cortical channels, in the S12 and S2 regions.

Cross frequency coupling

To see that there is indeed comodulated frequencies present in the data, consider the plot of three separate frequency components from a region in S1 (Fig 5.17a), in the second before a seizure, and the contour plot of cross frequency coupling for this same data in Fig 5.17b. The higher frequency couplings seen in this contour plot may be artefacts, but further filtering also verifies that coupling in the 250 - 300 Hz range is present.

As a check, Fig. 5.18 shows that Broseledec's theorem (discussed in Section 5.2.5) is satisfied for this example, in that the high frequency components and also the base

[7]Further data on this is available, but not shown

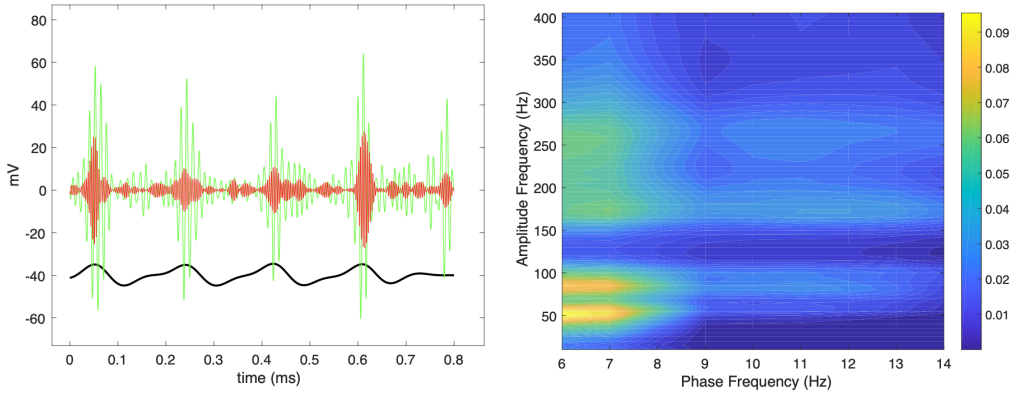

(a) **(b)**

Figure 5.17: Example of phase - amplitude cross frequency coupling (given by Eq. 5.12) in underlying oscillations from data, obtained directly by applying three filters to one data segment. (a) A two-second snippet of data, from the S2 region (rat 1, recording #202207), bandpass filtered at three frequencies : 260 ± 10 Hz (red); 90 ± 10 Hz (green) and between 5 - 9 Hz (black - this last waveform attenuated by a factor of 100 and shifted for clarity), showing detail of the relationship between higher frequency components.(b) Sample contour plot of cross frequency coupling for this data

frequency waveform share the same origin in the complex plane.

To see whether any common features may be present across all seizures, and to compare how these features may differ across each of S1, the junction region S12, and S2, Figs 5.19 and 5.20 show the histograms of cross frequency coupling above a set threshold value as a function of frequency in adjacent cortical regions at different time points in the progression of seizures.

To generate these histograms a threshold of statistical significance was set at 0.75 × the median coupling value at each coupled frequency bin tested, as discussed in Section 5.2.5, after a surrogate analysis to determine this using both pre- and inter-ictal data. Figs 5.19 and 5.20 display counts exceeding this threshold. The first observation from these results is that cross frequency coupling is markedly higher in S2 and S12 than in S1. Secondly, increased coupling is seen with the high gamma frequencies (150 - 200 Hz), and also in the 250 - 350 Hz bands, building successively two seconds and one second before a seizure. Again this is highest in the S12 region. These observations are consistent with the results of the comodulation analysis presented earlier. Fig 5.20 shows the cross frequency coupling seen immediately (the first second) after seizure termination. Coupling with

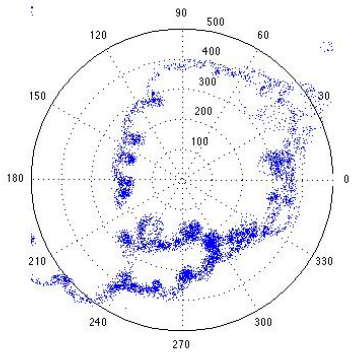

Figure 5.18: Example using the data from S2 cortex (rat 1, recording #202207) used in Fig 5.17, showing that the lower dominant frequency component contains the origin of the complex plane

higher frequencies was seen to markedly decrease after seizure termination (this data is not shown), suggestive of post ictal cortical depression, before again gradually increasing in the inter ictal period. Before seizure termination, the activity in S12 slows first, and in the first second post seizure termination it is lowest in S1.

Figs 5.19 and 5.20 show that the histogram plots are often more than 50% lower for S1.

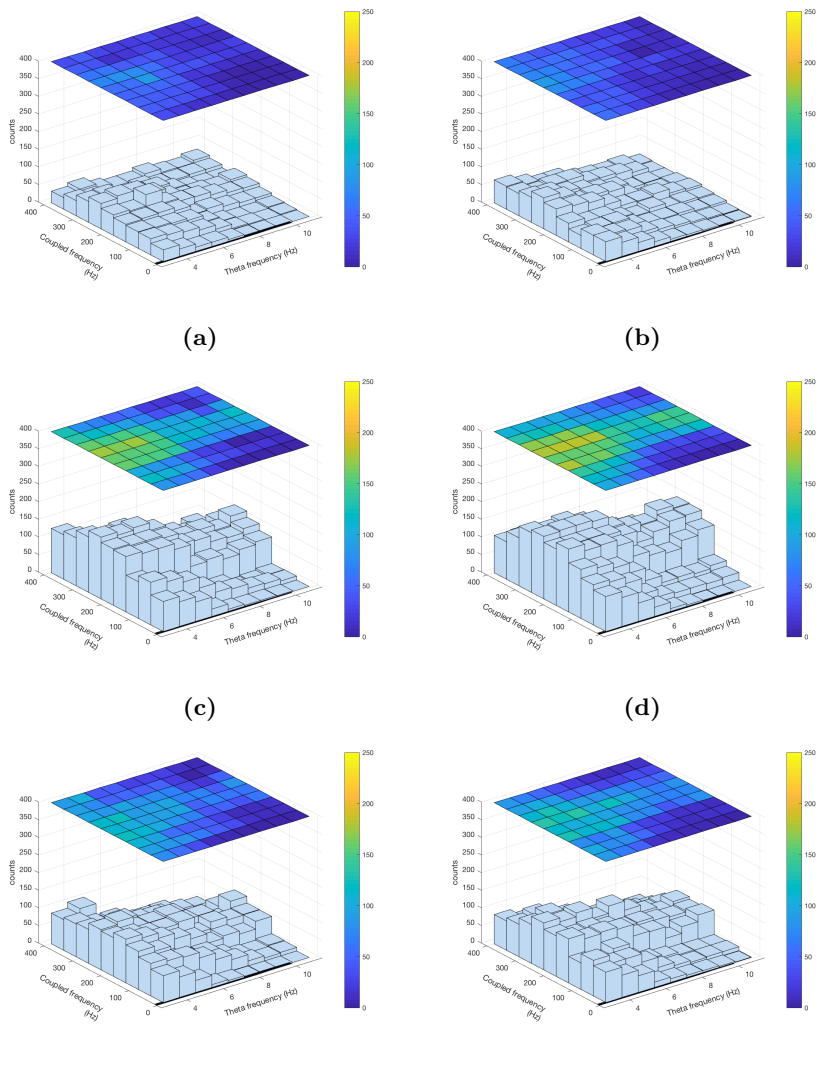

Figure 5.19: Plots of cumulative histograms of cross frequency coupling for all seizures by region, Left : 4 seconds before a seizure (a) S1,(c) S12 region and (e) S2. Right : for the last 2 seconds before seizure onset (b) S1, (d) S12, (f) S2

The occurrence of High Frequency Oscillations with SWDs

Looking at the plot of the instantaneous power spectrum (fig 5.5) and also the results of cross frequency coupling for higher frequencies (Figures 5.19, 5.20, and 5.21) it can be

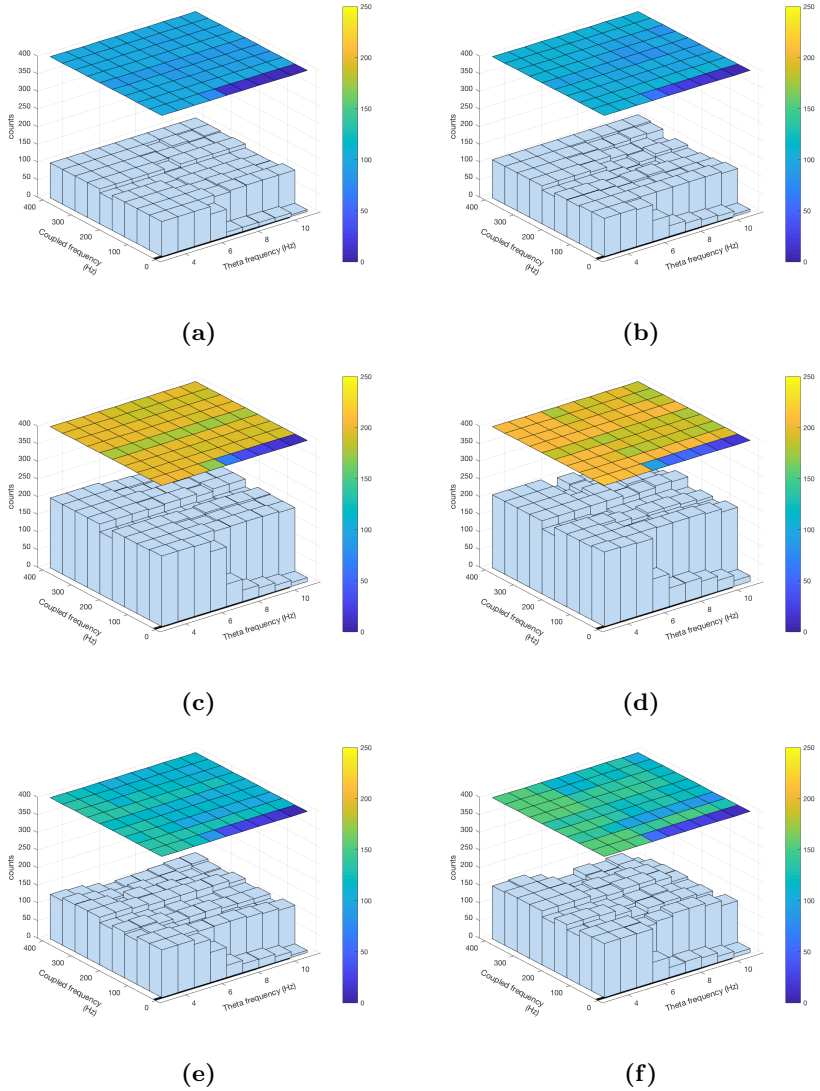

Figure 5.20: Left : Plot of the cumulative histograms of cross frequency coupling in the first second after seizure onset. (a) S1,(c) S12 region and (e) S2. Right : Similarly, for the last second before termination of SWDs, (b) S1, (d) S12, (f) S2

seen that higher frequency power also coincides with the theta peaks. By visual inspection of Figs 5.17a and 5.17b, it becomes clear that these are not artefactual as one sees the bandpass filtered signal overlaid with the theta peak. Additionally, the use of surrogate testing to set the threshold for histograms also demonstrates this. Further statistical

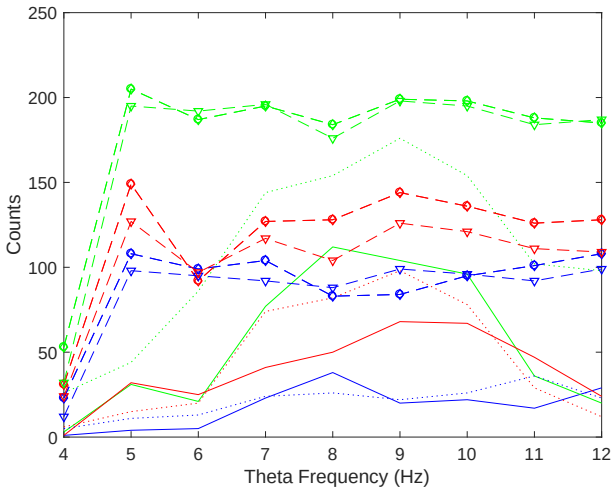

Figure 5.21: plot of significant counts of cross frequency coupling, Eq. 5.10, between frequencies of 250±20 Hz and theta frequencies between 4 and 12 Hz used for the T test of Table 5.1, for all tetrode data in relation to seizures shown in Figures 5.19 and 5.20. Significance was set above a threshold value of 0.75×(median), which was above a significance threshold found from surrogate inter - and pre - ictal data (Section 5.2.5). Each cortical area is represented as S12 - green; S2 - red; S1 - blue. I need to add legend here

analysis by groups with a T test also bears out a statistically significant difference between regions (Table 5.1). Taken together, these results suggest that high frequency oscillations themselves also are aligned with the theta rhythm.

To see that this is the case, and that they are related to the peaks of the theta rhythm, consider Fig 5.22. To generate this figure, snippets of higher frequency bandpass filtered data which aligned with 15 successive peaks of the 5±2 Hz rhythm were found, and then averaged together. To find the centre point for aligning these segments the maxima of the theta rhythm was used, however this was a trade off as too 'aggressive' filtering of the theta rhythm changed this time by bringing it forward. From here, the higher frequency snippets of data were chosen as ±2500 data points either side of this central peak. The

Difference between means - cross frequency coupling at 250 Hz				
Time	stat	S1→S12	S1→S12	S1→S12
4s before	95% CI	52.6 - 90.06	4.57 - 48.33	35.76 - 54.02
	p	2.2×10^{-5}	0.0237	3.3×10^{-6}
1s before	95% CI	61.22 - 99.61	27.92 - 53.86	25.5 - 53.58
	p	1.1×10^{-5}	8.6×10^{-5}	0.0002
First SWD	95% CI	95.07 - 100.92	61.96 - 70.48	28.58 - 55.01
	p	8.6×10^{-13}	4×10^{-13}	1.5×10^{-8}
last SWD	95% CI	95.38 - 101.73	51.27 - 59.46	40.27 - 46.17
	p	1.6×10^{-12}	1.2×10^{-9}	6.3×10^{-10}
after sz termination	95% CI	95.38 - 101.73	51.27 - 59.46	40.27 - 46.17
	p	1.6×10^{-12}	1.2×10^{-9}	6.3×10^{-10}
inter ictal	95% CI	52.6 - 90.06	4.57 - 48.33	35.76 - 54.02
	p	2.2×10^{-5}	0.0237	3.3×10^{-6}

Table 5.1: Summary of results of paired T test for significant differences between mean cross frequency coupling between regions, for all tetrode data prior in relation to seizures, shown in Figures 5.19 and 5.20

inset panel in Fig 5.22 shows the appearance of each snippet before being averaged.

This method was again adapted from [226] (see his Figure 3B, page 20518). It more or less follows the idea of Fig 5.17a, that bandpass filtering the data clearly identifies cross frequency interactions (but without the method for calculating the strength of cross frequency comodulation, i.e. Eq. 5.10). Fig 5.22 also provides evidence that HFOs are actually present.

To investigate what association may exist between higher gamma frequency spectral power and seizures, the power in these averaged data snippets was calculated for 10 Hz bandpass frequencies centred between 80 Hz and 400 Hz in 5Hz intervals. Each data point in this figure represents an average power from that calculated from all seizures in that recording location (range $n = 1$ to $n = 9$). The results of these calculations are shown in Fig D.6.

From these results a minority of HFOs arising from S1 had the highest HFO power. This is somewhat surprising when we consider that the S1 power spectrum was much higher than other regions at higher frequencies (Fig 5.2). S1 and S12 region data have more of a spreaded range of HFO power whereas the S2 data clumped together towards the highest power ranges at most frequency ranges, and at all times investigated relative

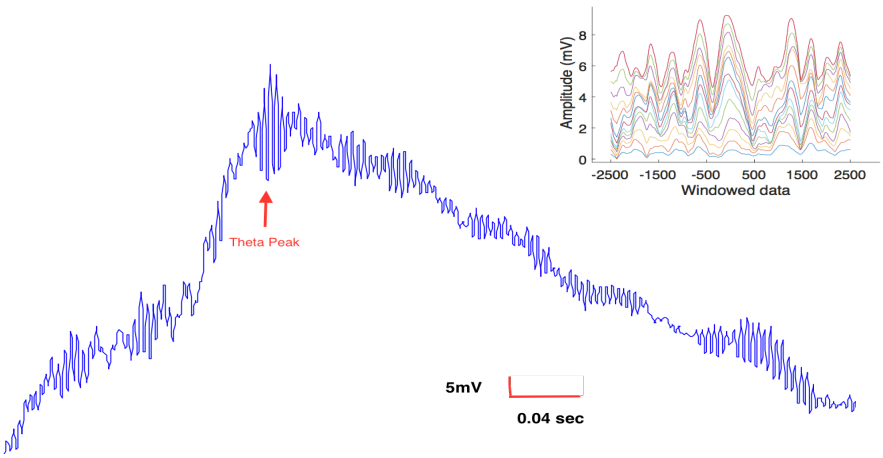

Figure 5.22: Cumulative plot of High frequency oscillations occurring at the peak of SWDs, showing that these are locked to the theta peaks during a seizure (tetrode data from rat 1, recording #202207). Inset figure shows a superposition plot of 15 consecutive theta peaks, band pass filtered at 250 Hz $\pm$ 10Hz centred at the time point of the maxima of the 5Hz theta rhythm, and averaged to generate the main figure. If HFO activity was not phase locked we would see the oscillations average out, however they can still be clearly seen.

to seizure onset. S2 also seemed to increase in HFO power more than other regions, at higher frequency ranges, and interestingly all data points from S2 apart from one in each figure are grouped around the maximum. We also see that there are increases in HFO power before seizures, as one may expect.

The instantaneous theta frequency plots of 5.5 and the results shown in Fig D.6 suggest that these oscillations gradually increase in the seconds before a seizure, in a non trivial way, becoming more phase locked to the theta rhythm.

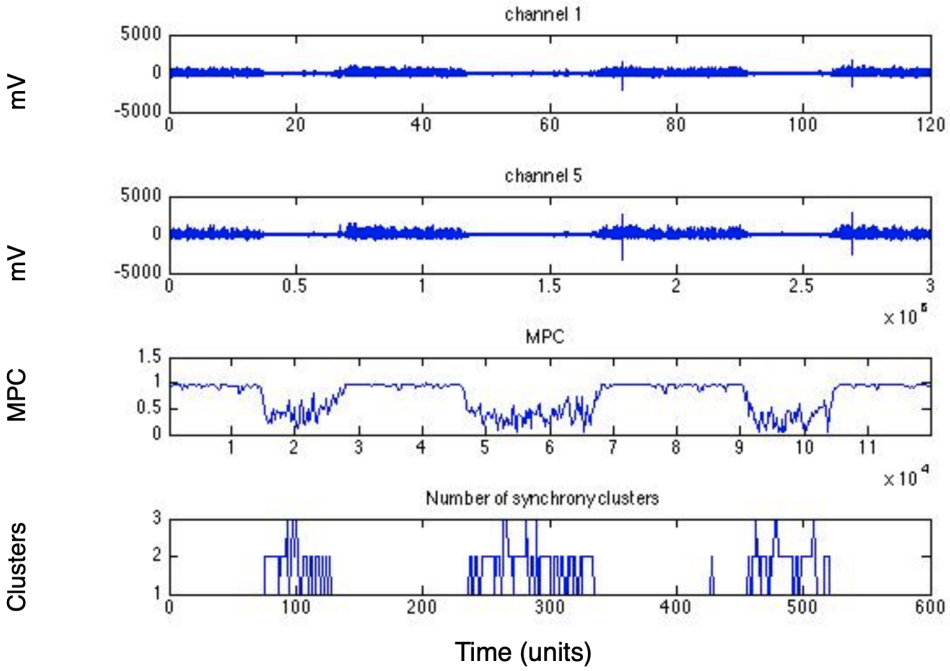

Figure 5.23: Example of synchrony clustering between cortical channels, found by eigenvalue decomposition of Eq 5.14. The top three panels show two data channels and mean phase coherence between cortex and thalamus over 120 seconds' recording. The lowest panel shows a plot of the number of synchrony clusters found by eigenvalue decomposition over a minute of recording

5.3.6 Clustering of synchrony prior to seizures

Using the eigenvalue decomposition method described in Section 5.2.6, the number of synchronous processes forming and the duration of synchrony clustering was examined. Using Equation 5.15 the significant clusters were counted at each 200 millisecond block between seizures. An example of the formation and peak in clusters during the interictal period is seen in Fig 5.23. The duration of these clusters in time was quantified by counting the length of time in which clusters remained consecutively significant. A histogram of the lengths of duration of synchronous activity was determined For all available tetrode data for each cortical region, and is shown in Fig 5.24. From these results it can be seen that the S1 region tends to have briefer, ($\sim$2 sec) shorter duration of synchronous activity, whereas the S12 region has a wider, relatively even distribution of durations, seen in the middle panel. There was no statistical difference in the number of synchronous processes by region.

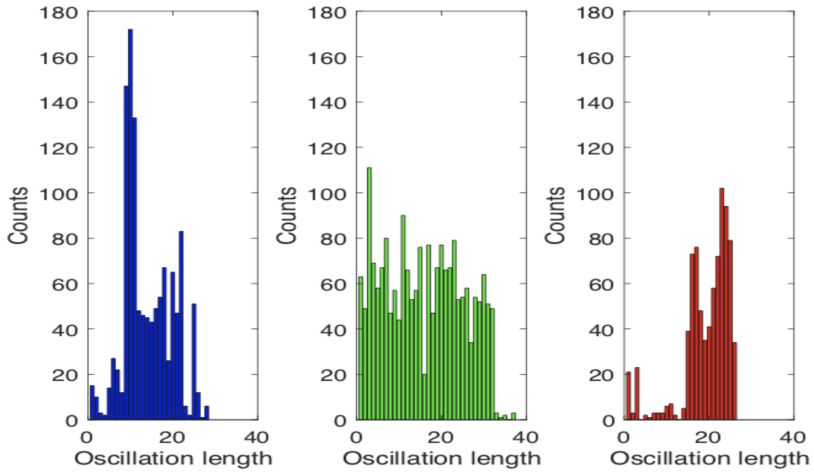

Figure 5.24: Histogram of the duration of synchrony clusters, for each cortical region, as defined as persistently significant clusters of synchrony using Equation 5.15. Units of time for the x axis are 200msec each. Colour code is S1 - blue; S12 - green; S2 - red.

5.3.7 Results of dynamical analysis

Finite Scale Lyapunov Exponent

To investigate difference in dynamical stability between regions the Finite Scale Lyapunov Exponent was calculated for the 4 seconds leading to the seizure shown in Fig 5.25 [117]. However, analysis of 87 consecutive seizures from depth electrode data do not show any statistically significant differences when comparing the difference between each lyapunov exponent and that of a control area (here, the contralateral motor cortex was used) for each seizure[8]. Additionally, there are not signifcant changes before seizures with inter ictal periods.

How do regions vary in their sensitivity to perturbation

As above the method of Letz et al's [110] analysis is based on the FSLE analysis of response to cortical microsimulations. Fig 5.27 shows some sample qualitative results for depth electrode data (rat # 7), over the first 1200 data points of a seizure in S2 (approximately 9 seconds). The phase plot in Fig 5.27a shows the reduction in phase space expected

[8] this data is not shown

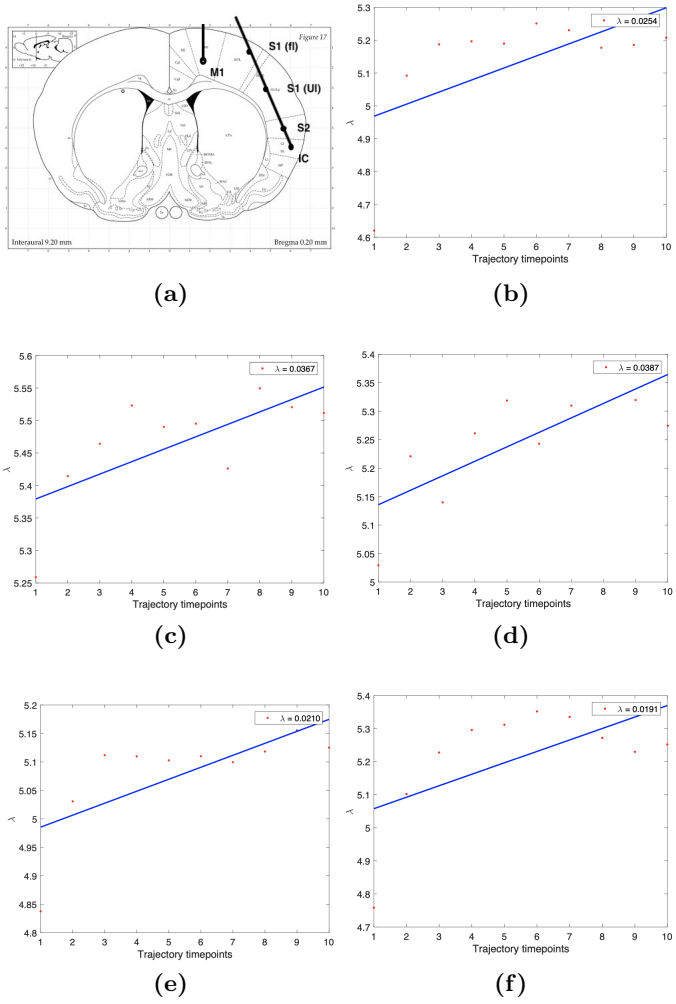

Figure 5.25: Finite Scale Lyapunov Exponent for simultaneously recorded depth electrode data of 4 second's duration (approx. 1000 data points) in the lead up to a seizure in GAERS rat #7. a) approximate depth electrode positions and corresponding channels. b) - f) : Finite Scale Lyapunov analysis for ten scales described in the text shown on the horizontal axis. Linear best fit shown in blue. The gradient of this line gives the FSLE for this scale region as respectively (b) 0.0254 for insular cortex (IC); (c) 0.0387 for S2; (d) 0.0367 for S1Ul; (e) 0.0210 for S1Fl; and for comparison purposes - (f) 0.0191 for motor cortex

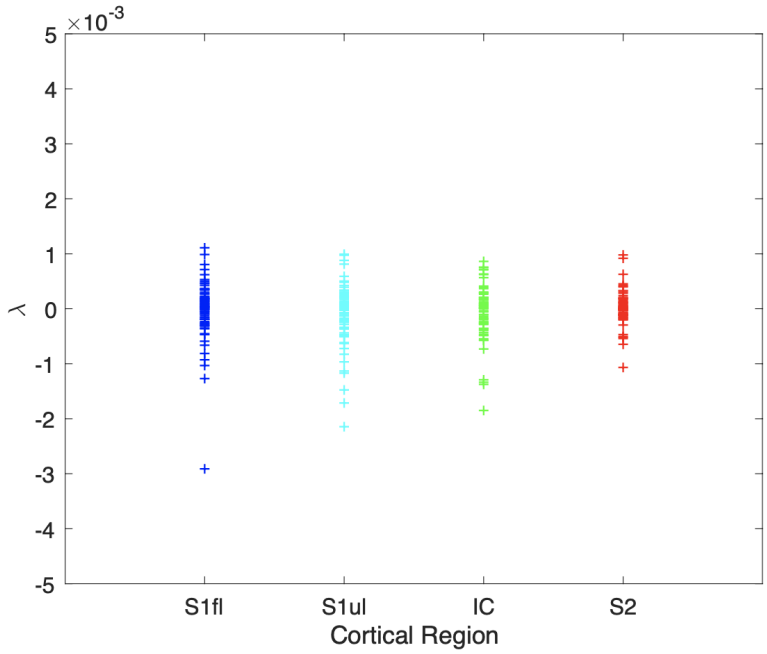

Figure 5.26: Plot of Finite Scale Lyapunov exponents prior to 77 consecutive seizures for depth electrode recordings for Rat # 7

and a sample path (shown in red) is the reference trajectory for perturbations amongst other available trajectories from the embedded data in green. The optimal τ, discussed in Section 3.3.4 and [31],[5], for this data is 16 data points (a little over 0.06 seconds - found as the time taken for the data's autocorrelation function to decay to $\sim e^{-1}$). The oscillatory path of larger perturbations, for example seen in fig 5.27c, is consistent with a largest local Lyapunov exponent of zero as seen in Fig 5.27b, and in the results of the FSLE analysis shown in Fig. 5.26.

5.4 Discussion

This chapter has explored the progression in network electrophysiology behaviour between different somatosensory cortical regions and their thalamic connections in the GAERS rat in relation to spontaneous seizures. The question of how and where resonance occurs during seizure generation has been addressed by sequentially looking for evidence of changes in characteristic amplitude and phase coherence, phase clustering, cross-frequency phase-

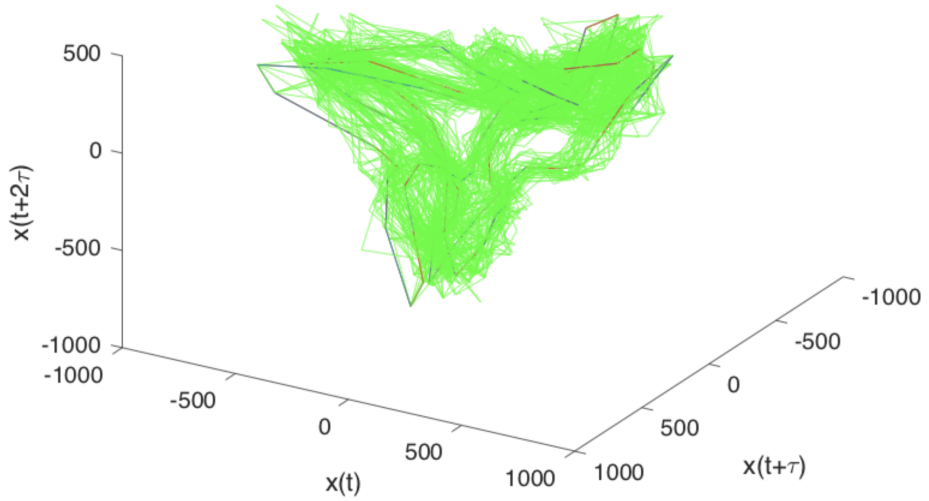

(a)

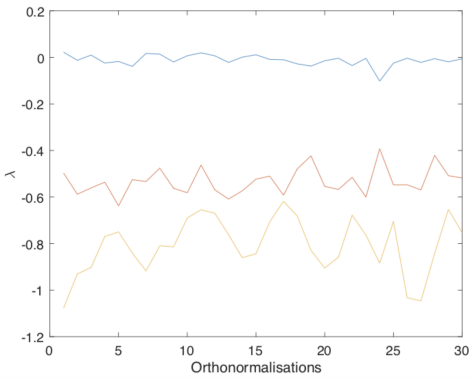

(b)

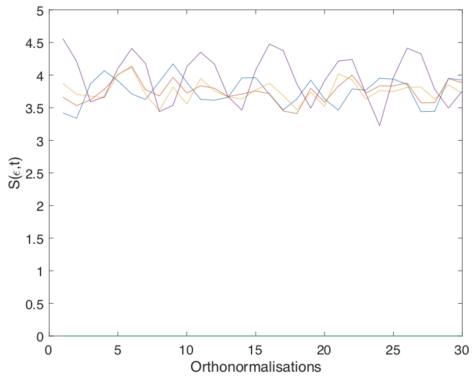

(c)

Figure 5.27: Example of perturbation analysis based on Letz et al.'s method [110], for rat Depth01, depth electrode data, in the second prior to a seizure. Parameters used for the delay embedding are $\tau = 16$ and $m = 3$. (a) Phase plot for the data used for these parameters, where a 'reference' trajectory is shown in red, and all nearest neighbour trajectories, representing possible perturbations for this embedding of the data, are shown in green. (b) Lyapunov spectrum for the same data. (c), Scale dependent stability numbers $S(\varepsilon, t)$ are plotted as a percentage perturbation of the largest dimension of the signal in phase space

amplitude coupling, and dynamical characteristics such as the ECoG complexity and stability as measured by the FSLE.

A number of characteristics support the hypothesis of resonance in all areas of cortex examined around the time of onset of seizures. However these appear strongest in the S12 junction region and S2. Although there appears to be a number of mechanisms behind this resonance that accompanies seizure generation, some patterns emerge.

There is no difference in the temporal onset of seizures between the thalamus and different cortical regions (Section 5.3.1). Time lags between seizure onset in either ventroposteromedial or VB thalamus and the first SWD seen in micro-networks in deep cortical layers of each of the different somatosensory regions S1, S12, and S2 showed no discernible difference.

Amplitude power (Figure 5.2) and amplitude coherence (C_{xy}, Eq. 5.2) can be interpreted as a measure of coincident recruitment of cortical areas in synchrony with thalamus. In these experiments, amplitude coherence (Sec. 5.2.3) did not show significant difference between cortical regions. Similarly, there was no difference in higher harmonic power (Section 5.2.2), or phase clustering analysis using Kalitzin's Phase Cluster Index method up to the fifth harmonic in the second before seizure between the regions (this analysis was not shown).

However, Mean Phase Coherence ($\varphi_{1,1}(t)$, Section 5.2.3, here called 'MPC') did show changes with seizure onset (Eq. 5.7 and Section 5.3.3). Insular cortex and S2 cortex had higher levels of mean phase coherence leading to seizures in depth electrode recordings compared with NEC rats (where the pattern was reversed and S1Ul and S1Fl were higher), however S1Fl also showed a significantly increased spread in MPC in GAERS rats also. It is interesting that the ANOVA results of Figure 5.10 show that the greatest increase in MPC between the non epileptic control rats and GAERS rats was in the S2 region. Additionally, an analysis of MPC by frequency range in tetrode recorded data (Fig. 5.9) suggests that the S2 region showed the largest statistically significant increases in MPC just prior to seizures, with a higher mean increase in MPC over a wide range of frequencies from the theta band of 5 - 9 Hz to the lower gamma band of up to 80 Hz. Interestingly, despite the fact that higher frequency spectral power was highest in S1 cortex prior to

seizures (Fig. 5.2), this region was found to have lower phase coherence and the lowest cross-frequency coherence changes just prior to seizures.

When analysed at the level of tetrode channels, consisting of micro-networks of multiples of single cells, it was found that individual thalamocortical neuronal MPC was erratic and very irregular. Despite this, between very close recording locations across adjacent thalamic and deep cortical tetrode locations, there tended to be consistent across one recording location for a number of seizures in two minutes (see, for example, the results of Fig D.2). In comparison with the results found by Truccolo and colleagues [227] where marked heterogeneity of single unit recordings was observed during seizures, electrophysiology studies of deep cortical layer cells prior to seizures in GAERS rats[249] indicated that the majority of cells (approximately 70%) were engaged in rhythmic activity.

Considering the results of mean phase difference entropy (H_n) analysis (Equation 5.9, Section 5.2.4), the S12 region showed a greater range of phase clustering and a bimodal distribution with lower entropy values, implying a tendency for a subset of neurons to phase lock more tightly. This trend was present in both interictal data and was also found prior to seizures. Between cortical and thalamic channels, the S12 region showed the largest reduction in mean phase difference entropy (i.e. tighter phase clustering), seen in the differences in means between interictal and pre-ictal phase clustering were significant for all frequencies studied up to 120 Hz (Fig. 5.14). This indicates a change in distribution of phase entrainment with the onset of seizures over a wide range of gamma frequencies. With respect to cortico-cortical phase clustering behaviour, the frequency range of changes was more widespread, and significant for frequencies from 40 Hz, up to 250 Hz.

Permutation entropy ($H_p(n)$, Eq. 5.8) analysis shows a reduction of complexity was greatest in the IC and S1Fl regions in the EEG prior to seizures (Section 5.3.4). This would be expected to be associated with a greater oscillatory component in the signal. Interestingly, the eigenvalue analysis of Section 5.2.6 did not show an increase in the number of separate oscillatory components across different cortical areas, although the length of time synchrony was maintained was observed to differ between regions(see, for example, Figure 5.23. It is possible that an increased strength of oscillations could be demonstrated, for example, with empirical mode decomposition methods, but this has not

been completed in the present work.

As shown in previous work [249] the theta rhythm is a central dominant contributing rhythm during the onset of seizures. Results obtained from the instantaneous power plots of Fig. 5.5 show that higher frequencies are entrained to this rhythm approximately one second after seizure onset, but not interictally.

The theta time locked instantaneous power was found to dramatically increase during seizures, but this increase was found to be delayed until approximately one second after the first SWD, and did not seem to coincide with seizure onset. This observation is consistent with the results of analysis of cross frequency coupling between theta and higher gamma rhythms and also our observations [249] of increased rhythmic cortical rhythms of the large majority of single cell recordings made in that study. It is also consistent with findings of increased cross frequency coupling occurring during seizures as demonstrated here (Section 5.3.5). Higher frequencies are amplitude - coupled to the peak of this theta rhythm even though amplitude coherence, or harmonic power is not increased. All regions show a high degree of coupling of the theta rhythm to higher gamma frequencies leading up to seizures, but the S12 and S2 regions showed more marked co-modulation (Figs 5.15 and 5.16) and cross frequency coupling (Figs 5.19 and 5.20) than the S1 region.

The pattern of cross frequency coupling was found to vary between regions and between inter ictal, pre ictal and post ictal periods. It was found that cross frequency coupling gradually increased until just before seizure termination, with a marked decrease after this point. The S2 and S12 regions showed higher degrees of cross frequency coupling than S1. Interestingly, S12 cortex was seen to decrease in the degree of coupling first, before other cortical regions, just prior to seizure termination.

Of the different spectral frequencies which were found to be coupled to the dominant theta rhythm, higher frequency oscillations above 250Hz seemed to be most marked. In our work of [249] we demonstrate the existence of high frequency oscillations for the first time. The study of HFOs in this chapter confirm this finding and, again, that these are also coupled to the theta rhythm. The S2 region was found to have higher combined HFO power with the progression of seizures (Fig D.6).

Taken together, the results of this chapter, from tetrode experiments in three rats, of whom two had seizures, and depth electrode experiments in five rats, show that phase dynamics between both small and larger scale cortical networks and thalamus provide evidence of increased resonance prior to seizures.

These results also suggest that phase-amplitude cross frequency coupling is a plausible factor in the resonance found by cortex in the beginning of a seizure. Although there is growing evidence that cross frequency coupling is an important method of information coding[149] and part of the normal functioning of the thalamocortical network[95], the results of cross frequency coupling are consistent with at growing amount of recent prior literature documenting it's presence in relation to mechanisms increasing neuronal excitability[200] and seizures. For example, Giurgis and colleague's study[118] showed that expert systems using a combination of phase synchrony and cross frequency coupling more consistently predicted pending seizures; Fitzgerald's findings[69] also demonstrated the presence of CFC in extra temporal epilepsy in intracranial EEG studies (Section 1.3.2).

There are potential weaknesses in the analysis methods presented here. The most obvious weakness is the relatively small number of animals. Despite this, the results presented here show statistical significance even for these small numbers. It is also possible that the instantaneous theta power analysis included the presence of artefacts which could exaggerate the degree of entrainment seen during seizures. This can be associated with the windowing used to obtain the amplitude envelopes for this analysis. Similarly it has been described by Kramer and colleagues [2] that measures of cross frequency coupling can be associated with edge effects leading to spurious frequency co-modulation, most likely in the presence of sharp discontinuities in the base rhythm as can be seen in SWDs. To minimise the risk of this, the analysis presented in this chapter was preceded by a surrogate analysis aimed at reducing the risk of statistically non-significant coupling, and the results presented here show relative values of cross frequency coupling above the same threshold. This threshold was chosen conservatively, with a margin above the 'base' threshold suggested by the surrogate analysis. As discussed, the intensity of coupling at higher frequencies is higher in the S12 and S2 regions than in S1. Similarly the presence of increased power in high frequency oscillations timed with theta peaks are also consistent

with this result being a true rather than a spurious finding. Lastly, the increase in theta instantaneous power and presence of entrainment only occurred one second after seizure onset, and was not present before this i.e. at the initial commencement of SWDs, when artefactual increases would be expected to occur.

5.4.1 Dynamics associated with seizures in GAERS rats

A dynamical analysis of phase space characteristics in the face of perturbation was outlined based on the work of [110]. From an available perusal of all of the published references to Letz and colleague's work, this is the first application of this technique in epilepsy. This showed variability in trajectories with increasing perturbation, associated with a dominant largest Lyapunov exponent of zero. The FSLE analysis of cortical regions in the seconds before seizures of Fig. 5.26 and after electrical stimulation (data not shown) however did not show differences in dynamics between regions.

This method allowed direct visualisation of the effect of finite perturbations to the trajectories of this dynamical system at different scales in phase space, and also quantitative determination of stability. The plots of scale dependent stability number $S(\varepsilon, t)$, shown in Fig 5.27c, which are based on actual trajectories of nearest neighbours, shown in Fig 5.27a for depth electrode data at the start of a seizure are in agreement with the findings of a Finite Scale Lyapunov Exponent fluctuating around a value of zero. This is consistent with the calculated Lyapunov spectrum from the same data in Fig 5.27b, and also the oscillatory pattern in phase space of all the SWD data available.

There are subtle differences in the maximum scale dependent lyapunov exponent between regions and at different scales which would support previous evidence for intermitent chaos. However the Finite Scale Lyapunov Exponent shows no difference between the three cortical regions prior to seizures. All values of this measure tended towards zero, consistent with the presence of sustained oscillations in the dominant SWD rhythm. When the Scale Dependent Lyapunov Exponent, $\lambda(\epsilon)$, was examined in relation to seizures, complex variation of this was seen qualitatively, in a pattern suggestive of intermittent chaos but these findings were difficult to interpret quantitatively with this measure. A more con-

vincing demonstration of intermittent chaos is of Suffrzynski's (2006) model of stochastic forcing.

When considering the one dimensional Fokker Planck analysis presented in chapter 3, there were differences in the modelled drift and diffusion coefficients in the lead up to seizures between regions (Section 3.4.3). Statistical analysis (regression and plot of gradient of the drift coefficient) shows some variability in these measures with each seizure between regions, but with some differences between groups and means of these groups also. That stochastic analysis revealed differences in the linear damping behaviour between cortical regions, and a relative collapse in this prior to seizures is suggestive of variance in the underlying 'driving process' underneath, rather than this being due to noise (for example). This is an interesting question for further study. Modelling the theta component separately did not change the drift coefficients (this data was not shown, but is available). Also, the two dimensional Fokker Planck analysis showed only a weak dependence of the diffusion coefficient of the gamma frequencies on the inter ictal theta rhythm. This observation again supports the conclusion that the theta rhythm is a dominant rhythm, as suggested from the above findings showing higher frequency rhythms phase locked to the theta rhythm, and increased cross frequency coupling. These observations also are in keeping with our understanding of the modes of operation of the thalamocortical network, as outlined in Section 1.2.1.

Evidence of intermittency in the dynamics underlying seizure transitions

The question of intermittent chaos in GAERS rats has previously been explored using wavelet analysis techniques, by Sitnikova and colleagues [206], [148]. Their method was a Morlet wavelet based automatic detection of oscillations, using a threshold for synchronised activity at wavelet scales corresponding to the frequencies of interest. They calculated the instantaneous wavelet energy for the kth wavelet scale is $\omega(\tau) = \int |\mathcal{W}_{k,\tau}| d\tau$, and then detect the conditions under which the averaged quantity of this instantaneous energy $\langle \omega_k(t) \rangle$ was greater than some threshold value. In their method this threshold value is found by inspection of the data record. They fitted the duration of these events to a power

law, with exponent -3/2, suggesting that this is characteristic of on-off intermittency [206]. Similarly Suffrczynski [220] found that the durations of interictal periods and seizures in GAERS rats statistically fitted a gamma distribution, which was well described by a Langevin model accounting for 'drift' into and out of a more unstable dynamic, leading him to postulate that stochastic forcing may be driving the process of ictal transitions.

From another angle, Goodfellow (2013) in a very elegant modelling study found a mathematical model for intermittent transitions between desynchronised 'turbulent' EEG and large amplitude oscillatory behaviour [82]. They found in their model that heterogeneity in cortical activity can account for transitions and after discharge behaviour (also noted in [116]).

Analysis of our data using the Scale Dependent Lyapunov Exponent, $\lambda(\epsilon)$, provides further evidence for intermittency more directly [79]. In all interictal and ictal data investigated with this measure, a convex curve to the SDLE at larger scales suggested the presence of periodic change in the forcing of $\lambda(\epsilon)$.

This is consistent with previous studies documenting the presence of intermittency in human partial epilepsy on the basis of recurrence mapping, and return times [234]. The presence of intermittency is consistent with the findings of multifractal scaling, and correlations at different spatial scales found in chapter 3.

It is conjectured that if intermittent dynamics are present, as found in a number of prior studies, then stochastic forcing is a component in the changing phase characteristics prior to seizures found above. It is possible that the changes in (for example) cross frequency coupling are also an expression of these more subtle dynamical changes which might correlate with the timescale separation found in the Lyapunov spectrum analysis in chapter 3, but which are not seen in the FSLE measures used here.

5.5 Conclusion

The results presented in this Chapter support the hypothesis that resonance does occur prior to seizures in GAERS rats, and that this is highest in the S12/S2 and IC cortical regions. This resonance was found to be most likely through the processes of phase coherence, increased phase clustering and cross frequency coupling rather than either increased power of oscillatory activity or a sudden, marked change in underlying system dynamics. It is consistent with the conjecture that there is a cortical focus at work in the thalamocortical network, which increases the animals' susceptibility to seizures.

Chapter 6

Discussion

The goals of this thesis were to document the network changes which underlie the transition from a normal, functioning thalamocortical network, to the abnormal hyper-synchrony seen in SWDs during seizures in the GAERS rat. Further goals were to analyse what alterations in dynamics accompanied these changes.

Accordingly it was found that there is evidence to indicate critical slowing prior to seizures in the GAERS rat and alterations in scaling behaviour both in relation to seizure on- and offset, and also that scaling behaviour varied in different cortical regions.

Although only a very limited number of animals were used for depth electrode and tetrode electrophysiology studies to answer these questions, statistical analyses indicated significance in the changes in network synchrony dynamics between thalamic and cortical neurons leading up to seizures. It could be argued that the important goal is the study of enough networks relevant to seizure generation, before than the number of animals[1], although it would clearly be ideal to include more animals in further analysis. A novel aspect of the present work is that analysis of these phenomena in a living animal at the level of single neurons within specific areas of thalamus and somatosensory cortex of the thalamocortical network are rare.

In Chapter 4, it was found that cortex did drive thalamus in the first second of seizure onset. This result is in agreement with Meeren's [131] surface EEG study and also our previous work[249]. It is also consistent with the cortical focus theory of absence seizure generation. To account for the oscillatory nature of the thalamocortical network, cortical -

[1] for example, increasing numbers of animals introduce other variables such as variations in depth of anaesthesia and cortical temperature, all of which will affect cortical and seizure dynamics

thalamic driving relationships were analysed at timescales of the order of the time constant of this system, and also at different "phases"[2] in the timing of the SWD cycle. Importantly, this finding was concordant in two complementary methods which were suited to nonlinear EEG signal analysis, and which operated in very different ways : nonlinear association, and via measures of phase difference in the frequency domain. It is also notable that in comparison to previous studies, in this study, multiple areas of cortex (including the S1, S2, and junction S12 region) were studied in relation to their relevant ventrobasilar thalamic connections, using high-resolution tetrode recordings, and simultaneous depth electrode recordings in different cortical areas (S1, including S1Fl and S1Ul, S2, insular cortex, and motor cortex) allowed a large area of cortex for analysis.

Analysis just prior to the SWD peak found stronger driving behaviour in the S12 region, compared with the average driving strength across the first second of SWD was slightly stronger for the S1 region. It is notable that at fine timescales, both measures also found alternating direction of 'influence' between cortex and thalamus, as also reported by Freestone and colleagues [177]. This is also consistent with our understanding of the interplay between deep layers of cortex and thalamus as found by Pinault [161] where these cortical areas were seen to lead thalamus at that time.

The finding of positive drive from cortex is also consistent with theories suggesting loss of inhibition by the thalaamic reticular nucleus, although this was not studied here.

In Chapter 5, details behind widespread historical observations of increased synchrony between cortex and thalamus during seizures was examined.

When the power spectrum of GAERS rats was analysed in cortex, the only notable finding was of increased power in the range above the higher gamma frequency range in the S1 region. There were no significant differences in thalamic power in any frequency range. Similarly, when amplitude coherence was analysed from tetrode data, no statistically significant difference between regions was found. On the other hand, significant differences were found in phase coherences and the distributions of both phase dispersion and phase clustering leading to seizures. There were also significant differences between cortical regions.

[2] in the literary sense rather than the physical or dynamical sense

Although the 'proximal' S1 region (that which corresponds to the homunculus of the S1Fl somatosensory area) showed higher gamma frequency spectral power than the S2 and S12 regions, the S1 region had the lowest degree of cross frequency coupling and lower phase coherence. Results of analysis of the distribution of phase entrainment, using the phase difference entropy measure defined by Eq. 5.9 and shown in Figure 5.14 revealed that the S12 region exhibited the greatest clustering of distributed phases across a wide range of frequencies. This suggests that entrainment of phase is 'tighter' in this cortical region prior to seizures.

Although there were not significant differences in amplitude coherence, phase coherence changed prior to seizures, and also between regions. Mean phase coherence was found to be higher in the S2 and IC regions in the depth recordings of GAERS rats when compared with NEC rats, although when comparing cortical mean phase coherence between somatosensory cortical regions and motor cortex, S2, IC, and S1Fl all had high coherence. Notably, increases in mean phase coherence were most marked just prior to seizures.

Further evidence that phase entrainment is an important contributor to increased synchrony and cortical resonance with seizure onset is provided by analysis of instantaneous power, which was phase-locked to the theta rhythm after the first second of SWDs, but not before this time. Cross frequency phase-amplitude coupling between the theta frequency and higher frequencies was found to be statistically highest for the S12 region. This gradually increased until seizure termination, where a marked decoupling occurred. Higher frequency oscillations, first described in our earlier work [249], were shown to be coupled to the theta rhythm as well. This again suggests that although a number of different phase entrainment mechanisms occur, the dominant mode of resonance with onset of SWDs in GAERS rats seems to be via phase coupling rather than amplitude coupling.

The 'edge effect' noted by Kramer [2] may account for some of the comodulation or cross frequency changes found, as this likely account for some of the theta instantaneous power centring on the theta rhythm as a windowing effect. However, a number of arguments support the conclusion that this is not merely a spurious result. Firstly, an inspection of the phase space of data after the onset of SWDs seen in Figure 3.16b shows that the data enters into a limit cycle of a frequency corresponding to the theta rhythm.

Secondly, the superposition of high frequency oscillations of Figure 5.22 show this entrainment. Additionally, the histograms of cross frequency coupling were calculated against a threshold of statistical significance generated by surrogates from the data itself. As a comparison between regions, it is clear at least from the very limited number of rats and seizures analysed here, that the S12 and S2 regions had a higher degree of cross frequency coupling at seizure onset, and also that these regions were the first to subside at seizure termination. These regions were also most suppressed after seizures terminated.

It is also unlikely that the 'edge effect' phenomenon of [2] would influence the Lyapunov spectrum, although it is likely that the choices of τ and embedding dimension will affect this. This separation in the dominant exponents of the Lyapunov spectrum was found for a number of embedding dimensions $m = 3, 4, 5,$ (and less reliably but still present for $m = 6, 7$) and so were not merely an artifact of embedding. Further, the reverse Lyapunov spectrum did show consistency, suggesting the Abarbanel and Brown's method did capture changes in the dynamics in the data. It is also noteworthy that the statistics of the separation in timescales, $\Delta\lambda_{12}$, varied more smoothly outside of SWDs as well as during seizures, so would be less likely to be influenced by this phenomenon.

The characteristics of the way synchrony was sustained also appeared to differ between cortical regions. The results of an eigenvalue decomposition showing the number and duration of synchronous clusters forming in the inter ictal period showed a greater sustained duration of synchrony in the S12 region compared with the S1 region which showed briefer, less sustained synchronous activity. Permutation entropy analysis points to the emergence of dominant reduction in complexity, or variability, of the signals in the IC region and S1Fl region, from depth electrode studies, presumably reflecting earlier oscillatory behaviour in these regions prior to seizures. This is again consistent with the results of our earlier work[249].

For these reasons, it can be concluded that changes in phase dynamics (including coherence, phase dispersion in cortico-cortical networks, and cross frequency coupling), rather than coincident recruitment of recorded neurons (as might be suggested by an increase in signal power or amplitude coherence), and the way synchrony is sustained was the dominant factor behind any increased resonance that might underlie the increased

cortical drive at seizure onset inferred from the results of Chapter 4. In support of the suggestion that increased resonance is a feature of cortical driving at the initiation of SWDs, higher frequencies were coincident with the theta rhythm, and higher frequency oscillations also had a higher mean power in the S2 region.

In Chapter 3, differences in scaling behaviour were found between cortical regions, as well as changes in scaling prior to seizures. Changes in scaling behaviour prior to seizures are intuitively not unexpected - for example, change in multifractal scaling has been described in EEG analysis and correlated with fMRI for behavioural tasks previously[229]. Here, the main result is that such changes differed in each of the cortical regions studied prior to seizures. These changes were verified using a number of complementary methods. The method of Extended Self Similarity, using structure functions was in agreement with the changes in wavelet scaling, and also the measured change in drift coefficients at different times found from Fokker-Planck analysis.

Although there was no clear change in the Finite Scale Lyapunov exponents, the distribution of spread between the first and second Lyapunov exponents in the spectrum, $\Delta\lambda_{12}$, did change in distribution with seizure onset. A number of markers of critical slowing were found in the GAERS rat model at seizure onset, ranging from statistical markers also found by previous authors (e.g. inverse coefficient of variation [132]) to alterations in multifractal scaling behaviour. A number of findings such as the collapse of scaling of the drift coefficient $D^{(1)}$ prior to seizures, a 'red shift' in spectral power, or changes in inverse coefficient of variation, are consistent with the phenomenon of critical slowing. A separation in timescales in the dynamics, as indicated by a gap between the two largest Lyapunov exponents in the spectrum, suggests an alteration in frequency response in the system at seizure onset as well. This was found to varying degrees in all cortical regions studied. This seemed to vary with seizure onset in depth electrode recordings. Supporting evidence for this result was also found in the skewing of the statistics of $\Delta\lambda_{12}$ in tetrode recordings. This varied also with seizure on- and offset.

The first Kramers Moyal coefficients were used to reconstruct a phase space of $\theta - \gamma$ activity, from which a description of the dynamics between these two bands was derived for inter ictal data. Changes in dynamics, as seen through the largest exponent of the

Lyapunov spectrum, were not found. These results are consistent with the null findings using the Finite Scale Lyapunov Exponent found in Chapter 5. One might argue, however, that this method required very long data sets to reconstruct the dynamics fro the 2 dimensional drift coefficients, so any alteration in dynamics in the time of the window used will not be apparrent.

The scaling changes found in Chapter 3 are relevant when considering the findings of differences in phase dispersion (as measured with the phase difference entropy), phase -amplitude coupling and mean phase coherence between regions. How each of these phenomena relate is however less clear. Results indicating a different degree of cortical excitability, and characteristics of resonance or phase entrainment correlate with these findings.

These variations in scaling behaviour in different cortical locations is also consistent with the results of permutation entropy analysis. A decrease in permutation entropy was found prior to seizures, suggesting that the complexity of the time series data decreases in the lead up to a seizure. It was also seen that the permutation entropy changes at different rates for each of the four different somatosensory regions S1Fl and S1Ul, S2 and insular cortex, and M1 motor cortex.

The findings of changes in permutation entropy prior to seizures in Section 5.3.4 are consistent with findings from previous studies (for example Li's [111], and Mammone's [122] studies), and also in line with changes in underlying dynamics prior to seizures as found by Pijn in 1991 [159], which suggest progressive increases in oscillations to a limit cycle prior to seizures. A new finding is that our results suggest differences in these permutation entropy changes in different cortical regions.

Scaling behaviour as measured by the first Kramers Moyal coefficient is a measure of 'drift', or equivalently the change in probability distribution of increment 'jumps' in phase space with time. The differences which were seen between cortical regions with regard to the changes in complexity of the depth electrode ECoG data in different cortical regions as measured by permutation entropy prior to seizures in Section 5.3.4, is also consistent with differences that were found in sensitivity to perturbation, studied empirically in our earlier work [249].

There are interesting parallels between these observations, the study of changes in resonance between cortex and thalamus prior to seizures explored in Chapter 5, and also these alterations in scaling behaviour found in Chapter 3.

For example, the measured instantaneous power, found to be time-locked to the theta rhythm in chapter 5, varied in frequency across different areas of cortex (Section 5.3.2). Coincidentally, the scaling behaviour of drift coefficients also varied between different areas of cortex. It was also found that the base theta frequency found by careful inspection of the instantaneous theta power results was slightly different for each of the four different cortical areas.

As discussed in Chapter 5, the patterns of changes in cross frequency coupling between theta band and higher gamma frequency bands, permutation entropy, and also corticothalamic mean phase coherence all pointed to increased resonance in the seconds preceding seizures. Here, it was also found that instantaneous higher frequency power was phase locked with theta peaks and also that higher frequency oscillations were phase locked with theta peaks. The Lyapunov spectrum was observed to peak in the ramping phase to these theta oscillations even though there was no difference in the value of Finite Scale Lyapunov Exponent.

A Fokker Planck analysis suggested that the theta rhythm was the dominant frequency band contributing to the inferred drift coefficient dynamics, in that the form of $D^{(1)}$ was almost identical for theta-band filtered data (i.e. a pass band of between 5 - 12 Hz) and a pass-band filtered data, of between 0.5 to 600 Hz[3]. It was also found from two dimensional Fokker Planck analysis that the scaling of the theta band did not depend on higher frequency gamma band activity. Given these findings and the results of cross frequency coupling found in Chapter 5, the theta rhythm was found to be a dominant contributor to dynamics prior to seizures. This is again in agreement with the findings of our previous work[249], and that of others [161],[166].

A zero net change in FSLE does not necessarily mean that there are not changes in dynamics prior to seizures. This may simply reflect that this is not sensitive to changes in dynamics and so not the best measure to investigate this problem. Changes in scaling

[3]these results are available on request, but not shown

behaviour could point to either altered dynamics or stochastic forcing [220], and have been demonstrated from reconstructed drift coefficients previously[12]. There is clear evidence of altered sensitivity to perturbation in different cortical regions from our prior work ([249]). It is interesting that despite the differences in scaling, summary statistics indicating critical slowing, or Lyapunov spectrum timescale separation, the finite scale Lyapunov exponent did not show any clear change with seizures onset, or any difference between cortical regions. One reason for this may be that this measure is subject to too much noise. Despite choosing 1 000 data points from depth electrode recordings in the four second interval prior to seizures, this may be too short to allow accurate differences using this measure, as already noted by Lai [106] in regards to Iasemedis's earlier work suggesting that short time Lyapunov exponents may be useful in seizure prediction. It is now reasonably widely accepted that these measures are not reliable in this setting.

It is possible that changes in drift coefficients with seizure onset indicates a change in the influence of a driving dynamic. Marked changes in dynamics, as measured using Finite Scale Lyapunov exponents were not found as supporting evidence of dynamical change prior to seizures, even though evidence of both critical slowing and alteration in the statistics of $\Delta\lambda_{12}$ do point to dynamical changes prior to seizures. Analysis using the Scale Dependent Lyapunov Exponent [79] do show qualitative changes suggestive of intermittency, though the results of these investigations are the subject of further work and have not been reported in this thesis.

6.1 Further work

The results of this thesis support the results of our earlier work [249] that the insular cortex and S2 cortex were important parts of the seizure generating network in GAERS rats. That work in turn built on the results of single cell electrophysiology experiments of Pinault [161], suggesting that the rhythmic thalamocortical oscillations comprising SWDs are the result of resonance between thalamus and cortex.

For example, when considering the previous work of Jones and others on the pacemaker roles of thalamus and Steriade's work on thalamocortical network changes between wake-

fulness and sleep (discussed in Section 1.2.1), one would naturally suspect that information 'coding' on multiple scales might be part of the normal function of the thalamocortical circuit. This is compatible the role of the thalamocortical circuit in the wakeful state is to facilitate information transfer between sensory cortex and heteromodal cortex involved in downstream neural information processing at multiple scales.

Recent interest in the role of cross frequency coupling in somatosensory cortex indeed supports this conclusion[95], and throws further light on the ways in which this occurs in individual neurons[200] and also populations[149].

Further questions then arise. For example, the results of this thesis demonstrate the changes in cortical resonance which occur with seizures, but do not shed light on which of these changes are cause or effect of seizures. What aspects of cortical resonance are 'normal', as opposed to those contributing to SWDs in generalised epilepsy, as demonstrated in this thesis, and so outside the normal bound of thalamocortical functioning? Are the changes in resonance documented here prior to seizures (for example corticothalamic mean phase coherence, cortical phase clustering, or cross frequency coupling) evidence of altered dynamics (excitability), or merely evidence of alterations in network synchrony and neuronal behaviour which play a part in driving resonance prior to seizures? In other words, are these phenomena cause or effect of altered dynamics?

One might tackle these questions from a number of perspectives. A starting point presented in this thesis has been to document how such 'indicators' of resonance in somatosensory cortex change in the GAERS rat between interictal period and during seizure generation, and termination. What is less clear, currently, is how changes in scaling behaviour might reflect either an alteration in underlying dynamics, or alternatively changes in network functional connectivity which results in altered synchrony between regions.

It would be important to disentangle this question further, because this may open up new pathways for treatment interventions for patients with absence seizures.

Using the analysis methods detailed here, further experiments investigating the effect of various antiepileptic drugs on the thalamocortical circuit and indicators of cortical resonance should offer new insights into the mechanism of action of these drugs in epilepsy.

This may pave the way for methods of more effective treatment delivery for patients. For example, focal intracortical or intrathecal delivery of much smaller doses of AEDs might alleviate side effects and hopefully improving the efficacy of AED treatment for absence seizures or other types of generalised seizures. Further, experiments studying the alteration in thalamocortical network dynamics with emergence of seizures in the GAERS rat model as they mature will also detail the pathological processes involved in epileptogenesis.

Following on from the work of this thesis, the following questions will be studied, with a view to addressing the challenges outlined in the paragraphs above :

1. What aspects of altered thalamocortical functioning are pathological and most related to seizures?

The results of this thesis support the hypothesis that altered signal phase characteristics in the ECoG of deep layers of cortex, including enhanced phase entrainment, cross frequency coupling and phase coherence are manifestations of increased resonance and associated with seizures. In other words, although these phenomena are also present inter-ictally in normal brain functioning, it seems they are abnormally enhanced, leading to resonance and are a factor in the development of seizures in this model.

Phenomena such as cross frequency coupling have been demonstrated as a mechanism in many aspects of cortical information processing [95]. For example, O'Connell [149] examined phase-amplitude coupling in auditory sensory processing of repetitive stimuli in monkeys showed how higher frequency responses on multiple scales can either augment or suppress activity in downstream neurons, presumably as a means of filtering or selecting information for further sensory processing. Several authors have previously explored how cross frequency coupling is altered during seizures (Section 1.3.2). From a theoretical viewpoint and using a neural network model, Shroeder and Lakatos [200] showed that input oscillations can control neuronal excitability and response. One can see the way in which such resonance may be relevant to the development of seizures in the GAERS rat.

There is evidence that altered dynamics can result in altered neuronal resonance at different frequencies. Using a neural network model, Rotstein [189] has shown that preferred frequency responses of neurons for both input spike trains and also output are altered with changes in sub-threshold dynamics. This change in resonance manifests as

an altered response time scales (i.e. frequencies on a population level), and also altered phase of spike timing output. Vanhatalo [232] showed how slow oscillations were strongly synchronised with faster dynamics responsible for modulating inter ictal excitabiliy in the EEG of patients with nocturnal seizures. Baud and colleagues [15] also found that interictal epileptiform activity varied with the subjects' circadian rhythm in addition to subject-specific factors, of between 20 or 30 day duration.

These observations suggest that alterations in frequency coupling might indicate signs of altered neural dynamics. From a theoretical viewpoint, the questions of how frequency coupling may relate to alteration in resonance and dynamics has been studied by Veltz and Sejnowski [235] in an inhibitory state network model.

In further work, it would be important to account for the way in which changes in scaling behaviour and frequency coupling and phase coupling related to changes in dynamics prior to seizures, to address the question of whether alteration in frequency coupling and phase coupling which leads to resonance is a cause, or effect, of increased neuronal excitability. Question 2a below addresses the related issue of whether altered dynamics in the EEG cause scaling changes in itself.

2a. Are dynamics altered with seizures?

Alterations in frequency coupling and resonance would make one suspect either underlying dynamical changes, or alternatively changes in network functional connectivity which results in altered synchrony between regions. One could explore these hypotheses in the following ways.

One possibility is to examine the 'physiological time constant' of the thalamocortical network. If there are differences between GAERS rats and their non-epileptic control strain, this offers a starting point for further investigations.

One aspect worthy of study is which part of the thalamocortical loop is associated with this resonance. One practical way of differentiating between alterations in cortical properties or thalamocortical conduction times might be to cool down the temperature of cortex during experiments. This would have the effect of slowing down more energy intensive synaptic transmission than axonal conduction. Alteration in conduction time

could be documented using single cell experiments in TRN or thalamic relay nuclei, as described in [161].[4]

Another aspect worthy of study is what networks in cortex are altered with the changes in resonance described here (for example, the increased local field potential entrainment in cortical neurons, which was increased from the results of Fig. 5.14). It will be important to correlate these network changes with physiological mechanisms such as receptor or ion channel changes (e.g. the T type calcium channel mutations described in Section 1.2.1).

Ways of documenting the 'physiological' cortical "frequency response" could be through stimulation experiments using different theta frequencies either directly to relevant deep layers of somatosensory cortex or through other means (e.g. transcranial magnetic stimulation to simulate a square wave, or mechanical stimulation of vibrissae to stimulate S1 cortical neurons).

2b. Are measured dynamical quantities altered with seizures?

Changes in scaling behaviour would indicate that the system is approaching an alteration in system dynamics, as suggested if critical slowing is also present. Especially if the physiological investigations into thalamocortical behaviour suggest alterations between non epileptic control animals and GAERS rats, and if there are altered dynamics prior to seizures, one would like to know that measured dynamical quantities of interest can capture these changes.

The basis of most investigations into underlying dynamics involve an embedding of the time series data, which require a choice of m or τ. It is mostly assumed that these quantities do not change with either brain state, or disease conditions, although some authors have studied this question ([159],[160],[55]).

However, changes in dynamics, or scaling, with seizure on- or offset raise the question of how stable the parameters of time constant τ, embedding dimension m, and dynamical dimension actually are. It is important to know if or how the dimensionality of EEG data changes with time, or scale, are stable in the brain generally as well as prior to seizures. This question was briefly assessed empirically prior to the analysis of chapter 3, and will

[4] in those experiments, simultaneous spiking in TRN and thalamic relay nuclei was studied in relation to the SWD peak, and observed to occur 12 msec prior (Section 1.2.2).

also be the subject of further study.

While it has previously been found that the correlation dimension does indeed change subtly between seizures and inter ictal periods[160], the meaning of such changes are less clear. Unless accounted for, such subtle alterations may invalidate results from traditional nonlinear analysis if these are present.

2c. Finding indications of altered timescales in seizure transitions

Finding the most relevant timescales for seizure generation, or the stability of cortical oscillations in relation to seizures is an important extension to the results of this thesis. To date, only a few studies have correlated the associated scales of dynamical complexity with ECoG activity, and this will be the subject of further work. From the techniques used in the studies presented in this thesis, we have developed further techniques for studying these 'microscales' and mapping changes in these prior to seizures.

In this work, a number of features suggestive of critical slowing were found prior to seizures. These included changes in the summary statistics of the data and separation in timescales as suggested by a widening Lyapunov spectrum. These changes occurred coincidentally with a breakdown in scaling behaviour, seen with both a breakdown in differences between scaling of the drift coefficient $D^{(1)}$ in different cortical regions prior to seizures and changes in wavelet scaling and structure function analysis in the pre seizure period. Indications of timescale separation was seen in the Lyapunov spectrum prior to seizures across different cortical areas and at the two different spatial and temporal data scales used in this thesis. In these same instances, changes in the maximal Lyapunov exponents were not found.

Findings suggestive of critical slowing are consistent with our previous observations [249] that seizures could be electrically stimulated across all somatosensory cortex and insular cortex, which are all parts of the thalamocortical network known to be important in absence seizure generation. In that work, we showed that seizures were more easily electrically stimulated in the S2 and insular cortex, at a lower threshold.

In Chapter 5, a 'perturbation observation' technique was presented and used to show that there was not divergence in the system phase space suggestive of a positive Lyapunov

exponent at seizure onset. Hence, one would assume that studies of other indicators might provide more information.

But, the presence of critical slowing with seizure onset is debated, with most of the evidence against coming from studies of summary statistics suggestive of this phenomenon. Milanowski and Suffzynski [133] found evidence of critical slowing from a reanalysis of Meeren's data [131], evidence of critical transitions in the data from 300 human patients undergoing iEEG for epilepsy surgery from the same statistical inidicators was found in only 8% of patients. This raises the interesting possibility that either the dynamics preceding seizures in the two species are different, or that the statistics of timescale changes (or scaling changes) in the data are different, and warrants further investigation. It was found in the analysis of this thesis that alterations in the window used to assess summary statistics and autocorrelation width would alter the appearance, or not, of critical slowing.

Another possible explanation of Milanowski's findings could be that the most relevant timescales in the data had changed to be more favourable for seizure generation. Our further work plans to address this question, and consider manifestations of differences in network electrophysiological behaviour at larger scales (such as coherence and cross frequency coupling) in this light.

Two possible methods for accomplishing this involve stochastic analysis. O'Regan and colleagues [146] have theoretically investigated the effects of noise in critical transitions, and the way these might be expressed in summary statistics of the data. To do this they assumed a normal distribution of statistics in the increments (i.e. $\Delta x = x(t+\tau) - x(t)$) in the data, and obtained a general form for a Fokker-Planck equation expressing the evolution of dynamics experiencing a perturbation from equilibrium. In analogy with Figure 5.1, they found that 'external noise' (possibly representing altered variables of specific frequencies of model parameters in the system) had a multiplicative effect in the dynamics as an expression of stochastic resonance as seen in the yellow histogram of Fig 5.1c, contrasting with 'internal noise' (from within the system, for example the blue histogram generated from surrogate data seen in Fig 5.1c).

3. Are the anti-seizure effects of AEDs related to altering cortical resonance? An examination of how the action of antiepileptic drugs alter the processes underlying

cortical resonance would provide further evidence of the altered dynamics in the thalamocortical circuit during seizures, and would also provide important information regarding the mode of action of these drugs. Further experiments are planned in which antiepileptic drugs are injected focally into specific areas of cortex to study this.

For example, do these medications cause changes in the indicators of resonance found here (e.g. cross frequency coupling, mean phase coherence, phase dispersion between regions) between populations of neurons in cortex? Agents which are well known to either suppress (such as sodium valproate) or exacerbate (such as carbamazepine) SWDs, and the techniques used in this work could shed further light on their mode of action at the network level.

To further correlate presumed changes in the thalamocortical network with the process of epileptogenesis in the GAERS rat model, it would also be possible to study the maturing thalamocortical network for markers of altered cortical resonance around the time that seizures emerge.

Chapter 7

Conclusion

In this thesis, the network dynamics of the thalamocortical system were studied during absence seizures in the GAERS rat model, in the whole, behaving animal, at the contrasting spatial scales of cortical ECoG signals from multiple large areas of cortex, and at finer scales, of tetrode data from groups of single neurons. Adding to a growing body of work that aims to uncover the factors underlying absence epilepsy by our group and others, this thesis presents the following main findings.

- Chapter 3: The scaling behaviour and evidence for an accompanying alteration in dynamics was investigated in relation to seizure onset and termination. This was contrasted with findings from the inter ictal period, and also across different parts of deep layers of somatosensory cortex, with their relevant thalamic relay cells, using ECoG recordings obtained from implanted tetrodes.

  Using stochastic analysis with a Fokker Planck formalism as well as the methods of Extended Self Similarity and Morlet wavelet coefficients, the changes in scaling behaviour of the ECoG was analysed leading to seizures. The validity of the Fokker Planck approach was verified as valid for increments in the EEG data[1]. Evidence was found for differences in scaling behaviour in the drift coefficient $D^{(1)}$ in different parts of cortex from simultaneous depth electrode recordings. Scaling behaviour was also seen to change between inter ictal data epochs, and prior to seizures, where

[1] that is, it was verified that increments in the data showed a Markovian property was present by satisfying a Chapman Kolmogorov equation. It was also shown that the first two coefficients of the Kramers-Moyal expansion were sufficient to describe changes in the increments of the data by showing that Pawula's theorem was satisfied. The Markovian condition was satisfied up until the second prior to the commencement of seizures only, after which this condition broke down

clear differences between regions was observed to break down. In a two dimensional Fokker-Planck analysis of the relation between the theta and lower gamma frequencies were examined. It was found that the theta rhythm was a dominant contributor to drift and diffusion coefficients, and that gamma band oscillations were only weakly coupled in this case.

Alterations in scaling behaviour with seizure onset was seen to be consistent across both the Fokker-Planck, Extended Self Similarity and wavelet scaling analysis in that differences were found between different somatosensory cortical areas, and also between inter-ictal periods and the seconds immediately preceding seizures.

Turning to dynamical analysis, evidence for altered dynamics prior to seizures was found in the timescale separation in the largest exponents of the Lyapunov spectrum, which occurred both at the onset and termination of seizures. This was found in both depth electrode data in GAERS, but notably, not NEC rats, and also found in tetrode data as a change in the statistical distribution of the gap between the largest and second largest Lyapunov exponent, $\Delta\lambda_{12}$. Observation of the patterns of changes in histograms of $\Delta\lambda_{12}$ between the inter-ictal period and then progressing to seizures showed that these distributions became increasingly skewed prior to the onset of seizures. An analysis of summary statistical indicators of critical slowing (such as the inverse coefficient of variation) also supported the hypothesis of critical slowing prior to seizures in these rats.

- Chapter 4 : The nonlinearity of the EEG and ECoG was studied using the simplectic geometric method of Convergent Cross Mapping[78], in which increasing degrees of nonlinearity were found at smaller scales.

  In agreement with prior observations by Meeren [131] and others, it was found that cortex leads thalamus at the commencement and during the first second of seizures. Two complimentary analysis methods, the Phase Slope Index and nonlinear association, as a measure of amplitude correlation, were in agreement. At finer scales of spatial and temporal resolution it was found that driving influence alternated between cortex and thalamus, as one may expect given this is consistent with previous

results[177], but also that it is consistent with our understanding of the function of the thalamocortical network, and of the anatomical relations between these structures and their physiology. Notably, it was also found that the S12 junction region of somatosensory cortex had an increased intensity of driving relationship with thalamus prior to the spike in each SWD cycle.

- Chapter 5 : Here, the question was asked whether there were identifiable resonance between the somatosensory cortex and related thalamic nuclei, and if found, whether this could be attributable to alterations in amplitude coupling or characteristics of phase coupling within the thalamocortical network.

  Evidence for increased resonance was analysed both between cortical microcircuits and between cortex and thalamus, using tetrodes, and between distant cortical areas using depth electrodes. Evidence for increased resonance found here included increased mean phase coherence in the insular cortex and also the secondary somatosensory cortex prior to seizures. Evidence was also found for tighter phase entrainment in the S12 junction region, in both the thalamocortical network and also between adjacent cortical channels in tetrode recordings with seizure onset, and increased cross frequency coupling and comodulation of higher frequency oscillations with the dominant theta rhythm across recorded channels in these areas. Notably, the S12 region was observed to be the first region to increase cross frequency coupling and comodulation prior to commencement of seizures, and the first region to reduce coupling prior to seizure termination.

  These findings of increased phase coupling and entrainment were not associated with statistically significant differences in amplitude coherence between cortical regions, and were not correlated with increased spectral power that may have accounted for these findings, which might otherwise have been suggestive, for example, of increased recruitment of cortex. In fact the primary somatosensory cortex was found to have increased spectral power at higher frequencies prior to seizures, but significantly lower cross frequency coupling at that time.

  Measures of complexity changes in the EEG supported these observations. Analysis

of permutation entropy showed that this decreased earlier, and to a greater degree, in secondary somatosensory cortex than other cortical areas before seizures. This is also in agreement with our previous work [249] where we found that stimulation of S2 cortex resulted in seizures earlier and a lower stimulation frequency. The finding of increased phase entrainment found here is also congruent with findings in that work of high rates of synchronous, rhythmic firing of cortical neurons in deep layers of cortex prior to seizures.

These findings broaden our understanding of the mechanisms behind alterations in thalamocortical network dynamics during seizures. The further evidence of critical slowing, suggested by alteration in summary statistics, a 'red shift' phenomenon suggested in alterations of scaling behaivour, or the timescale separation in the dynamics as suggested through analysis of the Lyapunov spectrum, support the results from previous studies showing indicators of critical slowing from summary statistics of their data. The complimentary methods of Extended Self Similarity, wavelet scaling analysis and Fokker-Planck analysis show altered scaling behaviour with seizure onset, but these analyses also show altered scaling behaviour in different parts of cortex. Self-consistent changes such as a breakdown in multifractal scaling with seizure onset coincide with findings of a decrease in signal complexity, as seen from the results of permutation entropy analysis, which was also found to differ between cortical regions.

Although differences were less clear between individual parts of somatosensory cortex when averaged across the first second of seizure onset, it was found that cortex generally drives the thalamus at the commencement of seizures. A stronger driving relationship between cortex and thalamus was found in the S12 region just prior to the SWD peaks in our data. This finding is consistent with findings of increased resonance in this cortical region prior to seizures, reported in Chapter 5. It also demonstrates the importance of taking into account the alternating pattern of drive between cortex and thalamus at timescales appropriate for this analysis, in line with the physiology of the thalamocortical system.

The phenomenon of resonance was demonstrated prior to seizure onset, and it was

further found that this differed between the different regions of somatosensory cortex. Results of Chapter 5 indicate that the mechanisms behind increased resonance more likely relate to altered phase characteristics between signals from cortical populations, rather than increased cortical recruitment, as might have been found if amplitude coherence and signal power was increased.

Evidence of alterations in phase dynamics prior to and during seizures include the tighter phase entrainment between close neighbours of deep-layer cortex, and between cortex and thalamus across a wide distribution of frequencies, most marked in the S12 region; increases in mean phase coherence in depth electrode data in the S2 and IC regions; and larger increases in cross frequency coupling with the theta rhythm in the S12 region and S2 region prior to seizures. Analysis of changes in cross frequency coupling also showed that the S12 and S2 regions were the first to subside after seizure termination also. An eigenvalue analysis of synchrony clusters between thalamus and cortex also showed that synchrony tended to be more sustained in duration in the S12 region. An analysis of high frequency oscillations during SWDs showed that these were phase-locked to the theta peak, and that the S2 region showed a higher power than other regions during seizures. It is perhaps an omission that an analysis of high frequency oscillations in non-epileptic control rats was not done for comparison, and this omission will be rectified in further work.

Taken together the above findings support the hypothesis that the S2 cortex and insular cortex are important areas of the seizure generating circuit in the GAERS rat, as suggested in our previous work[249]. While the links have not been fully clarified in this thesis, the observation that scaling behaviour, phase coupling and cross frequency coupling all change with seizure onset, consistent with increased resonance at that time, correlate with the timescale separation in the Lyapunov spectrum at the onset of seizures also, just as cortical driving strength also increases prior to theta peaks. Not only does the presence of timescale separation suggest an altered frequency response of the network at that time[2], it also suggests subtle alterations in dynamics at the point of seizure onset. This finding is also consistent with some phenomena found in critical dynamics, such as the phenomenon

[2]or at least, the attractor modelled which produces the time series data

of rate tipping[3]. The findings presented in this thesis are consistent with the cortical focus theory of absence seizure development in the GAERS rat, and complement the findings of [249] at larger scales. These results also help to provide context for findings such as an increased sensitivity to perturbation by electrical stimulation in S2 and insular cortex more than other areas in that work.

Future Work

The work presented in this thesis provides a grounding for future studies, to further determine the thalamocortical changes most central to the development of absence seizures in the GAERS rat. As mentioned in the Introduction, important components of the seizure generating circuit, such as posterior thalamic nuclei and the thalamic reticular nucleus, were not included in these experiments. Given that these areas have also been implicated in the development and the termination of seizures, it would be important to also include recordings of these areas simultaneously with somatosensory cortex and ventrobasilar thalmic nuclei during the development, and onset, of seizures.

To improve the statistical robustness of the results presented here, more experiments involving tetrode recordings are planned. These will include more areas of thalamus, including posterior thalamus and the reticular thalamic nucleus, to also improve our understanding of the dynamics between these structures in absence epilepsy.

Further, experiments are also planned to investigate the effects of antiepileptic drugs such as sodium valproate or ethosuxamide in attenuating seizures, and carbamazapine, often found to exacerbate absence seizures, on the thalamocortical circuit of GAERS rats. These studies may lead to more locally targeted drug treatments for this syndrome, which in humans is unfortunately often refractory to medical therapies.

[3]However, it has not been demonstrated that rate tipping is occurring here

Appendix A

The Kramers Moyal Expansion and physical interpretation of Jump Moments

A physical understanding of the scaling of increments follows directly from the derivation of the Kramers Moyal expansion and the concept of *jump moments* [7]. A brief recap of the derivation of the KM expansion clarifies the physical interpretation of jump moments.

Starting with a master equation describing the 'probability flow' of states in some domain, Y,

$$\partial_t P(y,t) = \int dy' [W(y|y')p(y',t) - W(y'|y)P(y,t), \tag{A.1}$$

we can interpret the first term as the 'gain' term of state transitions from other states to y, and the second term as a 'loss' or transition from y to other states. If we next express W as a function of the size of a jump r from some configuration y' to y, $r = y - y'$ provides a change of 'coordinates' such that $W(y|Y')$ is now a function of jump size $W(y';r)$ and the master equation reads

$$\partial_t P(y,t) = \int dr W(y-r;r)p(y-r;r) - P(y,t)\int dr W(y;-r). \tag{A.2}$$

This is only valid in the assumption that jumps are small enough that $W(y';r)$ remains sharply peaked to satisfy the Markov condition of exponential decay as a function of r. A Taylor expansion around r gives

$$\partial_t P(y,t) = \int dr W(y,r)p(y,t) - \sum_m^\infty \frac{(-1)^m}{m!}\int dr r^m \frac{\partial}{\partial y^m} W(y;r)P(y,t) \tag{A.3}$$

$$= \sum_{m}^{\infty} \frac{(-1)^m}{m!} \frac{\partial}{\partial y^m} \Big[\int dr r^m W(y;r) P(y,t) \Big], \tag{A.4}$$

which leads to the Kramers Moyal expansion

$$\partial_t P(y,t) = \sum_{m=1}^{\infty} \frac{(-1)^m}{m!} \frac{\partial}{\partial y^m} \Big[a^{(m)}(y,t) P(y,t) \Big]. \tag{A.5}$$

This equation represents the dynamic evolution of probabilities (in the case of the Langevin equation) or probability density functions (in the case of the Fokker Planck equation). By analogy with Figures 1.8a and 1.8b we interpret the drift term $D^{(1)} \sim \partial_y a^{(1)} p$ as the term describing the "deterministic" dynamics for the evolution of $\langle y \rangle$; the diffusion term $D^{(2)}$ describes the spread of probability around it's mean with time.

The jump moments, $a^{(m)}$, are given by $\int dr r^m W(y;r)$. A more helpful expression for these arises if we recall that W(y;r) = W(y'—y), so

$$\int dr r^m W(y;r) = \int dy' (y'-y)^m W(y'|y) = \int dy' (y'-y)^m P(y', t+\tau | y, t). \tag{A.6}$$

The conditional probabilities $P(.)$ can be calculated directly from the data as the conditional average of the binned increments of the stochastic variable Y found from the PMF distributed from the time series data[72]. In other words, as described in Section 3.3.3 and Equation 3.11 the integral in the above equation is the conditional average $\langle [y(t+\tau) - y(t)]^m \rangle$ evaluated for the instance $y(t)$ equal to some value y.

Appendix B

Karhunen Loeve analysis and coherent structures in thalamocortocal networks

The rationale behind this section is to find the dominant spatial and temporal correlations, and to define a temporal correlation length in the data leading to seizures.

There is no general, effective numerical way of finding system bifurcation behaviour directly, or deducing model equations from data for this to be possible. One approximation is to generate a lower dimensional expansion of the system and analyse this (connection between conditional probability distributions and Takens and Ruelle's work on describing a strange attractor....). the Karhunen-Loeve expansion (also called proper orthogonal decomposition or principal components analysis) optimally represents that data in a L^2-norm (least squares) sense.

Lets say our system has provided an ensemble of observations $\mathbf{U}$ but the dynamics are unknown, and we assume that it could be represented by some N-dimensional PDE

$$\partial_t \mathbf{U} = f(U, \partial_x U, \partial^2_{xy} U, ..., \mathbf{x}, t) \tag{B.1}$$

We suppose that this system can be described by a solution to the above of a form $u(x,t)$, given by

$$u(x,t) = \sum_{n=1}^{\infty} a_n(t)\phi_n(x) \tag{B.2}$$

where ϕ_n is any set of orthogonal functions belonging to an inner (Hilbert) space such that $\langle \phi_j(x)\phi_k(x) \rangle \equiv \int \phi_j \phi_k d\mathbf{x} = \delta_{jk}$. We could choose any basis set but in this instance we want to describe the dynamics to lowest order possible, so it makes sesne to choose

an empirical set pf basis functions directly from the data, directly from a singular value decomposition. Physically, the basis functions do not distinguish between space and time, but since we want to describe coherent structures in the system we choose the inner space comprising of spatial (in a phase space sense) functions, with some functions a_n describing time varying amplitude changes of the system.

For some data X which has a dimension of N channels $\times$ T samples, the singular value decomposition of X is

$$\mathbf{X} = \mathbf{U}\mathbf{\Sigma}\mathbf{V} = \begin{bmatrix} u_1 \\ u_2 \\ \vdots \\ u_n \end{bmatrix} \begin{bmatrix} \sigma_1 & 0 & \dots & 0 \\ 0 & \sigma_2 & \dots & 0 \\ \vdots & \vdots & \ddots & \sigma_n \\ 0 & 0 & \dots & 0 \end{bmatrix} \begin{bmatrix} \phi_1 \\ \phi_2 \\ \vdots \\ \phi_n \end{bmatrix} \tag{B.3}$$

Σ is diagonal with non-negative elements $\sigma_1 \geq \sigma_2 \geq ... \geq 0$ comprising the *singular values* of X. $\mathbf{U}$ and $\mathbf{V}$ are the eigenvalues of the covariance matrices $\mathbf{X}\mathbf{X}^*$ and $\mathbf{X}^*\mathbf{X}$ respectively.

Expanding

gives the decomposition of the kth row of $\mathbf{X}$

$$\mathbf{X}_k = \sum_{j=1}^{n} \sigma_j u_{kj} \phi_j \tag{B.4}$$

i.e. the set of orthogonal basis functions describing each row of data in X. Elements ϕ_j of this basis are the *POD modes* of the data. The contribution of each mode ϕ_j in the expansion approximating the data is given by the relative 'energy' contained in that mode

$$E_j = \frac{\sigma_j^2}{\sum_{i=1}^{N} \sigma_i^2} \tag{B.5}$$

Appendix C

Multitaper Spectral Analysis

Frequency domain analysis is an important technique for time-varying data in that it can provide information about oscillations in the data, and alternative information about degrees of freedom which may not have been apparent in the time domain. Estimation of the power spectrum is often done via a periodogram, but the problem is that this estimation is inherently biased for finite-length data sets.

This can be seen if we consider the power spectral density (PSD) of a finitely sampled data set $\{f_n\}$, from the Weiner-Kinchin theorem, as a Fourier transform of its autocorrelation function. Consider the autocorrelation function $\phi = \mathrm{E}[f_n f_{n+m}]$, and its Fourier transform, $\hat{\Phi}_f(k) = \frac{1}{T}|F(w)|^2$. The bias in this estimate is a consequence of the limited number of 'shifts' in the autocorrelation, which does decrease as data length $N \to \infty$. Unfortunately the variance in this estimate does not similarly decrease with increasing data lengths. The third problem in the 'simple' periodogram approach is the implicit effect of windowing in taking finite data lengths, such that the resultant power spectrum is the Fourier transform of the "true" autocorrelation of the data multiplied by the window function, whichever form this takes.

Multitaper spectral analysis offers a way of minimising some of these problems when computing power spectra from limited data. In this approach, data is binned into sequences of bandwidth W, and averaging the spectral estimates from a set of orthogonal (uncorrelated) taper functions of taper length N. Often Slepian sequences are chosen because these allow optimal localisation in frequency for a given W and taper length N.

Appendix D

Supplementary Results

Table D.1: Statistical significance of ANOVA results for differences in means of the phase clustering entropy by frequency range and cortical area, shown in Fig D.5. Each data point in Fig D.5 is an average of all channels and seizures in that recording (range of one to nine seizures in between 60 and 120s). Total number of average points are respectively 88 for S1, 81 for S12, and 67 for S2

Frequency range	p
40 to 80 Hz	0.0003
80 to 120 Hz	0.52
120 to 250 Hz	0.11
250 to 450 Hz	0.0008

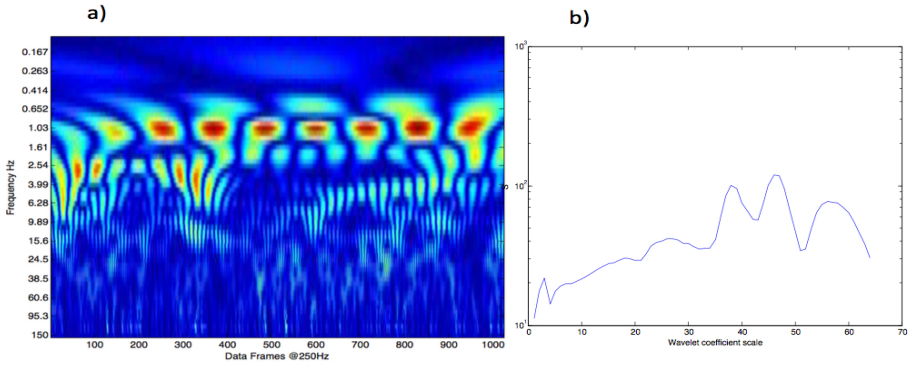

Figure D.1: Spectral analysis for the Ising model at critical temperature : (a) Morlet wavelet analysis, and (b) Scaling functions for this model

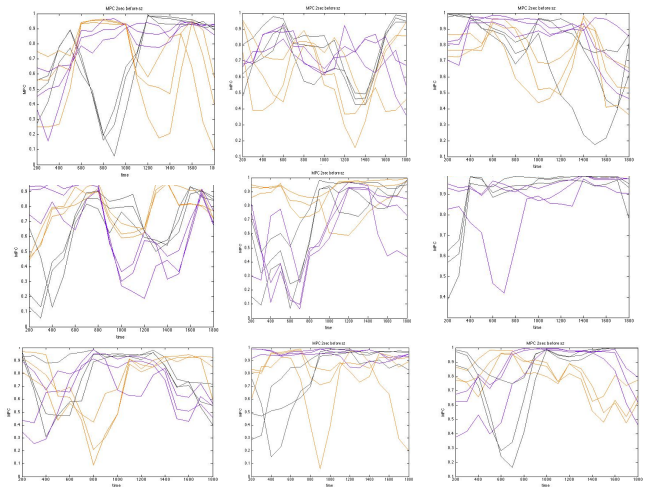

Figure D.2: Mean Phase Coherence between thalamus and cortex, now for each of the three regions. Left most, from top to bottom, S1; middle graphs (top to bottom), S12; and right most, S2. Slightly higher phase coherence is seen for S12 and S2. The three colours in each graph (orange, purple, black) represent each of three thalamic channels.

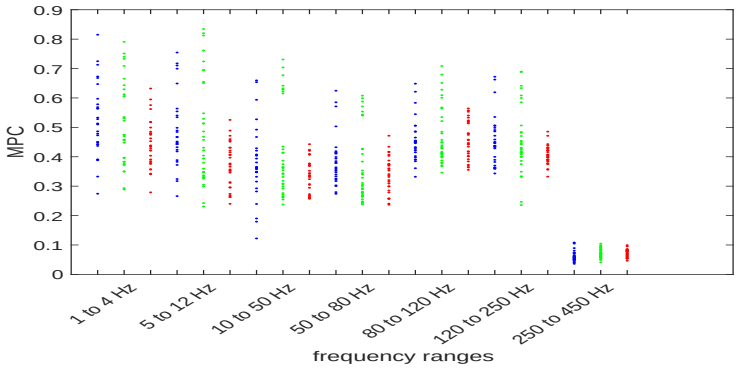

(a)

[-1.5in] [-10ex]

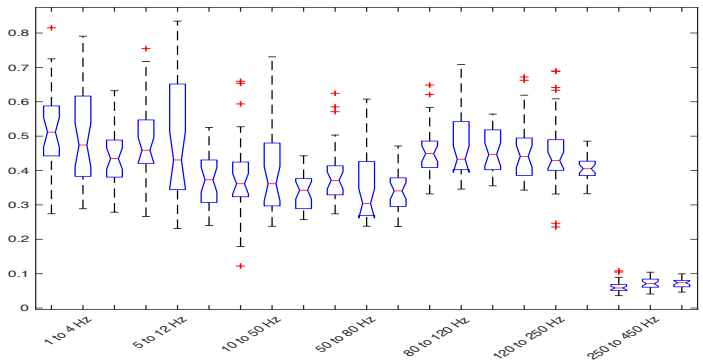

(b)

[-10ex]

Figure D.3: (a) combined analysis of Mean Phase Coherence of all data between thalamus and each of three regions of cortex colour-coded blue : S1; green - S12; and red - S2, repeated for band passed data in the consecutive frequency ranges shown. For 1 - 4 Hz calculation a two second window was used, otherwise all MPC calculations were calculated by averaging across all data channels for the second immediately before a seizure. (b) three way ANOVA for statistically significant differences in means between cortical regions for of the above data

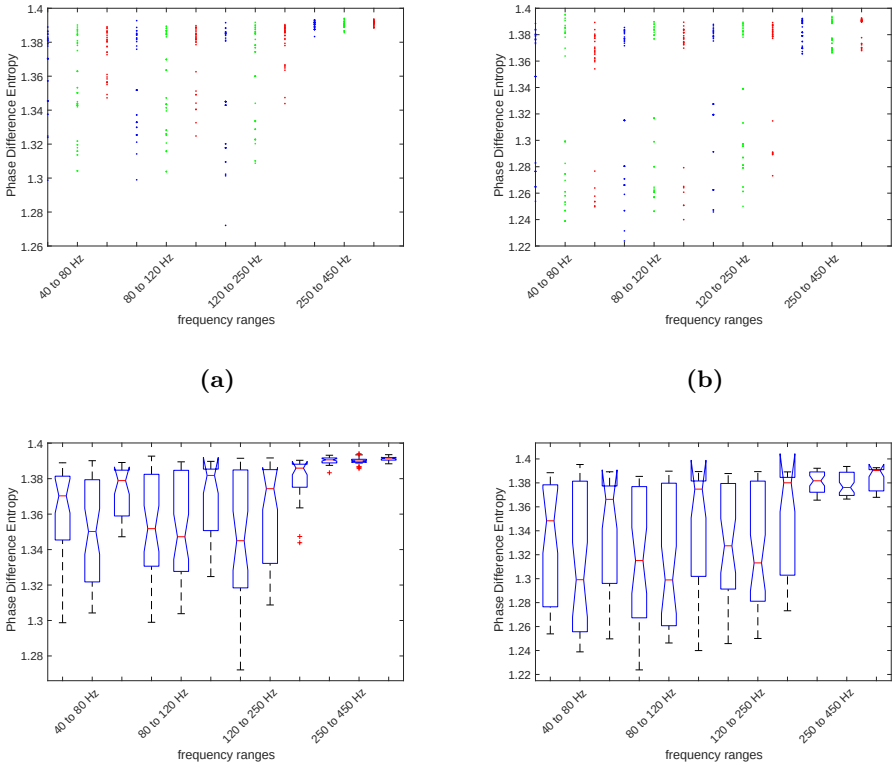

Figure D.4: Mean Phase difference entropy as a measure of the "clumpedness" of phases distributed inter ictally (a) between thalamus and cortex, and (b) between adjacent tetrode cortical channels. (c) and (d) show boxplots for ANOVA for the data in a) and b) respectively. Colour code is blue : S1, green : S12, and red : S2

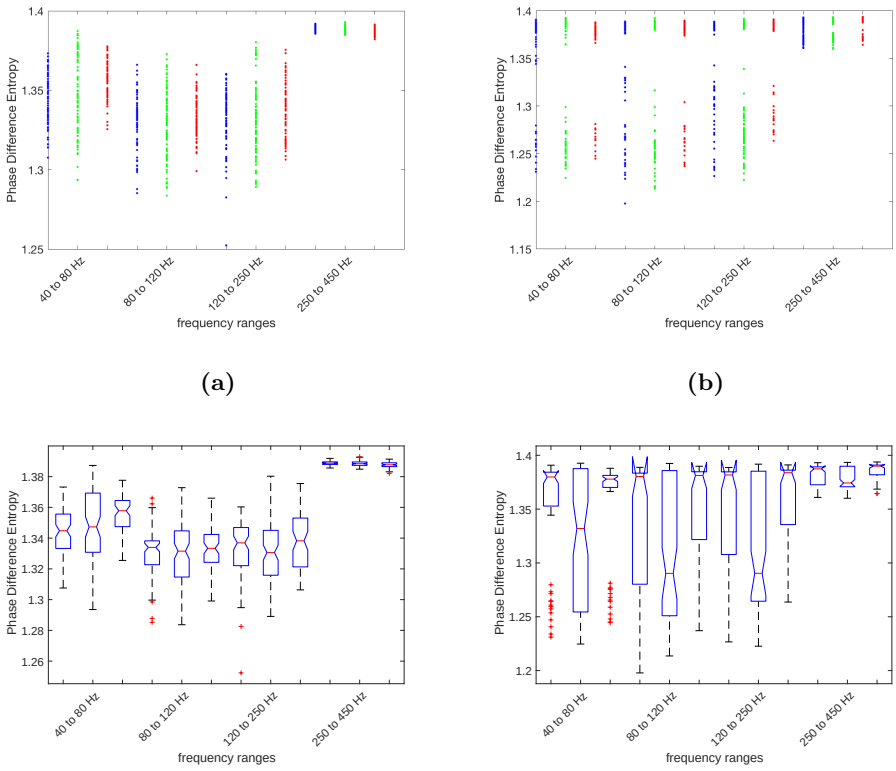

Figure D.5: Mean Phase difference entropy as a measure of the "clumpedness" of phases distributed in the last second before a seizure (a) between thalamus and cortex, and (b) between adjacent tetrode cortical channels. (c) and (d) show boxplots for ANOVA for the data in a) and b) respectively. Colour code is blue : S1, green : S12, and red : S2

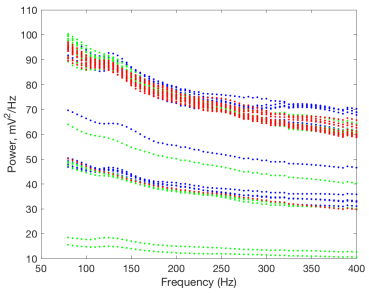

(a)

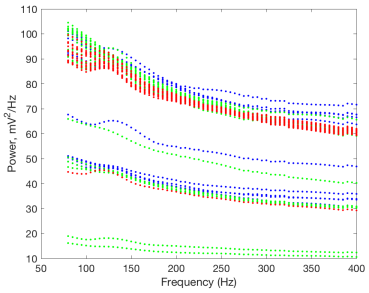

(b)

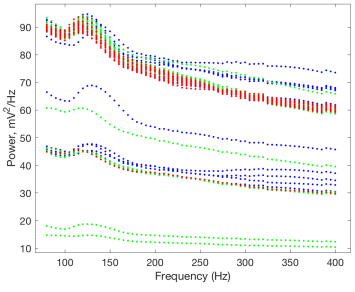

(c)

Figure D.6: Plots of higher frequency oscillation power, in the averaged HFO waveforms found to be phase locked with the theta peaks as in the method used to generate Fig 5.22. From bottom to top : in the first second before seizure onset, at seizure onset, and one second after the first sWD.

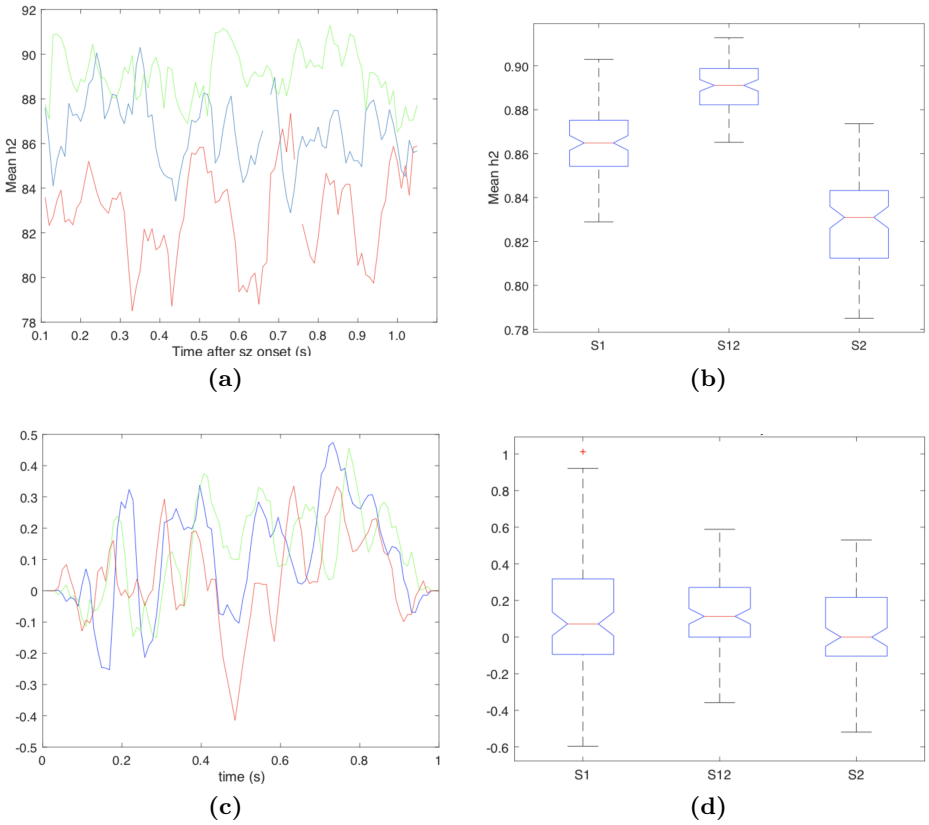

Figure D.7: Pooled mean data from all seizures in three experiments for each of S1 (blue), S12 (green) and S2 (red) for thalamocortical coupling as calculated for the first second of the seizure, using the FieldTrip nonlinear association and PSI routines rather than the analysis of Chapter 4. The 0 second mark corresponds to the first SWD(a)Average of $h^2_{y|x}$ for cortico thalamic channels of 160 seizures and (b) ANOVA boxplot showing statistical significant difference in means. (c) Average of PSI for the same data as in (a), and (d) corresponding boxplot

Bibliography

[1] A. Luttjohann A, Zhang S, de Peijper R, and van Luijtelaar G, *Electrical stimulation of the epileptic focus in absence epileptic wag/rij rats: assessment of local and network excitability*, Neuroscience **188** (2011), 125 – 134.

[2] Kramer M A, Tort A B L, and Kopell N J, *Sharp edge artifacts and spurious coupling in eeg frequency comodulation measures*, Journal of Neuroscience Methods **170** (2008), no. 2, 352 – 357.

[3] Luttjohann A, Schoffelen J-M, and van Luijtelaar G, *Peri-ictal network dynamics of spike-wave discharges: Phase and spectral characteristics*, Experimental Neurology **239** (2013), 235 – 247.

[4] ———, *Termination of ongoing spike-wave discharges investigated by corticothalamic network analyses*, Neurobiology of Disease **70** (2014), 127 – 137.

[5] H D. I. Abarbanel and M B. Kennel, *Local false nearest neighbors and dynamical dimensions from observed chaotic data*, Phys. Rev. E **47** (1993), 3057–3068.

[6] C Allefield and J Kurths, *An approach to multivariate phase synchronisation analysis and it's application to event-related potentials*, International Journal of Bifurcation and Chaos **14** (2004), no. 02, 417–426.

[7] Alexander Altland and Ben D. Simons, *Condensed matter field theory*, 2 ed., Cambridge University Press, 2010.

[8] Ramal R. Angles d'Auriac J.C., Maynard R., *Critical dynamics of the finite ising model.*, Journal of Statistical Physics **2** (1981), no. 28, 307 – 323.

[9] W R Ashby, *Principles of the self-organizing system*, Principles of Self-Organization: Transactions of the University of Illinois Symposium (H. Von Foerster and G. W. Zopf Jr, eds.), Pergamon Press, 1962, pp. 255–278.

[10] E Aurell, G Boffetta, A Crisanti, G Paladin, and A Vulpiani, *Predictability in the large: an extension of the concept of lyapunov exponent*, Journal of Physics A: Mathematical and General **30** (1997), no. 1, 1–26.

[11] M Avoli and P Gloor, *Interaction of cortex and thalamus in spike and wave discharges of feline generalized penicillin epilepsy.*, Experimental Neurology **76** (1982), no. 1, 196 – 217.

[12] A Bahraminasab, F Ghasemi, A Stefanovska, P V E McClintock, and R Friedrich, *Physics of brain dynamics: Fokker-planck analysis reveals changes in eeg interactions in anaesthesia*, New Journal of Physics **11** (2009), no. 10, 103051.

[13] C Bandt and B Pompe, *Permutation entropy: A natural complexity measure for time series*, Phys. Rev. Lett. **88** (2002), 174102.

[14] A M. Bastos and J-M Schoffelen, *A tutorial review of functional connectivity analysis methods and their interpretational pitfalls*, Frontiers in Systems Neuroscience **9** (2016), 175.

[15] M Baud, J Kleen, E Mirro, J Andrechak, D King-Stephens, E Chang, and V Rao, *Multi-day rhythms modulate seizure risk in epilepsy*, Nature Communications **9** (2018).

[16] C Bedard, H Kroger, and A Destexhe, *Does the 1/f frequency scaling of brain signals reflect self-organized critical states?.*, Physical Review Letters **97** (n.d.), no. 11.

[17] JM Beggs, *The criticality hypothesis: how local cortical networks might optimize information processing.*, Philosophical Transactions of the Royal Society A - Mathematical Physical and Engineering Sciences **366** (n.d.), no. 1864, 329 – 343.

[18] JM Beggs and D Plenz, *Neuronal avalanches in neocortical circuits.*, Journal of Neuroscience **23** (n.d.), no. 35, 11167 – 11177.

[19] R Benzi, S Ciliberto, R Tripiccione, C Baudet, F Massaioli, and S Succi, *Extended self-similarity in turbulent flows.*, Physical Review E **48** (1993), no. 1, R29 – R32.

[20] H. Berger, *Über das elektrenechalogramm des menschen (on the human electroencephalogram)*, Archiv f. Psychiatrie u. Nervenkrankheiten (1929), no. 87, 527:70.

[21] S F Berkovic, *Genetics of epilepsy in clinical practice.*, Epilepsy Currents **15** (2015), no. 4, 192 – 196.

[22] S F. Berkovic, J C. Mulley, I E. Scheffer, and S Petrou, *Human epilepsies: interaction of genetic and acquired factors*, Trends in Neurosciences **29** (2006), no. 7, 391 – 397, Nature and nurture in brain development and neurological disorders.

[23] W Bialek, A Cavagna, I Giardina, T Mora, E Silvestri, M Viale, and A M. Walczak, *Statistical mechanics for natural flocks of birds*, Proceedings of the National Academy of Sciences **109** (2012), no. 13, 4786–4791.

[24] H Blumenfeld, *Cellular and network mechanisms of spike-wave seizures*, Epilepsia **46**, no. s9, 21–33.

[25] H. Blumenfeld, J. P. Klein, U. Schridde, M. Vestal, T Rice, D S. Khera, C Bashyal, K Giblin, C Paul-Laughinghouse, F. Wang, A. Phadke, J F. Mission, R. Agarwal, D. Englot, J. Motelow, H Nersesyan, S. Waxman, and A. Levin, *Early treatment suppresses the development of spike?wave epilepsy in a rat model*, Epilepsia **49** (2008).

[26] H. Blumenfeld, J.P. Klein, U. Schridde, M. Vestal, T. Rice, D.S. Khera, C. Bashyal, K. Giblin, C. Paul-Laughinghouse, and F. Wang, *Early treatment suppresses the development of spike-wave epilepsy in a rat model.*, Epilepsia (2008), no. 3, 400.

[27] B. Boashash, *Estimating and interpreting the instantaneous frequency of a signal. ii. algorithms and applications*, Proceedings of the IEEE **80** (1992), no. 4, 540–568.

[28] M Botcharova, S F Farmer, and L Berthouze, *Markers of criticality in phase synchronization*, Frontiers in systems neuroscience **8** (2014).

[29] M Breakspear, *Nonlinear phase desynchronization in human electroencephalographic data*, Human Brain Mapping **15**, no. 3, 175–198.

[30] B Brett-Green, M Paulsen, R J. Staba, E Fifkova, and D S. Barth, *Two distinct regions of secondary somatosensory cortex in the rat: Topographical organization and multisensory responses*, Journal of Neurophysiology **91** (2004), no. 3, 1327–1336, PMID: 14586034.

[31] R Brown, P Bryant, and H D I Abarbanel, *Computing the lyapunov spectrum of a dynamical system from an observed time series*, Physical Review A **43** (1991), no. 6, 2787.

[32] T Budde and H-C Pape, *Thalamic neurons and networks related to absence epilepsy.*, Encyclopedia of Basic Epilepsy Research (2009).

[33] G. Buzsaki, *The thalamic clock: Emergent network properties*, Neuroscience **41** (1991), no. 2, 351 – 364.

[34] Perretti C T., Munch S B., and Sugihara G, *Model-free forecasting outperforms the correct mechanistic model for simulated and experimental data.*, Proceedings of the National Academy of Sciences **110** (2013), no. 13, 5253.

[35] P Camfield and C Camfield, *What happens to children with epilepsy when they become adults? some facts and opinions*, Pediatric Neurology **51** (2014).

[36] R. T. Canolty, E. Edwards, S. S. Dalal, M. Soltani, S. S. Nagarajan, H. E. Kirsch, M. S. Berger, N. M. Barbaro, and R. T. Knight, *High gamma power is phase-locked to theta oscillations in human neocortex*, Science **313** (2006), no. 5793, 1626–1628.

[37] L Cao, *Practical method for determining the minimum embedding dimension of a scalar time series*, Physica D **110** (1997), no. 1-2, 43–50.

[38] P Carney and G Jackson, *Insights into the mechanisms of absence seizure generation provided by eeg with functional mri*, Frontiers in neurology **5** (2014), 162.

[39] M. A. Castro-Alamancos, *Properties of primary sensory (lemniscal) synapses in the ventrobasal thalamus and the relay of high-frequency sensory inputs.*, Journal of Neurophysiology (2002), no. 2, 946.

[40] M.A. Castro-Alamancos, *Cortical up and activated states: Implications for sensory information processing.*, Neuroscientist (2009), no. 6, 625.

[41] W. Chaovalitwongse, L.D. Iasemidis, P.M. Pardalos, P.R. Carney, D.-S. Shiau, and J.C. Sackellares, *Performance of a seizure warning algorithm based on the dynamics of intracranial eeg*, Epilepsy Research **64** (2005), no. 3, 93 – 113.

[42] M. Chavez, M. Le Van Quyen, V. Navarro, M. Baulac, and J. Martinerie, *Spatio-temporal dynamics prior to neocortical seizures: amplitude versus phase couplings*, IEEE Transactions on Biomedical Engineering **50** (2003), no. 5, 571–583.

[43] D R. Chialvo, P Balenzuela, and D Fraiman, *The brain: What is critical about it?.*, AIP Conference Proceedings **1028** (2008), no. 1, 28 – 45.

[44] P T. Clemson and A Stefanovska, *Discerning non-autonomous dynamics*, Physics Reports **542** (2014), no. 4, 297 – 368.

[45] S. Cocco and R. Monasson, *Adaptive cluster expansion for inferring boltzmann machines with noisy data*, Physical Review Letters **106** (2011), 090601.

[46] S Cocco and R Monasson, *Adaptive cluster expansion for the inverse ising problem: Convergence, algorithm and tests*, Journal of Statistical Physics **147** (2011).

[47] Berkovic S Murphy M Morokoff A Fabinyi G D'Souza W Yerra R Archer J Litewka L Hosking S. Cook M, O'Brien T, *Prediction of seizure likelihood with a long-term, implanted seizure advisory system in patients with drug-resistant epilepsy: a first-in-man study*, Lancet Neurology **12** (2013), no. 6.

[48] F Crick, *Function of the thalamic reticular complex: The searchlight hypothesis*, Proceedings of the National Academy of Sciences of the United States of America **81** (1984), 4586–90.

[49] J. H Cross, G Kluger, and L Lagae, *Review article: Advancing the management of childhood epilepsies.*, European Journal of Paediatric Neurology **17** (2013), 334 – 347.

[50] V Crunelli and N Leresche, *Childhood absence epilepsy: genes, channels, neurons and networks*, Nature reviews. Neuroscience **3** (2002), 371–82.

[51] ———, *Childhood absence epilepsy: genes, channels, neurons and networks.*, Nature Reviews. Neuroscience **3** (2002), no. 5, 371 – 382.

[52] FHL da Silva, W Blanes, SN Kalitzin, J Parra, P Suffczynski, and DN Velis, *Dynamical diseases of brain systems: Different routes to epileptic seizures.*, IEEE Transactions on Biomedical Engineering **50** (n.d.), no. 5, 540 – 548.

[53] D Delignieres and V Marmelat, *Fractal fluctuations and complexity: Current debates and future challenges*, Critical Reviews in Biomedical Engineering **40** (2012), no. 6, 485–500.

[54] A Depaulis, O David, and S Charpier, *Invited review: The genetic absence epilepsy rat from strasbourg as a model to decipher the neuronal and network mechanisms of generalized idiopathic epilepsies.*, Journal of Neuroscience Methods **260** (2016), no. Methods and Models in Epilepsy Research, 159 – 174.

[55] A Destexhe, *Spatiotemporal aspects of slow-waves and seizures in humans.*, Brain: A Journal of Neurology **133** (2010), no. Pt 9, 2514 – 2515.

[56] E. Di Pasquale, K. D. Keegan, and J. L. Noebels, *Increased excitability and inward rectification in layer v cortical pyramidal neurons in the epileptic mutant mouse stargazer.*, Journal of Neurophysiology (1997), no. 2, 621.

[57] P D. Ditlevsen and S J. Johnsen, *Tipping points: Early warning and wishful thinking*, Geophysical Research Letters **37** (2010), no. 19, n/a–n/a, L19703.

[58] L G Dominguez, R A. Wennberg, W Gaetz, D Cheyne, O. C Snead, and J L P Velazquez, *Enhanced synchrony in epileptiform activity? local versus distant phase synchronization in generalized seizures*, Journal of Neuroscience **25** (2005), no. 35, 8077–8084.

[59] Sitnikova E and van Luijtelaar G, *Cortical and thalamic coherence during spikewave seizures in wag/rij rats*, Epilepsy Research **71** (2006), no. 2, 159 – 180.

[60] Jones E G., *Thalamic circuitry and thalamocortical synchrony.*, Philosophical Transactions: Biological Sciences **357** (2002), no. 1428, 1659.

[61] ———, *Thalamic circuitry and thalamocortical synchrony.*, Philosophical Transactions: Biological Sciences **357** (2002), no. 1428, 1659.

[62] J. P. Eckmann, S. Oliffson Kamphorst, D. Ruelle, and S. Ciliberto, *Liapunov exponents from time series*, Phys. Rev. A **34** (1986), 4971–4979.

[63] J.-P. Eckmann and D. Ruelle, *Ergodic theory of chaos and strange attractors*, pp. 273–312, Springer New York, New York, NY, 2004.

[64] S El Boustani and A Destexhe, *Brain dynamics at multiple scales: can one reconcile the apparent low-dimensional chaos of macroscopic variables with the seemingly stochastic behavior of single neurons?*, International Journal of Bifurcation and Chaos **20** (2010), no. 06, 1687–1702.

[65] R C. Elson, A I. Selverston, R Huerta, N F. Rulkov, M I. Rabinovich, and H D. I. Abarbanel, *Synchronous behavior of two coupled biological neurons*, Physical Review Letters **81** (1998), 5692–5695.

[66] A K. Engel, P Fries, and W Singer, *Dynamic predictions: Oscillations and synchrony in top-down processing.*, Nature Reviews Neuroscience **2** (2001), no. 10, 704 – 716.

[67] Mormann F, Kreuz T, Andrzejak R G, P David, Lehnertz K, and E Elger C E, *Epileptic seizures are preceded by a decrease in synchronization*, Epilepsy Research **53** (2003), no. 3, 173 – 185.

[68] C D. Ferrie, *Epileptic syndromes in childhood and adolescence.*, Paediatrics & Child Health **19** (2009), no. 5, 210.

[69] T Fitzgerald, A Valentin, R Selway, and M Richardson, *Cross-frequency coupling within and between the human thalamus and neocortex*, Frontiers in Human Neuroscience **7** (2013), 84.

[70] D Fraiman, P Balenzuela, J Foss, and DR Chialvo, *Ising-like dynamics in large-scale functional brain networks.*, Physical Review E **79** (n.d.), no. 6.

[71] N Friedman, S Ito, B A. W. Brinkman, M Shimono, R. E. L DeVille, K A. Dahmen, J M. Beggs, and T C. Butler, *Universal critical dynamics in high resolution neuronal avalanche data*, Physical Review Letters **108** (2012), 208102.

[72] R Friedrich, J Peinke, M Sahimi, and M. R R Tabar, *Approaching complexity by stochastic methods: From biological systems to turbulence*, Physics Reports **506** (2011), no. 5, 87 – 162.

[73] R. Friedrich, S. Siegert, Joachim Peinke, Stephan Lck, Malte Siefert, Michael Lindemann, Jan Raethjen, Gnther Deuschl, and Gerd Pfister, *Extracting model equations from experimental data*, Physics Letters A **271** (2000), 217–222.

[74] P Fries, *A mechanism for cognitive dynamics: neuronal communication through neuronal coherence.*, Trends in Cognitive Sciences **9** (n.d.), no. 10, 474 – 480.

[75] Buzsaki G, Buhl D L, Harris K D, Csicsvari J, Czh B, and Morozov A, *Hippocampal network patterns of activity in the mouse*, Neuroscience **116** (2003), no. 1, 201 – 211.

[76] Buzski G and D Andreas, *Neuronal oscillations in cortical networks.*, Science **304** (2004), no. 5679, 1926.

[77] Paxinos G and Watson C, *The rat brain in stereotaxic coordinates*, Academic Press, 2007.

[78] Sugihara G, May R, Y Hao, Hsien C-h, Dayle E, Fogarty M, and Munch S, *Detecting causality in complex ecosystems.*, Science **338** (2012), no. 6106, 496.

[79] J Gao, Y Cao, W Tung, and J Hu, *Multiscale analysis of complex time series: integration of chaos and random fractal theory, and beyond*, John Wiley & Sons, 2007.

[80] F A. Gibbs, W G. Lennox, and E L. Gibbs, *The Electro-encephalogram in diagnosis and in localization of epileptic seizures*, Archives of Neurology Psychiatry **36** (1936), no. 6, 1225–1235.

[81] P. Gloor, *Generalized cortico-reticular epilepsies some considerations on the pathophysiology of generalized bilaterally synchronous spike and wave discharge*, Epilepsia **9**, no. 3, 249–263.

[82] Marc Goodfellow and Paul Glendinning, *Mechanisms of intermittent state transitions in a coupled heterogeneous oscillator model of epilepsy*, The Journal of Mathematical Neuroscience **3** (2013), no. 1, 1–14.

[83] C. W. J. Granger, *Investigating causal relations by econometric models and cross-spectral methods*, Econometrica **37** (1969), no. 3, 424–438.

[84] R.W. Guillery and S. M Sherman, *Review: Thalamic relay functions and their role in corticocortical communication. generalizations from the visual system.*, Neuron **33** (2002), 163 – 175.

[85] Bokil H, Andrews P, Kulkarni J E, Mehta S, and Mitra P P, *Chronux: A platform for analyzing neural signals*, Journal of Neuroscience Methods **192** (2010), no. 1, 146 – 151.

[86] H. Haken, *Synergetics. an introduction. springer-verlag, berlin-heidelberg-new york 1977. xii, 325 s., 125 abb., dm 72.*., Biometrical Journal **20** (1978), no. 2, 197–197.

[87] T E Harris, *The theory of branching processes*, New York : Dover Publications, 1989, c1963., 1989.

[88] JM Hurtado, LL Rubchinsky, and KA Sigvardt, *Statistical method for detection of phase-locking episodes in neural oscillations.*, Journal of Neurophysiology **91** (n.d.), no. 4, 1883 – 1898.

[89] L. D. Iasemidis, , J. C. Sackellares, P. M. Pardalos, and A. Prasad, *Dynamical resetting of the human brain at epileptic seizures: application of nonlinear dynamics and global optimization techniques*, IEEE Transactions on Biomedical Engineering **51** (2004), no. 3, 493–506.

[90] LD Iasemidis, JC Sackellares, HP Zaveri, and WJ Williams, *Phase space topography and the lyapunov exponent of electrocorticograms in partial seizures*, Brain topography **2** (1990), no. 3, 187201.

[91] G M. Ibrahim, S Wong, B R. Morgan, N Lipsman, A Fallah, A G. Weil, V Krishna, R A. Wennberg, and A A. Lozano, *Phase-amplitude coupling within the anterior thalamic nuclei during seizures*, Journal of Neurophysiology **119** (2018), no. 4, 1497–1505, PMID: 29357461.

[92] E Ising, *Beitrag zur theorie des ferromagnetismus*, Z. Physik **31** (1925), 253–258.

[93] Y Itoh and S Ueda, *The ising model for changes in word ordering rule in natural language*, Physica D Nonlinear Phenomena **198** (2001).

[94] Anton I. Ivanov, Christophe Bernard, Pascale P. Quilichini, Viktor K. Jirsa, and William C. Stacey, *On the nature of seizure dynamics*, Brain **137** (2014), no. 8, 2210–2230.

[95] Aru J, Aru J, Priesemann V, Wibral M, Lana L, Pipa G, Singer S, and Vicente R, *Untangling cross-frequency coupling in neuroscience*, Current Opinion in Neurobiology **31** (2015), 51 – 61, SI: Brain rhythms and dynamic coordination.

[96] J. Jeong, J.-H. Chae, S. Y. Kim, and S.-H. Han, *Nonlinear dynamic analysis of the eeg in patients with alzheimer's disease and vascular dementia.*, Journal of Clinical Neurophysiology (2001), no. 1, 58.

[97] P Jiruska, M de Curtis, J Jefferys, C Schevon, S Schiff, and K Schindler, *Synchronization and desynchronization in epilepsy: Controversies and hypotheses.*, The Journal of physiology **591** (2012).

[98] E.G. Jones, *Synchrony in the interconnected circuitry of the thalamus and cerebral cortex.*, Annals - New York Academy of Sciences (2009), 10.

[99] S. Kalitzin, D. Velis, S. Claus, and F. L. da Silva, *Electrical brain stimulation for assessment and control of epileptic transitions*, (2011), 659–662.

[100] CJ Keller, W Truccolo, JT Gale, E Eskandar, T Thesen, C Carlson, O Devinsky, R Kuzniecky, WK Doyle, JR Madsen, DL Schomer, AD Mehta, EN Brown, LR Hochberg, I Ulbert, E Halgren, and SS Cash, *Heterogeneous neuronal firing patterns during interictal epileptiform discharges in the human cortex.*, Brain **133** (2010), no. Pt 6, 1668 – 1681.

[101] MG Kitzbichler, ML Smith, SR Christensen, and E Bullmore, *Broadband criticality of human brain network synchronization.*, PLoS Computational Biology **5** (n.d.), no. 3.

[102] M A. Kramer, U T. Eden, E D. Kolaczyk, R Zepeda, E N. Eskandar, and S S. Cash, *Coalescence and fragmentation of cortical networks during focal seizures*, **30** (2010), no. 30, 10076–10085.

[103] M A. Kramer, Wilson Truccolo, U T. Eden, K Q. Lepage, L R. Hochberg, E N. Eskandar, J R. Madsen, J W. Lee, A Maheshwari, E Halgren, C J. Chu, and S S. Cash, *Human seizures self-terminate across spatial scales via a critical transition*, Proceedings of the National Academy of Sciences **109** (2012), no. 51, 21116–21121.

[104] J-P Lachaux, E Rodriguez, J Martinerie, and F J. Varela, *Measuring phase synchrony in brain signals*, Human Brain Mapping **8**, no. 4, 194–208.

[105] S J. Lade and T Gross, *Early warning signals for critical transitions: A generalized modeling approach.*, PLoS Computational Biology **8** (2012), no. 2, 1 – 6.

[106] Y-C Lai, I Osorio, M G. Frei, and M A F. Harrison, *Are correlation dimension and lyapunov exponents useful tools for prediction of epileptic seizures?*, Computational Neuroscience in Epilepsy (I Soltesz and K Staley, eds.), Academic Press, San Diego, 2008, pp. 471 – 495.

[107] M Le Van Quyen and A Bragin, *Analysis of dynamic brain oscillations: methodological advances.*, Trends in Neurosciences **30** (n.d.), no. 7, 365 – 373.

[108] A Lenartowicz and S K. Loo, *Use of eeg to diagnose adhd*, Current Psychiatry Reports **16** (n.d.), no. 11.

[109] William G. Lennox, *The heredity of epilepsy as told by relatives and twins*, Journal of the American Medical Association **146** (1951), no. 6, 529–536.

[110] T Letz and H Kantz, *Characterization of sensitivity to finite perturbations*, Phys. Rev. E **61** (2000), 2533–2538.

[111] X Li, G Ouyang, and D A. Richards, *Predictability analysis of absence seizures with permutation entropy.*, Epilepsy Research **77** (2007), no. 1, 70 – 74.

[112] K Linkenkaer-Hansen, V V. Nikouline, J. M Palva, and R J. Ilmoniemi, *Long-range temporal correlations and scaling behavior in human brain oscillations.*, The Journal of Neuroscience **21** (2001), no. 4, 1370 – 1377.

[113] B Litt, R Esteller, J Echauz, M D'Alessandro, R Shor, T Henry, P Pennell, C Epstein, R Bakay, M Dichter, and G Vachtsevanos, *Epileptic seizures may begin hours in advance of clinical onset: A report of five patients*, Neuron **30** (2001), no. 1, 51 – 64.

[114] R Llinas and M Steriade, *Bursting of thalamic neurons and states of vigilance*, Journal of neurophysiology **95** (2006), 3297–308.

[115] G Luijtelaar, E Sitnikova, and I Midzyanovskaya, *Cortical control of absence seizures : focal initiation, spreading and modulation*, pp. 93–117, 01 2006.

[116] Annika Luttjohann and Gilles van Luijtelaar, *Dynamics of networks during absence seizures on- and offset in rodents and man*, Frontiers in Physiology **6** (2015), no. 16.

[117] Cencini M and Vulpiani A, *Finite size lyapunov exponent: review on applications*, Journal of Physics A: Mathematical and Theoretical **46** (2013), no. 25, 254019.

[118] Guirgis M, Chinvarun Y, del Campo M, Carlen P L, and Bardakjian B L, *Defining regions of interest using cross-frequency coupling in extratemporal lobe epilepsy patients*, Journal of Neural Engineering **12** (2015), no. 2, 026011.

[119] Steriade M, *Interneuronal epileptic discharges related to spike-and-wave cortical seizures in behaving monkeys*, Electroencephalography and Clinical Neurophysiology **37** (1974), no. 3, 247 – 263.

[120] Steriade M and Yossif G, *Spike-and-wave afterdischarges in cortical somatosensory neurons of cat*, Electroencephalography and Clinical Neurophysiology **37** (1974), no. 6, 633 – 648.

[121] Kaushik Majumdar, Pradeep D. Prasad, and Shailesh Verma, *Synchronization implies seizure or seizure implies synchronization?*, Brain Topography **27** (2013), no. 1, 112–122.

[122] Nadia Mammone, Domenico Labate, Aime Lay-Ekuakille, and Francesco Morabito, *Analysis of absence seizure generation using eeg spatial-temporal regularity measures*, International journal of neural systems **22** (2012), 1250024.

[123] D Marinazzo, G Wu, M Pellicoro, L Angelini, and S Stramaglia, *Information flow in networks and the law of diminishing marginal returns: Evidence from modeling and human electroencephalographic recordings*, PLOS One **7** (2012), no. 9, 1–9.

[124] J Martinerie, C Adam, M Le Van Quyen, M Baulac, S Clemenceau, B Renault, and F.J. Varela, *Epileptic seizures can be anticipated by non-linear analysis*, Nature medicine **4** (1998), 1173–6.

[125] Iacopo Mastromatteo and Matteo Marsili, *On the criticality of inferred models*, Journal of Statistical Mechanics **2011** (2011).

[126] D A McCormick and H C Pape, *Properties of a hyperpolarization-activated cation current and its role in rhythmic oscillation in thalamic relay neurones.*, The Journal Of Physiology **431** (1990), 291 – 318.

[127] P McSharry, *The danger of wishing for chaos.*, Nonlinear Dynamics, Psychology, And Life Sciences **9** (2005), no. 4, 375 – 397.

[128] P E McSharry, L A Smith, and L Tarassenko, *Prediction of epileptic seizures: are nonlinear methods relevant?*, Nature Medicine **9** (2003), no. 3, 2412; author reply 242.

[129] KD Mease, S Bharadwaj, and S Iravanchy, *Timescale analysis for nonlinear dynamical systems*, Journal of guidance, control, and dynamics **26** (2003), no. 2, 318–330.

[130] H. Meeren, G. van Luijtelaar, F. L. da Silva, and A. Coenen, *Evolving concepts on the pathophysiology of absence seizures: The cortical focus theory.*, Archives of Neurology (2005), no. 3, 371.

[131] H K. M. Meeren, J P M. Pijn, E L. J. M. Van Luijtelaar, A M. L. Coenen, and F H. Lopes da Silva, *Cortical focus drives widespread corticothalamic networks during spontaneous absence seizures in rats*, Journal of Neuroscience **22** (2002), no. 4, 1480–1495.

[132] Christian Meisel, Alexander Storch, Susanne Hallmeyer-Elgner, Ed Bullmore, and Thilo Gross, *Failure of adaptive self-organized criticality during epileptic seizure attacks.*, PLoS Computational Biology (2012), no. 1.

[133] P Milanowski and P Suffczynski, *Seizures start without common signatures of critical transition*, International Journal of Neural Systems **26** (2016), no. 08, 1650053, PMID: 27633895.

[134] T Mora and W Bialek, *Are biological systems poised at criticality?*, Journal of Statistical Physics **144** (2010).

[135] F Mormann, R G. Andrzejak, T Kreuz, C Rieke, P David, C E. Elger, and K Lehnertz, *Automated detection of a preseizure state based on a decrease in synchronization in intracranial electroencephalogram recordings from epilepsy patients*, Physical Review E **67** (2003), 021912.

[136] F Mormann, K Lehnertz, P David, and CE Elger, *Mean phase coherence as a measure for phase synchronization and its application to the eeg of epilepsy patients.*, Physica D - Nonlinear Phenomena **144** (n.d.), no. 3-4, 358 – 369.

[137] T I. Netoff and S J. Schiff, *Decreased neuronal synchronization during experimental seizures*, Journal of Neuroscience **22** (2002), no. 16, 7297–7307.

[138] C. Neuper and G. Pfurtscheller, *Event-related dynamics of cortical rhythms: frequency-specific features and functional correlates.*, International Journal of Psychopathology (2001), no. 1, 41.

[139] E Niedermeyer, *Sleep Electroencephalograms In Petit Mal*, Archives of Neurology **12** (1965), no. 6, 625–630.

[140] D Nolan and J Fink, *Genetics of epilepsy.*, Handbook Of Clinical Neurology **148** (2018), 467 – 491.

[141] G Nolte, A Ziehe, N Krmer, F Popescu, and K-R Mller, *Comparison of granger causality and phase slope index*, Proceedings of Workshop on Causality: Objectives and Assessment at NIPS 2008 (Whistler, Canada) (Isabelle Guyon, Dominik Janzing, and Bernhard Schlkopf, eds.), Proceedings of Machine Learning Research, vol. 6, PMLR, 12 Dec 2010, pp. 267–276.

[142] G Nolte, A Ziehe, V V. Nikulin, A Schloegl, N Kraemer, T Brismar, and K-R Mueller, *Robustly estimating the flow direction of information in complex physical systems.*, Physical Review Letters **100** (2007), no. 23.

[143] Stelt O van der, B Aysenil, and Lieberman J A., *Macroscopic fast neuronal oscillations and synchrony in schizophrenia.*, Proceedings of the National Academy of Sciences of the United States of America **101** (2004), no. 51, 17567.

[144] IE Ohiorhenuan, F Mechler, KP Purpura, AM Schmid, Q Hu, and JD Victor, *Sparse coding and high-order correlations in fine-scale cortical networks.*, Nature **466** (n.d.), no. 7306, 617 – U4.

[145] L Onsager, *Crystal statistics. i. a two-dimensional model with an order-disorder transition*, Phys. Rev. **65** (1944), 117–149.

[146] S M. O'Regan and D L. Burton, *How stochasticity influences leading indicators of critical transitions.*, Bulletin of Mathematical Biology **80** (2018), no. 6, 1630 – 1654.

[147] I Osorio, M G. Frei, D Sornette, J Milton, and Y-C Lai, *Epileptic seizures: Quakes of the brain?*, Phys. Rev. E **82** (2010), 021919.

[148] A. A. Ovchinnikov, A. E. Hramov, A. Luttjehann, A. A. Koronovskii, and G. Luijtelaar, *Method for diagnostics of characteristic patterns of observable time series and*

its real-time experimental implementation for neurophysiological signals, Technical Physics **56** (2011), no. 1, 1–7.

[149] M. N. OConnell, A. Barczak, D. Ross, T. McGinnis, C. E. Schroeder, and P. Lakatos, *Multi-scale entrainment of coupled neuronal oscillations in primary auditory cortex*, Frontiers in Human Neuroscience **9** (2015), 655.

[150] Fries P, Reynolds J H., Rorie A E., and Desimone R, *Modulation of oscillatory neuronal synchronization by selective visual attention.*, Science **291** (2001), no. 5508, 1560.

[151] C. P. Panayiotopoulos, *The epilepsies : seizures, syndromes and management : based on the ilae classifications and practice parameter guidelines.*, NCBI bookshelf, Oxfordshire, UK : Bladon Medical Pub., 2005., 2005.

[152] J. Peinke, M.R.R. Tabar, and M. Wachter, *The fokkerplanck approach to complex spatiotemporal disordered systems*, Annual Review of Condensed Matter Physics **10** (2019), no. 1, 107–132.

[153] W Penfield and H Jasper, *Epilepsy and the functional neuroanatomy of the brain*, Southern Medical Journal **47** (1954), no. 7, 704.

[154] E Pereda, RQ Quiroga, and J Bhattacharya, *Nonlinear multivariate analysis of neurophysiological signals.*, Progress in Neurobiology **77** (n.d.), no. 1-2, 1 – 37.

[155] R Perin, TK Berger, and H Markram, *A synaptic organizing principle for cortical neuronal groups.*, Proceedings of the National Academy of Sciences **108** (n.d.), no. 13, 5419 – 5424.

[156] T Petermann, T C. Thiagarajan, M A. Lebedev, M A. L. Nicolelis, D R. Chialvo, and D Plenz, *Spontaneous cortical activity in awake monkeys composed of neuronal avalanches*, Proceedings of the National Academy of Sciences **106** (2009), no. 37, 15921–15926.

[157] M Pievani, W de Haan, T Wu, W W Seeley, and G B Frisoni, *Review: Functional network disruption in the degenerative dementias.*, Lancet Neurology **10** (2011), 829 – 843.

[158] Lopes da Silva F. Pijm J.P., *Propagation of electrical activity: Nonlinear associations and time delays between eeg signals.*, In: Zschocke S., Speckmann EJ. (eds) Basic Mechanisms of the EEG. Brain Dynamics, Birkhuser, Boston, MA, 1993.

[159] J P Pijn, J Van Neerven, A Noest, and F H. Lopes da Silva, *Chaos or noise in eeg signals; dependence on state and brain site*, Electroencephalography and Clinical Neurophysiology **79** (1991), no. 5, 371 – 381.

[160] JP Pijn, DN Velis, MJ van der Heyden, J DeGoede, CW van Veelen, and FH Lopes da Silva, *Nonlinear dynamics of epileptic seizures on basis of intracranial eeg recordings*, Brain topography **9** (1997), no. 4, 249270.

[161] D Pinault, *Cellular interactions in the rat somatosensory thalamocortical system during normal and epileptic 59 hz oscillations*, The Journal of Physiology **552**, no. 3, 881–905.

[162] ———, *Review: The thalamic reticular nucleus: structure, function and concept.*, Brain Research Reviews **46** (2004), 1 – 31.

[163] D. Pinault and M. Deschenes, *Projection and innervation patterns of individual thalamic reticular axons in the thalamus of the adult rat: A three-dimensional, graphic, and morphometric analysis.*, Journal of Comparative Neurology (1998), no. 2, 180.

[164] D Pinault, N Leresche, S Charpier, J M Deniau, C Marescaux, M Vergnes, and V Crunelli, *Intracellular recordings in thalamic neurones during spontaneous spike and wave discharges in rats with absence epilepsy.*, The Journal Of Physiology **509 (Pt 2)** (1998), 449 – 456.

[165] D Pinault and T J O'Brien, *Cellular and network mechanisms of genetically-determined absence seizures*, Thalamus & Related Systems **3** (2005), no. 3, 181203.

[166] D Pinault, A Slzia, and L Acsdy, *Corticothalamic 59 hz oscillations are more pro-epileptogenic than sleep spindles in rats*, The Journal of Physiology **574**, no. 1, 209–227.

[167] D Pinault, M Vergnes, and C Marescaux, *Medium-voltage 59-hz oscillations give rise to spike-and-wave discharges in a genetic model of absence epilepsy: in vivo dual extracellular recording of thalamic relay and reticular neurons.*, Neuroscience **105** (2001), 181 – 201.

[168] Steve Pincus, *Approximate entropy as a measure of system complexity*, Proceedings of the National Academy of Sciences of the United States of America **88** (1991), 2297–301.

[169] A Pitknen, P S. Buckmaster, A S. Galanopoulou, and S L. Mosh, *Models of seizures and epilepsy.*, Elsevier : Academic Press, 2017.

[170] D Plenz and TC Thiagarajan, *The organizing principles of neuronal avalanches: cell assemblies in the cortex?.*, Trends in Neurosciences **30** (n.d.), no. 3, 101 – 110.

[171] P-O Polack, I Guillemain, E Hu, C Deransart, A Depaulis, and S Charpier, *Deep layer somatosensory cortical neurons initiate spike-and-wave discharges in a genetic model of absence seizures*, Journal of Neuroscience **27** (2007), no. 24, 6590–6599.

[172] P. O. Polack, S. Mahon, M. Chavez, and S. Charpier, *Inactivation of the somatosensory cortex prevents paroxysmal oscillations in cortical and related thalamic neurons in a genetic model of absence epilepsy.*, Cerebral Cortex (2009), no. 9, 2078.

[173] K.L. Powell, M. Kyi, C.A. Reid, L. Paradiso, G.M. D'Abaco, A.H. Kaye, S.J. Foote, and T.J. O'Brien, *Genetic absence epilepsy rats from strasbourg have increased corticothalamic expression of stargazin.*, Neurobiology of Disease **31** (2008), 261 – 265.

[174] T Prosen, B Buca, and TH Seligman, *Correlation matrices at the phase transition of the ising model*, arXiv preprint arXiv:1403.7218 (2014).

[175] J Prusseit and K Lehnertz, *Measuring interdependences in dissipative dynamical systems with estimated fokker-planck coefficients*, Physical Review E **77** (2008), 041914.

[176] C Quinto, I. Pimentel, A Andrade, J Foreid, and E Ducla-Soares, *Correlation dimension maps of eeg from epileptic absences*, Brain topography **11** (1999), 201–9.

[177] Freestone D R, Grayden D B, Lai A, Nelson T S, Halliday A, Burkitt A N, and Cook M J, *The thalamocortical circuit and the generation of epileptic spikes in rat models of focal epilepsy.*, 2009 Annual International Conference of the IEEE Engineering in Medicine and Biology Society, Engineering in Medicine and Biology Society, 2009. EMBC 2009. Annual International Conference of the IEEE (2009), 1533.

[178] Llinas R, Urbano F J, Leznik E, Ramirez R R, and van Marle H J F, *Rhythmic and dysrhythmic thalamocortical dynamics: Gaba systems and the edge effect*, Trends in Neurosciences **28** (2005), no. 6, 325 – 333, INMED/TINS special issue: Multiple facets of GABAergic synapses.

[179] Llinas R, Ribary U, Contreras D, and Pedroarena C, *The neuronal basis for consciousness*, Philosophical Transactions: Biological Sciences **353** (1998), no. 1377, 1841–1849.

[180] Llinas R R, Ribary U, Jeanmonod D, Kronberg E, and Mitra P P, *Thalamocortical dysrhythmia: A neurological and neuropsychiatric syndrome characterized by magnetoencephalography.*, Proceedings of the National Academy of Sciences of the United States of America **96** (1999), no. 26, 15222.

[181] R Renganathan and N Delanty, *Juvenile myoclonic epilepsy: under-appreciated and under-diagnosed*, Postgraduate Medical Journal **79** (2003), no. 928, 78–80.

[182] Joshua Richman and Joseph Moorman, *Physiological time-series analysis using approximate entropy and sample entropy*, American journal of physiology. Heart and circulatory physiology **278** (2000), H2039–49.

[183] M. Riedl, A. Muller, and N. Wessel, *Practical considerations of permutation entropy.*, European Physical Journal Special Topics (2013), no. 2, 249.

[184] P Rinn, P G Lind, M Wchter, and J Peinke, *The langevin approach: An r package for modeling markov processes*, Journal of Open Research Software **4** (2016), no. 1.

[185] J A Roberts, T W Boonstra, and M Breakspear, *The heavy tail of the human brain*, Current Opinion in Neurobiology **31** (2015), 164 – 172, SI: Brain rhythms and dynamic coordination.

[186] P A. Robinson, C Rennie, A Phillips, J W Kim, and J A Roberts, *Phase transitions in physiologically-based multiscale mean-field brain models*, pp. 179–201, Springer, 2010.

[187] M.G. Rosenblum, A Pikovsky, and J Kurths, *Phase synchronization of chaotic oscillators*, Physical Review Letters **76** (1996), 1804–1807.

[188] M T. Rosenstein, J J. Collins, and C J. De Luca, *A practical method for calculating largest lyapunov exponents from small data sets*, Physica D: Nonlinear Phenomena **65** (1993), no. 1, 117 – 134.

[189] H Rotstein, *Spiking resonances in models with the same slow resonant and fast amplifying currents but different subthreshold dynamic properties*, Journal of Computational Neuroscience **43** (2017).

[190] M Rybarsch and S Bornholdt, *Avalanches in self-organized critical neural networks: A minimal model for the neural soc universality class.*, PLoS One **9** (n.d.), no. 4.

[191] Sherman S. M and Guillery R. W., *The role of the thalamus in the flow of information to the cortex.*, Philosophical Transactions: Biological Sciences **357** (2002), no. 1428, 1695.

[192] M. Sano and Y. Sawada, *Measurement of the lyapunov spectrum from a chaotic time series*, Phys. Rev. Lett. **55** (1985), 1082–1085.

[193] S Saremi and T J. Sejnowski, *Hierarchical model of natural images and the origin of scale invariance*, Proceedings of the National Academy of Sciences **110** (2013), no. 8, 3071–3076.

[194] ———, *On criticality in high-dimensional data*, Neural Computation **26** (2014), no. 7, 1329–1339, PMID: 24708368.

[195] J. Sarnthein, A. Morel, A. von Stein, and D. Jeanmonod, *Thalamic theta field potentials and eeg: high thalamocortical coherence in patients with neurogenic pain, epilepsy and movement disorders.*, Thalamus and Related Systems (2003), no. 3, 231.

[196] S Sato, M Sano, and Y Sawada, *Practical Methods of Measuring the Generalized Dimension and the Largest Lyapunov Exponent in High Dimensional Chaotic Systems*, Progress of Theoretical Physics **77** (1987), no. 1, 1–5.

[197] M. Scheffer, J. Bascompte, W. A. Brock, V. Brovkin, S. R. Carpenter, V. Dakos, H. Held, E. H. van Nes, M. Rietkerk, and G. Sugihara, *Early-warning signals for critical transitions.*, Nature (2009), no. 7260, 53.

[198] M Scheffer, S R. Carpenter, T M. Lenton, J Bascompte, W Brock, V Dakos, J van de Koppel, I A. van de Leemput, S A. Levin, E H. van Nes, M Pascual, and J Vandermeer, *Anticipating critical transitions*, Science **338** (2012), no. 6105, 344–348.

[199] A Schnitzler and J Gross, *Normal and pathological oscillatory communication in the brain.*, Nature Reviews. Neuroscience **6** (2005), no. 4, 285 – 296.

[200] C Schroeder and P Lakatos, *Low-frequency neural oscillations as instruments of sensory selection*, Trends in neurosciences **32** (2008), 9–18.

[201] E. Schulz-DuBois and I. Rehberg, *Structure function in lieu of correlation function.*, Applied Physics A: Materials Science Processing **24** (1981), no. 4, 323.

[202] S. M. Sherman and R. W. Guillery, *Functional organization of thalamocortical relays.*, Journal of Neurophysiology (1996), no. 3, 1367.

[203] M. Siegel, T. H. Donner, and A. K. Engel, *Spectral fingerprints of large-scale neuronal interactions.*, Nature Reviews Neuroscience (2012), no. 2, 121.

[204] Samantha Simons, Pedro Espino, and Daniel Absolo, *Fuzzy entropy analysis of the electroencephalogram in patients with alzheimers disease: Is the method superior to sample entropy?*, Entropy **20** (2018), no. 1.

[205] W Singer and CM Gray, *Visual feature integration and the temporal correlation hypothesis*, Annual Review of Neuroscience **18** (1995), 555 – 586.

[206] E Sitnikova, A E. Hramov, V V. Grubov, A A. Ovchinnkov, and A A. Koronovsky, *On-off intermittency of thalamo-cortical oscillations in the electroencephalogram of rats with genetic predisposition to absence epilepsy*, Brain Research **1436** (2012), 147 – 156.

[207] E. Sitnikova and G. van Luijtelaar, *Cortical control of generalized absence seizures: effect of lidocaine applied to the somatosensory cortex in wag/rij rats.*, Brain Research (2004), no. 1-2, 127.

[208] H Sohanian Haghighi and Amir H. Davaie Markazi, *A new description of epileptic seizures based on dynamic analysis of a thalamocortical model*, Scientific Reports **7** (2017).

[209] C.J. Stam, T. Montez, B.F. Jones, S.A.R.B. Rombouts, Y. van der Made, Y.A.L. Pijnenburg, and Ph. Scheltens, *Disturbed fluctuations of resting state eeg synchronization in alzheimer's disease*, Clinical Neurophysiology **116** (2005), no. 3, 708 – 715.

[210] M Stead, M Bower, BH Brinkmann, K Lee, WR Marsh, FB Meyer, B Litt, J Van Gompel, and GA Worrell, *Microseizures and the spatiotemporal scales of human partial epilepsy.*, Brain **133** (2010), no. Pt 9, 2789 – 2797.

[211] A Stefanovska, P Clemson, and Y Suprunenko, *Introduction to chronotaxic systems systems far from thermodynamics equilibrium that adjust their clocks*, pp. 227–246, 12 2016.

[212] K E Stephan, E B Binder, M Breakspear, P Dayan, E C Johnstone, A Meyer-Lindenberg, U Schnyder, X-J Wang, D R Bach, P C Fletcher, J Flint, M J Frank,

A Heinz, Q J M Huys, P R Montague, M J Owen, and K J Friston, *Charting the landscape of priority problems in psychiatry, part 2: pathogenesis and aetiology.*, The Lancet. Psychiatry **3** (2016), no. 1, 84 – 90.

[213] G J. Stephens, T Mora, G Tkačik, and W Bialek, *Statistical thermodynamics of natural images*, Phys. Rev. Lett. **110** (2013), 018701.

[214] M. Steriade, *Review: Grouping of brain rhythms in corticothalamic systems.*, Neuroscience **137** (2006), 1087 – 1106.

[215] M. Steriade and D. Contreras, *Spike-wave complexes and fast components of cortically generated seizures i. role of neocortex and thalamus.*, Journal of Neurophysiology (1998), no. 3, 1439.

[216] IH Stevenson, JM Rebesco, LE Miller, and KP Kording, *Inferring functional connections between neurons.*, Current Opinion in Neurobiology **18** (2009), no. 6, 582 – 588.

[217] M L. Steyn-Ross, D.A. Steyn-Ross, and J.W. Sleigh, *Modelling general anaesthesia as a first-order phase transition in the cortex*, Progress in Biophysics and Molecular Biology **85** (2004), no. 2, 369 – 385, Modelling Cellular and Tissue Function.

[218] P A. Stokes and P L. Purdon, *A study of problems encountered in granger causality analysis from a neuroscience perspective*, Proceedings of the National Academy of Sciences **114** (2017), no. 34, E7063–E7072.

[219] U. Strauss, M. H. Kole, A. Bräuer, J. Pahnke, R. Bajorat, A. Rolfs, R. Nitsch, and R. A. Deisz, *An impaired neocortical ih is associated with enhanced excitability and absence epilepsy*, European Journal of Neuroscience **19** (2004).

[220] P Suffczynski, F H L Da Silva, J Parra, D N Velis, B M Bouwman, C M Van Rijn, P Van Hese, P Boon, H Khosravani, and M Derchansky, *Dynamics of epileptic phenomena determined from statistics of ictal transitions*, IEEE Transactions on Biomedical Engineering **53** (2006), no. 3, 524–532.

[221] M. V. Sysoeva and I. V. Sysoev, *Mathematical modeling of encephalogram dynamics during epileptic seizure*, Technical Physics Letters **38** (2012), no. 2, 151–154.

[222] E Tagliazucchi, D R. Chialvo, M Siniatchkin, E Amico, J-F Brichant, V Bonhomme, Q Noirhomme, H Laufs, and S Laureys, *Large-scale signatures of unconsciousness are consistent with a departure from critical dynamics*, Journal of The Royal Society Interface **13** (2016), no. 114, 20151027.

[223] F Takens, *Detecting strange attractors in turbulence. lecture notes in mathematics*, vol. 898, pp. 366–381, 11 2006.

[224] P. Tass, M. G. Rosenblum, J. Weule, J. Kurths, A. Pikovsky, J. Volkmann, A. Schnitzler, and H.-J. Freund, *Detection of $n : m$ phase locking from noisy data: Application to magnetoencephalography*, Physical Review Letters **81** (1998), 3291–3294.

[225] J Theiler, *On the evidence for low-dimensional chaos in an epileptic electroencephalogram*, Physics Letters A **196** (1994), no. 1, 335 – 341.

[226] A B L Tort, M A Kramer, C Thorn, D J Gibson, Y Kubota, A M Graybiel, and N J Kopell, *Dynamic cross-frequency couplings of local field potential oscillations in rat striatum and hippocampus during performance of a t-maze task*, Proceedings of the National Academy of Sciences **105** (2008), no. 51, 20517–20522.

[227] W Truccolo, J Donohoe, L Hochberg, E Eskandar, J Madsen, Anderson S W, E Brown, E Halgren, and S S Cash, *Single-neuron dynamics in human focal epilepsy*, Nature neuroscience **14** (2011), 635–41.

[228] I A. van de Leemput, M Wichers, A O. J. Cramer, D Borsboom, F Tuerlinckx, P Kuppens, E H. van Nes, W Viechtbauer, E J. Giltay, S H. Aggen, C Derom, N Jacobs, K S. Kendler, H L. J. van der Maas, M C. Neale, F Peeters, E Thiery, P Zachar, and M Scheffer, *Critical slowing down as early warning for the onset and termination of depression*, Proceedings of the National Academy of Sciences **111** (2014), no. 1, 87–92.

[229] D Van De Ville, J Britz, and C M. Michel, *Eeg microstate sequences in healthy humans at rest reveal scale-free dynamics*, Proceedings of the National Academy of Sciences **107** (2010), no. 42, 18179–18184.

[230] van Luijtelaar G, Sitnikova E, and Luttjohann A, *On the origin and suddenness of absences in genetic absence models*, Clinical EEG and Neuroscience **42** (2011), no. 2, 83–97, PMID: 21675598.

[231] M van Putten, *Nearest neighbor phase synchronization as a measure to detect seizure activity from scalp eeg recordings*, Journal of clinical neurophysiology **20** (2003), 320–5.

[232] S. Vanhatalo, J. M. Palva, M. D. Holmes, J. W. Miller, J. Voipio, and K. Kaila, *Infraslow oscillations modulate excitability and interictal epileptic activity in the human cortex during sleep*, Proceedings of the National Academy of Sciences **101** (2004), no. 14, 5053–5057.

[233] F. Varela, J.-P. Lachaux, E. Rodriguez, and J. Martinerie, *The brainweb: phase synchronization and large-scale integration.*, Nature Reviews Neuroscience (2001), no. 4, 229.

[234] J. L. Perez Velazquez, H Khosravani, A Lozano, B. L. Bardakjian, P L. Carlen, and R Wennberg, *Type iii intermittency in human partial epilepsy*, European Journal of Neuroscience **11**, no. 7, 2571–2576.

[235] R Veltz and T J. Sejnowski, *Periodic forcing of inhibition-stabilized networks: Nonlinear resonances and phase-amplitude coupling*, Neural Computation **27** (2015), no. 12, 2477–2509, PMID: 26496044.

[236] M Vergnes and C Marescaux, *Cortical and thalamic lesions in rats with absence epilepsy.*, Journal of Neural Transmission (1992), 71 – 83.

[237] M Vergnes, C Marescaux, and A Depaulis, *Mapping of spontaneous spike and wave discharges in wistar rats with genetic generalized non-convulsive epilepsy.*, Brain Research **523** (1990), no. 1, 87 – 91.

[238] M Vinck, M van Wingerden, T Womelsdorf, P Fries, and C M.A. Pennartz, *The pairwise phase consistency: A bias-free measure of rhythmic neuronal synchronization*, NeuroImage **51** (2010), no. 1, 112 – 122.

[239] A von Stein and J Sarnthein, *Different frequencies for different scales of cortical integration: from local gamma to long range alpha/theta synchronization*, International Journal of Psychophysiology **38** (2000), no. 3, 301 – 313.

[240] Zheng T W, *Cortical and thalamic network mechanisms underlying absence seizure generation and their modulation by anti-epileptic drugs*, Ph.D. thesis, University of Melbourne, 2010.

[241] F Wagner, W Truccolo, J Wang, and A Nurmikko, *Spatiotemporal dynamics of optogenetically-induced and spontaneous seizure transitions in primary generalized epilepsy.*, Journal of neurophysiology **113** (2014), jn.01040.2014.

[242] F. Wendling, F. Bartolomei, J.J. Bellanger, and P. Chauvel, *Interpretation of interdependencies in epileptic signals using a macroscopic physiological model of the eeg*, Clinical Neurophysiology **112** (2001), no. 7, 1201 – 1218.

[243] A Wolf, J B Swift, H L Swinney, and J A Vastano, *Determining lyapunov exponents from a time series*, Physica D: Nonlinear Phenomena **16** (1985), no. 3, 285–317.

[244] G A. Worrell, Ca S, D. Cranstoun, J Echauz, and B Litt, *Evidence for self-organized criticality in human epileptic hippocampus*, Neuroreport (2002), 2017–2021.

[245] T-L Yao, H-F Liu, J-L Xu, and W-F Li, *Lyapunov exponent spectrum from noisy time series*, International Journal of Bifurcation and Chaos **23** (2013), no. 06, 1350103.

[246] S Yu, D Huang, W Singer, and D Nikolic, *A small world of neuronal synchrony.*, Cerebral Cortex **18** (n.d.), no. 12, 2891 – 2901.

[247] S Yu, H Yang, H Nakahara, G S. Santos, D Nikolić, and D Plenz, *Higher-order interactions characterized in cortical activity*, Journal of Neuroscience **31** (2011), no. 48, 17514–17526.

[248] S Yu, H Yang, O Shriki, and D Plenz, *Universal organization of resting brain activity at the thermodynamic critical point*, Frontiers in Systems Neuroscience **7** (2013), 42.

[249] T W. Zheng, T J. OBrien, M J. Morris, C A. Reid, V Jovanovska, P OBrien, L van Raay, A K. Gandrathi, and D Pinault, *Rhythmic neuronal activity in s2 somatosensory and insular cortices contribute to the initiation of absence-related spike-and-wave discharges*, Epilepsia **53** (2012), no. 11.